MICROSYSTEMS BASED ON MICROBIAL BIOSENSING

Memòria presentada per

Xavier Muñoz Berbel

per optar al grau de doctor en Biotecnologia

Centre Nacional de Microelectrònica

Bellaterra, maig de 2008

Aquesta tesi, que porta per títol "Microsystems Based on Microbial Biosensing", ha estat realitzada en els laboratoris del Grup de Biosensors i BioMEMs del Departament de Micro i Nano Sistemes del Centre Nacional de Microelectrònica sota la direcció del Dr. Francesc Xavier Muñoz Pascual, investigador científic del Consejo Superior de Investigaciones Científicas.

Bellaterra, febrer de 2008

Francesc Xavier Muñoz Pascual

Vist-i-plau del Dr. Jaume Farrés Vicén, professor titular del Departament de Bioquímica i Biologia Molecular de la Universitat Autònoma de Barcelona i tutor d'aquest treball.

Jaume Farrés Vicén

Al meus, als que hi són
i als que desgraciadament no

Quan un metge va darrera el fèretre del seu pacient,

a vegades la causa segueix l'efecte

Robert Koch,

metge alemany considerat el pare de la bacteriologia

CONTENTS

CONTENTS

CHAPTER 5: MONITORING OF THE BIOFILM GROWTH ON METALLIC SURFACES USING ELECTROCHEMICAL IMPEDANCE SPECTROSCOPY

CHAPTER 11: DETERMINATION OF THE ROLE OF SEVERAL PROTEINS FROM PHOTORHABDUS LUMINESCENS IN THE FORMATION OF BIOFILMS, EARLY ATTACHMENT, MOTILITY AND VIRULENCE

CHAPTER 12: CONCLUSIONS

ANNEX

ABBREVIATIONS, SYMBOLS AND UNITS

ABBREVIATIONS, SYMBOLS AND UNITS

ABBREVIATIONS

Symbol	Meaning
(E)QCM(-D)	(Electrochemical) Quartz Crystal Microbalance (with Dispersion)
(RT)-PCR	(Reverse Transcription)-Polymerase Chain Reaction
ABMM	AB Minimal Medium
AC	Alternating Current
ADC	Analogue-to-Digital Converter
AIA	All Injection Analysis
ANN	Artificial Neural Network
APHA	American Public Health Association
CE	Counter Electrode
CH1	Channel 1
CH2	Channel 2
CME	Chemically Modified Electrode
CNM	Centre Nacional de Microelectrònica
CPE	Constant Phase Element
CSIC	Centre Superior d'Investigacions Científiques
CSLM	Confocal Scanning Laser Microscopy
CVA	Canonical Variate Analysis

Symbol	Meaning
DA	Discriminant Analysis
DAC	Digital-to-Analogue Converter
DAPI	4'-6-DiAmidino-2-Phenylindole
DAQ	Data Acquisition
DC	Direct Current
DFA	Discriminant Function Analysis
EIS	Electrochemical Impedance Spectroscopy
ENFET	ENzyme Field Effect Transistor
FET	Field Effect Transistors
FIA	Flow Injection Analysis
FISH	Fluorescent In Situ Hybridization
FTIR	Fourier Transform Infrared
GDM	Gradient Descent with Momentum
HCA	Hierarchical Cluster Analysis
HOMO	Highest Occupied Molecular Orbital
IDS	InterDigitated Structure electrode
IMB	Institut de Microelectrònica de Barcelona
ISE	Ion-Selective Electrode
ISFET	Ion-Selective Field Effect Transistor
IUPAC	International Union of Pure and Applied Chemistry
KNN	K-Nearest Neighbour
LB	Luria-Bertani medium
LM	Levenberg-Marquardt
LPS	LypoPolySaccharide
LUMO	Lowest Unoccupied Molecular Orbital
MCFIA	Multi-Commuted Flow Injection Analysis
MPS	Multi-Pumped System
MSB	Modified Scholten's Broth
MSFIA	Multi-Syringe Flow Injection Analysis
MVP	Modular Valve Position
NASBA	Nucleic Acid Sequence-Based Amplification
OCP	Open Circuit Potential
PBS	Phosphate Buffered Saline
PC	Personal Computer
PCA	Principal Component Analysis
PCB	Print Circuit Board
PECVD	Plasma Enhanced Chemical Vapour Deposition
PLC	Partial Least Square
PTFE	PolyTetraFluoro-Ethylene

Symbol	Meaning
RE	Reference Electrode
RI	Refractive Index
RIE	Reactive Ion Etching
RMSE	Root Mean Squared Error
SFA	Segmented Flow Analysis
SIA	Sequential Injection Analysis
SIMCA	Soft Independent Modelling of Class Analogy
SPR	Surface Plasmon Resonance
TIR	Total Internal Reflection
UAB	Universitat Autònoma de Barcelona
VI	Virtual Instrumentation
WE	Working Electrode

SYMBOLS

Symbol	Meaning
α_A	coefficient of anodic transfer
α_C	coefficient of cathodic transfer
A	area of the bare electrode
Abs_{550}	absorbance magnitude at 550 nm
A_C	coating area
A_{CE}	area of the counter electrode
$Ag43$	Antigen 43
A_P	area of the cross-sectional channels in the coating
β	parameter linked with the phase angle in Constant Phase Elements
B	susceptance
C	capacitance
C^*_O	concentration of oxidizing species in the bulk
C^*_R	concentration of reducing species in the bulk
$C_{bacteria}$	capacitance of the bacteria
C_{BC}	capacitance of the molecules composing the attached biofilm
$C_{biofilm}$	biofilm capacitance
C_C	coating capacitance
C_{dl}	double layer capacitance
$C_{dl(CE)}$	double layer capacitance for the counter electrode
$C_{dl(WE)}$	double layer capacitance for the working electrode

Symbol	Meaning
C_i	total measured interface capacitance
c_{ij}	expected concentration value
$\hat{c}_{ij}$	concentration value provided by the ANN
CPE_i	interface Constant Phase Element
C_{Pt}	bare electrode capacitance
C_{ref}	capacitance associated with the reference electrode
C_S	capacitance of the solution
δ	thickness of the diffusion layer
$\Delta K_i(t)$	normalized value of the magnitude of the constant phase element at time t
$\Delta K_i(4)$	normalized value for the 10^4 CFU mL^{-1} sample
$\Delta\theta$	differential surface plasmon resonance angle
$\Delta\theta_m$	minimum reflection angle shift
d	geometrical thickness of the material deposited on the gold
d	distance between electrodes
D	average value of the diffusion coefficients of the species in solution
d_C	coating thickness
d_{dl}	distance between charged layers
$d_{dl(CE)}$	distance between charged layers in the counter electrode
D_O	diffusion coefficient of the oxidizing species
d_p	length of the channels in the coating
D_R	diffusion coefficient of the reducing species
ε_0	permittivity of the free space
ε_C	coating permittivity
ε_{dl}	permittivity of the double layer
$\varepsilon_{dl(CE)}$	permittivity of the counter electrode double layer
ε_r	relative permittivity of the medium
e	alternating potential
E	alternating potential amplitude
Eq	equation
ϕ	phase angle
f	frequency
F	Faraday constant
Fig	figure
g	per gravity
η	overpotential
i	alternating current
I	alternating current amplitude
i_0	exchanged current density

IV

Symbol	Meaning
j	$\sqrt{-1}$
κ	conductivity
K	conductance
κ_C	conductivity of the electrolyte solution retained in the polymer
K	constant phase element magnitude
K_i	magnitude of the interface CPE
$K_i(1)$	magnitude of the CPE after 1 min attachment
$K_i(3.5)$	magnitude of the CPE after 3.5 days of incubation
$K_i(c)$	magnitude of the interface CPE at any bacteria concentration
$K_i(it)$	magnitude of the CPE_i at any incubation time
$K_i(m)$	magnitude of the CPE_i of the culture medium without bacteria
$K_i(t)$	magnitude of the CPE at time t
$K_i(wb)$	magnitude of the interface CPE in absence of bacteria
$k_{ph(i)}$	wave vector of incident photons
$k_{ph(r)}$	wave vector of reflected photons
λ	wavelength
l_d	decay length
n	number of electrons exchanged
n	refractive index of the material
N_P	number of channels in the coating
OD_{550}	Optical Density at 550 nm
θ	incidence angle
$\theta(t)$	coverage bacteria factor
θ_C	critical incidence angle
θ_m	minimum reflection angle
q	charge
R	resistance
R	constant of the ideal gases
$R_{biofilm}$	the resistance of the biofilm pores
R_C	coating-porous resistance
R_{CT}	the charge-transfer resistance
R_P	polarization resistance
R_S	solution resistance
σ	Warburg coefficient
S/N	signal-to-noise relationship
T	temperature
t	time
ω	angular frequency

Symbol	Meaning
Xc	capacitive reactance
$Y(w)$	admittance
Z	impedance magnitude
$|Z|$	impedance modulus
$Z(\omega)$	impedance
$Z_{CE}(\omega)$	impedance of the counter electrode
$Z_{cell}(\omega)$	impedance of the electrochemical cell
$Z_{CPE}(\omega)$	impedance of a constant phase element
$Z_E(\Omega)$	impedance of the electrodes
$Z_{eq}(\omega)$	equivalent impedance
$Z_{im}(\omega)$	imaginary component of the impedance
$Z_{re}(\omega)$	real component of the impedance
$Z_S(\omega)$	impedance of the solution
Z_W	Warburg's impedance
$Z_{WE}(\omega)$	impedance of the working electrode

UNITS

Symbol	Meaning
CFU	Colony Forming Units
F	Farad
h	Hour
Hz	Hertz
L	Litre
m	Meter
min	Minute
PFU	Plaque-Forming Units
rpm	Revolutions per minute
s	Second
UA	Unity of Absorbance
V	Volt
Ω	Ohm

VI

SUMMARY

SUMMARY

The present thesis was focused on the development of new electrochemical instrumentation for microbial biosensing to complement or to substitute the classical microbiological methods. The traditional microbiological methods, mainly based on plating on agar or staining-imaging processes, although highly specific and sensitive, still require considerable experience as well as time. Sensors in general and electrochemical sensors in particular have been thought to be a good alternative to them because of their simplicity, low cost, efficiency and their possibility to be compacted, miniaturized, automated and to supply information at real-time.

In terms of bacterial attachment, Electrochemical Impedance Spectroscopy (EIS) and Surface Plasmon Resonance (SPR) have been demonstrated to be sensitive methods for the real-time monitoring of bacteria attachment to metallic surfaces and they have shown good correlation with the traditional staining methods. Focusing on impedance measurements, the interface Constant Phase Element (CPE_i) has been found responsive to the bacterial coverage of the electrode, especially at the initial stage of attachment: the very early attachment or pre-attachment step.

The CPE_i has been also used to on-line monitor the formation and maturation of bacterial biofilms on the surface of platinum or gold electrodes, although another parameter of the equivalent circuit, the biofilm capacitance ($C_{biofilm}$), has been probed to be even more sensitive to the biofilm growth and maturation than the CPE_i. Both capacitances have shown good correlation with traditional microbiological techniques. Further, the removal capacity of several solutions has been checked using EIS, being the concentrated samples of peroxides the most efficient in the detachment of biofilms.

EIS has been applied to the detection of bacteriophages, virus that specifically infect bacteria, by following the degradation of mature biofilms of specific bacteria. 6-days mature biofilms grown on the electrode surface were incubated for 24 h in bacteriophages samples. The bacteriophages infection and degradation of the biofilm changed the $C_{biofilm}$, which variation correlated well with Optical and Confocal Microscopy measurements.

The changes produced in the electrode-solution interface by microbial attachment have been applied to the bacteria quantification using EIS. After short attachment times (below 2 min of attachment), the change in the CPE_i magnitude (K_i) was found to correlate well with the suspended concentration of bacteria in a wide range of concentrations, from 10^1 to 10^7 Colony Forming Units per mL (CFU mL^{-1}). This impedimetric approach was very sensitive to the applied potential and the aging of the sensor. The sensitivity of the measurement was enhanced by applying more positive potentials on the working electrode which favoured bacterial attachment. On the other hand, sensors were found to lose their capacity to discriminate between concentrations with time, especially low concentrations, although, the sensitivity (in terms of slope of the calibration curve) remained invariant.

The impedimetric approach to quantify suspended bacteria has been applied to *real* samples directly extracted from an incubator. In this case, also the influence of the metabolic products from the fermentation in the impedimetric measurement has been tested using centrifuged samples only containing metabolites or cells. It was seen that in the experimental condition in use only attached cells could produce a detectable change in K_i and showed a good correlation with the suspended concentration value from

plating on agar and Epifluorescence Microscopy counting. Thus, the impedimetric approach was found insensitive to the presence of metabolites in the medium.

The real-time and automatic monitoring of suspended bacteria concentration using EIS has been achieved by developing a new Virtual Instrumentation (VI) implemented in LabView to manage the automatic flow system and to synchronize it with the measurement system. In this case, the VI controlled the transport of the microbiological samples (from the incubator to the electrochemical cell and their elimination to the wasting recipient), the cleaning and sterilization of the electrochemical cell and the synchronization of the flow and measurement systems to make the EIS measurements after 15 s of the complete inoculation of the bacterial sample in the electrochemical cell. Good correlations were found between the bacteria concentration from classical microbiological methods and EIS when using this VI.

The K_i has been also applied to the resolution of binary microbial mixtures by following the changes produced in the electrode-interface capacitance by several concentrations of different species of microorganisms. This was achieved by combining this impedimetric approach used in bacterial quantification with chemometric tools, namely Artificial Neural Networks (ANNs). Very good correlations were obtained by comparing the predicted values (from the ANN) against the expected ones (from plating on agar), with comparison lines indistinguishable from the theoretical values (slope equal to one with zero intercept in the three cases under study).

Finally, attachment information from SPR data, together with biofilm formation (in the air-liquid interface) information, motility results (from the swimming process) and virulence assays (using *Galleria mellonella* larvae) of several *Pseudomonas luminescens* TT01 mutants has been combined for the prediction of the function of some structural proteins. Although characterization of the role of these proteins has been only achieved at a very basic level, the combination of used techniques, and particularly SPR, is capable of supplying relevant information rapidly and easily.

RESUM

Aquesta tesi s'ha centrat en el desenvolupament de nova instrumentació electroquímica per a la detecció microbiana que permetés complementar o, fins i tot, substituir els mètodes microbiològics clàssics. Els mètodes microbiològics tradicionals, principalment basats en processos de cultiu en placa o de tinció i observació microscòpica, encara que són altament sensibles i específics, requereixen un elevat grau d'experiència de l'usuari, així com llargs temps de mesura. En aquest sentit, s'ha pensat en els sensors en general i particularment en els sensors electroquímics com una bona alternativa a aquests mètodes per la seva gran simplicitat, baix cost i eficiència, així com per la facilitat que mostren per ser compactats, miniaturitzats, automatitzats i subministrar informació de qualitat a temps real.

Pel que fa a l'adhesió bacteriana, l'Espectroscòpia Electroquímica d'Impedàncies (EEI) i la Ressonància de Plasmó Superficial (RPS) han demostrat ser mètodes útils en el seguiment a temps real de l'adhesió bacteriana en superfícies metàl·liques, en mostrar gran concordança amb els mètodes tradicionals de tinció i observació microscòpica. Centrant-nos en les mesures impedimètriques, l'Element de Fase Constant de la interfase elèctrode-solució (EFC$_i$) s'ha mostrat molt sensible al procés de recobriment

bacterià de l'elèctrode, especialment en els primers estadis d'adhesió bacteriana, coneguts com adhesió inicial o *preadhesió*.

L'EFC$_i$ també s'ha fet servir pel monitoratge de la formació i maduració de biofilms bacterians en la superfície d'elèctrodes de platí i or. No obstant, un altre element del circuit equivalent, concretament la capacitat del biofilm ($C_{biofilm}$), ha demostrat ser fins i tot més sensible al creixement i maduració del biofilm. Ambdues capacitats mostraven bones correlacions amb els mètodes microbiològics tradicionals. Per altra banda, la impedància també es va fer servir per determinar la capacitat que tenien diferents solucions per eliminar biofilms, sent les mostres concentrades de peròxids les que mostraven un major poder desincrustant.

L'EEI també s'ha aplicat a la detecció de bacteriòfags, virus que específicament infecten bacteris, mitjançant el seguiment de la degradació de biofilms madurs de determinats bacteris. Després de 6 dies de creixement dels biofilms sobre la superfície dels elèctrodes, aquests van ser incubats durant 24 h en mostres que contenien bacteriòfags. La infecció i posterior degradació dels biofilms bacterians per part dels bacteriòfags canviava la $C_{biofilm}$, la variació de la qual mostrava bona correlació amb les mesures obtingudes mitjançant Microscòpia Òptica i Confocal.

Els canvis produïts en la interfase elèctrode-solució pel procés d'adhesió microbiana s'han utilitzat per a la quantificació bacteriana fent servir EEI. Després d'un temps d'adhesió curt (per sota els 2 min) es va observar que el canvi produït en la magnitud de l'EFC$_i$ (K_i) es podia correlacionar molt bé amb la concentració de bacteris en suspensió en un ampli rang de concentracions, entre 10^1 i 10^7 Unitats Formadores de Colònies per mL (UFC mL^{-1}). Aquesta aproximació impedimètrica era molt sensible al potencial aplicat a la superfície de l'elèctrode de treball i al procés d'envelliment del sensor. La sensitivitat de la mesura es veia incrementada en aplicar potencials més positius a la superfície de l'elèctrode de treball, els quals afavorien el procés d'adhesió bacteriana. Per altra banda, es va observar que els sensors perdien la seva capacitat per discriminar entre diferents concentracions amb el temps, especialment quan aquestes concentracions eren baixes, encara que la sensitivitat (considerada com el pendent de la recta de calibrat) no variava.

Aquesta aproximació impedimètrica per a la quantificació de bacteris en solució s'ha aplicat a mostres *reals* directament extretes d'un incubador. En aquest cas, la influència dels productes metabòlics produïts durant la fermentació en les mesures impedimètriques va ser testada mitjançant mostres centrifugades que únicament contenien metabòlits o cèl·lules. Sota les condicions experimentals utilitzades, únicament les cèl·lules adherides produïen canvis detectables en el valor de K_i. A més, els canvis mostraven una molt bona correlació amb el valor de concentració de bacteris en suspensió obtingut mitjançant recompte en plaques d'agar o Microscòpia d'Epifluorescència. Per tant, l'aproximació impedimètrica aquí descrita era pràcticament insensible a la presència de metabòlits en el medi.

El monitoratge de la concentració de bacteris en suspensió a temps real i de forma automàtica s'ha aconseguit mitjançant el desenvolupament de nova Instrumentació Virtual (IV) implementada en LabView que s'encarregava de regular el sistema de flux així com de sincronitzar-lo amb el sistema de mesura. En aquest cas, l'IV controlava el transport de les mostres microbiològiques (del fermentador a la cel·la electroquímica i la seva posterior eliminació al recipient de rebuig), la neteja i esterilització de la cel·la electroquímica i la sincronització entre el sistema de flux i el de mesura, per tal de realitzar les mesures impedimètriques exactament 15 s després de la completa inoculació de les mostres bacterianes a la cel·la electroquímica. Es van obtenir bones correlacions entre els valors de concentració bacteriana obtinguts mitjançant mètodes microbiològics i els obtinguts mitjançant l'EEI quan s'utilitzava l'IV.

La K_i també s'ha emprat en la resolució de mescles binàries de microorganismes. En aquest cas, es van tenir en compte els canvis produïts, en la interfase elèctrode-solució, per vàries concentracions de diferents espècies bacterianes. La resolució de les mescles es va aconseguir mitjançant la combinació de l'aproximació impedimètrica, utilitzada en la quantificació bacteriana, i d'eines quimiomètriques com les Xarxes Neuronals Artificials (XNAs). En comparar els valors predits per la XNA amb els esperats (obtinguts mitjançant el recompte amb plaques d'agar), es van obtenir bones correlacions, amb rectes ajustades indistingibles de les ideals, és a dir, amb el pendent igual a 1 i amb l'ordenada a l'origen passant per zero.

7

Finalment, la combinació de la informació d'adhesió obtinguda mitjançant RPS, la de formació de biofilms en la interfase aire-aigua, la de mobilitat bacteriana i la de virulència emprant *Galleria mellonella*, obtinguda de varis mutants de *Pseudomonas luminescens* TT01, s'ha utilitzat en la predicció de la funció de diverses proteïnes estructurals. Encara que el paper d'aquestes proteïnes només s'ha pogut determinar a un nivell molt bàsic, la combinació de tècniques emprada, i particularment la RPS, ha demostrat ser capaç de subministrar informació rellevant de forma ràpida i senzilla.

CHAPTER 1: INTRODUCTION

CHAPTER 1: INTRODUCTION

In this Chapter, general concepts for the suitable positioning of the thesis in the current biotechnological research are introduced. Chemical sensors are next defined, paying special attention to the electrochemical sensors. This Chapter also includes a detailed description of the most relevant measurement methods used in the development of the present thesis, fundamentally Electrochemical Impedance Spectroscopy (EIS) and Surface Plasmon Resonance (SPR). Finally, an overview of biological concepts, basically focused on the bacteria structure and colonization mechanism until biofilm formation, is included.

1.1   GENERAL INTRODUCTION: BIOTECHNOLOGY CONCEPT AND FUTURE PERSPECTIVES

Biotechnology is a multidisciplinary science which combines biological disciplines (e. g. molecular biology, cell biology, microbiology, biochemistry or genetics) with other sciences and engineering (e.g. physics, chemistry, electronics, informatics or chemical engineering), as illustrated in Fig. 1.1.
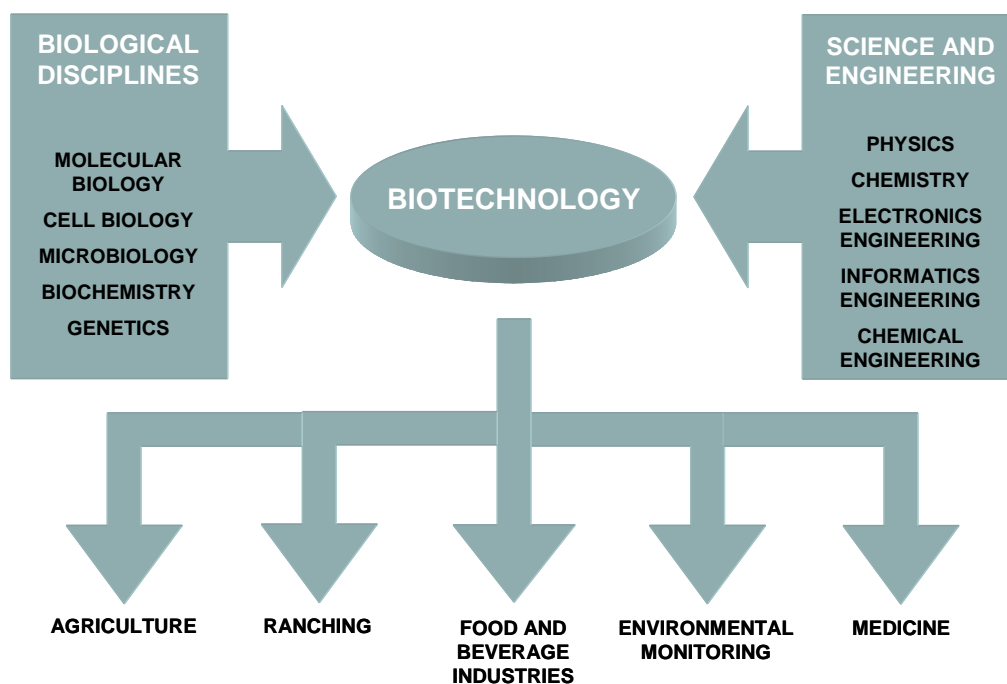
Fig. 1.1 Schematic representation of the huge variety of disciplines that biotechnology involves and the more representative areas where biotechnology plays an important role.

In 1992, the United Nations Convention on Biological Diversity of Rio de Janeiro defined the term biotechnology as "any technological application that uses biological systems, living organisms, or derivatives thereof, to make or modify products or processes for specific use". Regarding this, the paper of biotechnology is critical in several areas and thus, biotechnologists have become important in some fields, such as agriculture (development of transgenic plants)[1-3], ranching (development of transgenic animals)[4-6], food and beverage industries (improvement on the production and control systems)[7-10], environmental monitoring (systems for the control of plagues, for

monitoring biological contamination and residues and for the regeneration of contaminated lands)[11-15] or medicine (production of drugs and systems of analysis)[16, 17].

In the environmental monitoring, biotechnology is basically focused on the substitution of classical methods for the detection of biofilms, bacteria, viruses, toxins and other biohazard particles for simple, cheap, sensitive, efficient, compacted, miniaturized, automated and real-time systems. Sensors, and particularly those based on optical and electrochemical measurements, comply most of these features.

1.2   CHEMICAL SENSORS: DEFINITION AND IDEAL PROPERTIES

The International Union of Pure and Applied Chemistry (IUPAC) define a chemical sensor as "a device that transforms chemical information, ranging from the concentration of a specific sample component to total composition analysis, into an analytically useful signal. The chemical information, mentioned above, may be originated from a chemical reaction of the analyte or from a physical property of the system investigated"[18].
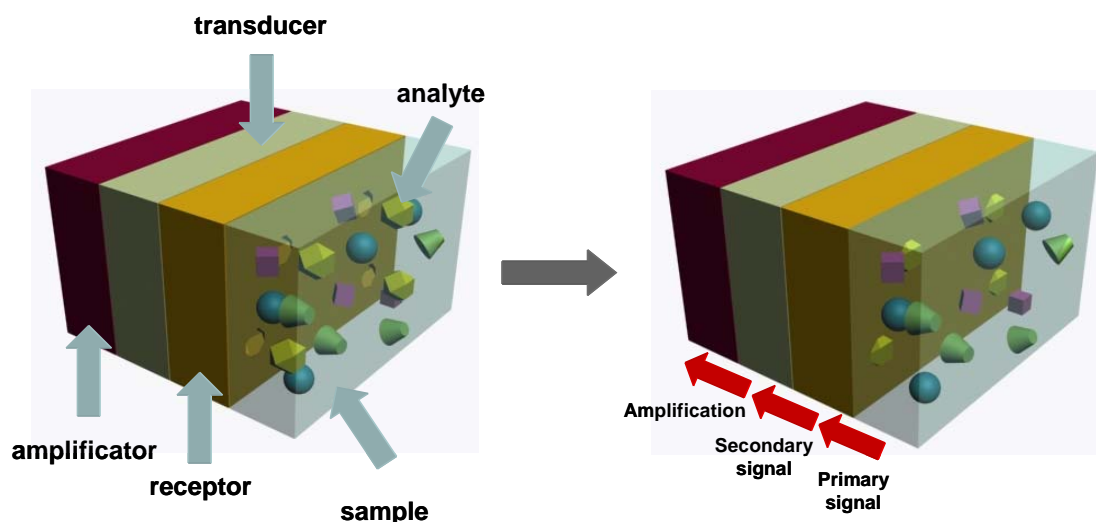
Fig. 1.2 Basic representation of the mechanism of information transfer for a chemical sensor.

Chemical sensors are composed of two principal functional parts, namely the receptor and the transducer parts. In the receptor part, the receptor element (a molecular or ionic

recognition material) selectively interacts with the analyte of the sample. The generated chemical information is subsequently transformed into a form of energy that can be measured by a transducer, predominantly electrical, optical, thermal or mass energy. The transducer is a device that converts the primary recognition signal carrying the chemical information of the sample into a useful analytical signal, usually from the electric domain. In some cases, the electrical signal is too complex to be directly interpreted and requires additional amplification or processing steps. The mechanism of information transfer for a chemical sensor is shown in Fig. 1.2. The receptor and the transducer parts can be close, separate or directly coupled but, for the suitable information transfer, they have to be physically connected.

Ideally, chemical sensors should be integrated, miniaturized, robust, easy-to-use and portable devices, coupled to automatic systems and capable to continuously supply quality analytical information. The use of chemical sensors should simplify the classical analytical process[19]. In terms of response, an ideal chemical sensor should fulfil the following conditions: (1) a signal output proportional to the amount of analyte of the sample, (2) without hysteresis, which means that the sensor response should return to baseline after responding to the analyte, (3) fast response times, especially for on-line applications, (4) good signal-to-noise (S/N) characteristics, (5) good selectivity and (6) good sensitivity[20].

1.2.1 *Chemical sensors classification: electrochemical sensors*

Chemical sensors are commonly classified following two main criteria: (1) the nature of the recognition element or (2) the transduction mechanism. Regarding the nature of the recognition elements, chemical sensors can be divided into **chemosensors**, when using ionophores or macromolecular receptors, and **biosensors**, when using enzymes, antibodies, oligonucleotides or chemical receptors. Biosensors, which use biologic material of high selectivity, are much more selective than chemosensors. This fact favours the biosensors development[21]. On the other hand, the transduction mechanism divides the chemical sensors into **optical** (absorbance, reflectance or luminescence sensors), **electrochemical** (potentiometric, amperometric or impedimetric sensors or Field Effect Transistors, FETs), **electric** (metal-oxide-semiconductor sensors, organic

semiconductor sensors, electrolytic conductivity sensors or electric permittivity sensors), **mass** (piezoelectric or acoustic wave devices), **magnetic**, **thermometric** and **radiometric sensors**.

Most of chemical sensors use electrochemical transduction. Electrochemical sensors play a relevant role in the development of chemical sensors because of their simplicity, clear correlation with the amount of analyte in the sample, easy miniaturization (which could involve a decrease in the reagents consumption and in the sensor size), low detection limits and wide response range[22]. Table 1.1 shows the classification of the electrochemical sensors regarding the measurement technique (transduction mode)[23]. The common transducers and the usual analytes for each type of measurement are also shown.

Table 1.1 Classification of the electrochemical sensors regarding the measurement type and the analytes more frequently reported.

Measurement type	Transducer	Usual analytes
1. Potentiometric	Ion-Selective Electrodes (ISEs)	K^+, Cl^-, Ca^{2+}, F^-
	Glass electrodes	H^+, Na^+
	Gas electrodes	CO_2, NH_3
	Metal electrodes	Redox species
2. Amperometric	Metal or carbon electrodes	O_2, sugars, alcohols
	Chemically Modified Electrodes (CMEs)	sugar, alcohols, phenols, oligonucleotides
3. Impedimetric	InterDigitated Structure (IDS) electrodes	Urea, charged species, oligonucleotides
	Metal electrodes	
4. Field effect	Ion-Selective Field Effect Transistors (ISFETs)	H^+, K^+
	ENzyme Field Effect Transistor (ENFETs)	

Thus, in the development of electrochemical sensors, the recognition element, chemical or biological, and the measurement transduction have to be previously chosen. In terms of electrochemical mechanisms of transduction, potentiometric and amperometric sensors are the most frequently reported in the literature[24-29]. Both phenomena are governed by simple equations which allow an easy correlation between the response signal and the amount of analyte in the sample. The use of impedimetric sensors has currently increased a lot, although it has been especially limited for the huge complexity

of the data interpretation: EIS measurements cannot be always correlated to the analyte concentration directly but they require the use of complex mathematical methods (see Section 1.3.2)[30-32]. However, the development of simple commercial software which allows the fitting of impedimetric data without mathematical considerations has extended their application to new areas.

1.3   ELECTROCHEMICAL IMPEDANCE SPECTROSCOPY

This Section aims to provide a general overview of the principles underpinning EIS, paying special attention to the interpretation and fitting of the impedance data.

1.3.1   Fundamentals of EIS

Electrochemical techniques study interfacial phenomena by looking at the relation between current and potential. The experimentalist imposes a perturbation in either the current or the potential of the working electrode (WE) and observes how the dependent variable responds to those perturbations. The study of such dependence then gives access to a wealth of information about the system under study (kinetic, thermodynamic and mechanistic). The most commonly used electrochemical techniques are based on the application of direct currents, such as the case of Chronoamperometry or Voltammetry.

In the case of EIS, the nature of the perturbation is a sine wave, commonly a potential (e, in V) of small amplitude (E, in V) which oscillates around a fixed set potential [Direct Current (DC) potential, in V] with an angular frequency ($\omega = 2\pi f$, where f is the frequency in Hz):

$$e = E\sin\omega t \tag{1.1}$$

This exciting signal generates a sine wave response, frequently a current (i, in F) of different amplitude (I, in F) and phase ($\omega t + \phi$, where ϕ is the phase angle, in radians):

$$i = I \sin(\omega t + \phi) \tag{1.2}$$
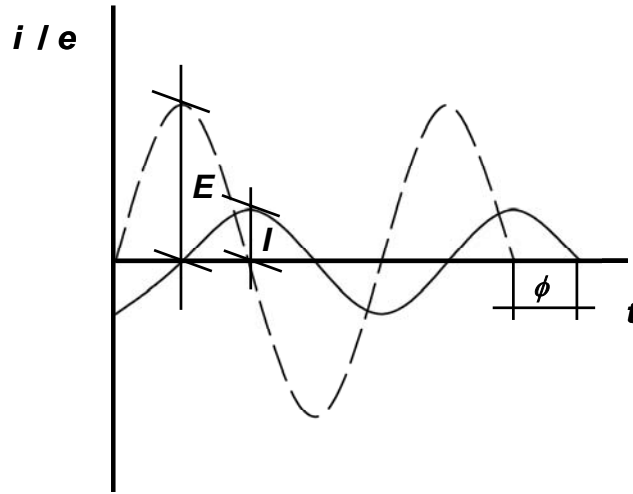
Fig. 1.3 Diagram showing the relationship between Alternating Current (AC) potential and current signals in terms of amplitude and ϕ.

Fig. 1.3 shows the difference between the exciting and the response signals in terms of amplitude and phase. The magnitude of the exciting signal amplitude plays a critical role in the EIS measurements. Small amplitudes ensure the linear response of the electrochemical system (Fig. 1.4), but the excitation of non-linear systems produces more complex responses which, despite of being periodic, have lost its sinusoidal nature[33-35]. This thesis has been assumed to be made under linear conditions.

The general Ohm's law defines the impedance ($Z(\omega)$, in Ω) as the relationship between the applied sinusoidal voltage and the recorded current (Eq. 1.3). Complex number notation, and particularly the Euler relationship (Eq. 1.4), allows impedance deconvolution into its real ($Z_{re}(\omega)$, in Ω) and imaginary ($Z_{im}(\omega)$, in Ω) components (Eq. 1.5):

$$Z(\omega) = \frac{e}{i} = \frac{E}{I} \frac{\sin \omega t}{\sin (\omega t + \phi)} = Z \frac{\sin \omega t}{\sin (\omega t + \phi)} \tag{1.3}$$

$$e^{j\phi} = \cos \phi + j \sin \phi \tag{1.4}$$

$$Z(\omega) = \frac{E e^{j\omega t}}{I e^{j(\omega t - \phi)}} = Z e^{j\phi} = Z(\cos\phi + j\sin\phi) = Z_{re}(\omega) - jZ_{im}(\omega) \qquad (1.5)$$
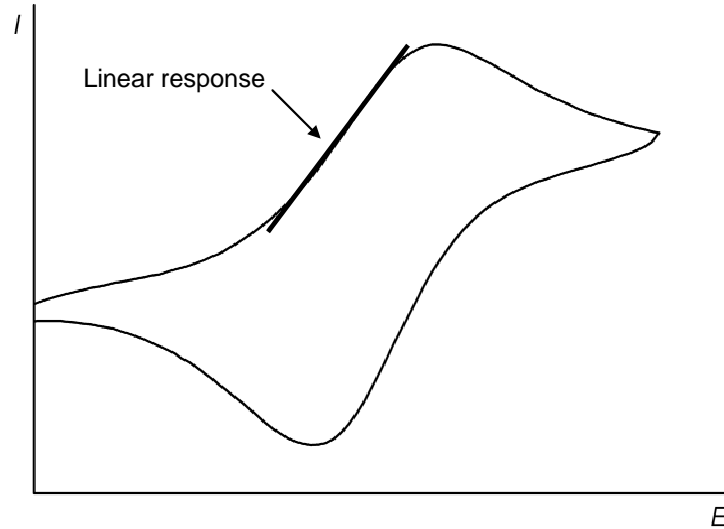
Fig. 1.4 Representation of a current-voltage plot. In the *linear response region* the exciting and the response signals show a linear correlation.
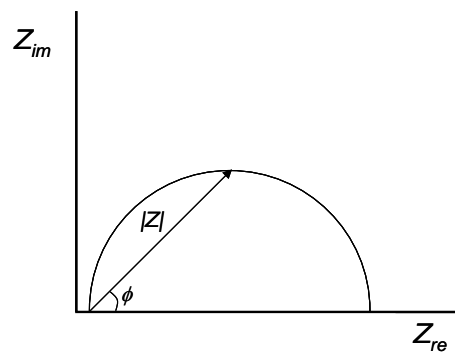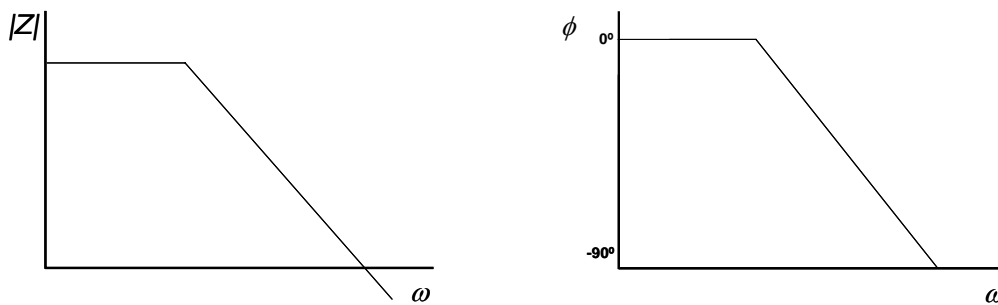
Fig. 1.5 Representation of classical Nyquist and Bode plots.

Regarding Eq. 1.5, impedance can be plotted as a vector by representing the $Z_{im}(\omega)$ and the $Z_{re}(\omega)$ along the ordinary and the abscissa axis, respectively. This representation is frequently referred to as complex plane plot or Nyquist plot. Each point in the plot corresponds to a single EIS measurement and represents a vector whose modulus coincides with the impedance modulus ($|Z|$) and with an angle between the vector and the ordinary axis equals to the ϕ (Fig. 1.5-a). EIS is also commonly represented as a function of the frequency in Bode plots. The $|Z|$, the $Z_{im}(\omega)$, the $Z_{re}(\omega)$ or the ϕ can be plotted versus the ω, in logarithm terms. An example is shown in Fig. 1.5-b.

a) Nyquist plot

Z_{im}

Z_{re}

b) Bode plots

$|Z|$

ω

ϕ 0º

-90º

ω
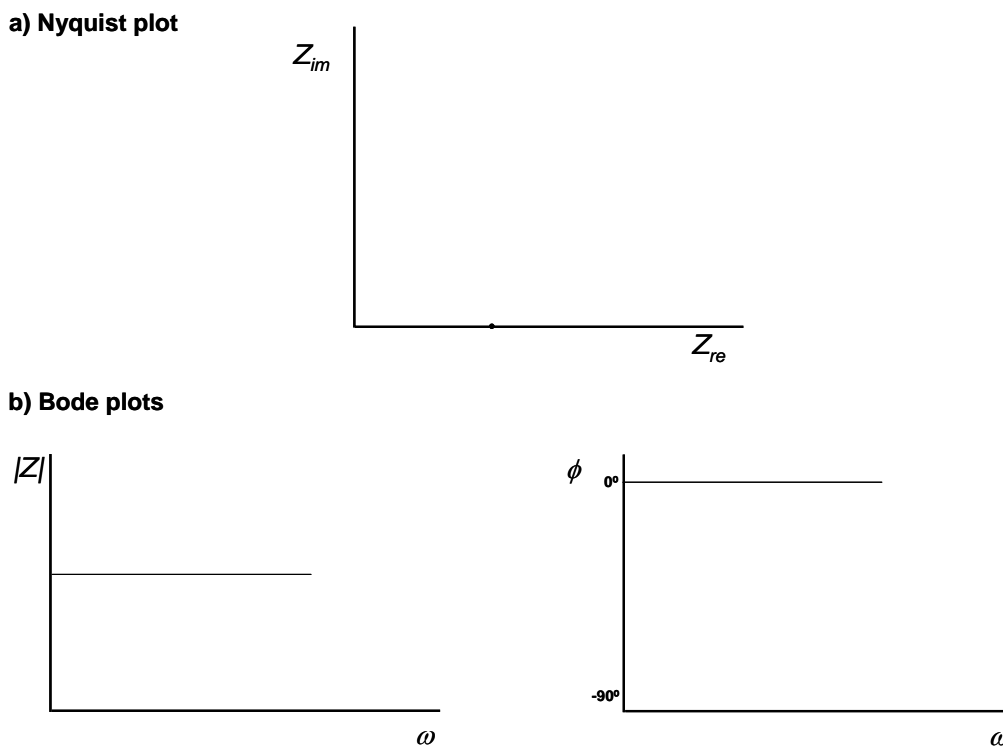
Fig. 1.6 Representation of the Nyquist and Bode plots for a pure resistance.

EIS data are commonly analysed in terms of equivalent circuit using commercial and simple software. In the equivalent circuit, complex physical and chemical phenomena are defined as simple electrical elements, basically resistances and capacitances that model their behaviour. The impedimetric response of these basic elements is described below.

For pure resistances (R) current and voltage are *in phase* ($\phi = 0$) and impedance only have real component:

$$Z(\omega) = Z(\cos\phi) = Z_{re} \tag{1.6}$$

Fig. 1.6 shows the Nyquist and Bode plots for a pure resistance. The Nyquist plot, a point in the real axis, supplies too much lower information and thus, Bode plots for the $|Z|$ and the ϕ are more commonly used. Resistances are unaffected by the frequency and give straight lines in the modulus representation. The resistance magnitude (in Ω) coincides with $|Z|$. On the other hand, the ϕ is constant at 0°.

a) Nyquist plot

b) Bode plots
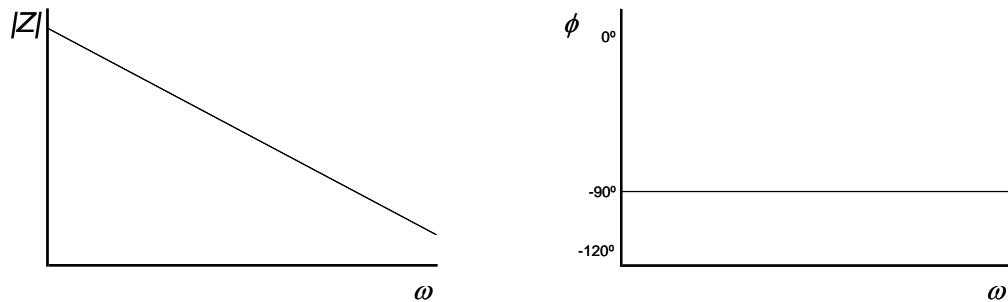
Fig. 1.7 Representation of the Nyquist and Bode plots for a pure capacitance.

By definition, the magnitude of an ideal capacitance, C, (two parallel-plates of infinite size separated a constant distance) depends on the charge residing on the plates (q) and the difference of potential between the plates (e):

$$q = C \cdot e \tag{1.7}$$

Expressing the current as the variation of the charge with time, the resulting impedance of a pure capacitance shows a phase shift of -90º (ϕ = -π/2) with only imaginary component (see Eq. 1.8 and Eq. 1.9). The parameter Xc, widely used in EIS, is called capacitive reactance and is defined as $1/\omega C$.

$$i = \frac{dq}{dt} = C\frac{de}{dt} = -\omega CE\cos\omega t = \frac{E}{Xc}\sin(\omega t - \frac{\pi}{2}) \qquad (1.8)$$

$$Z(\omega) = \frac{1}{\omega C}e^{-j\frac{\pi}{2}} = \frac{-j}{\omega C} = \frac{1}{j\omega C} \qquad (1.9)$$

Fig. 1.7-a shows the Nyquist plot for an ideal capacitance: a straight line on the imaginary axis. More information can be obtained from the Bode plots. Fig. 1.7-b shows the frequency-dependence of the impedance of a capacitance: the $|Z|$ continuously decreases with the frequency. In terms of the ϕ, capacitances should show a constant angle of -90º.

1.3.2 Fitting and interpretation of impedance data

The impedimetric response of real systems is much more complicated because of the huge number of physical and chemical phenomena which should be considered. Although there are many ways to analyse EIS data, the most common way consists in defining the system under scrutiny and laying out its equivalent circuit in terms of electrical components, basically resistances and capacitances. In order to adequately build the equivalent circuit, it is advisable to identify the more relevant events occurring during the EIS measurements with suitable electrical elements, regarding the nature of the physic-chemical event. Once the equivalent circuit is defined, the experimental data is fitted to it using non-linear least square fitting techniques.

The equivalent circuits are combinations of capacitances and resistances in series and / or in parallel. In circuit theory, the overall impedance experimentally measured for an electrochemical system is called equivalent impedance, $Z_{eq}(\omega)$. For an equivalent circuit

of i elements combined in series, the $Z_{eq}(\omega)$ is the sum of the impedance of each element:

$$Z_{eq}(\omega) = \Sigma_i Z_i(\omega) \qquad (1.10)$$

When the l elements are combined in parallel, the reciprocal of $Z_{eq}(\omega)$ is equal to the sum of the individual reciprocal impedance of each element:

$$\frac{1}{Z_{eq}(\omega)} = \Sigma_e \frac{1}{Z_e(\omega)} \qquad (1.11)$$

The reciprocal of the impedance ($1/Z_{eq}(\omega)$) is known as admittance, $Y(\omega)$, and it is vastly used for describing parallel combinations of elements. Table 1.2 summarizes the relationships between the $Z(\omega)$ and the $Y(\omega)$.

Table 1.2 Summary of the relationships between the $Z(\omega)$ and the $Y(\omega)$.

Impedance [$Z(\omega)$]		Admittance [$Y(\omega)$]	
Real component	Imaginary component	Real component	Imaginary component
($Z'(\omega)$ or $Z_{re}(\omega)$)	($Z''(\omega)$ or $Z_{im}(\omega)$)	($Y'(\omega)$ or $Y_{re}(\omega)$)	($Y''(\omega)$ or $Y_{im}(\omega)$)
Resistance (R)	Reactance (X_c)	Conductance (K)	Susceptance (B)

However, real systems are much more complicated and interpretation of the results is usually quite cumbersome. In order to correctly fit EIS data, suitable equivalent circuits are necessary. The acquisition of a good equivalent circuit requires knowledge both on the events taking place along the current paths and on their connections. The removal of parasitic elements and artefacts from EIS data is also important, for example inductive elements (with ϕ higher than 0). Inductive artefacts are commonly found at high frequencies when using too long cables, although they has been also reported when measuring coupled chemical reactions[36].

It is worth pointing out that EIS experiments determine the impedance of the whole electrochemical cell, $Z_{cell}(\omega)$, and not simply that corresponding to the working

electrode. However, experimentally only the electrodes and the solution properties have been found to markedly influence $Z_{cell}(\omega)$ since the features of the experimental set-up, cables, connections and welding have shown to produce extremely small or even null changes in the recorded impedance. Once the relevant features are recognised, it is very important to suitably combine them in an adequate equivalent circuit. In the construction of the circuit, simultaneous events are generally described by elements combined in parallel, whereas consecutive events require series elements. The impedance of most electrochemical systems may be simplistically considered to be the series combination of the impedances of the electrodes, $Z_E(\omega)$ (sum of the impedance of the working, $Z_{WE}(\omega)$, and the counter electrodes, $Z_{CE}(\omega)$) and the impedance of the electrolyte solution between them, $Z_S(\omega)$:

$$Z_{cell}(\omega) = Z_E(\omega) + Z_S(\omega) = Z_{WE}(\omega) + Z_{CE}(\omega) + Z_S(\omega) \tag{1.12}$$

Considering this general equation, the individual terms will be deeply analyzed in the following sections.

1.3.2.1 Impedance of the solution

The $Z_S(\omega)$ includes two electrical elements: the capacitance of the electrolyte (C_S, in F) and the resistance of the solution (R_S, in Ω). The C_S is a measurement of the charge stored in the electrolyte solution between the electrodes and the R_S quantifies the difficulty of transferring charge through the same medium. Both events occur at the same time (simultaneously) and the corresponding elements appear combined in parallel in the equivalent circuit (Fig. 1.8). However, the empirical expression of $Z_S(\omega)$, Eq. 1.13, can be simplified regarding experimental evidences which show that at low frequencies (below 100 kHz), $j\omega\, C_S R_S$ is much smaller than unity[37] (Eq. 1.14):

$$\frac{1}{Z_S(\omega)} = \frac{1}{R_S} + j\omega C_S \tag{1.13}$$

$$Z_S(\omega) = \frac{R_S}{1 + j\omega C_S R_S} \approx R_S \tag{1.14}$$

Thus, in most electrochemical systems, the $Z_S(\omega)$ can be simplified to R_S.

The R_S basically depends on the conductivity of the medium, κ (in S m^{-1}), although some geometrical parameters of the electrochemical system, namely the area of the electrode (A, in m^2), and the distance between electrodes (d, in m), could also modify its magnitude:

$$R_S = \frac{1}{\kappa}\frac{d}{A} \qquad (1.15)$$

Experimentally, the κ and the R_S are highly influenced by the temperature: higher temperatures increase κ, decreasing R_S.
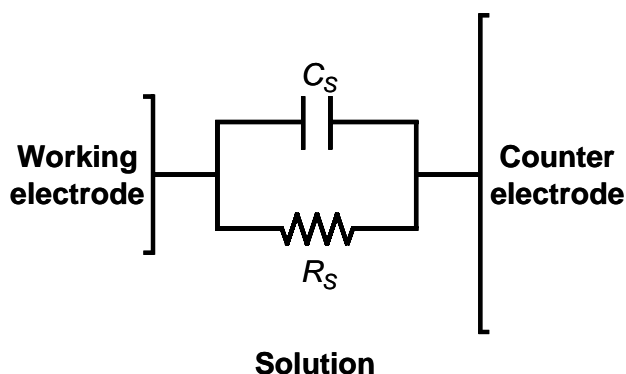
Fig. 1.8 Schematic representation of the equivalent circuit containing the solution elements, namely the C_S and the R_S.

1.3.2.2 Impedance of the electrodes

In a reduction process, electrons jump from the Fermi level of the metal into the Lowest Unoccupied Molecular Orbital (LUMO) of the ions in solution, while in an oxidation process, electrons are transferred from the Highest Occupied Molecular Orbital (HOMO) of the species in solution to the Fermi level of the metal. Regarding the molecular orbital theory, in the simplest case of a metal electrode immersed in an electrolyte solution, the energy gap exiting between the Fermi level of the metal an the levels HOMO / LUMO of the electrolyte causes a charge separation which can be

modelled as a capacitance in the electrode-solution interface: the double layer capacitance, C_{dl} (in F). However, the charge separation also generates a resistance associated to the polarization process, R_P (in Ω), which should appear in series versus the C_{dl} in the equivalent circuit (Fig. 1.9).
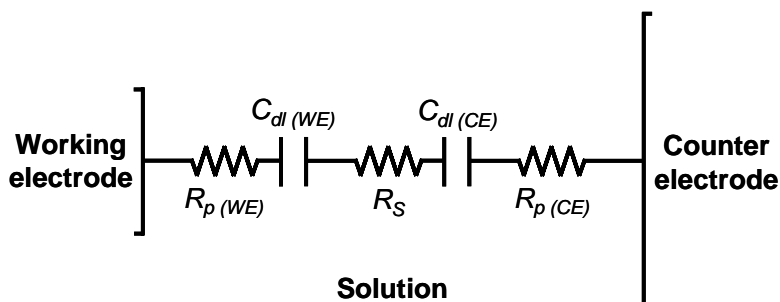
Fig. 1.9 Schematic representation of the equivalent circuit containing the R_S and the parameters of the electrode-solution interface, namely the C_{dl} and the R_P. The elements labelled as WE and CE corresponds to the working and counter electrodes, respectively.

In most electrochemical systems, R_P is much smaller than the R_S[37] and the $Z_E(\omega)$ is assumed to be exclusively dependent on C_{dl}. Thus, the $Z_E(\omega)$, which includes the $Z_{WE}(\omega)$ and the $Z_{CE}(\omega)$, could be simplified by only considering the C_{dl} of each electrode:

$$Z_E(\omega) = \frac{1}{j\omega C_{dl(WE)}} + \frac{1}{j\omega C_{dl(CE)}} \qquad (1.16)$$

The C_{dl} is frequently assumed to behave as an ideal capacitance of parallel plates and thus, its magnitude would depend on the permittivity of the solution-electrode interface medium, ε_{dl} (in F m^{-1}), on the distance between the charged layers of the double-layer, d_{dl} (in m), and on the electrode area, A (in m^2). The ε_0 is the free space permittivity constant:

$$C_{dl} = \varepsilon_0\, \varepsilon_{dl}\, \frac{A}{d_{dl}} \qquad (1.17)$$

The C_{dl} has been found to be very sensitive to the changes of the ε_{dl} and the d_{dl}. The ε_{dl} evaluates the capacity of the dielectric material of the interface to store charge[38] and is

hardly influenced for the temperature and superficial modifications, such as generation of thin oxide layers, adsorption of impurities, electrodeposition of isolating or conducting coatings or other processes, which may change its value. The d_{dl}, commonly of tens of angstroms, is basically influenced by the κ: increases of conductivity in the interface region would compact the double layer.

Experimentally, the counter electrode size is frequently much bigger than the working electrode to ensure a near-homogeneous polarization of the working electrode during the impedimetric measurements[39]. This areas relationship also influences the recorded $Z_E(\omega)$ since, regarding Eq. 1.16, the area increase dramatically decreases the $Z_{CE}(\omega)$ magnitude and the $Z_E(\omega)$ can be considered to be exclusively influenced by the $Z_{WE}(\omega)$:

$$Z_E(\omega) = Z_{WE}(\omega) = \frac{1}{j\omega C_{dl(WE)}} \tag{1.18}$$

1.3.2.2.1 Non-ideal capacitances: the Constant Phase Element

On most solid electrodes, the double layer does not behave as a pure capacitance[35, 40] but, usually its ϕ is slightly smaller than 90º. The reasons for this effect are subject to continuous discussion, although a roughness factor appears to be one important cause. As a consequence, a Constant Phase Element (CPE) is very frequently used to fit the C_{dl}. CPEs are non-intuitive circuit elements with a ϕ of constant value and independent of the frequency. Fig. 1.10 shows the Nyquist and Bode plots for a CPE. The impedance of most interfacial CPEs in non-electroactive electrolyte are described by the expression[37]:

$$Z_{CPE}(\omega) = \frac{1}{K(j\omega)^\beta} \tag{1.19}$$

$Z_{CPE}(\omega)$ is the impedance of a CPE (in Ω), K is the CPE magnitude (in $\Omega^{-1}s^{-\beta}$), ω is the angular frequency (in s^{-1}) and β (in radiant) is a parameter linked with the ϕ which oscillates from 1, for planar surfaces, to 0.5, for very rough ones[41, 42]. The relationship between the parameter β and the ϕ is shown in Eq. 1.20:

$$\phi = -\beta \frac{\pi}{2} \tag{1.20}$$

Common values for the β on solid-state electrodes oscillate between 0.8 and 1.

a) Nyquist plot
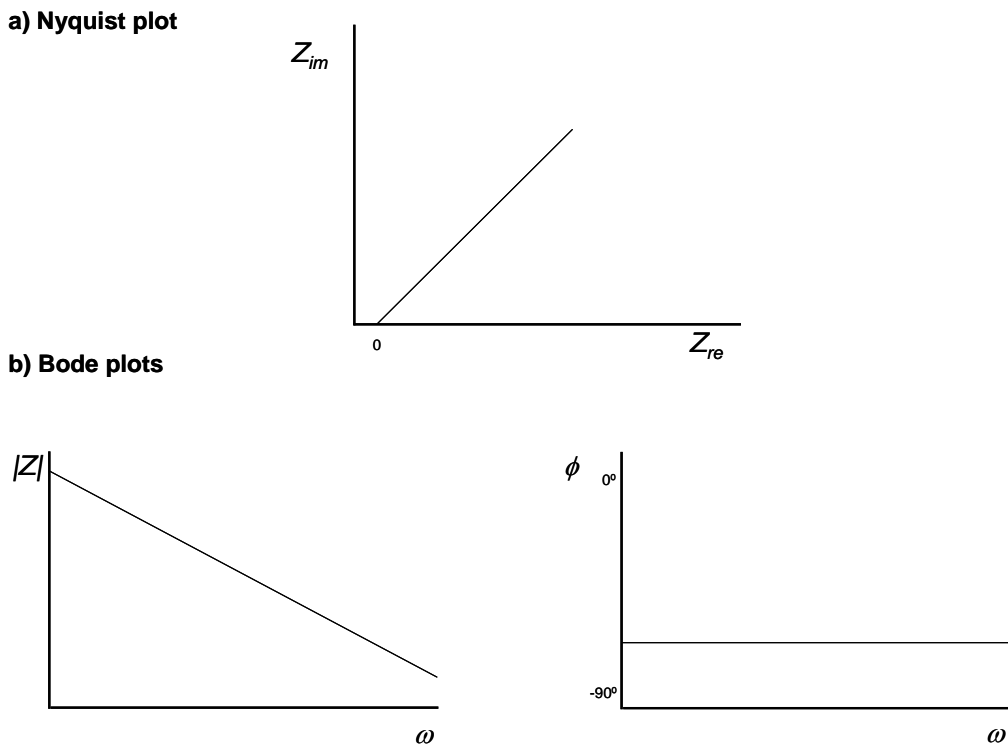
b) Bode plots

Fig. 1.10 Representation of the Nyquist and Bode plots for a CPE.

1.3.2.3 Presence of electroactive species: faradaic parameters

The circuit introduced in Fig. 1.11-a, whose elements have been widely discussed above, represents the general starting point for most electrochemical systems. However, the presence of electroactive species in the medium, which can exchange charge with the electrode, would modify both the charge flux and the $Z_{cell}(\omega)$ magnitude. The existence of at least one process involving electron exchange produces new interfacial parameters generally known as interfacial faradaic elements (because of the electronic transference that they entail). Employing the same terminology, C_{dl} is defined as an interfacial non-faradaic element since its presence in the circuit is not linked to electron transfer. Faradaic and non-faradaic processes take place simultaneously in the interface

and thus generate parallel parameters in the equivalent circuit. The faradaic processes cannot be represented by a single linear circuit element since they involve several physical and chemical events of complex nature. In most electrochemical systems, faradaic processes are represented by only two electrical elements in series in the equivalent circuit: the charge-transfer resistance, R_{CT}, and the Warburg's impedance, Z_W. The equivalent circuit which contains all of these parameters is known as equivalent circuit of Randles (Fig. 1.11-b). These elements will be analyzed in detail below.
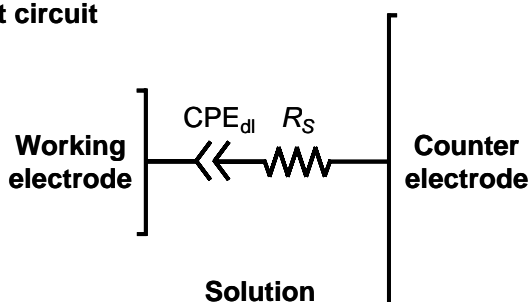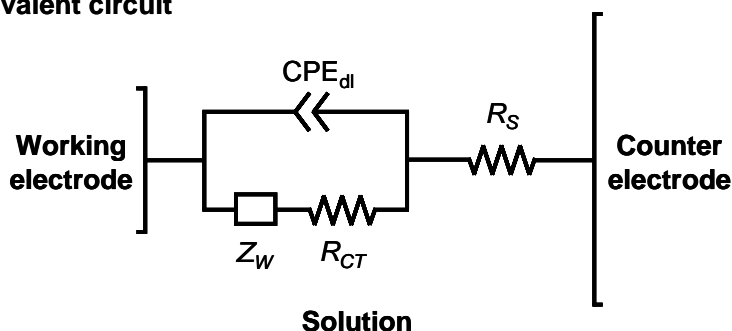
Fig. 1.11 a) Equivalent circuit for electrochemical systems without electroactive species. b) The Randles equivalent circuit containing the R_S, the Z_W, the R_{CT} and the the C_{dl} as a CPE (CPE_{dl}).

1.3.2.3.1 Charge-transfer resistance

The charge transfer is mainly limited by the capacity of the electrode material to exchange electrons with the electroactive species of the medium. Using the same material or materials with similar properties, the charge transfer becomes dependent of the electroactive species. Redox couples show different kinetics, mechanisms and stoichiometries modulated by the experimental conditions, essentially the temperature, the reagents concentration and the potential applied to the electrode. Depending on the

efficiency of the electron exchange, the electrochemical system is claimed to be under diffusion or kinetic control. Under diffusion control, reactions are usually limited by the mass transport from the medium to the electrode. These reactions are called fast reactions in opposition to slow reactions, which are under kinetic control, where the electron exchange is led by the velocity of the electron transfer process[43].

Electrochemical systems under kinetic control are commonly assumed to follow the Butler-Volmer model[34, 36]:

$$i = i_0 \left[e^{\left(\frac{\alpha_A nF}{RT} \eta \right)} - e^{-\left(\frac{\alpha_C nF}{RT} \eta \right)} \right] \tag{1.21}$$

i_0 is the exchanged current density, η is the overpotential ($\eta = e - e_0$), n is the number of electrons exchanged in the reaction, R is the constant of the ideal gases, F is the Faraday constant, T is the temperature and α_A and α_C are the coefficient of anodic and cathodic transfer, respectively.

These reactions may be considered to be practically reversible ($\alpha_A = \alpha_C = 0.5$) in the equilibrium. Regarding this and under a very small η, Eq. 1.21 can be further simplified by using the first order Taylor's expansion (exposed in Eq. 1.22):

$$e^x \approx 1 + x \tag{1.22}$$

$$i = i_0 \left[1 + \frac{nF}{2RT} \eta - 1 + \frac{nF}{2RT} \eta \right] \tag{1.23}$$

$$i = i_0 \frac{nF}{RT} \eta \tag{1.24}$$

$$\frac{\eta}{i} = R_{CT} = \frac{RT}{nFi_0} \tag{1.25}$$

Hence, the R_{CT} is a function of the properties of the electrode material, the characteristics of the redox couple and the structure of the interface[34].

1.3.2.3.2 The Warburg impedance

Additionally, if the potential is such that the charge extent is sustained, eventually the supply of material to and from the bulk of the solution towards the electrode surface is limited by mass transport. Mass transport can take several forms, namely convection (when the transport is produced by the stirring of the solution), migration (when the transport is produced by a charge gradient) and diffusion (when the transport is produced by a concentration gradient). The experimental conditions are normally chosen so that close the electrode surface the limitation comes from diffusion. The thickness of the diffusion layer in the interface depends on some experimental parameters, such as the type of molecules, the stirring or the temperature. This mass transport limitation brings about an additional term, named the Z_W, placed in series with the previously observed R_{CT} (Fig. 1.11-b).

Diffusion is defined by the Fick's laws. In the case of EIS, where a sine wave changes the electrode potential with time, diffusion and Z_W are precisely described by the Fick's second law. For planar diffusion fields of finite thickness, the Z_W is also called "finite" Warburg. The value of the "finite" Warburg basically depends on the average value of the diffusion coefficients of the species which are diffusing, D, the thickness of the diffusion layer, δ (in m) and the Warburg coefficient, σ:

$$Z_W = \sigma \, \omega^{-\frac{1}{2}} (1-j) \tanh\left[\delta \left(\frac{j\omega}{D} \right)^{\frac{1}{2}} \right] \tag{1.26}$$

The Warburg coefficient is a complex parameter influenced by the properties of the redox couple (particularly, the number of exchanged electrons and the diffusion coefficient of the oxidizing and reducing species, respectively D_O and D_R), geometrical features (the area of the electrode) and experimental conditions (the concentration of the oxidizing and reducing species in the bulk, respectively C^{*O} and C^{*R}):

$$\sigma = \frac{RT}{n^2 F^2 A \sqrt{2}} \left(\frac{1}{C^{*O}\sqrt{D_O}} + \frac{1}{C^{*R}\sqrt{D_R}} \right) \tag{1.27}$$

Eq. 1.26 can be simplified by considering diffusion layers of large or infinite thickness. The resulting Z_W, called "infinite" Warburg, exhibits identical values for the $Z_{re}(\omega)$ and the $Z_{im}(\omega)$:

$$Z_W = \sigma(\omega)^{-\frac{1}{2}}(1-j) \tag{1.28}$$

1.3.2.4 The equivalent circuit of Randles: kinetic and diffusion control

In 1947 J. E. Randles published a simplified equivalent circuit for EIS measurements which included the most relevant events occurring in the electrochemical system (Fig. 1.11-b). The frequency modulates the weight of each element of the equivalent circuit in the measured $Z_{cell}(\omega)$, particularly the Z_W, which has been proved to be extremely sensitive to the frequency. The weight of the R_{CT} and the Z_W in the $Z_{cell}(\omega)$ magnitude can be used as a measurement of the balance between the kinetic and the diffusion control of the redox reaction under study. At low frequencies, the electrode potential changes very slowly and reactants have time to diffuse from the bulk to the electrode. In this case, the electrochemical system is under diffusion control and the Z_W gains importance respect to R_{CT}. Eqs 1.29 and 1.30 illustrate the $Z_{re}(\omega)$ and $Z_{im}(\omega)$ for electrochemical systems under diffusion control:

$$Z_{re}(\omega) = R_S + R_{CT} + \sigma(\omega)^{-\frac{1}{2}} \tag{1.29}$$

$$Z_{im}(\omega) = \sigma(\omega)^{-\frac{1}{2}} + 2\sigma^2 C_{dl} \tag{1.30}$$

The combination of Eqs 1.29 and 1.30 correspond to the Nyquist plot for an electrochemical system under diffusion control:

$$Z_{im}(\omega) = Z_{re}(\omega) - R_S - R_{CT} + 2\sigma^2 C_{dl} \tag{1.31}$$

The Nyquist plot, illustrated in Fig. 1.12-a, shows a straight line of unit slope which intercepts in $Z_{re}(\omega)$ on $R_S + R_{CT} - 2\sigma^2 C_{dl}$.

a) Diffusion control   **b) Kinetic control**
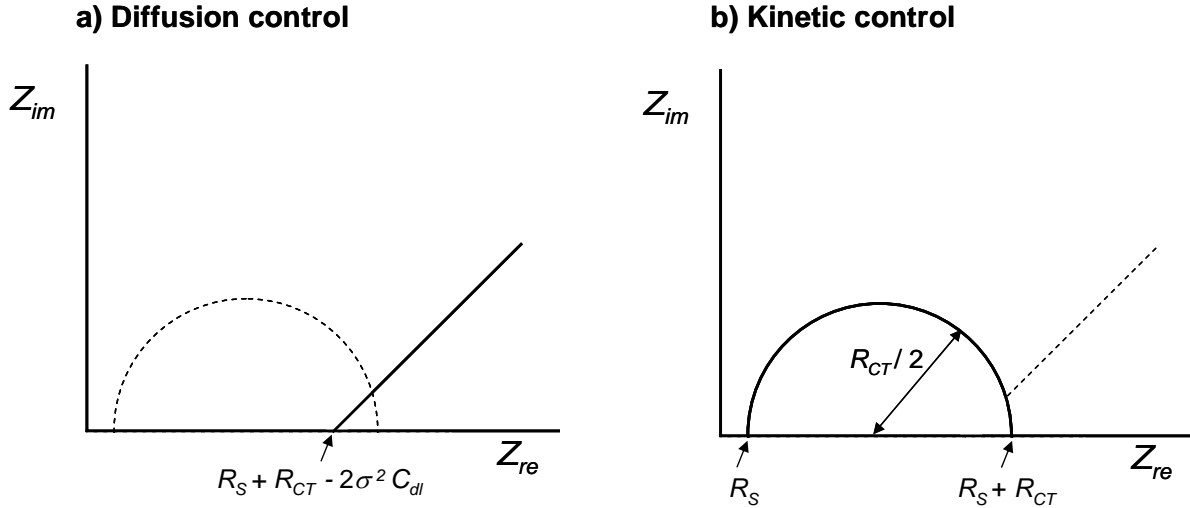
Fig. 1.12 Nyquist plots for electrochemical systems under a) diffusion and b) kinetic control.

At high frequencies, the potential of the electrode rapidly change with time, which does not allow diffusion to manifest itself. Under kinetic control, the influence of the Z_W is very small or even null and the $Z_{cell}(\omega)$ is mainly governed by the R_{CT}. Eqs 1.32 and 1.33 describes the $Z_{re}(\omega)$ and the $Z_{im}(\omega)$ for electrochemical systems under kinetic control:

$$Z_{re}(\omega) = R_S + \frac{R_{CT}}{1 + \omega^2 C_{dl}^2 R_{CT}^2} \tag{1.32}$$

$$Z_{im}(\omega) = \frac{C_{dl} R_{CT} \omega}{1 + \omega^2 C_{dl}^2 R_{CT}^2} \tag{1.33}$$

The combination of both equations, representative of the Nyquist plot, is a circle of radius $R_{CT}/2$ which crosses twice in the $Z_{re}(\omega)$ axis at R_S and $R_S + R_{CT}$ (Fig. 1.12-b):

$$\left(Z_{re} - R_S - \frac{R_{CT}}{2} \right)^2 + Z_{im}{}^2 = \left(\frac{R_{CT}}{2} \right)^2 \tag{1.34}$$

1.3.2.5 Electrodes modified with coating films

The modification of the electrode brings about important changes in the definition of the equivalent circuit. Thus, it is no longer convenient talk about double layer capacitance but to leave it all in terms of an overall interface capacitance. The presence of a coating film on the electrode surface can change both the $Z_{cell}(\omega)$ value and the equivalent circuit. In terms of circuit, thick coating films, especially those with isolating properties (e.g. bacterial biofilms), require additional elements for fitting EIS spectra adequately. In 1995, Amidurin et. al. described a simple equivalent circuit, illustrated in Fig. 1.13, that modelled electrodes modified with coating polymers by adding two extra elements to the equivalent circuit of Randles: the coating capacitance, C_C (in F), and the coating-porous resistance, R_C (in Ω)[44]. The C_C and the R_C, which describe simultaneous events, appear in parallel in the equivalent circuit and are combined in series with the elements of the Randles equivalent circuit since they describe consecutive events.
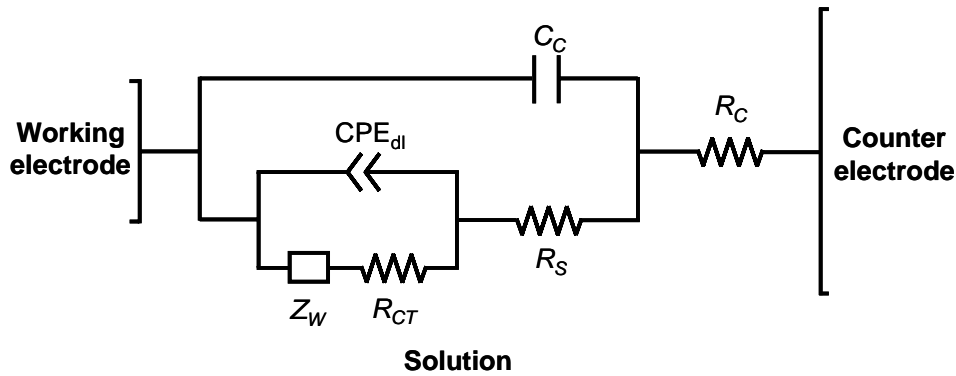
Fig. 1.13 Equivalent circuit for electrodes modified with coating films, previously proposed by Amirudin et. al. by following the corrosion of polymer-coated metals[44].

The C_C is fundamentally sensitive to the permittivity, ε_C (in F m^{-1}), the area, A_C (in m^2) and the thickness, d_C (in m), of the coating:

$$C_C = \varepsilon_0 \, \varepsilon_C \, \frac{A_C}{d_C} \qquad\qquad (1.35)$$

Basically, the C_C magnitude depends on the material but it can also be used to measure the capacity of the polymer to absorb water (water permeation). Most organic coatings show small permittivity, between 4 and 8 F m^{-1}. Adsorbed water, which has a permittivity of 80.1 F m^{-1} at 20 ºC, dramatically increases the C_C[45]. The area and the thickness of the coating commonly increase with the polymer growth until stabilization.

The R_C measures the resistance of the electrolyte solution retained in the polymeric structure and basically depends on the conductivity of this electrolyte solution retained in the polymer, κ_C (in S m^{-1}), although other parameters related to the structure of the porous [the number of channels in the coating, N_P, the average cross-sectional area of the channels, A_P (in m^2) and the length of the channels, d_P (in m)] can also modify its magnitude, as follows:

$$R_C = \frac{1}{\kappa_C} \frac{d_P}{N_P A_P} \qquad\qquad (1.36)$$

1.3.3 Configuration of the EIS measurements

EIS is a robust electrochemical technique which offers different strategies depending on the interest of the measurement. Each strategy is focused on the measurement of a specific property of the electrochemical system and differs from the others in the number of electrodes and the configuration of the EIS equipment. Most impedimetric approaches use four, three or two electrodes configurations which respectively focus on the properties of the bulk (changes of medium conductivity), on the charge-transfer process of specific redox species and on the electrode-solution interface. These configurations are described below.

1.3.3.1 Two and three electrodes configurations

The two electrodes configuration involves the use of a working and an auxiliary electrode (Fig. 1.14-a).

a) Two electrodes configuration
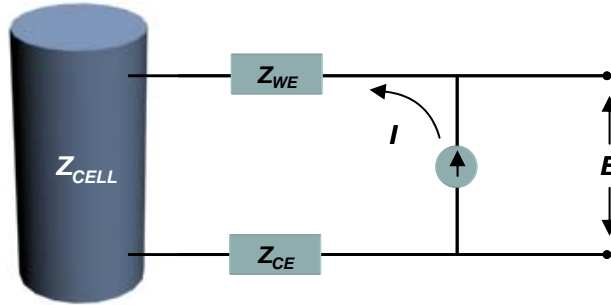
b) Three electrodes configuration
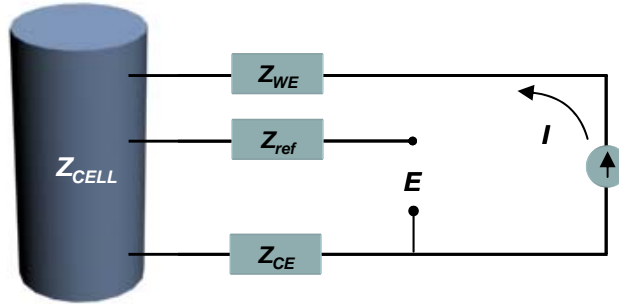
Fig. 1.14 Scheme of the measurement system for a) two and b) three electrodes configurations.

In this case, the exciting signal and the current response are applied and measured over the same pair of electrodes. Thus, both electrodes are highly polarized and their impedance commonly exceeds the $Z_S(\omega)$:

$$Z_{cell}(\omega) \approx Z_E(\omega) = Z_{WE}(\omega) + Z_{CE}(\omega) \tag{1.37}$$

This configuration is recommended to monitor interfacial events, especially those linked with the electrode-solution interface which does not require charge transfer (non-faradaic interface elements).

The main drawback is that this configuration cannot accurately control the electrode potential, which becomes critical when electroactive species are present in the medium. The three electrode configuration solves this problem by adding an extra electrode in the electrochemical system, acting as reference electrode, and a potentiostat to monitor the potential of the working electrode (Fig. 1.14-b). In this case, the $Z_{cell}(\omega)$ is also mainly governed by the $Z_E(\omega)$, although the presence of the reference electrode allows an accurate control of the redox processes. However, the use of a reference electrode usually involves the appearance at high frequencies of a parasitic capacitance associated to the reference electrode, C_{ref} (Fig. 1.15)[46]. The C_{ref} commonly shows small magnitudes and can be easily isolated from the EIS measurement.
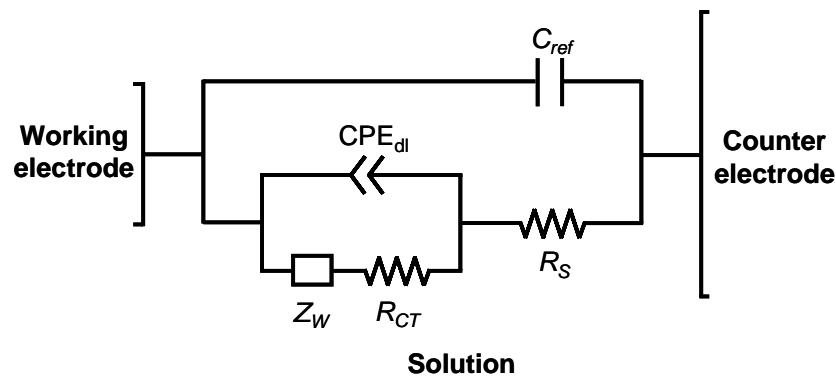
Fig. 1.15 Representation the equivalent circuit of Randles including the C_{ref}.

1.3.3.2 Four electrodes configuration

In a four electrodes configuration, the exciting signal is applied in a pair of electrodes and the resulting response is measured using two more electrodes, which are not polarized (Fig. 1.16). Thus, when measuring with four electrodes configurations, the influence of the $Z_E(\omega)$ in the $Z_{cell}(\omega)$ is much smaller than previously and the $Z_{cell}(\omega)$ magnitude basically depends on $Z_S(\omega)$:

$$Z_{cell}(\omega) \approx Z_S(\omega) \qquad (1.38)$$
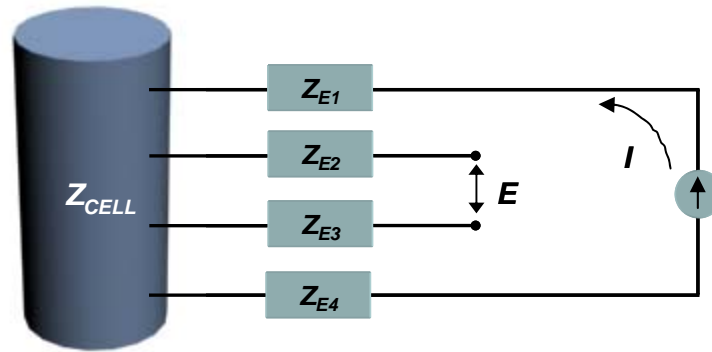
Fig. 1.16 Scheme of the EIS measurement using a four electrodes configuration.

Thus, this configuration is highly recommended to monitor solution events, especially those related to changes in the medium conductivity.

1.4   SURFACE PLASMON RESONANCE

The SPR is a complex optical technique widely used in the field of biosensing, especially to characterize the binding process of specific or unspecific analytes. This Section includes the basis of the physical principles governing this technique and the experimental features of the measurement.

1.4.1   Fundamentals of SPR

In 1900, Drude described the Drude model for electric conduction[47, 48]. This model considers metals to be composed of immobile positively charged ions and a quasi-free electron gas, also called plasmon. The SPR is based on a quantum optical-electrical phenomenon arising from the interaction of light with superficial plasmons. Under certain conditions, the energy carried by photons is transferred to plasmons on a metal surface. This energy transfer occurs only at a specific resonance wavelength, namely at the wavelength where the quantum energy carried by the photons exactly equals the quantum energy level of the plasmon[49].

1.4.1.1 Photons direct reflection at dielectric-metal interfaces

In order to understand the excitation of surface plasmons by light, the simple reflection of photons at planar dielectric-metal interfaces will be described. The wave vector of reflected photons, $k_{ph(r)}$, is sensitive to the incidence angle, θ, varying from 0, for perpendicular angles, to the maximum, which coincides with the wave vector of the incident photons, $k_{ph(i)}$, for large angles of incidence:

$$k_{ph(r)} = k_{ph(i)} \sin \theta \qquad (1.39)$$

Experimentally, polarised light has found to be insufficient to match the quantum energy level of the plasmon and cannot be directly used to excite plasmons. This problem has been solved by using coupling techniques, basically prism coupling and grating coupling[50, 51], which enhance the photon wave vector. The bases of the prism coupling, the most widely used technique, are detailed below.

1.4.1.2 Prism coupling: Total Internal Reflection

For a complete understanding of the prism coupling process, a brief description of the Total Internal Reflection (TIR) concept is required. When the incident light crosses a boundary between materials of different refractive index, part of the light is reflected and part is transmitted to the other side of the boundary. The amount of light transmitted depends on the θ. The incident light is Totally (Internally) Reflected when the θ exceeds the critical incidence angle (θ_C). Fig. 1.17 shows that below θ_C the reflectivity exponentially decays following Eq. 1.40, where l_d is the decay length:

$$l_d = \frac{\lambda}{2\pi\sqrt{(n \sin \theta)^2 - 1}} \qquad (1.40)$$

λ is the wavelength and n is the refractive index of the material. The θ_C is given by the Snell's law and depends on the refractive indexes of the two boundary materials:

$$n_1 \sin \theta_1 = n_2 \sin \theta_2 \qquad (1.41)$$

$$\sin \theta_C = \frac{n_2}{n_1} \qquad (1.42)$$

The TIR only occurs when the light travels from a medium of higher refractive index (n_1) to another of lower refractive index (n_2).
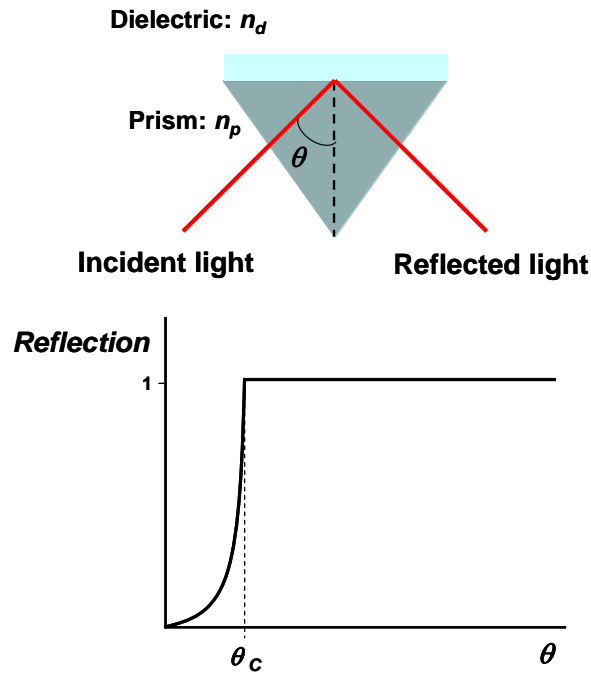
Fig. 1.17 TIR at a glass prism in contact with a dielectric material.

In prism coupling, photons are coupled to the metal-dielectric interface via the evanescent tail of light totally internally reflected at the base of a high-index prism. The high n of the prism glass ensures the TIR of the light. Commonly, the energy of this enhanced light exceeds the quantum energy level of the plasmon[52] and cannot be directly transferred. However, the energy of the reflected light can be modulated by θ and, after choosing the appropriate angle, the coupling between photons and plasmons can be achieved. This resonant coupling was first described by Turbadar in 1958[53, 54]. Experimentally, the excitation of surface plasmons can be found by following the change in the intensity of the reflected light with the θ. The energy transfer process appears as a sharp minimum in the totally reflected intensity. Fig. 1.18 shows the minimum reflection angle, θ_m, where the energy transfer occurs.
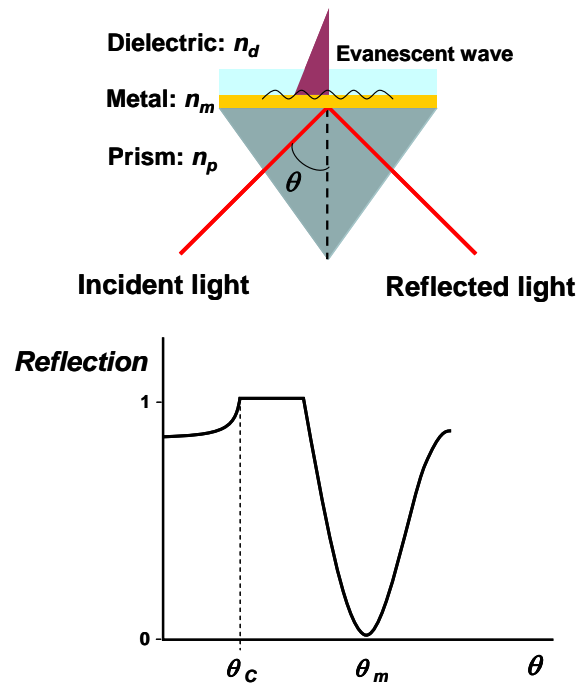
Fig. 1.18 Attenuated TIR at a metal film.

When TIR occurs, the reflected photons create an electrical field on the opposite side of the interface which propagate parallel to the plane of the interface[55]. In prism coupling, this field causes oscillation of the electrons in the dielectric material which, at the same time, induces the collective movement of the free delocalised electrons of the metal[56]. The collective excitation states of the quasi-free electron gas are called plasmon surface polaritons. The resonance coupling has been found to enhance the electric field at the interface between 15 and 20 times in the case of gold and 80 times for silver films[57]. Gold thin layers of tens of nanometres are widely used.

1.4.2 SPR measurements

The SPR equipment is compost of very fragile optical and electronic components (lasers, photodiodes, amplifiers or lenses) calibrated under specific conditions. Fig. 1.19 shows the typical scheme for a SPR device. In order to reduce equipment manipulation, most of SPR devices are coupled with fluidic systems which allow working in continuous or in batch (stopping the flux at the moment of the measurement). SPR equipment can be mainly divided into single and two channels devices, which are detailed below.
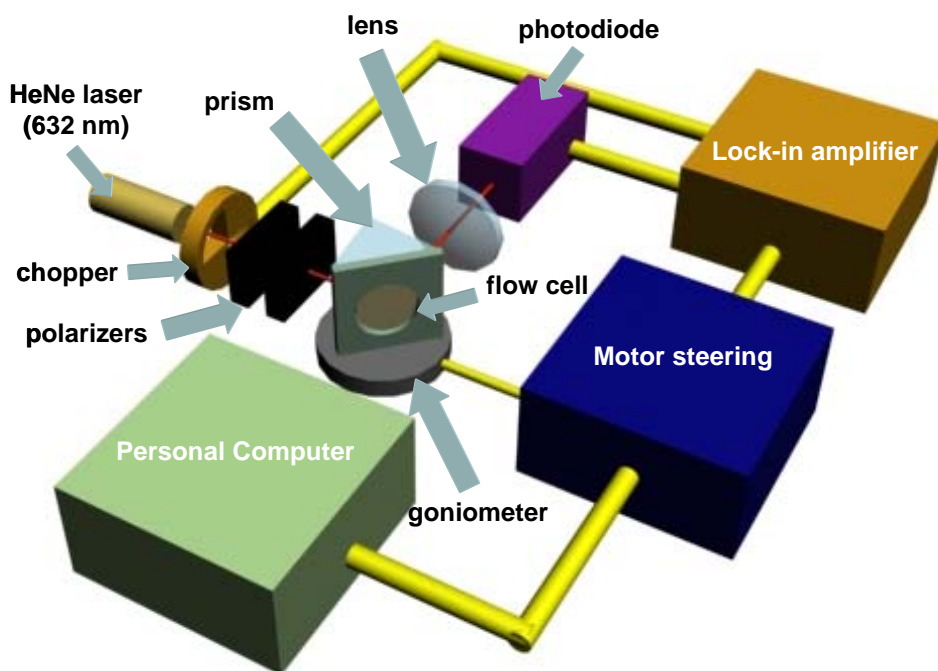
Fig. 1.19 Schematic representation of a standard SPR setup. The red ray represents the laser light.

1.4.2.1 Single channel measurements

After the localization of the position of the θ_m for the specific experimental conditions of the measurement, this angle is continuously monitored with time. A frequent reflectivity scan-curve is given in Fig. 1.18. The angle is chosen to have about 20-25 % reflectivity, as at this point the change in reflectivity is nearly linear. Experimentally, the unspecific adsorption or the covalent binding of molecules on the gold layer, namely DNA sequences[58], antibodies[59, 60], whole cells[61] and aptamers[62], changes the position of the θ_m.

The deposition of ultrathin layers of material with a higher refractive index than the ambient dielectric (e.g. n_{air} = 1, n_{buffer} = 1.33) increases the overall refractive index integrated over the evanescent field. The net effect is a slight shift of the θ_m to again couple the energy of the photons with the momentum of the surface plasmons[63]. Fig. 1.20 shows a characteristic shift plot.
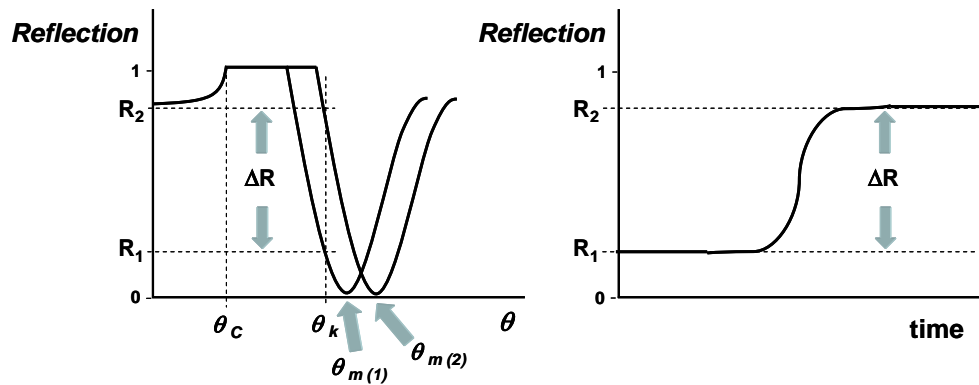
Fig. 1.20 On the left, typical angular SPR scans before (1) and after (2) the adsorption of molecules on the metal. The kinetic measurement is made at the angle θ_k. On the right, it is shown the kinetic SPR mode, where the reflected intensity is recorded at a fixed angle of incidence, θ_k, as a function of time.

The angular dependence of the overall reflectivity can be computed and compared with the measured curves. The θ_m shift ($\Delta\theta_m$) can be related to the n and the geometrical thickness, *d*, of the material deposited on the gold:

$$\Delta\theta_m \propto n\,d \tag{1.43}$$

This relation gives the fundamentals of SPR, but also shows its limits, as either thickness or refractive index have to be determined by another method, to obtain reliable results. For biomolecules, the n is difficult to obtain, as they do not form a closed layer on the surface. Therefore a refractive index of 1.41 is assumed and the focus is laid on the differences between measurements, not on the absolute thickness values obtained by modelling the data.

1.4.2.2 Two channels measurements

The two channels instruments duplicate the optic and electronic components in a single device which permit performing two independent SPR experiments at the same time, with the same gold disk and under identical experimental conditions. Each individual experiment is made as described in the previous Section (Section 1.4.2.1). Commonly, one of the channels is used as an internal control to subtract artefact and to make measurements more accurate. In this case, the SPR software simultaneously follows the

θ_m of both channels with time. In two channels systems, the parameter more frequently used is the difference between angles or differential angle, $\Delta\theta$. This parameter monitors the changes of the θ_m produced exclusively by the deposition of material since environmental artefacts are eliminated.

1.5   OVERVIEW OF BIOLOGICAL CONCEPTS

In this Section, a brief historical introduction describing the most relevant events in the development of the bacteriology is included. The most frequent bacterial morphological and metabolic characteristics are also enumerated. Next, bacterial structure and its colonization mechanism are detailed, with special attention to the biofilm formation process.

1.5.1   Bacteria: brief history and general considerations

Bacteriology can be considered to start in 1876 when Anton van Leeuwenhoek observed the first bacteria using a home-made single-lens microscope[64]. However, the term bacterium was introduced many years later, in 1828, by Christian Gottfried Ehrenberg. From this moment until now, lots of distinguished researchers have made important contributions to the development of bacteriology. The most relevant contributions for the development of bacteriology are chronologically enumerated in Table 1.3.

Table 1.3 Relevant contributions for the development of bacteriology.

Year	Contribution
1859	**Louis Pasteur** probed that fermentations were caused by microorganisms.
1878	**Pasteur** published the germ theory of diseases.
1886	**Hans Christian Gram** discovered the Gram stain as a method for bacterial differentiation.

Year	Contribution
1905	**Robert Koch** was awarded with a Nobel Prize for probing the germ theory of diseases.
1910	**Paul Ehrlich** developed arsphenamine, the first antibacterial developed, which was effective in curing syphilis.
1977	**Carl Woese** discovered that archaea had a separated line of evolutionary descent from bacteria.

Bacteria are small prokaryotic and unicellular microorganisms. Morphologically, bacteria display a vast diversity of shapes and sizes, oscillating from 0.5 to 5.0 μm in length. The bacteria shape depends on the cell wall (see Section 1.5.1.1) and on the cytoskeleton, a dynamic structure constituted by proteins, such as the tubulin-like protein FtsZ or the actin-like protein MreB[65, 66]. Frequent bacterial shapes are: **cocci** (spherical), **bacilli** (rod-shaped), **vibrio** (slightly curved or comma-shaped), **spirilla** (spiral-shaped) or **spirochetes** (tightly coiled). In the natural environment, bacteria can be found alone or associated in characteristic patterns, basically combined in pairs (diploid), forming chains or clusters (like bunch of grapes) (Fig. 1.21).
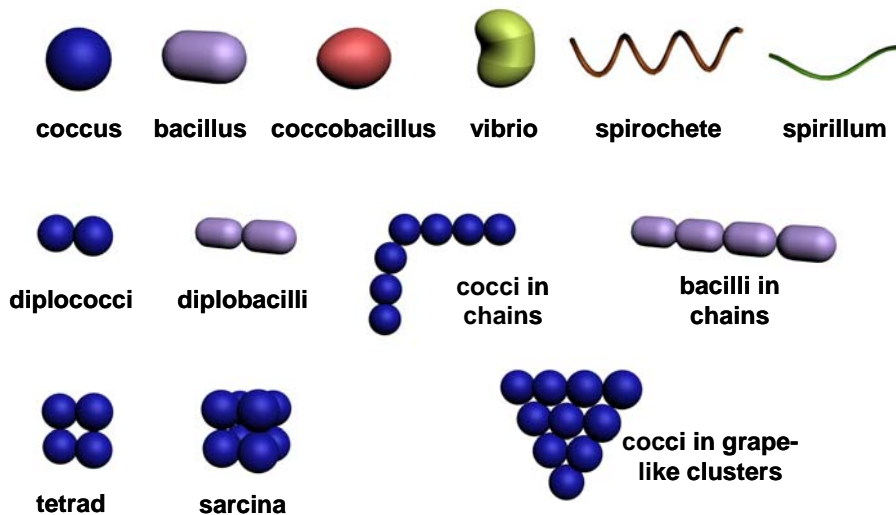
Fig. 1.21 Illustration of the more representative cell morphology of bacteria.

In terms of metabolism, bacteria cover a huge variety of possibilities. They are commonly classified on the basis of three main criteria: (1) *the carbon source*, which

distinguishes between **heterotrophic** (when using organic carbon compounds) and **autotrophic** bacteria (when fixing carbon dioxide), (2) *the electron donors*, which distinguishes between **lithotrophic** (when using inorganic electron donors) and **organotrophic** (when using organic electron donors) and (3) *the energy source* used in the metabolism, which distinguishes between **phototrophic** (when using light as energy source) and **chemotrophic** bacteria (when using chemical substances, oxidized organic or inorganic compounds as electron acceptors).

The Gram stain is the most popular criteria to classify bacteria. This is a simple method to experimentally classify bacteria in Gram-positive or Gram-negative regarding the composition of their cell walls. The classification can also be based on the cell structure, on the cellular metabolism or on differences in cell components such as DNA, fatty acids, pigments, antigens or other elements. Regarding genetics, most bacteria have a single circular chromosome ranging from 160.000 to 12 million of bases and also plasmids, which are small extra-chromosomal DNA sequences, typically circular and double-stranded, capable of autonomous replication, sometimes involved in the transmission of genetic information between bacteria.

1.5.1.1 Bacterial structure

From a structural point of view, prokaryotic cells have a rather simple structure, with a non-distinct cytoplasm, where the **DNA**, **plasmids**, **ribosomes**, **mesosomes** and **storage granules** are confined, surrounded by a plasma membrane (Fig. 1.22)[67]. The **plasma membrane** is a lipid bilayer with a huge number of transmembrane proteins and external receptors moving within or upon it, respectively. Most of transmembrane proteins are involved in the transport of water, ions, nutrients and metabolism residues across the membrane. Thus, the plasma membrane acts as a selective barrier controlling the ion exchange between the cytoplasm and the external medium and thus, allowing the existence of asymmetries in ion concentration in both sides of the membrane, which result in a permanent membrane potential.
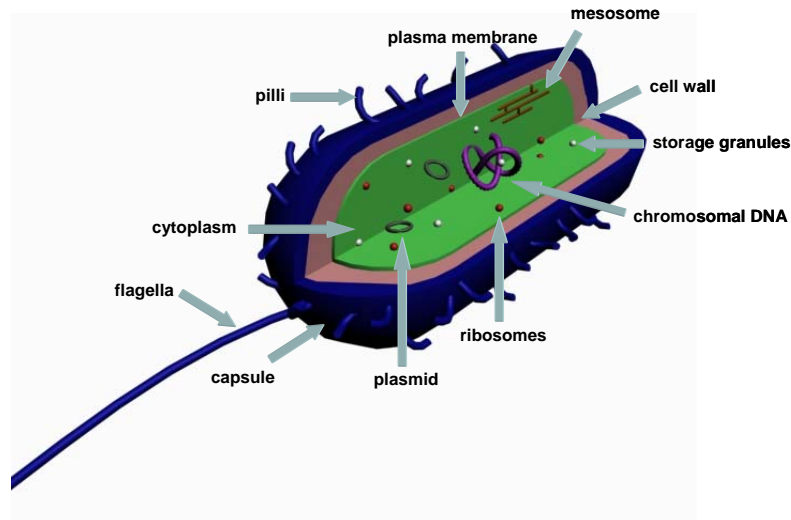
Fig. 1.22 Schematic representation of the main components of the bacteria structure.

Outside the plasma membrane, a multilayered **cell wall** is found. The cell wall structure depends on the type of microorganism. Gram-positive bacteria possess a thick cell wall containing many layers of peptidoglycan and teichoic acids. In contrast, Gram-negative bacteria have a relatively thin cell wall consisting of a few layers of peptidoglycan surrounded by a second lipid membrane containing lipopolysaccharides and lipoproteins (Fig. 1.23)[68]. These lipopolysaccharides have linear or slightly branched structures projected into the external medium and contain a large number of functional groups susceptible of ionization, mainly charged carboxyl, phosphate and amine groups. The grade of protonation and dissociation of these groups modulates the cell surface charge, which basically depends on the pH. At physiological pH values, the number of charged carboxyl and phosphate groups exceeds the number of charged amino groups and thus, most bacterial strains are negatively charged. When bacteria are immersed in ionic media, these charged external macromolecules attract a cloud of opposite charges forming a diffusive "electric double layer" on the cell wall surface[69, 70].

Most bacteria also have another layer outside of the cell wall or the outer membrane called **capsule** or **glycocalyx** (Fig. 1.22). This layer, usually composed of polysaccharides, is known to mediate attachment of bacterial cells to particular surfaces and the formation of biofilms[71]. These external structures are also involved in the protection of the cell against the engulfment by predatory protozoa or white blood cells and against antimicrobial agents[72].
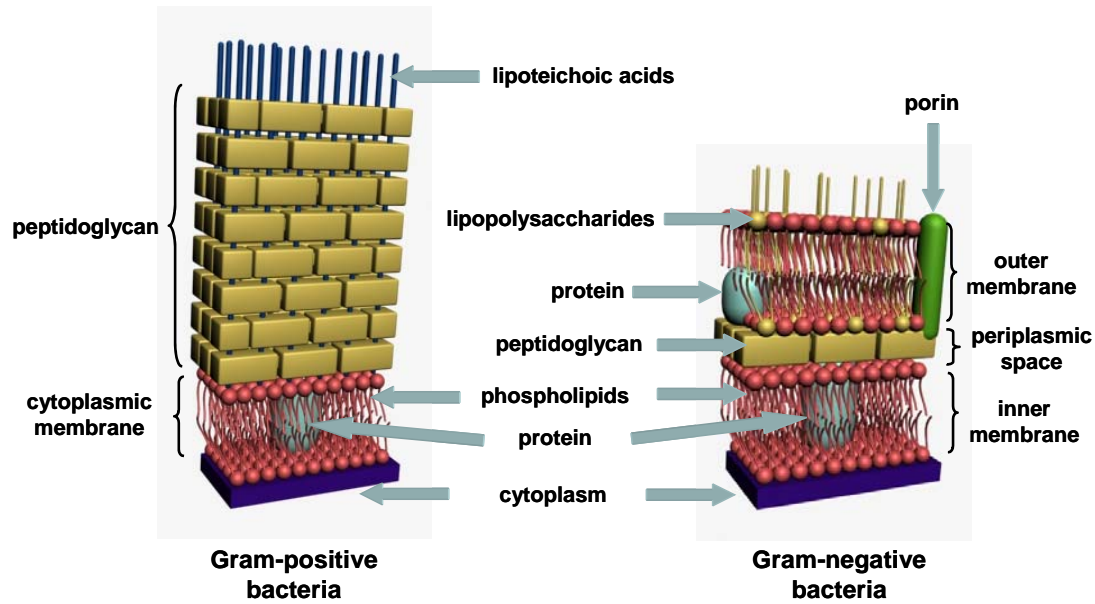
Fig. 1.23 Illustration of the transversal section of the cell wall for Gram-positive and Gram-negative bacteria.

Finally, bacteria can also present external appendages, namely **pili**, **fimbriae** and **flagella**. Flagella are long protein appendages anchored on the plasma membrane (Fig. 1.22). Their complex structure can be simplified considering flagella to be composed of a long tail and a *motor* which rotates the entire flagella. This appendage is basically involved in motility and in attachment to surfaces. On the other hand, pili and fimbriae are interchangeable terms used to designate short protein structures on the surface of bacteria (Fig. 1.22). Fimbriae are shorter and slightly smaller in diameter than common pili. Both of them are mainly involved in the attachment of the cell to surfaces in the nature and often play a relevant role in colonization. For instance, it is probed that fimbriae structure and composition has a relevant paper in formation of *Escherichia coli* biofilms[73]. A special pilus, the sex pilus, is not involved in the attachment but in the transference of substances between cells, basically genetic material.

1.5.1.2 Bacterial colonization mechanism: biofilm formation

The bacteria colonization mechanism is a complex multi-step process which can vary depending on the bacteria. In the natural environment, bacterial colonization is known to involve at least five stages, namely **(1) the preconditioning of the surface**, **(2) the bacterial attachment**, **(3) the biofilm formation**, **(4) the biofilm growth** and **(5) the**

biofilm maturation and stabilization[74, 75]. After each step, microorganisms become more firmly attached and more protected from the action of cleaners and sanitizers. Fig. 1.24 illustrates the main steps in the bacterial colonization mechanism.
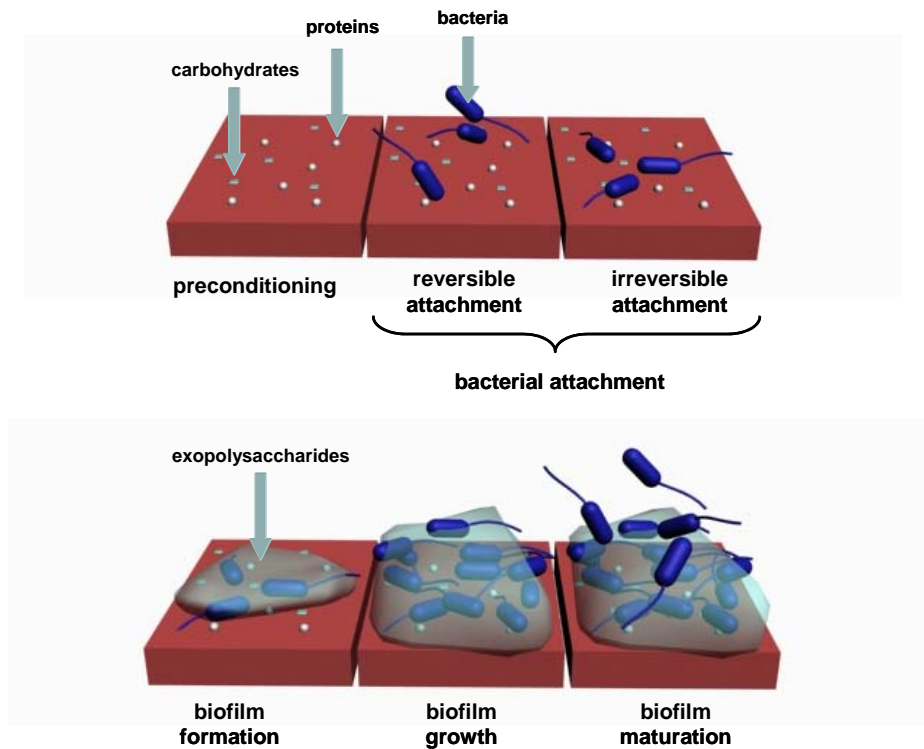
Fig. 1.24 Representation of the stages in the biofilm formation.

(1) The **preconditioning** involves the formation of an adherent layer, composed of proteins and carbohydrates, on the surface of the material. After few seconds of exposure, the proteins and carbohydrates of the surrounding environment adsorb and coat the surface by specific or non-specific chemical reactions. This stage does not involve bacterial attachment and is not usually considered a *real* colonization step. However, the layer that results from conditioning is absolutely necessary for the suitable colonization of the surface and may provide receptor sites for the firm attachment of bacteria subsequently.

(2) Attachment, considered the first *real* stage in bacterial colonisation, is relatively poorly understood since its study requires very sensitive and preferably real time instrumentation and methods. The presence of charged groups (carboxyl, phosphate or amine groups) and hydrophobic zones in bacterial membranes partly controls their

ability to flocculate or to adsorb onto surfaces[76, 77]. The attachment to surfaces is generally thought to be a two stage process, although both steps may take place simultaneously[78]. Stage 1, called **reversible attachment**, is a fast initial adsorption phase, governed by physical forces such as electrostatic charges, Brownian motion and van-der-Waals forces and it is likely that bacterial swimming, which requires flagella, is required for initial attachment to allow the bacteria to overcome these physical forces and come into close proximity to the surface. The reversible attachment occurs after some minutes of exposure and only allows a weak and non-permanent adsorption of bacteria which can easily leave the colonized surface. Stage 2, called **irreversible attachment**, is a slower cellular phase whereby bacteria tightly adhere to the surface via pili, binding proteins and polysaccharides from the conditioning layer. Bacteria irreversible attached to the surface are commonly found after few hours of exposure (1-2 hours). Thus, this stage is much slower than the reversible attachment since it requires the suitable interaction between mobile suspended bacteria and immobile molecules from the conditioning layer.

(3) Within 8 to 24 hours of exposure, cells strongly attached to the conditioning layer are stimulated to produce and to subsequently secrete exopolysaccharides[79]. A currently unknown hormone is though to be the responsible of the change in the genetic expression of bacteria[80]. Secreted polysaccharides create a glue-like matrix which covalently entraps bacteria within. This complex bacterial-polymeric structure, strongly attached to the surface is called **biofilm**[74, 75].

(4) After the initial biofilm formation, this structure starts **growing** basically through cell division and recruitment from the bulk. Biofilms contain bacterial cells in highly specialized microenvironments, created by bacteria, which provide nutrients and protection and favour cell division. Under these conditions, biofilms grow not only laterally across the surface, but in all directions (increase of thickness) and may cover the complete surface within days to months, depending on the external conditions and the bacteria.

(5) Finally, biofilms become **mature**. In this case, the number of cells within the film and its thickness remain practically constant with time. This requires the balance between the uptake cells, from cell division and recruitment, and the released ones, from

the detachment of individual cells or superficial layers. Bacteria growing in biofilms possess distinct characteristics from their free-floating or swimming counterparts. For instance, bacteria in biofilms become resistant to antimicrobial treatments and to the immune defence of hosts[81, 82]. Mature biofilms provide advantages to bacterial development. Essentially, biofilms facilitates nutrient uptake through complex diffusion channels, improve bacterial activity, stimulate microbial interactions and offer protection against toxic agents, cleaners and sanitizers, impeding their penetration within the structure[75].

The study of bacterial attachment on solid surfaces is important, as many pathogenic bacteria attach and colonise them, forming highly antibiotic resistant biofilms. For example, a serious human pathogen, *Pseudomonas aeruginosa* colonises the lungs of persons with Cystic Fibrosis, often leading to their premature death, and Gram-positive bacteria such as *Staphylococcus aureus* are known to infect medical devices such as urinary catheters leading to infection[83, 84].

1.6   REFERENCES

[1] G. Giddings, G. Allison, D. Brooks, A. Carter, *Nature Biotechnology*, **18** (2000) 1151-1155

[2] A. Hiatt, R. Caffferkey, K. Bowdish, *Nature*, **342** (1989) 76-78

[3] Y. Ishida, H. Saito, S. Ohta, Y. Hiei, T. Komari, T. Kumashiro, *Nature Biotechnology*, **14** (1996) 745-750

[4] L.A. Donehower, M. Harvey, B.L. Slagle, M.J. McArthur, C.A. Montgomery, J.S. Butel, B. Allan, *Nature*, **356** (1992) 215-221

[5] K. Hsiao, P. Chapman, S. Nilsen, C. Eckman, Y. Harigaya, S. Younkin, F. Yang, G. Cole, *Science*, **274** (1996) 99-103

[6] D. Games, D. Adams, R. Alessandrini, R. Barbour, P. Borthelette, C. Blackwell, T. Carr, J. Clemens, T. Donaldson, F. Gillespie, T. Guido, S. Hagopian, K. Johnson-Wood, K. Khan, M. Lee, P. Leibowitz, I. Lieberburg, S. Little, E. Masliah, L. McConlogue, M. Montoya-Zavala, L. Mucke, L. Paganini, E. Penniman, M. Power, D. Schenk, P. Seubert, B. Snyder, F. Soriano, H. Tan, J. Vitale, S. Wadsworth, B. Wolozin, J. Zhao, *Nature*, **373** (1995) 523-527

[7] N. Adányi, M. Váradi, N. Kim, I. Szendrö, *Current Applied Physics*, **6** (2006) 279-286

[8] C. Champagne, C. Lacroix, I. Sodini-Gallot, *Critical Reviews in Biotechnology*, **14** (1994) 109.134

[9] M. Coakley, G. Fitzgerald, R.P. Ros, *Applied and Environment Microbiology*, **63** (1997) 1434-1440

[10] B. Lennox, G.A. Montague, H.G. Hiden, G. Kornfeld, P.R. Goulding, *Biotechnology and Bioengineering*, **74** (2001) 125-135

[11] A. Rompre, P. Servais, J. Baudart, M.-R. de-Roubin, P. Laurent, *Journal of Microbiological Methods*, **49** (2002) 31-54

[12] T.M. Straub, D.P. Chandler, *Journal of Microbiological Methods*, **53** (2003) 185-197

[13] G. Marrazza, I. Chianella, M. Mascini, *Analytica Chimica Acta*, **387** (1999) 297-307

[14] C.A. Rowe-Taitt, J.W. Hazzard, K.E. Hoffman, J.J. Cras, J.P. Golden, F.S. Ligler, *Biosensors and Bioelectronics*, **15** (2000) 579-589

[15] C.J. French, N.M. Dickinson, P.D. Putwain, *Environmental Pollution*, **141** (2006) 387-395

[16] A.E. Schnieke, A.J. Kind, W.A. Ritchie, K. Mycock, A.R. Scott, M. Ritchie, I. Wilmut, A. Colman, K.H.S. Campbell, *Science*, **278** (1997) 2130-2133

[17] D.A. Armbruster, *Clinical Chemistry*, **39** (1993) 181-195

[18] A. Hulanicki, S. Glab, F. Ingman, *Pure and Applied Chemistry*, **63** (1991) 1247-1250

[19] *Sensors: A comprehensive survey*. T. Grandke, W.H. Ko, eds. *Fundamentals and general aspects*. Weinheim, Wiley-VCH (1989)

[20] D. Diamond, ed. *Principles of Chemical and Biological Sensors*. New York, Wiley-Interscience (1998)

[21] P. Vadgama, P.W. Crump, *The Analyst*, **117** (1992) 1657-1670

[22] E. Bakker, *Analytical Chemistry*, **76** (2004) 3285-3298

[23] D.R. Thévenot, K. Toth, R.A. Durst, G.S. Wilson, *Pure and Applied Chemistry*, **71** (1999) 2333-2348

[24] C. Malitesta, F. Palmisano, L. Torsi, P.G. Zambonin, *Analytical Chemistry*, **62** (1990) 2735-2740

[25] N.C. Foulds, C.R. Lowe, *Analytical Chemistry*, **60** (1988) 2473-2478

[26] J. Wang, M. Musameh, *Analytical Chemistry*, **75** (2003) 2075-2079

[27] E. Bakker, E. Pretsch, P. Buhlmann, *Analytical Chemistry*, **72** (2000) 1127-1133

[28] T. Rosatzin, E. Bakker, K. Suzuki, W. Simon, *Analytica Chimica Acta*, **280** (1993) 197-208

[29] S. Daunert, S. Wallace, A. Florido, L.G. Bachas, *Analytical Chemistry*, **63** (1991) 1676-1679

[30] O. Ouerghi, A. Senillou, N. Jaffrezic-Renault, C. Martelet, H. Ben Ouada, S. Cosnier, *Journal of Electroanalytical Chemistry*, **501** (2001) 62-69

[31] A.E. Radi, J.L. Acero-Sanchez, E. Baldrich, C.K. O'Sullivan, *Analytical Chemistry*, **77** (2005) 6320-6323

[32] S. Grant, F. Davis, K.A. Law, A.C. Barton, S.D. Collyer, S.P.J. Higson, T.D. Gibson, *Analytica Chimica Acta*, **537** (2005) 163-168

[33] A.J. Bard, L.R. Faulkner, *Electrochemical Methods: Fundamentals and Applications*. New York, John Wyley & Sons (2001)

[34] A.C. Fisher, *Electrode Dynamics*. Oxford, Oxford University Press (1996)

[35] E. Barsoukov, J.R. Macdonald, eds. *Impedance Spectroscopy: Theory, Experiment, and Applications*. New Jersey, John Wiley & Sons (2005)

[36] C. Gabrielli, Identification of Electrochemical Processes by Frequency Response Analysis. 1984, Solartron-Schlumberger. p. 120.

[37] H. Fricke, *Philosophical Magazine*, **7** (1932) 310-318

[38] R. Pethig, *Dielectric and electronic properties of biological materials*. New York, Wiley (1979)

[39] J.E. Harrar, I. Shain, *Analytical Chemistry*, **38** (1966) 1148-1158

[40] A.L.G. van den Eeden, J.H. Sluyters, J.H. van Lenthe, *Journal of Electroanalytical Chemistry*, **171** (1984) 195-217

[41] M.J. Rodiguez Presa, R.I. Tucceri, M.I. Florit, D. Posadas, *Journal of Electroanalytical Chemistry*, **502** (2001) 82-90

[42] W.H. Mulder, J.H. Sluyters, T. Pajkossy, L. Nyikos, *Journal of Electroanalytical Chemistry*, **285** (1990) 103-115

[43] A.W. Bott, *Current separations*, **11** (1992) 61-65

[44] A. Amirudin, D. Thieny, *Progress in Organic Coatings*, **26** (1995) 1-28

[45] F. Geenen, *Characterization of Organic Coatings with Impedance Measurements; A Study of Coating Structure, Adhesion and Underfilm Corrosion*. Delft, Delft University of Technology (1991)

[46] G. Hsieh, S.J. Ford, T.O. Mason, L.R. Pederson, *Solid State Ionics*, **91** (1996) 191-201

[47] P. Drude, *The Theory of Optics*. Mineola, NY, Dover Publications (2005)

[48] M.S. M. Dressel, *Annalen der Physik*, **15** (2006) 535-544

[49] I.K. Vockenroth, *Investigations of tethered bilayer lipid membranes for their potential use in biosensing devices*. Bath, University of Bath (2007)

[50] J. Homola, S.S. Yee, G. Gauglitz, *Sensors and Actuators B: Chemical*, **54** (1999) 3-15

[51] W. Knoll, *Annual Review of Physical Chemistry*, **49** (1998) 569-638

[52] A. Otto, *Zeitschrift für Physik A Hadrons and Nuclei*, **216** (1968) 398-410

[53] T. Turbadar, *Proceedings of the Physical Society*, **73** (1959) 40-44

[54] T. Turbadar, *Optica Acta*, **11** (1964) 207-210

[55] D. Axelrod, *Journal of Luminescence*, **31-32** (1984) 881-884

[56] A.D. Boardman, ed. *Electromagnetic surfaces modes*. New York, John Wiley & Sons. (1982)

[57] M. Malmqvist, *Nature*, **361** (1993) 186-187

[58] L. He, M.D. Musick, S.R. Nicewarner, F.G. Salinas, S.J. Benkovic, M.J. Natan, C.D. Keating, *Journal of the American Chemical Society*, **122** (2000) 9071-9077

[59] E. Stenberg, B. Persson, H. Roos, C. Urbaniczky, *Journal of Colloid and Interface Science*, **143** (1991) 513-526

[60] L.A. Lyon, M.D. Musick, M.J. Natan, *Analytical Chemistry*, **70** (1998) 5177-5183

[61] A.T.A. Jenkins, A. Buckling, M. McGhee, R.H. ffrench-Constant, *Journal of The Royal Society Interface*, **2** (2005) 255-259

[62] S. Tombelli, M. Minunni, E. Luzi, M. Mascini, *Bioelectrochemistry*, **67** (2005) 135-141

[63] D.K. Kambhampati, W. Knoll, *Current Opinion in Colloid and Interface Science*, **4** (1999) 273-280

[64] A. Leewenhoeck, *Philosophical Transactions (1683-1775)*, **14** (1753) 568-574

[65] J. Errington, *Nature Cell Biology*, **5** (2003) 175-178

[66] P.L. Graumann, *Annual Review of Microbiology*, **61** (2007) 589-618

[67] M.T. Madigan, J.M. Martinko, J. Parker, *Brock Biology of Microorganisms*. Hertfordshire, U.K., Prentice Hall International (1997)

[68] Y.H. An, R.B. Dickinson, R.J. Doyle. *Mechanisms of Bacterial Adhesion and Pathogenesis of Implant and Tissue Infections*. Y.H. An, R.J. Friedman, eds. *Handbook of Bacterial Adhesion. Principles, Methods and Applications*. Totowa, New Jersey, USA, Humana Press (2000)

[69] J.N. Israelachvili, *Intermolecular and Surface Forces*. London, Academic Press (1992)

[70] D.L. Chapman, *Philosophical Magazine*, **25** (1913) 475-481

[71] M. Daffe, G. Etienne, *Tubercle and Lung Disease*, **79** (1999) 153-169

[72] R.W. Stokes, R. Norris-Jones, D.E. Brooks, T.J. Beveridge, D. Doxsee, L.M. Thorson, *Infection and Immunity*, **72** (2004) 5676-5686

[73] G.C. Ulett, A.N. Mabbett, K.C. Fung, R.I. Webb, M.A. Schembri, *Microbiology*, **153** (2007) 2321-2331

[74] J. Wiley. *Wiley series in ecological and applied microbiology*. W.G. Characklis, K.C. Marshall, eds. *Biofilms*. New York, John Wiley (1990)

[75] H.M. Lappin-Scott, J.W. Costerton, eds. *Microbial Biofilms*. Cambridge, Cambridge University Press (1995)

[76] H.H.M. Rijnaarts, W. Norde, E.J. Bouwer, J. Lyklema, A.J.B. Zehnder, *Applied and Environment Microbiology*, **59** (1993) 3255-3265

[77] V. Urbain, J.C. Block, J. Manem, *Water Research*, **27** (1993) 829-838

[78] Y.H. An, R.J. Friedman, *Journal of Biomedical Materials Research*, **43** (1998) 338-348

[79] D.G. Davies, A.M. Chakrabarty, G.G. Geesey, *Applied and Environment Microbiology*, **59** (1993) 1181-1186

[80] J.W. Costerton, P.S. Stewart, E.P. Greenberg, *Science*, **284** (1999) 1318-1322

[81] P.S. Stewart, J. William Costerton, *The Lancet*, **358** (2001) 135-138

[82] T.-F.C. Mah, G.A. O'Toole, *Trends in Microbiology*, **9** (2001) 34-39

[83] C. Moser, M. van Gennip, T. Bjarnsholt, H. Calum, P.O. Jensen, B. Lee, O. Ciofu, M. Givskov, S. Molin, N. Hoiby, *International Journal of Antimicrobial Agents*, **29** (2007) S40-S41

[84] G. Reid, C. Tieszer, *International Biodeterioration & Biodegradation*, **34** (1994) 73-83

CHAPTER 2: OBJECTIVES

CHAPTER 2: OBJECTIVES

This Chapter describes the scientific questions that induced the development of the present thesis. It is important to note that these objectives arose from a collaboration work between the Biosensors and BioMEMs group of the Centre Nacional de Microelectrònica (CNM-IMB, CSIC) of Barcelona, the Grup de Microbiologia Ambiental of the Universitat Autònoma de Barcelona (UAB) and the Department of Chemistry of the University of Bath (UK).

The present thesis was focused on the development of new electrochemical instrumentation for microbial biosensing to complement or to substitute the classical microbiological methods. The traditional microbiological methods, basically based on plating on agar and staining processes, although highly specifics and sensitive, still require considerable experience as well as time. Sensors in general and electrochemical sensors in particular have been thought to be a good alternative to them because of their simplicity, low cost, efficiency and their possibility to be compacted, miniaturized, automated and to supply information at real-time.

Briefly, the main objectives of the present thesis are:

1. The characterization of the early bacteria attachment to metallic surfaces using electrochemical (Electrochemical Impedance Spectroscopy, EIS) and optical (Surface Plasmon Resonance, SPR) measurements.

2. The monitoring of the formation of mature biofilms on metallic surfaces using EIS.

3. The detection of bacteriophages in water samples by following the degradation of mature biofilms of specific bacteria grown on the electrode surface using EIS.

4. The development and optimization of an impedimetric approach based on bacterial attachment for the quantification of suspended bacteria concentration.

5. The application of the previously exposed impedimetric approach to the real-time monitoring of bacteria growth.

6. The development of an automated flow system for the real-time monitoring of suspended bacteria concentration.

7. The resolution of binary mixtures of microorganisms using EIS and Artificial Neural Networks (ANNs).

8. The determination of the role of some *Photorhabdus luminescens* (*P. luminescens*) proteins in the biofilm formation, early bacteria attachment, motility and virulence.

CHAPTER 3: EXPERIMENTAL

CHAPTER 3: EXPERIMENTAL

This Chapter enumerates the chemical reagents, buffers, solutions and culture media used in the present thesis. An overview of the instrumentation, general measurement features and common experimental conditions for the most relevant techniques used in the development of this thesis are also included.

3.1   REAGENTS AND SOLUTIONS

In this work, analytical grade chemicals were used with no further purification. All the solutions were prepared using ultra pure de-ionized water (18 MΩ cm) by dissolving the appropriate amount of analyte.

For the microbiological preparations, culture media were also prepared using de-ionized water. Bacteria cultures were mostly grown in AB Minimal Medium, ABMM[1], and Luria-Bertani (LB) medium was used for the counting process. The ABMM was also used in the infection of bacteriophages and compared with a rich medium, the Modified Scholten's Broth (MSB) supplemented with nalidixic acid (250 µg mL^{-1})[2].

3.2   CHEMICAL SENSORS

This Section describes the design and principal characteristics of the electrochemical and optical sensors used in Electrochemical Impedance Spectroscopy (EIS) and Surface Plasmon Resonance (SPR) measurements, respectively. Also a brief description of the fabrication process for the electrochemical sensors used in this thesis is included.

3.2.1   Electrochemical sensors

The thin film gold and platinum sensors used in this thesis were fabricated under silicon microtechnology using photolithographic processes. Electrode production was carried out in the clean room of the Centre Nacional de Microelectrònica (CNM-IMB, CSIC) using silicon wafers of 4'' (10 mm of diameter) doped with 1-12 Ω cm phosphorous as substrate. An example of fabrication is illustrated in Fig. 3.1. It has to be noted that each fabrication step required the use of suitable masks, which were previously designed using the LASI software. Further information concerning the masks design and fabrication processes can be found in previous theses[3, 4] and publications[5] of the group.

The first step in the fabrication process consisted in thermally **growing an insulating silicon oxide coating layer** on the silicon substrate (Fig. 3.1-a). This layer isolated the silicon from the solution and from the metals subsequently deposited[6].

In the second step, a **platinum layer was deposited** (using electron beam metallization) on the electrodes region using an indirect process known as **lift-off**[6]. In the lift-off process, as in all *additive processes*, metals are added to those regions of the substrate unprotected by a resist. This process required four principal stages: **the deposition of the photoresist** (Fig. 3.1-b); **the elimination of the photoresist from the electrode regions** using suitable masks, UV light (to depolymerise the resist) and a developing step (to remove the depolymerised resist) (Fig. 3.1-c); **the addition of a metallic bilayer** composed of a thick platinum layer and a thin titanium layer (which favoured the platinum adhesion to the substrate) by electron beam metallization (evaporation of the metal and deposition on the substrate)[7] (Fig. 3.1-d); and **the definition of the desired structure** after removing the excess resist in an acetone bath (Fig. 3.1-e).

The following step consisted in **the deposition of gold** (on the electrodes and pads) using a **wet direct etching process**[7]. The direct etching is a *subtractive process* where resists protect the unexposed material from the attack of an etchant. This process had four main steps: **the deposition of a gold layer** over two thin layers of titanium and nickel (which improved the adhesion of gold and prevented possible electromigration problems) by sputtering metallization (metal ions were bombarded with a flux of inert-gas ions to the wafer)[7] (Fig. 3.1-f); **the addition of the photoresist on the electrode areas** to protect the gold from the attack of the etchant (Fig. 3.1-g); **the elimination of unwanted exposed metals** with suitable wet etchants (Fig. 3.1-h); and **the definition of the desired structure** after removing the excess resist in an acetone bath (Fig. 3.1-i).

Finally, **electrodes were isolated with a mixed silicon oxide / silicon nitride layer** deposited using a dry direct etching process. This process was composed of three main steps: **the deposition of the mixed layer on the wafer** using the Plasma Enhanced Chemical Vapour Deposition (PECVD) technique (Fig. 3.1-j); **the elimination of the insulating layer from the electrode regions** using suitable masks, the photoresist and the Reactive Ion Etching (RIE) process (a dry etching process based on the production of volatile compounds by the interaction between the chemically active gaseous ions of

the RIE plasma and the mixed layer, which were eliminated with the vacuum system) (Fig. 3.1-k); and **the definition of the desired structure** after removing the excess resist in an acetone bath (Fig. 3.1-l).
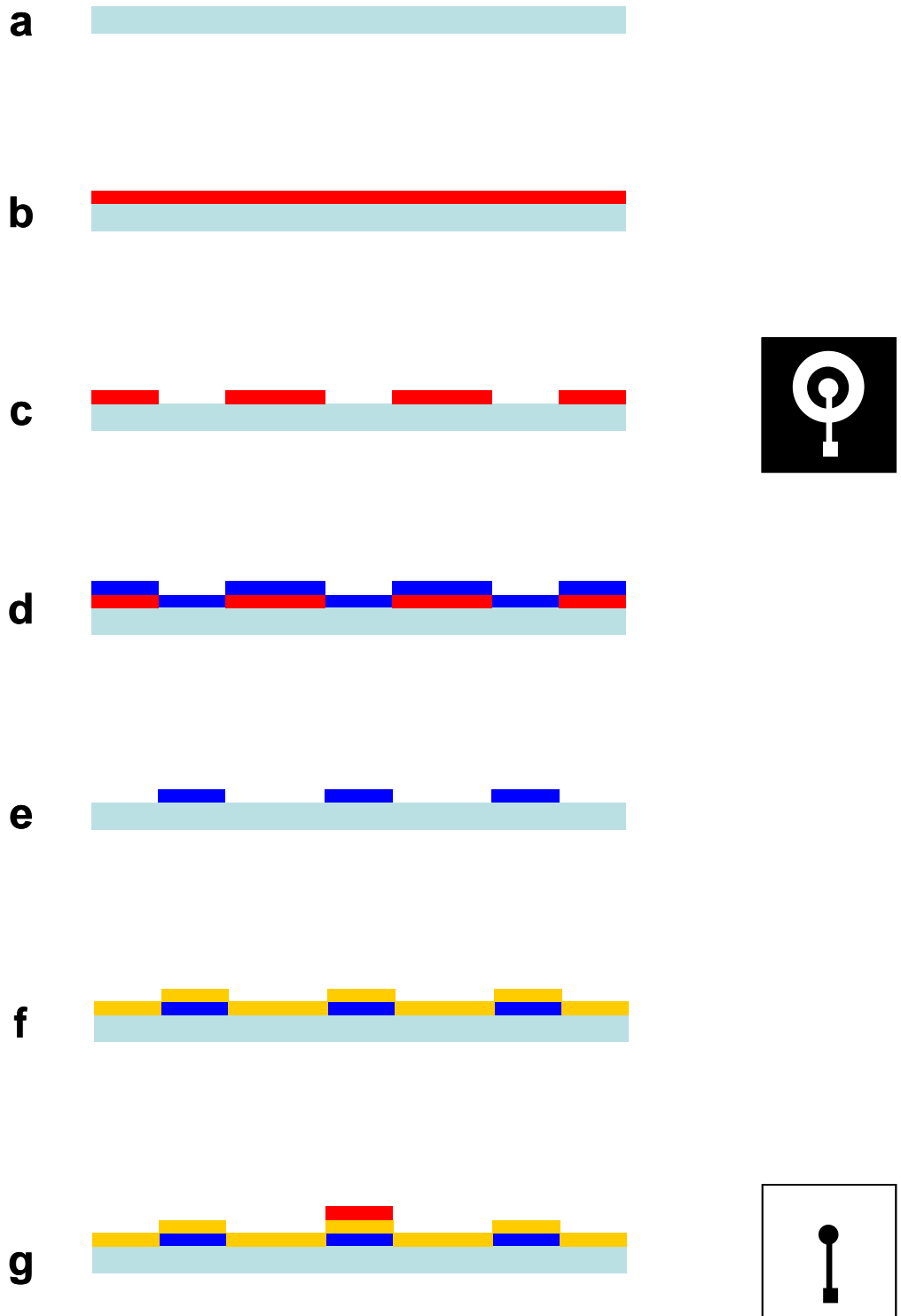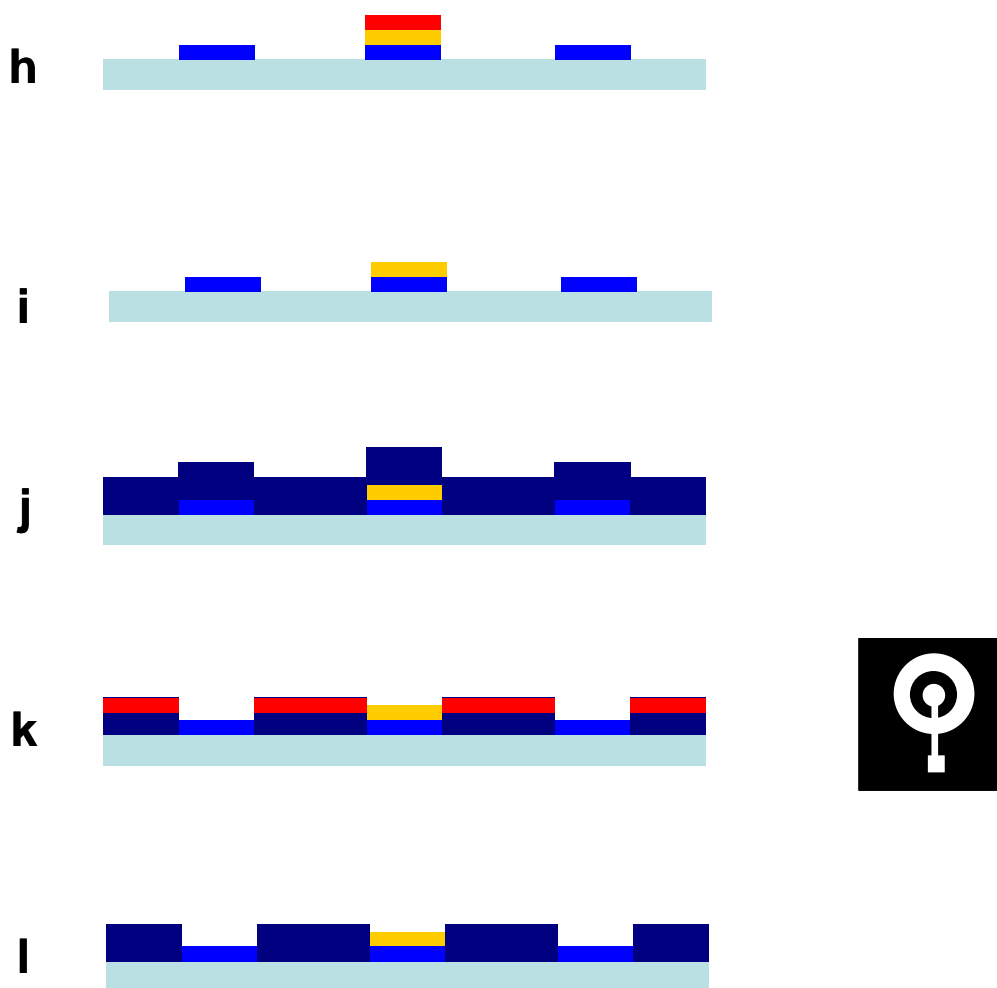
Fig. 3.1 Illustration of the fabrication process of the electrodes used in the present thesis. Diagrams of the masks are also provided to clarify with black and white zones which respectively impede and permit the UV light to cross. Neither the masks nor the relative thickness of the layers are drawn to scale.

After the fabrication process, the wafers were cut and the sensors were individualized (Fig. 3.2). Each individual sensor was transferred to a Print Circuit Board (PCB) holder. Wire bonds were made to provide electric contact between the chip and the connecting pads on the PCB. The chip and the connections were isolated from the electrolyte solution by encapsulating them with a photo-curable insulating resin.

The electrochemical sensors used in the development of the present thesis are shown in Fig. 3.2. Gold or platinum disc working electrodes (WEs) with an area of 0.5 mm^2 surrounded by a platinum counter electrode (CE) of 1.4 mm^2 were integrated on a silicon nitride substrate, following the fabrication process previously exposed. The

electrodes were 0.08 mm apart, ensuring near-homogeneous polarization of the WE[8]. The selection of the WE material depended on the application.

Silicon wafer after the microfabrication process

Gold electrode

gold working electrode

platinum counter electrodes

Platinum electrode

platinum working electrode

photo-curable resin　　**wire bonding**

PCB pad

PCB holder

sensor-chip

sensor pad
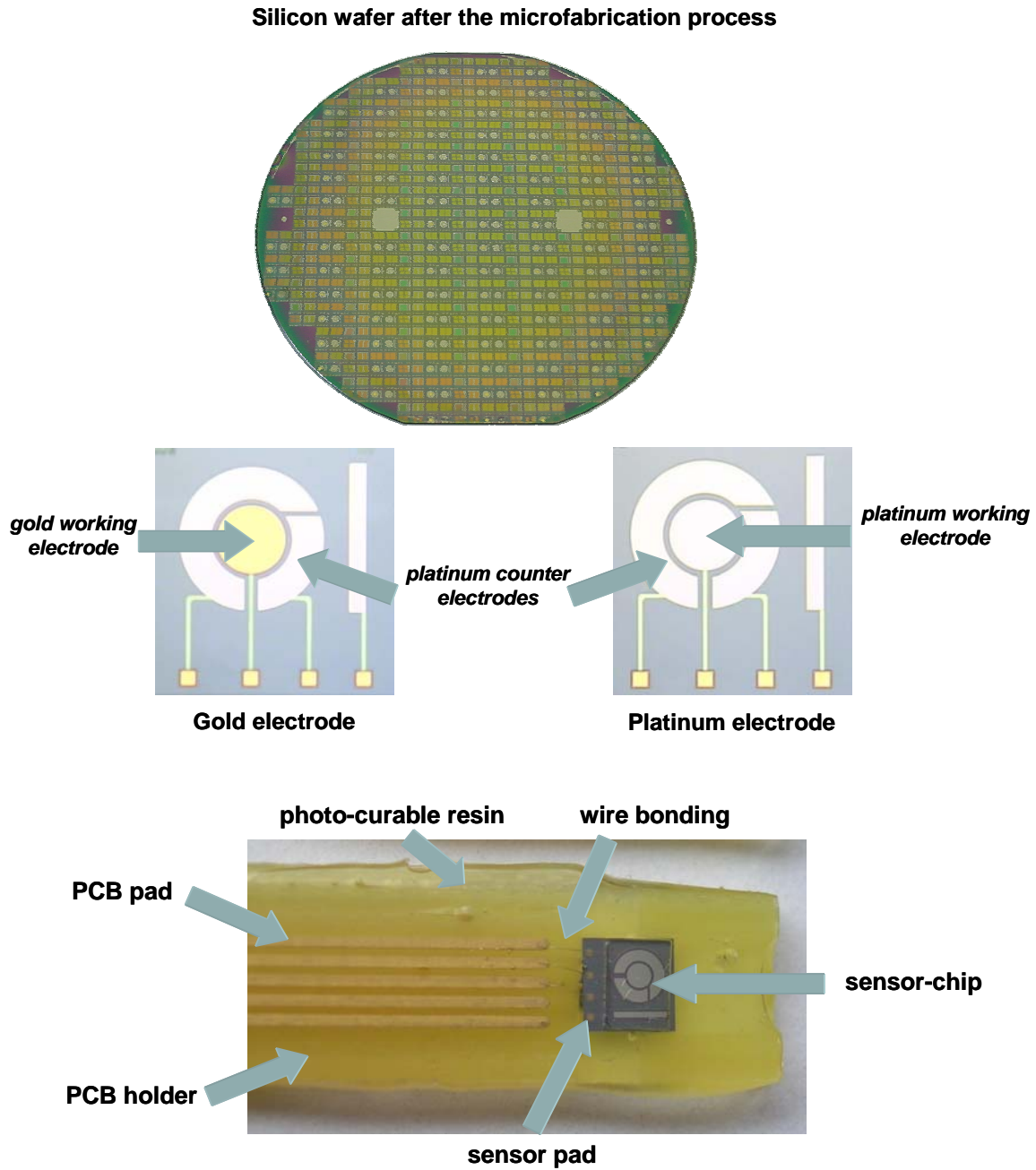
Fig. 3.2 Image of a processed silicon wafer with the electrochemical platinum and gold sensors used in the present thesis. The parts and connections of the sensor immobilized in a PCB are specified in the illustration.

3.2.2   Optical sensors

For the SPR measurements, prefabricated gold-coated glass disks (EcoChemie, BV, The Netherlands) were used as sensors. The glass disk was coated with a thin gold layer of 50 nm.

3.3   INSTRUMENTATION

This Section details the instrumentation employed in the development of the present thesis with a brief description of the frequent experimental conditions and protocols used.

3.3.1   EIS instrumentation and measurement conditions

Different instrumentation was used for the EIS measurements depending on the application. Most of them were made using an impedance analyzer Solartron SI 1260A (Solartron Analytical, Hampshire, UK) connected to a potentiostat Solartron 1287. In this case, impedance spectra were recorded using the Z-Plot software (Scribner Associates Inc., North Carolina, USA). This equipment showed high resolution in the impedance spectra in a wide range of frequencies, a short measurement time and a huge stability and reliability of the measurement.

However, portability problems and the difficulty to synchronize the Solartron equipment with the flow system suggested the use of the AUTOLAB PGSTAT 12 (EcoChemie, BV, The Netherlands) containing a FRA-2 module both when monitoring the real-time bacteria concentration and when detecting bacteriophages infection. In both cases, EIS spectra were registered using the FRA-2 software (EcoChemie, BV, The Netherlands). This equipment, which integrated the impedance analyzer and the potentiostat in a single device, was more portable and did not show calibration problems after moving. Further, this instrument could be easily synchronized to the automatic flow system using the *Project* application of the FRA-2 software via trigger signal.

EIS measurements were made as follows, independently of the equipment. Three electrodes configuration was chosen in all cases (see Chapter 1, Section 1.3.3.1). An external Ag|AgCl electrode, 5240 (Crison, Barcelona, Spain), was used as a Reference Electrode (RE). A 25 mV Alternating Current (AC) potential was applied at the cell Open Circuit Potential, OCP, (+ 0.26 ± 0.05 V versus Ag|AgCl) over a frequency range between 100 kHz and 10 Hz. The measurement time was around 50 s and 120 s (for the Solartron and the AUTOLAB equipment, respectively) after recording 17 points per frequency decade. All measurements made in this thesis are in relation to the Ag|AgCl RE.

3.3.2 SPR measurements and conditions

SPR data were acquired using the AUTOLAB ESPRIT (Eco Chemie, BV, The Netherlands). Measurements were made by following the change in the reflected light minimum angle (θ_m) with time, which is indicative of the change in optical properties of the interface as bacteria attach. The instrument had two independent channels allowing two experiments to be carried out simultaneously (see Section 1.4.2.2). In these experiments, one of the channels was used as an internal control to subtract artefacts, such as changes in bulk refractive index. Bacterial suspensions in Phosphate Buffered Saline (PBS) and buffer without bacteria were measured in Channel 1 (CH1) and 2 (CH2), respectively. Hence, the difference between the angles recorded in CH1 and CH2, called differential angle, was indicative of the change produced in the refractive index by bacterial attachment. The optical sensors described in Section 3.2.2 were placed on a hemispherical prism using index match fluid (RI = 1.518, Cargille), which ensured optical continuity. The system was allowed to stabilise for four min before addition of the corresponding sample in each channel. The difference in angle of SPR was thus recorded. Measurements were made every 3 s for the duration of the experiment.

3.3.3 Optical Microscopy

Optical Microscopy images were obtained using a Nikon Eclipse ME-600 microscope (Nikon Corporation, Japan). Electrodes containing attached bacteria or biofilms were commonly stained using the Gram stain kit (Sigma, Switzerland) before imaging.

3.3.4 Confocal Scanning Laser Microscopy

The Confocal Scanning Laser Microscopy (CSLM) was used for the characterization of the composition of mature biofilms and for the measurement of the biofilm thickness before and after the bacteriophages infection. The microscope Laser Confocal Leica TCS SP2 AOBS (Leica, Heidelberg, Germany) was used. Cells and exopolysaccharides of the biofilms were respectively stained for 5 min with 4'-6-DiAmidino-2-Phenylindole (DAPI) (Merck, Germany), concabalina A (Merck, Germany) and WGA (Merck, Germany) prior to imaging by CSLM. The biofilm thickness was determined by following the strategy described by Heydorn et al.[9, 10]. With this protocol, images were acquired between 1.0 and 2.0 μm intervals down through the biofilm, and therefore the number of images in each stack varied according to the thickness of the biofilm.

3.3.5 Epifluorescence Microscopy

Epifluorescence Microscopy was used both for imaging bacteria attached to the electrode and for quantifying suspended bacteria. In both cases, images were obtained using an Olympus BH Fluorescence Microscope (Olympus, California, USA) after staining with DAPI, as detailed in the previous Section. When quantifying the suspended bacteria concentration, cells were initially fixed with formaldehyde (CH_2O, Sigma) and filtered in 2 μm pore size GTBP filters (Millipore, Billerica, Massachusets, USA). Bacteria retained in the filters were stained with DAPI, imaged and counted. More than 20 different optical fields were counted.

3.3.6   Optical Density measurements

The magnitude of the Optical Density at 550 nm (OD_{550}) was used to control the suspended concentration of bacteria culture with time. An Ultrospec 1100 pro spectrophotometer (Biochrom, Cambridge, UK) was used.

3.3.7   Attached bacteria quantification by sonication and plating on agar

Attached bacteria were quantified by sonication and plating on agar. Briefly, electrodes were sonicated for 3 min in 5 mL of PBS to remove the attached bacteria from the surface of the electrodes. The supernatant was 1/10 serially diluted in PBS and 100 µL of the corresponding dilutions were then inoculated onto an agar plate containing LB medium. After overnight incubation at 37 ºC, bacteria were counted and the number of attached bacteria onto the chips was then estimated as Colony Forming Units per cm^2 ($CFU \ cm^{-2}$).

3.4   REFERENCES

[1] D. Balestrino, J.A.J. Haagensen, C. Rich, C. Forestier, *Journal of Bacteriology*, **187** (2005) 2870-2880

[2] Anonymous, "*Detection and enumeration of bacteriophages. Part 2: Enumeration of somatic coliphages*". ISO 10705-2: Water quality. Geneva, Switzerland, International Organisation for Standardisation (2000)

[3] J. Gonzalo-Ruiz, *Desarrollo de biosensores enzimáticos miniaturizados para su aplicación en la industria*. Cerdanyola del Vallès, Universitat Autònoma de Barcelona (2006)

[4] O. Ordeig-Sala, *Thin film based disc microelectrode arrays in water toxicity control*. Barcelona, UPC (2007)

[5] F.G. Chevallier, N. Fietkau, J. del Campo, R. Mas, F.X. Munoz, L. Jiang, T.G.J. Jones, R.G. Compton, *Journal of Electroanalytical Chemistry*, **596** (2006) 25-32

[6] S.P. Beeby, G. Ensel, M. Kraft, *MEMS Mechanical Sensors*. Norwood, Artech House INC (2004)

[7] N. Maluf, K. Williams, *An Introduction to Microelectromechanical Systems Engineering*. Norwood, Artech House INC (2004)

[8] J.E. Harrar, I. Shain, *Analytical Chemistry*, **38** (1966) 1148-1158

[9] A. Heydorn, A.T. Nielsen, M. Hentzer, C. Sternberg, M. Givskov, B.K. Ersboll, S. Molin, *Microbiology*, **146** (2000) 2395-2407

[10] A. Heydorn, B.K. Ersboll, M. Hentzer, M.R. Parsek, M. Givskov, S. Molin, *Microbiology*, **146** (2000) 2409-2415

CHAPTER 4: MONITORING OF THE EARLY BACTERIAL ATTACHMENT USING ELECTROCHEMICAL IMPEDANCE SPECTROSCOPY AND SURFACE PLASMON RESONANCE

CHAPTER 4: MONITORING OF THE EARLY BACTERIAL ATTACHMENT USING ELECTROCHEMICAL IMPEDANCE SPECTROSCOPY AND SURFACE PLASMON RESONANCE

This Chapter describes the characterization of the early bacterial attachment on metallic surfaces using Electrochemical Impedance Spectroscopy (EIS) and Surface Plasmon Resonance (SPR). *Escherichia coli* (*E. coli*) were chosen as model bacteria. As summary, SPR and EIS measurements were found to be very sensitive both to the concentration of bacteria in the solution and to the attachment time. Both of them were compared with classical measurements of bacterial attachment on identical surfaces such as staining / microscopy and bacterial removal by sonication and plating onto agar. In this Chapter, the relationship between the measured EIS of the electrode during attachment and the biophysical processes involved are discussed. A similar discussion is made by the SPR measurements. This work has been partially published in *Electrochemical Communications* (Annex I)[1] and in *Biosensors and Bioelectronics* (Annex II)[2].

4.1 INTRODUCTION

The study of bacterial attachment on solid surfaces is important, as many pathogenic bacteria attach and colonise them, forming highly antibiotic resistant biofilms. For example, a serious human pathogen, *Pseudomonas aeruginosa* colonise the lungs of persons with Cystic Fibrosis, often leading to their premature death, and Gram-positive bacteria such as *Staphylococcus aureus* are known to infect medical devices, especially urinary catheters, leading to infection[3, 4].

The early attachment step is generally thought to be a fast initial adsorption phase, governed by physical forces such as electrostatic charges, Brownian motion and van-der-Waals forces and it is likely that bacterial swimming, which requires flagella, is required for initial attachment to allow the bacteria to overcome these physical forces and come into close proximity to the surface. However, the exact adhesion process depends on the specific bacteria[5]. In the case of *E. coli*, various cell surface appendages were shown to be necessary to achieve a suitable attachment and mature biofilm development. Flagella and type I fimbriae are implicated in early adhesion steps, while the conjugative plasmid pili and the production both of a polysaccharide-rich matrix (cellulose, colanic acid, and poly-β-1,6-N-acetylglucosamine) and of short adhesins such as antigen 43 (Ag43) contributes to biofilm maturation[6].

E. coli is considered the most thoroughly studied of all species of bacteria, and has been used extensively as a model to study biofilm development due to its relevance to the human biotic environment and its genetic amenability. However, attachment, the first stage in bacterial colonisation, is relatively poorly understood since its study requires very sensitive and preferably real-time instrumentation and methods. The classical method for studying attached bacteria was pioneered by Robert Koch, back in the 19th century, where attached bacteria were stained with a dye and then studied by optical microscopy. This method is still one of the principal bacteriological methods used today. The disadvantage of staining is however that it can be difficult to accurately quantify the response, especially at low bacterial concentrations and is an 'end point' method. In recent years a number of new methodologies have been employed to study

bacterial attachment. These include Cyclic Voltammetry[7] and Quartz Crystal Microbalance with Dispersion (QCM-D)[8]. This Chapter describes the real-time characterization of the early bacterial attachment using EIS and SPR.

4.2 EXPERIMENTAL

This Section details the preparation of the microbiological samples for the characterization of the early bacteria attachment to metallic surfaces. Also the description of the experimental protocol for the EIS and SPR measurements is included. Optical Microscopy, Epifluorescence Microscopy and attached bacteria quantification by sonication and plating on agar measurements were made as shown in Chapter 3 (Section 3.3).

4.2.1 Impedimetric characterization of the early attachment to platinum electrodes

Bacterial suspensions were introduced to the electrochemical cell, containing the platinum working electrode / counter electrode (WE / CE) chip and an external Ag|AgCl reference electrode (RE). The electrochemical cell was thermostatically kept at 4 ºC. EIS measurements were made immediately and every periodic interval for 40 min, under the experimental conditions detailed in Chapter 3 (Section 3.3.1). It should be noted that these times were the time before measurement of the EIS spectrum – which itself took around 50 s.

After each sequence of measurements WE / CE chips were washed with 30 % v/v hydrogen peroxide (Sigma, Switzerland) for 2 min. This cleaning was proved to detach molecules and whole cells irreversibly adhered on the electrode during the measurement and to help regenerate the chip for future use. However, the hydrogen peroxide solution also damaged the coating used for isolating the connections of the chip from the solution and critically reduced the sensor life-time. Coating fragments attached to the electrode surface were eliminated by cleaning with 96 % v/v ethanol (Panreac, Spain). Electrodes and the electrochemical cell were finally cleaned with water and sterilized with ethanol. After the cleaning, chips were checked by measuring in AB Minimal

Medium (ABMM) without bacteria. Similar data were obtained in all cases [magnitude of the interface capacitance, $K_i = (1.57 \pm 0.08) \times 10^{-7}\ \Omega^{-1}\ s^{-\beta}$].

4.2.2 Characterization of the early attachment to gold surfaces using SPR

Before the analysis, glass disks with a gold coating were placed on a hemispherical prism using index match fluid (Refractive Index (RI) = 1.518, Cargille), which ensured optical continuity. The system was allowed to stabilise for four minutes in 50 μl of Phosphate Buffered Saline (PBS) before addition of 50 μl of the corresponding sample in each channel. Bacterial suspensions in PBS and buffer without bacteria were measured in channel 1 (CH1) and 2 (CH2), respectively. Hence, the difference between the angles recorded in CH1 and CH2, called differential angle, was indicative of the change produced in the RI by bacterial attachment. The difference in angle of SPR was thus recorded. Measurements were made every three seconds for the duration of the experiment.

4.2.3 Microbiological preparations

E. coli (CGSC 5073 K12) was grown overnight in ABMM at 37 ºC. An aliquot of 10 mL of culture was centrifuged for 15 min at 3500 *g* [Sigma 4-10 centrifuge (Sigma, Switzerland)]. The supernatant liquid was removed and cells (the pellet) were re-suspended in ABMM, when measured using EIS, or in PBS at pH 7.4, when measured using SPR. The process was repeated twice in order to remove metabolic products, membrane fragments and cytoplasmatic proteins. The final bacterial pellet was re-suspended in 10 mL of ABMM or PBS and then counted using plating on agar containing Luria-Bertani (LB) medium. The suspension was then serially diluted down to 1 Colony Forming Units per mL (CFU mL^{-1}) in decade steps. Before measurements, biological samples were stored in the fridge at 4 °C to slow growth. All of the manipulations were performed under sterile conditions.

4.3   RESULTS AND DISCUSSION

4.3.1   Fitting and interpretation of impedance spectra

Z-View software was used to fit impedance data to the equivalent circuit shown in Fig. 4.1. The circuit, a simplification of the Randles equivalent circuit[9], included a resistance modelling the solution resistance (R_S), a double layer capacitance, which appears as the interface Constant Phase Element (CPE_i), and an extra capacitance of small magnitude (nF) associated with the presence of an external reference (C_{ref}), whose value did not vary with the concentration of bacteria. Comparable equivalent circuits have been employed in similar applications[10]. The use of the CPE_i instead of a conventional double layer capacitance has to be discussed. In this work, as on most solid electrodes, the double layer impedance did not behave as a pure capacitance since its phase angle was slightly smaller than 90º [11]. Although this is currently under study, a roughness factor appears to be one important cause of this effect. As a consequence, a Constant Phase Element (CPE) is very frequently used to fit the double layer capacitance of the electrode. While this approach may be controversial, in the work reported in this Chapter, variation of the CPE parameters are important and used in themselves as parameters for following bacterial attachment. The impedance of most interfacial CPEs in non-electroactive electrolytes are described by the expression[12]:

$$Z = \frac{1}{K(j\omega)^{\beta}} \tag{4.1}$$

Z is the magnitude of the impedance (in Ω), K is the CPE magnitude (in $\Omega^{-1}s^{-\beta}$), ω is the angular frequency (in s^{-1}), $j = \sqrt{-1}$ and β is a parameter linked with the phase angle which oscillates from 1, for planar surfaces, to 0.5, for very rough ones[13]. In these experiments, where charged bacteria become part of the interfacial region, and in doing, modify the dielectric properties of the electrode, the obtained CPE will contain more parameters than those linked simply to roughness, such as bacterial density and the nature of the attached bacteria. For this reason, Fig. 4.1 shows a CPE labelled CPE_i as a generic element that accounts for many complex processes which cannot, themselves, be deconvoluted.

Fig. 4.1 shows impedance measurements after 1 and 40 min attachment. The change in the CPE_i with bacterial attachment can be clearly seen.
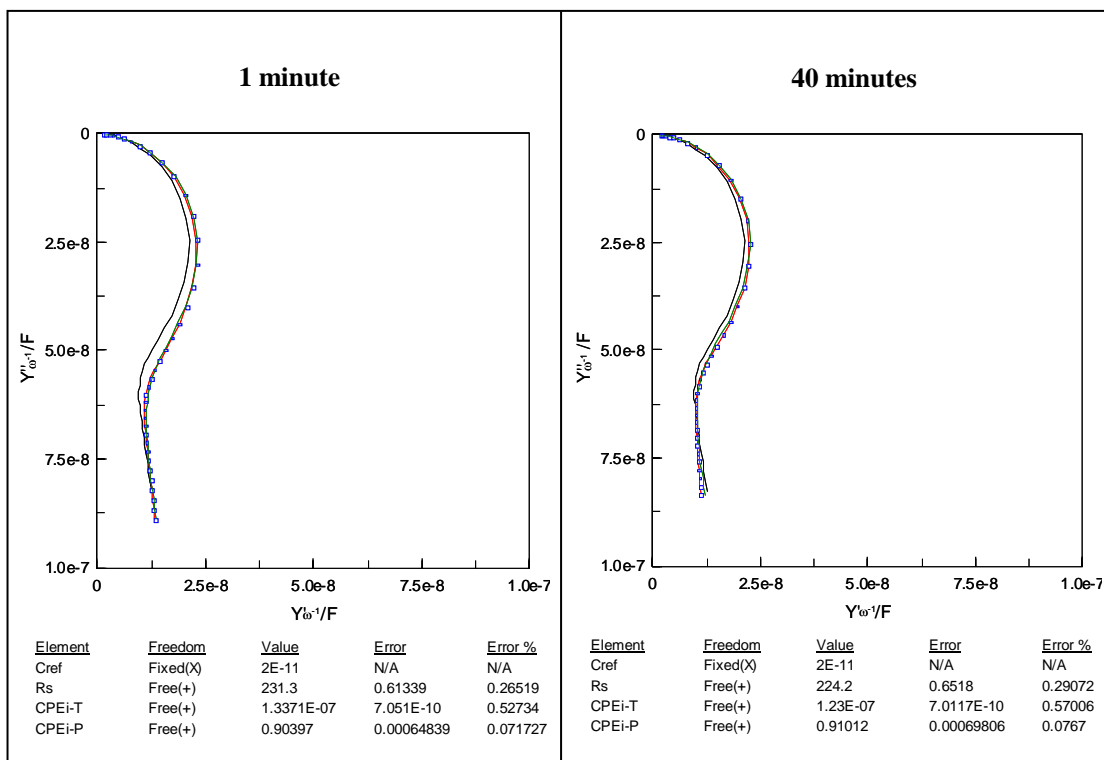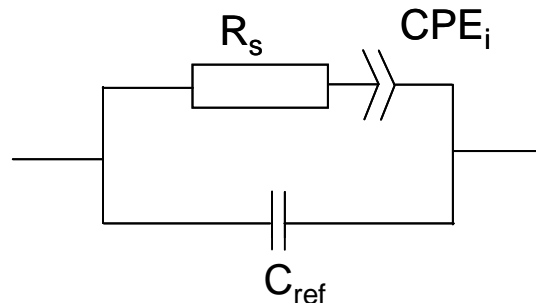
Fig. 4.1 Admittance complex plane plot for *E. coli* at a concentration of 10^7 CFU mL^{-1} after 1 and 40 min of attachment. The spectrum corresponding to the control (ABMM without bacteria) is also included in each plot (black line). The impedance spectra (points in the plot) were fitted to the equivalent circuit shown inset, which contained the C_{ref}, the R_S and the CPE_i. The ideal impedance spectra obtained from the fitting (line in the plot), the calculated values and errors using the *Z-View* software for each element of the equivalent circuit are also shown.

4.3.2   Effect of bacterial concentration on attachment when measured by EIS

The effect of bacterial concentration on the EIS response of the electrodes was measured as described in Section 4.2.1. Impedance spectra were recorded and fitted as detailed above. The results from the fitting are given in Fig. 4.2. A constant R_S value was obtained with time for each measurement regardless of concentration ($230 \pm 17\ \Omega$). Sample conductivity was measured separately with a conductance meter and found also to be sample invariant. However, the CPE_i magnitude (K_i) changed both as a function of attachment time and with concentration (Fig. 4.2).
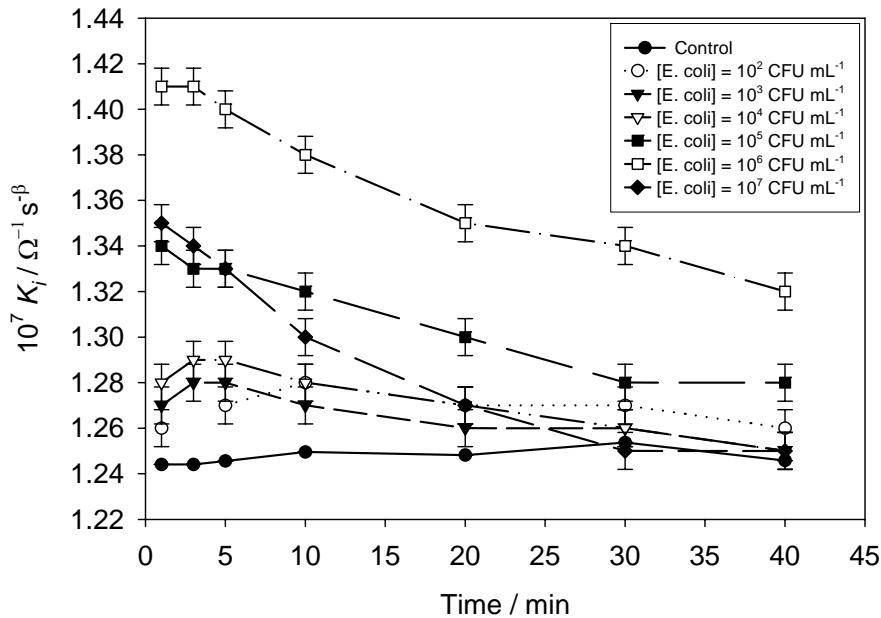
Fig. 4.2 Representation of the variation of the K_i with time by six bacterial concentrations and the control sample (ABMM without bacteria). Recorded changes were due to bacterial attachment to the electrode surface. Confidence intervals were calculated at the 95 % confidence level.

The effect on K_i was most pronounced with the higher concentrations (10^5 CFU mL^{-1} and above) of bacterial samples. After a small initial increase (for around 1 min), K_i decreased. In Fig. 4.3, the change in K_i was normalized ($\%K_i(t)$), as shown in Eq. 4.2. $K_i(t)$ is the value of the CPE magnitude at time t after the introduction of bacteria and $K_i(1)$ the value of the CPE after 1 min attachment.

$$\%K_i(t) = \frac{\left(K_i(t) - Ki(1)\right)}{K_i(1)} \times 100 \qquad (4.2)$$

It can be seen that the relative change in K_i was proportional to the concentration of the bacteria: higher concentration suspensions gave the greatest decrease after 40 min attachment.
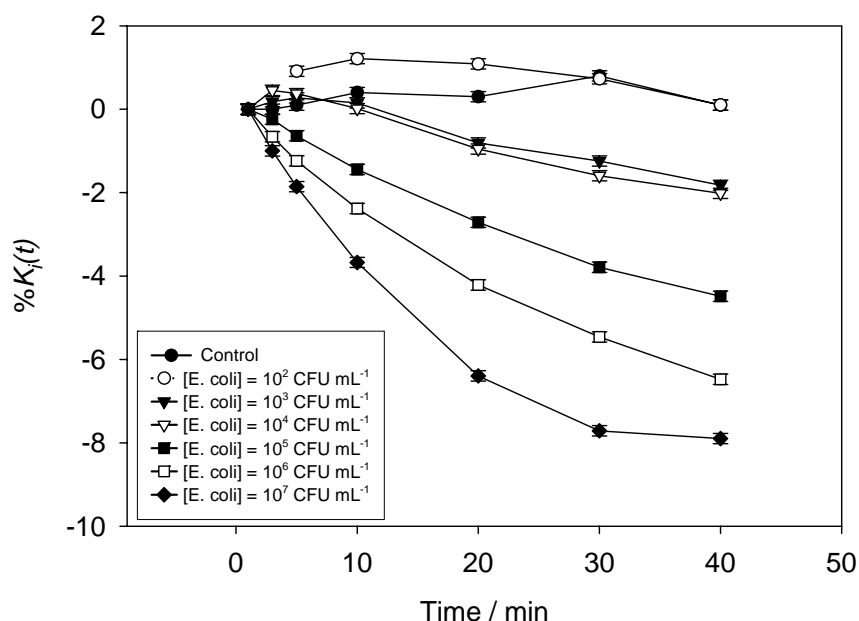
Fig. 4.3 Representation of the variation of the *%K_i(t)* with time by six bacterial concentrations and the control sample (ABMM without bacteria). Recorded changes were due to bacterial attachment to the electrode surface. Confidence intervals were calculated at the 95 % confidence level.

In all cases, K_i mainly decreased with time. In a separate study of EIS measurements of antibody-antigen binding, Katz reported that on antigen binding to an electrode immobilised antibody a decrease in the interfacial capacitance was measured[14]. This was ascribed to changes in the dielectric separation in the interfacial double layer. In this study of bacterial attachment, similar results were obtained. At frequencies below 100 MHz, current cannot cross the cell membranes and bacteria behave as isolating particles[15, 16]. Gingell reported that cell attachment did not affect the double layer capacitance since the lipid bilayer was not deposited directly onto the electrode surface,

but bacterial cells attached to the electrode usually being separated by a gap of 10-20 nm[17]. Thus, it is supposed that the aqueous gap between the cell membrane and the electrode would prevent a direct influence of the cell membrane on the impedance of the electrode[18]. However, the attachment of bacteria to the electrode may change the microstructure of the double layer, thus may result in a change in the double layer capacitance.

A more important mechanism may be the principal cause of this large decrease in CPE. Adhesion process can also be understood in terms of a decrease in the area, A, of bare electrode (in m^2) which causes a decrease in the double layer capacitance of the electrode, since:

$$C = \frac{\varepsilon_o \varepsilon_r A}{d} \qquad (4.3)$$

C is the capacitance magnitude (in F), ε_0 is the vacuum permittivity (in F m^{-1}), ε_r is the relative static permittivity and d is the distance between charged layers (in m). A reasonable, if simplistic model of the CPEs pertaining to the measured interfacial CPE can be understood if, for the sake of simplicity, we considered the measured CPE to be primarily capacitive in nature. In this case, the total measured capacitance (C_i, in F) is the sum of the bare electrode capacitance (C_{Pt}, in F) and the capacitance of the bacteria ($C_{bacteria}$, in F) modified by the coverage of bacteria, given by $\theta(t)$, Eq. 4.4:

$$C_i = \theta(t) C_{bacteria} + (1 - \theta(t)) C_{Pt} \qquad (4.4)$$

The magnitude of the capacitance of the plasmatic membrane[19] has been reported in the literature to be nearly 1 µF cm^{-2}. Providing $C_{bacteria}$ (below the pF when considering an area of the cell close to several µm^2) is lower in magnitude than C_{Pt} (experimentally found higher than 100 µF), the C_i will fall as bacteria attach, which is what is observed in Fig. 4.2 and Fig. 4.3. These results correlated well with the measurement of attached bacteria and the percentage of coverage (calculated regarding that each attached bacterium covered an area of 3.5 µm^2) made by sonication / removal and growth on agar plates (Table 4.1). This showed that higher concentrations of attached bacteria (or

larger covered areas) correlated with larger changes in K_i and with higher concentrations of bacteria in suspension. However, the percentage of attached cells decreased with the concentration and hence, higher concentrations of bacteria in suspension showed lower percentages of attachment. It is important to note, that at the time period used for these measurements only reversible, early stage attachment is taking place. Colonisation and associated growth of any extra polysaccharide matrix would takes several hours or days and was not measured here[20].

Table 4.1 Summary table of the amount of attached bacteria, percentage of attached bacteria, percentage of coverage of the electrode after sonication and the corresponding K_i value. Suspended concentrations and exposure times are included in the table.

Bacterial concentration (CFU mL^{-1})	Exposure time (min)	Adhered bacteria* (CFU mL^{-1})	Percentage of attached cells*	Percentage of coverage of bacteria*/**	10^7 K_i (Ω s$^{-\beta}$)
3.6×10^3	3	$(5.0 \pm 0.3) \times 10^1$	1.4 ± 0.8	0.015 ± 0.009	1.28 ± 0.08
1.5×10^4	1	$(1.9 \pm 0.5) \times 10^3$	1.1 ± 0.3	0.55 ± 0.16	1.34 ± 0.12
1.5×10^4	3	$(1.0 \pm 0.3) \times 10^3$	0.59 ± 0.17	0.29 ± 0.08	1.33 ± 0.07
1.5×10^4	5	$(3.8 \pm 0.9) \times 10^2$	0.23 ± 0.05	0.11 ± 0.03	1.33 ± 0.08
1.5×10^4	10	$(6.5 \pm 2.1) \times 10^2$	0.38 ± 0.12	0.19 ± 0.06	1.32 ± 0.08
1.5×10^4	20	$(5.8 \pm 1.8) \times 10^2$	0.34 ± 0.10	0.17 ± 0.05	1.30 ± 0.05
1.5×10^4	40	$(8.5 \pm 0.7) \times 10^2$	0.50 ± 0.04	0.25 ± 0.02	1.28 ± 0.06
5×10^7	3	$(5.4 \pm 0.6) \times 10^3$	0.0108 ± 0.0012	1.56 ± 0.18	1.34 ± 0.08

*From sonication. **Area of the *E. coli K12*: 3.5 μm^2; area of the WE / CE chip: 6 mm^2.

The change in EIS on attachment of lower concentrations of bacteria (below 10^4 CFU mL^{-1}) is less easy to understand. It is clear from Table 4.1 that the number of attached bacteria at these concentrations was relatively low. It can also be seen that on addition of bacteria to the chip at these low concentrations, different behaviour was observed. The CPE initially increases, by around 1 %, before slightly decreasing. A large decrease in CPE was not observed. The reason for the initial increase in the CPE is unclear, but

we speculate on the basis of reports in the literature[10, 21, 22] that this may be due to a decrease in the Debye length caused by increase in charge at the interface associated with weakly attached bacteria (since bacteria are themselves charged and therefore they have their own double layer charge region around them).

4.3.3 Determination of the effect of the initial bacterial concentration on the attachment of bacteria when using SPR

The effect of bacterial concentration on SPR measurements was determined as described in Section 4.2.2. Fig. 4.4 shows the change of the differential angle measured using SPR with time at three different bacteria concentrations.
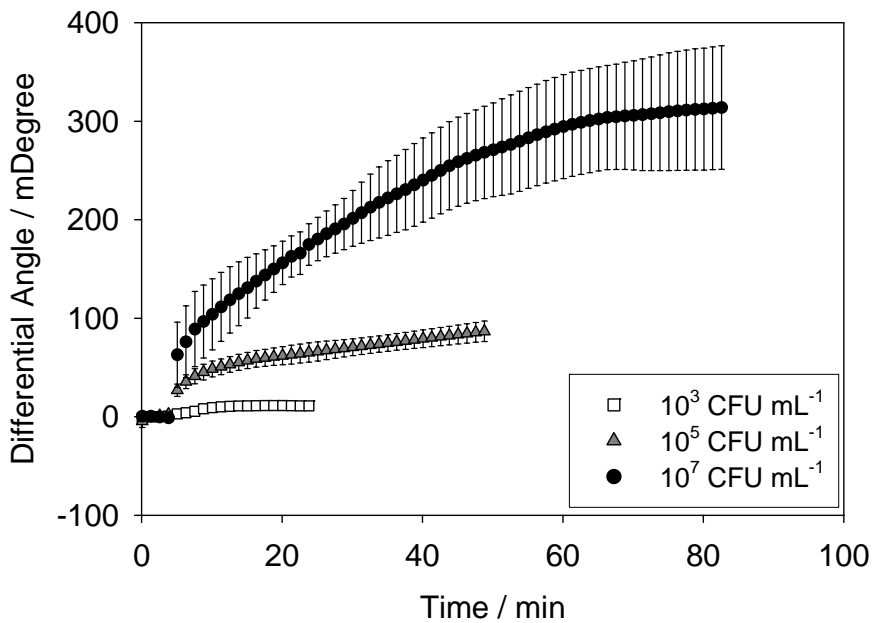
Fig. 4.4 Representation of the differential angle measured using SPR versus time for *E. coli* at a concentration of 10^3, 10^5 and 10^7 CFU mL^{-1}.

Fig. 4.4 shows that the differential angle measured using SPR also changed both as a function of attachment time and with concentration. The SPR measurement principle is based on the fact that the recorded angle (the angle of SPR) is highly sensitive to changes in the refractive index of the dielectric layer above the gold. Previous works

show that bacterial attachment to the gold changed the refractive index of the dielectric, which is observed in Fig. 4.4[23].

4.3.4   Verification of EIS data by Epifluorescence and Optical Microscopy

After EIS measurements were made, chips were rinsed with distilled water, dried under a nitrogen stream, suitably stained and imaged as detailed in Chapter 3 by Epifluorescence and Optical Microscopy imaging (Sections 3.3.5 and 3.3.3, respectively).

Fluorescence images of cells adhered on the chip surface were obtained (Fig. 4.5). The line crossing the pictures was taken as a spatial reference of the chip, to aid identification of electrodes. The WE was on the left side in A.1, B.2 and B.3 pictures, and on the right side in A.2, A.3 and B.1. These images show bacterial distribution on the chip. A rough estimation of the number of attached cells was made, but aggregation made bacterial counting difficult. These results were compared with Table 4.1.

Epifluorescence Microscopy images show that bacteria adhered to any surface. Attached bacteria were found on the platinum electrodes or the silicon nitride area. Bacteria actually adhered better on the silicon nitride area. Fig. 4.5-A illustrates attached bacteria on the chip after 2 min of exposure to 10^2, 10^5 and 10^7 CFU mL^{-1} samples, respectively. With increasing concentration, the number of adhered cells increased (Table 4.1). However, the level of aggregation also increased. After 2 min attachment, bacteria were mainly found attached around the edges of the working electrode. This may be due to two reasons. Firstly, the electric field lines around the edges are more densely packed and the electric field is more intense (although this will be still low in Alternating Current (AC) measurements without an applied Direct Current (DC) bias potential), favouring bacterial adhesion[24]. Moreover, bacteria quickly attached to the silicon nitride area, which surrounds the working electrode. Thus, for proximity, the edges would be the first covered region. The fast adhesion induced aggregation, especially in concentrated samples. Due to aggregation, bacteria covered less area. However, bacterial count showed proportionality between the number of attached cells and the logarithm of the concentration. This agreed with impedance data:

K_i plots shifted to higher values with the concentration after very short attachment times, before decreasing.
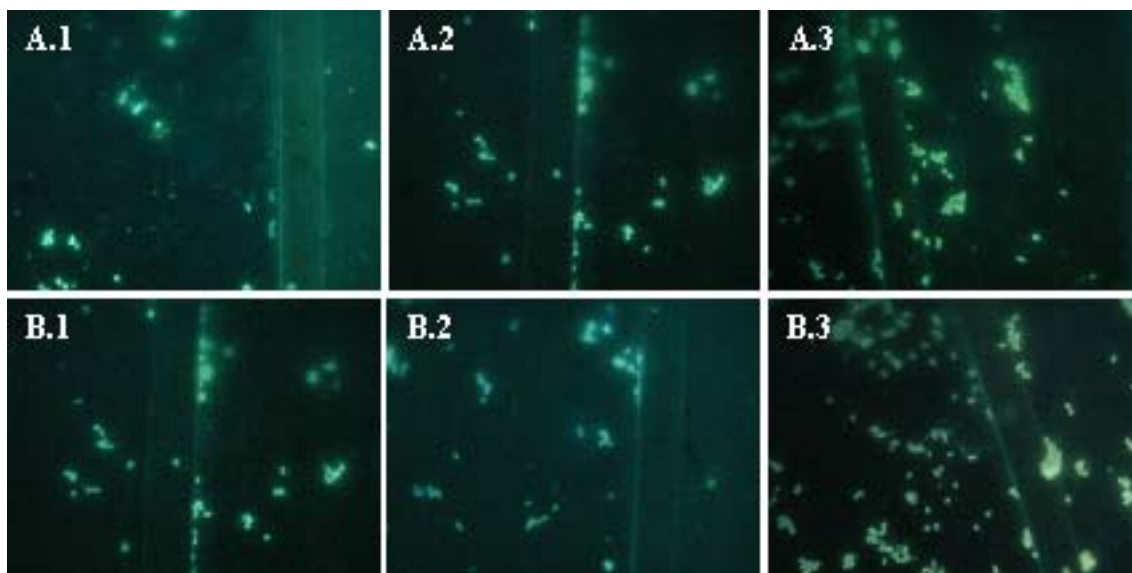
Fig. 4.5 Fluorescence images at 400 x of bacteria attached to platinum surfaces. (A) Chips immersed 2 min in (1) 10^2 CFU mL^{-1}, (2) 10^5 CFU mL^{-1} and (3) 10^7 CFU mL^{-1} bacterial samples. (B) Chips immersed in a 10^5 CFU mL^{-1} sample for (1) 2, (2) 5 and (3) 10 min.

In Fig. 4.5-B, chips were immersed in a 10^5 CFU mL^{-1} sample for 2, 5 and 10 min, respectively. The number of attached cells remained almost constant with time (Table 4.1) probably because of the fact that the flux of attaching cells was balanced with the flux of cells which, due to their weak attachment by physical forces, left the surface of the electrode. However, bacterial distribution changed significantly. Initially, bacteria attached around the electrode edges. With time, they expanded across the entire electrode area, although a higher bacterial density was found on the edges. This corroborated impedance measurements, which showed that bacterial adhesion on non-polarized electrode (an electrode at its Open Circuit Potential, OCP) is a spontaneous process and confirmed the time-dependence of the coverage of bacteria ($\theta(t)$) since the amount of covered area was shown to increase with time.

Optical Microscopy images also showed cells attached to the electrode surface. In this case, the number of attached bacteria also changed as a function of attachment time and

with concentration (Fig. 4.6). The number of attached cells was proportional to the concentration of the bacteria in suspension. With time, the number of attached cells seemed to increase until stabilization after 20 minutes attachment, although an expansion effect as shown in epifluorescence images (bacteria expanded across the entire electrode area) cannot be discarded.
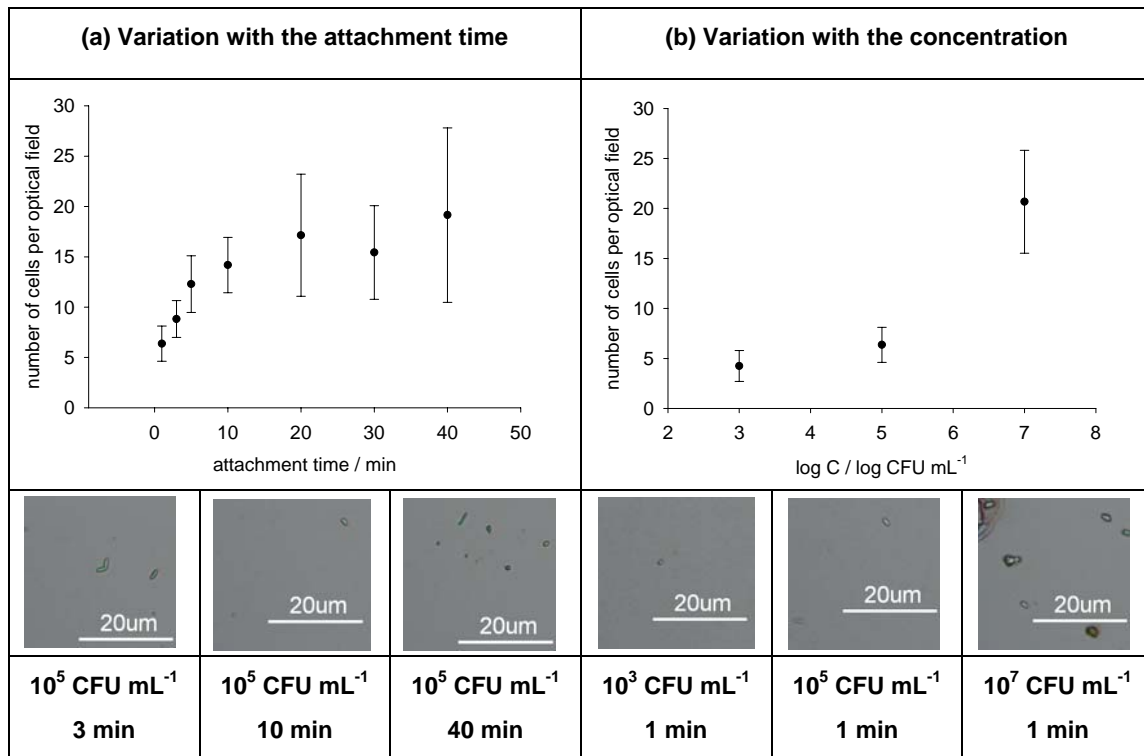
Fig. 4.6 (a) Variation of the number of attached cells for a 10^5 CFU mL^{-1} sample versus the time. (b) Variation of the number of attached cells after 1 min of exposure for 10^3, 10^5 and 10^7 CFU mL^{-1}. Relevant images of the attachment process are also included. The number of attached cells was found after counting 20 different optical fields.

4.3.5 Comparison of very early stage attachment (at 50 s) and later attachment effects on K_i

The discussion until now has largely focussed on measurement of attachment between 2 min up to 40 min. However, the very early stage attachment, at the point where bacteria can be considered to be behaving as simple charged colloidal particles is interesting, and quite a different effect on the CPE$_i$ was seen compared with later measurement times.
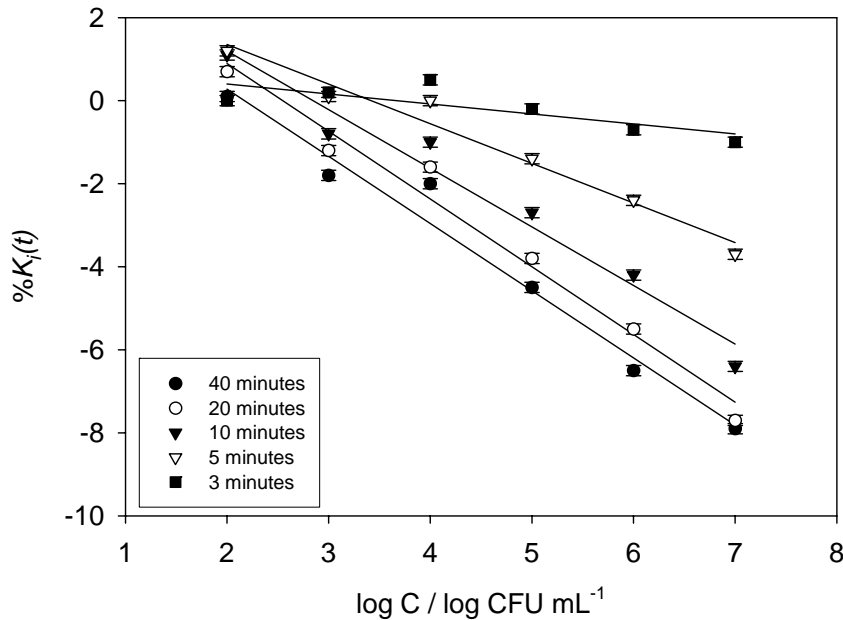
Fig. 4.7 Representation of the *%K$_i$(t)* after 3, 5, 10, 20 and 40 min of attachment versus bacterial concentration. Confidence intervals were calculated at the 95 % confidence level.

Fig. 4.7 shows the effect on the CPE of concentration and time of attachment. The general effect seen in Fig. 4.2 and Fig. 4.3 is also observed. However, in Fig. 4.8, the very early stage change in CPE at 50 s attachment is plotted against concentration of bacteria. A quite different effect was seen. Here the CPE actually *increased* with concentration of bacteria (rather than decreased as seen at longer times). Moreover, a correlation between concentration and increase in CPE was evident. An explanation for this very early stage behaviour is probably provided by again considering how the introduction of charged bacterial particles, with their associated counter-ions, affects the double layer at the electrode interface. In fact, the behaviour is perhaps the same as was observed in Fig. 4.2 for very low bacterial concentrations, where a pronounced early increase in CPE was also observed: that is a decrease in Debye length at the electrode double layer causes an initial increase in CPE, prior to the actual attachment of bacteria at later times. This early stage (at times lower than 2 min) could be termed as pre-attachment phase.
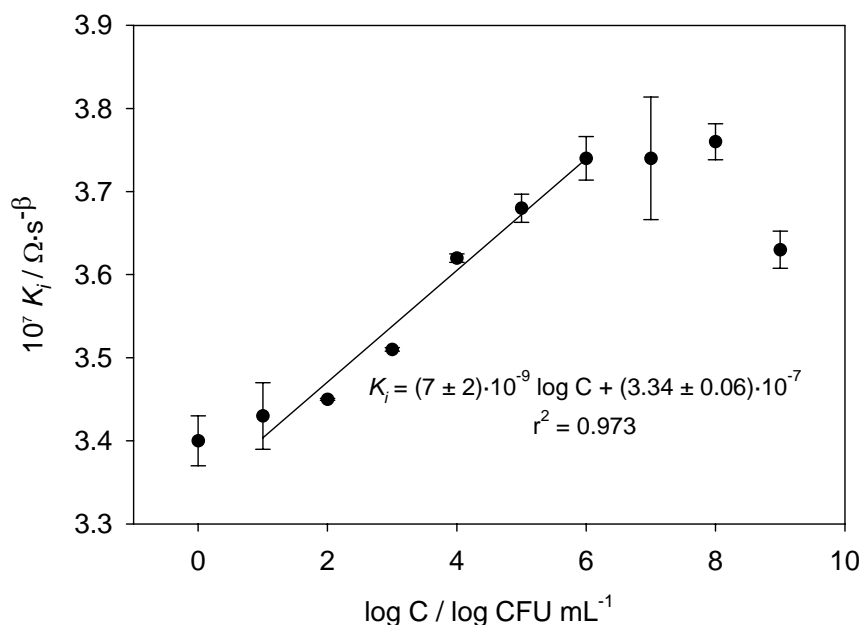
Fig. 4.8 Representation of the K_i after 50 s of attachment versus bacterial concentration. Confidence intervals were calculated at the 95 % confidence level.

4.4 CONCLUSIONS

In this Chapter, SPR and EIS have been demonstrated to be sensitive methods for the real-time monitoring of bacteria attachment to metallic surfaces and their measurements have shown good correlation with the traditional methods, namely staining / microscopy and bacterial removal by sonication and plating onto agar. EIS has found to be particularly sensitive to the very early attachment / pre-attachment. The most useful parameter of the electrical circuit, which related to coverage of bacteria on the electrode surface, was electrode CPE_i, approximately the electrode double layer capacitance, which decreased during early stage attachment. The change in CPE showed dependence on both the attachment time and the concentration of bacteria.

4.5   REFERENCES

[1] X. Muñoz-Berbel, N. Vigués, J. Mas, A.T.A. Jenkins, F.J. Muñoz, *Electrochemistry Communications*, **9** (2007) 2654-2660

[2] X. Munoz-Berbel, N. Vigués, A.T.A. Jenkins, J. Mas, F.J. Munoz, *Biosensors and Bioelectronics*, (Accepted)

[3] C. Moser, M. van Gennip, T. Bjarnsholt, H. Calum, P.O. Jensen, B. Lee, O. Ciofu, M. Givskov, S. Molin, N. Hoiby, *International Journal of Antimicrobial Agents*, **29** (2007) S40-S41

[4] G. Reid, C. Tieszer, *International Biodeterioration & Biodegradation*, **34** (1994) 73-83

[5] Y.H. An, R.J. Friedman, *Journal of Biomedical Materials Research*, **43** (1998) 338-348

[6] R. Van Houdt, C.W. Michiels, *Research in Microbiology*, **156** (2005) 626-633

[7] M.J. Vieira, I.A. Pinho, S. Giao, M.I. Montenegro, *Biofouling*, **19** (2003) 215 - 222

[8] T.A. Camesano, Y. Liu, M. Datta, *Advances in Water Resources*, **30** (2007) 1470-1491

[9] J.E.B. Randles, *Faraday Discussions of the Chemical Society*, **1** (1947) 11-19

[10] L. Yang, Y. Li, C.L. Griffis, M.G. Johnson, *Biosensors and Bioelectronics*, **19** (2004) 1139-1147

[11] E. Barsoukov, J.R. Macdonald, eds. *Impedance Spectroscopy: Theory, Experiment, and Applications*. New Jersey, John Wiley & Sons (2005)

[12] H. Fricke, *Philosophical Magazine*, **7** (1932) 310-318

[13] W.H. Mulder, J.H. Sluyters, T. Pajkossy, L. Nyikos, *Journal of Electroanalytical Chemistry*, **285** (1990) 103-115

[14] E. Katz, I. Willner, *Electroanalysis*, **15** (2003) 913-947

[15] H.P. Schwan, *Advances in Biological and Medical Physics*, **5** (1957) 147-209

[16] C.L. Davey, H.M. Davey, D.B. Kell, *Bioelectrochemistry and Bioenergetics*, **28** (1992) 319-340

[17] D. Gingell, "*Cell contact with solid surfaces*". R. Glaser, D. Gingell (Eds). Biophysics of the Cell Surface. New York, Springer (1990)

[18] R. Ehret, W. Baumann, M. Brischwein, A. Schwinde, K. Stegbauer, B. Wolf, *Biosensors and Bioelectronics*, **12** (1997) 29-41

[19] R. Holzel, *Biochimica et Biophysica Acta (BBA) - Molecular Cell Research*, **1450** (1999) 53-60

[20] M.T. Madigan, J.M. Martinko, J. Parker, *Brock Biology of Microorganisms*. Hertfordshire, U.K., Prentice Hall International (1997)

[21] R. Firstenberg-Eden, J. Zindulis, *Journal of Microbiological Methods*, **2** (1984) 103-115

[22] K. Futschik, H. Pfützner. *Electrode and Media Impedance for Detection and Characterization of Microorganisms*. in *Proceedings of the RC IEEE-EMBS & 14th BMESI*. 1995

[23] A.T.A. Jenkins, R. ffrench-constant, A. Buckling, D.J. Clarke, K. Jarvis, *Biotechnology Progress*, **20** (2004) 1233-1236

[24] A.J. Bard, L.R. Faulkner, *Electrochemical Methods: Fundamentals and Applications*. New York, John Wyley & Sons (2001)

CHAPTER 5: MONITORING OF THE BIOFILMS GROWTH ON METALLIC SURFACES USING ELECTROCHEMICAL IMPEDANCE SPECTROSCOPY

CHAPTER 5: MONITORING OF THE BIOFILMS GROWTH ON METALLIC SURFACES USING ELECTROCHEMICAL IMPEDANCE SPECTROSCOPY

This Chapter describes the use of an electrochemical technique, particularly Electrochemical Impedance Spectroscopy (EIS), for the real-time monitoring of the formation of bacterial biofilms on the surface of gold and platinum electrodes. *Pseudomonas putida* (*P. putida*) was chosen as model bacteria for biofilm formation. Briefly, the total measured interface capacitance, C_i, the parameter of the electrical circuit which modelled the electrode-solution interface, and the biofilm capacitance, $C_{biofilm}$, which modelled the biofilm, were both found to be sensitive to the biofilm growth. EIS measurements were discussed regarding Confocal Microscopy, Electronic Microscopy and Optical Microscopy imaging. In this Chapter, the biofilm removing and detaching capacity of peroxides, acid/bases and alcohol solutions has been evaluated using EIS. This work has been partially published in *Sensors and Actuators B: Chemistry* (Annex III)[1] and recently accepted for publication in *Electrochimica Acta* (Annex IV)[2].

5.1 INTRODUCTION

Bacteria biofilms are complex heterogeneous structures of cells grouped in a hydrated extracellular matrix[3, 4]. This construction provides several advantages to bacteria, especially in terms of nutrient uptake and protection against toxic agents (e.g. disinfectants and antibiotics)[5]. Their high resistance against toxic agents is particularly critical both in the clinical field, where biofilms can cause persistent infections of medical devices such as urinary catheters or the development of important diseases[6, 7], and in the environmental monitoring by the formation of resistant biofilms on the surface of water distribution network pipes[8].

The mechanism of biofilm formation includes different steps, which depend on the specific bacteria[9]. One of the most studied bacteria in this field, principally for their huge capacity to build thick and stable biofilms rapidly, is *Pseudomonas*. *Pseudomonas* is a Gram-negative rod bacterium, motile by means of a single polar flagellum, that causes several opportunistic human infections, mainly in the respiratory system[3, 10]. In the last 10 years, research studies performed on *Pseudomonas* biofilm formation on abiotic surfaces (e.g. glass and plastics) have revealed that biofilm formation proceeds through discrete steps: initial attachment, the formation of mature biofilms and ultimately dispersion, where a subpopulation of the community swims away from the mature biofilm, reinitiating the cycle (Fig. 5.1)[11]. These studies have also demonstrated a couple of important points. The first is that, in many cases, the biofilm culturing conditions can influence the requirement of a particular factor. For example, the requirement of the single polar flagellum for initial adherence to a surface depends upon the carbon source on which *Pseudomonas* is growing[12]. The second important point is that biofilm formation can be a fairly complex process with subpopulations within the community carrying out different behaviours that contribute to the final biofilm structure. It is not simply just bacteria attaching to a surface and multiplying. Several groups have demonstrated that *Pseudomonas* is capable of forming two general types of biofilms in the laboratory based on their structure[11]. A 'flat' biofilm is characterized by a relatively confluent, uniform community of bacteria on the surface (Fig. 5.1). A

'structured' biofilm consists of cell aggregates or 'mushrooms' separated by channels or spaces (Fig. 5.1).

Fig. 5.1 depicts stages in the formation of flat and structured biofilms. Initial attachment involved adherence of free-swimming cells to the surface. In the case of structured biofilms, Kirisits and Parsek presented two alternative routes to their formation[11]. The first was called 'Structured Biofilm I'. In the illustration, blue cells represent the immobile 'stalks' of structured biofilms, while red cells represent the motile subpopulation that produced the 'cap' as described by Klausen et al.[12]. The second was called 'Structured Biofilm II'. In that case, small cell aggregates grew clonally, forming large cell aggregates consisting of cells primarily derived from cells in the small cell aggregates. This was indicated by the large aggregate of blue cells in the figure, indicating that the cells in aggregate were progeny derived from the initial small aggregates. Finally, cells could actively leave the biofilm to reinitiate the cycle in a process called dispersion or detachment.
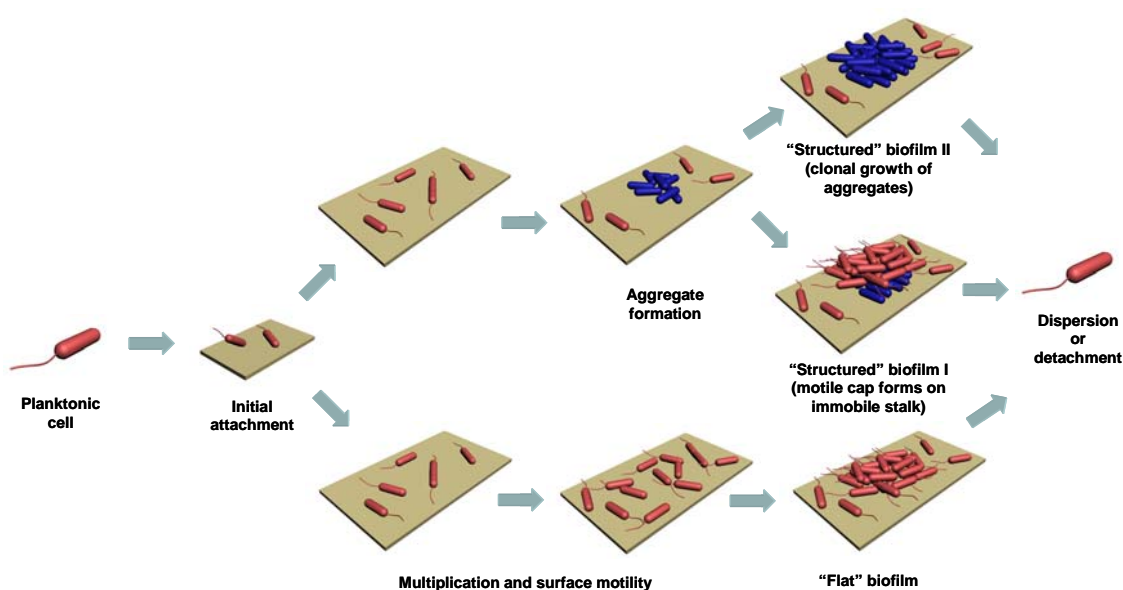
Fig. 5.1 Models for biofilm development in *Pseudomonas*.

The monitoring of biofilm formation has been attempted by combining gravimetric (Electrochemical Quartz Crystal Microbalances, EQCM), optical (Confocal Scanning Laser Microscopy, CSLM) and electrochemical techniques (amperometry)[13]. The main disadvantage of these techniques is however that it can be difficult to integrate them in a

flow system for the real-time monitoring of the biofilm growth. This Chapter describes the use of the EIS both for the direct monitoring of the biofilm formation on the electrode surface and for the evaluation of the biofilm detachment efficiency of strong acids and bases, ethanol and peroxide solutions.

5.2   EXPERIMENTAL

This Section details the experimental protocols and conditions used in the monitoring of bacterial biofilms formation with special attention to the EIS measurements. The equipment and experimental conditions used for growing bacteria are exposed. Finally, the reagents and the solutions evaluated in the biofilm removal and detachment are also included. Optical Microscopy, Epifluorescence Microscopy and CSLM imaging were made as detailed in Chapter 3.

5.2.1   Characterization of the Pseudomonas biofilm growth on platinum and gold electrodes using EIS

The gold and platinum working electrode / counter electrode (WE / CE) chips, described in Chapter 3 (Section 3.2.1), were aseptically introduced into a glass reactor containing a fresh bacterial culture, prepared as indicated below (Fig. 5.2).

Fig. 5.2 Image of three WE / CE chips inside the glass reactor.

Electrodes were kept in the reactor between 6 and 8 days to allow bacterial colonization. During the colonization process, the WE / CE chips were impedimetrically measured every 12-24 h (depending on the experiment). Before measurement, sensors were washed with sterile electrolyte solution to remove weakly attached compounds from the electrode surface. The optimum cleaning time was found to be between 10 and 15 min, as shown in Fig. 5.3.

After 10 min of cleaning, the WE / CE chips were introduced in the electrochemical cell, which also contained an external Ag|AgCl reference electrode (RE), and impedimetrically measured under the experimental conditions described in Chapter 3 (Section 3.3.1). The electrochemical cell was thermostatically kept at 25 ℃. Measurements were made in a sterile electrolyte solution, principally Phosphate Buffered Saline (PBS), to avoid osmolarity problems with the biofilm cells.
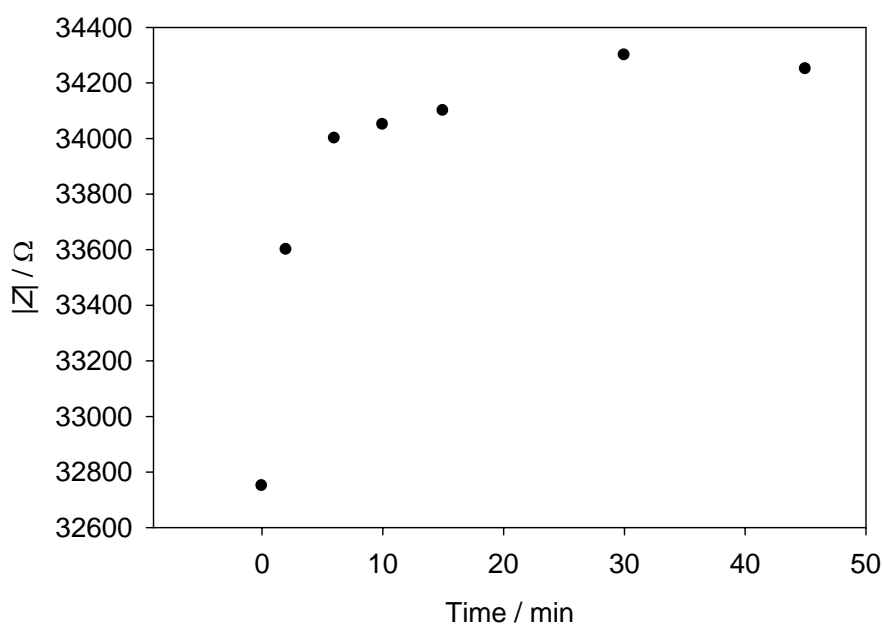
Fig. 5.3 Representation of the variation of the impedance modulus ($|Z|$) with the cleaning time.

5.2.2 Bacterial strains and culture conditions

For the stock culture preparation, *P. putida* was grown overnight in AB Minimal Medium (ABMM) at the room temperature (22 ℃, approximately). An aliquot of 50

mL was inoculated into a 500 mL glass reactor containing ABMM with glucose as carbon source. Bacteria were grown under constant agitation [MR 2000 (Heidolph, Germany)] and aeration [BioFlo (New Brunswick Scientific, New Jersey, USA)] (Fig. 5.4). After the inoculation, no nutrients were added into the reactor (batch process). These conditions (turbulent stirring and lack of nutrients) favoured the formation of biofilms[5]. All of the manipulations were performed under sterile conditions.
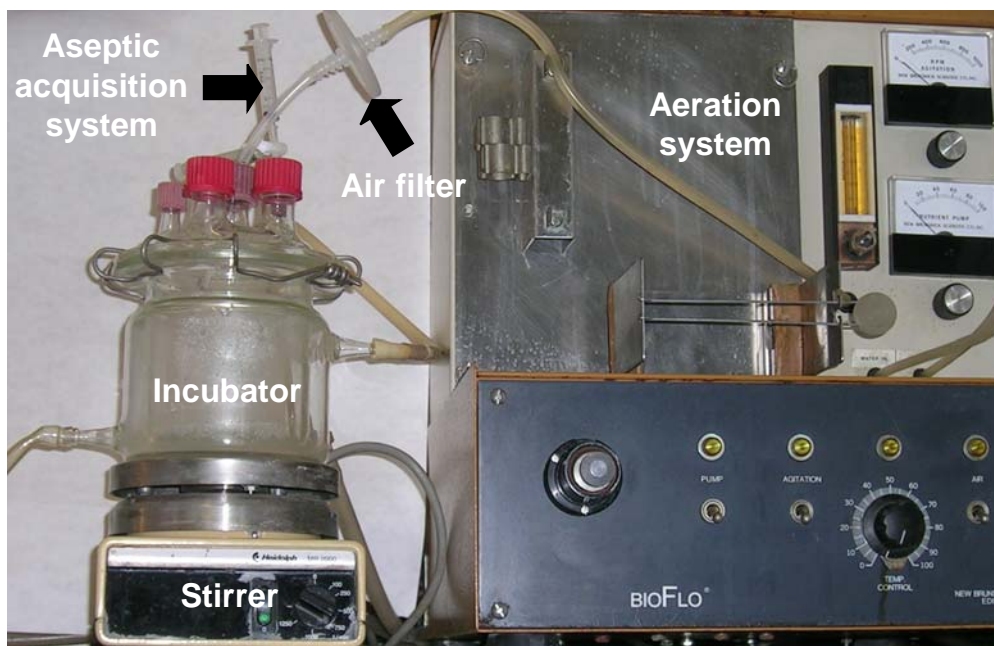
Fig. 5.4 Image of the glass reactor, the stirrer and the aeration system used for growing bacteria in controlled experimental conditions.

5.2.3 Reagents and solutions for the biofilm detachment and elimination

The biofilm detachment and elimination from the electrode surface was attempted by using 30 % H_2O_2 (Sigma-Aldrich, Switzerland), the combination of 3 M H_2SO_4 and 1 M NaOH or 96 % ethanol (Panreac, Spain) to evaluate the capacity of peroxides, hard acids and bases or alcohols to eliminate the different compounds of the structure of biofilms.

5.3 RESULTS AND DISCUSSION

5.3.1 Fitting and interpretation of impedance spectra

Z-View software was used to fit EIS data to a modification of the equivalent circuit previously proposed by Liu for corrosion studies[14]. This circuit, shown in Fig. 5.5, was composed of a resistance which modelled the solution, R_S, the biofilm capacitance, $C_{biofilm}$, the resistance of the biofilm pores, $R_{biofilm}$, the double layer capacitance, which appears as the interface Constant Phase Element, CPE_i, the charge-tranfer resistance, R_{CT}, and an extra capacitance of small magnitude (some nF) associated with the presence of an external reference, C_{Ref}, whose value did not vary with the biofilm growth. The use of the CPE_i instead of a conventional double layer capacitance has been discussed previously in Chapter 4 (Section 4.3.1).
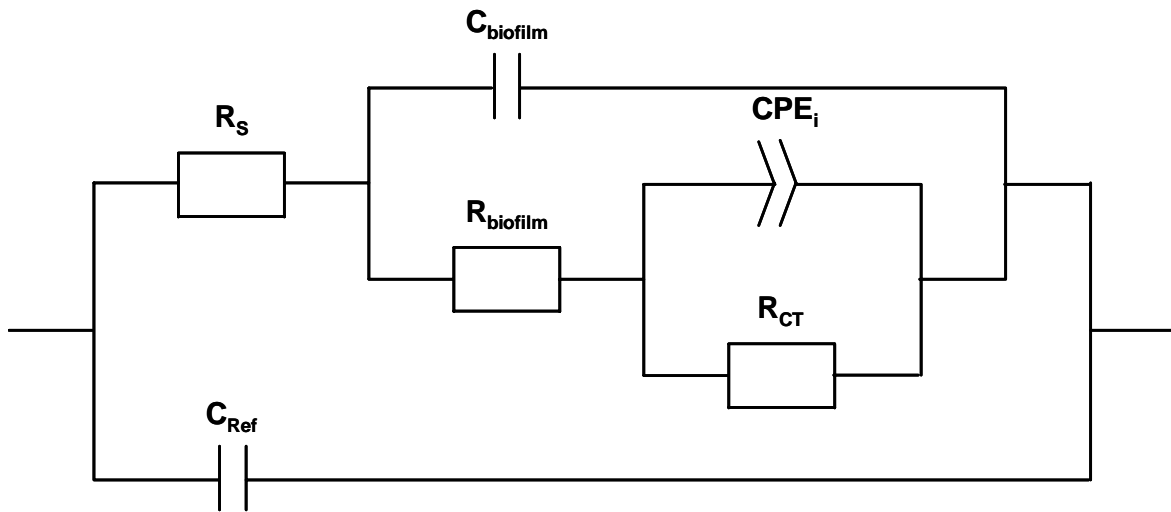
Fig. 5.5 Representation of the equivalent circuit used for fitting EIS spectra, which contains the R_{Ref}, the R_S, the $C_{biofilm}$, the $R_{biofilm}$, the CPE_i and the R_{CT}.

Fig. 5.6 shows the changes in the EIS spectra associated to biofilm formation. The magnitude of the CPE_i (shown in the figure as *Ki-T*), and the $C_{biofilm}$ were found very sensitive to the biofilm growth and maturation.

1 day biofilm	6 days biofilm

Element	Freedom	Value	Error	Error %
Cref	Free(+)	4.8426E-10	1.7441E-11	3.6016
Rs	Free(+)	486	2.1046	0.43305
Cbiofilm	Free(+)	3.3008E-08	6.6386E-10	2.0112
Rbiofilm	Free(+)	446.9	14.816	3.3153
Rct	Fixed(X)	1.5416E07	N/A	N/A
Ki-T	Free(+)	5.3212E-07	3.3633E-09	0.63206
Ki-P	Free(+)	0.76705	0.0011431	0.14903

Element	Freedom	Value	Error	Error %
Cref	Free(+)	4.4295E-10	1.0596E-11	2.3921
Rs	Free(+)	475.5	1.2874	0.27075
Cbiofilm	Free(+)	3.5266E-08	5.2666E-10	1.4934
Rbiofilm	Free(+)	380.7	9.5913	2.5194
Rct	Fixed(X)	1.5416E07	N/A	N/A
Ki-T	Free(+)	3.0174E-07	1.1456E-09	0.37966
Ki-P	Free(+)	0.81638	0.00088745	0.10871

Fig. 5.6 Admittance complex plane plot for *P. putida* biofilms after 1 and 6 days of incubation. The EIS spectra (points in the plot) were fitted to the equivalent circuit previously shown. The ideal EIS spectra obtained from the fitting (red line in the plot), the calculated values and errors using the *Z-View* software for each element of the equivalent circuit are also shown. The spectrum corresponding to the electrode before the introduction in the bacterial incubator is also included in each plot as control (blue line).

5.3.2 Effect of the biofilm formation when measured by EIS

P. putida made thick biofilms on the WE / CE chips surface quickly and easily. The effect of the biofilm formation on the electrode surface was measured using EIS as previously detailed. The most relevant results from the fitting are given in Fig. 5.7 and Fig. 5.10. The CPE$_i$ magnitude (K_i) and the $C_{biofilm}$ changed as a function of the attachment time.
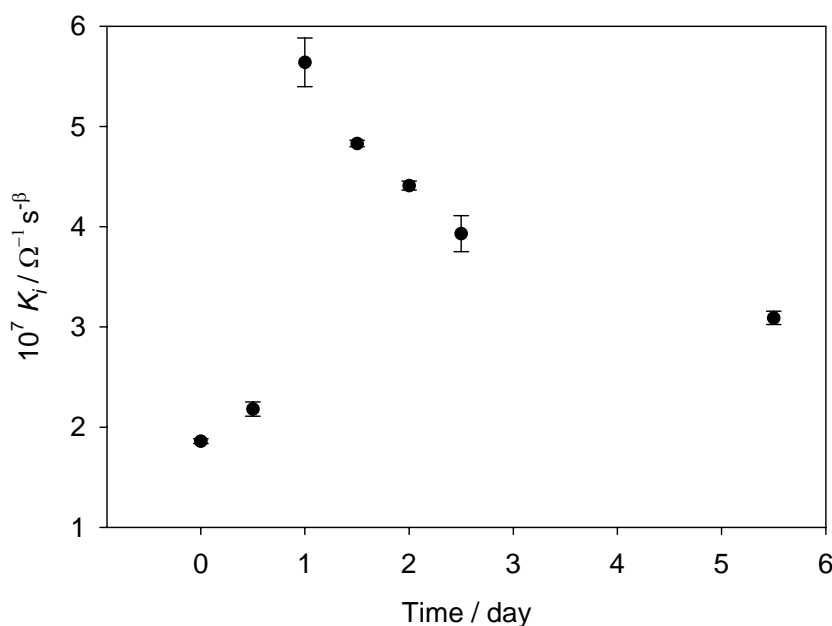
Fig. 5.7 Representation of K_i versus the incubation time during the formation of *P. putida* biofilms on the platinum WE / CE chips. This plot illustrates the changes caused by the biofilm growth in the CPE$_i$.

In Fig. 5.7, the K_i showed a pronounced early increase followed by a deep decrease. This behaviour coincided with that found by the early bacteria attachment when using platinum electrodes (Chapter 4). In that case, a pronounced early increase in CPE$_i$ was also observed prior to the massive attachment of bacteria, which decreased the CPE$_i$ later. The initial increase in CPE$_i$ was thought to be caused by the decrease in the Debye length at the electrode double layer for the attachment of single bacteria, behaving as simple charged colloidal particles, with their counter-ions.

Further, some compounds, basically salts, were found precipitated on the electrode surface during the initial biofilm formation steps (Fig. 5.8), which also involved an increase in the CPE_i magnitude.
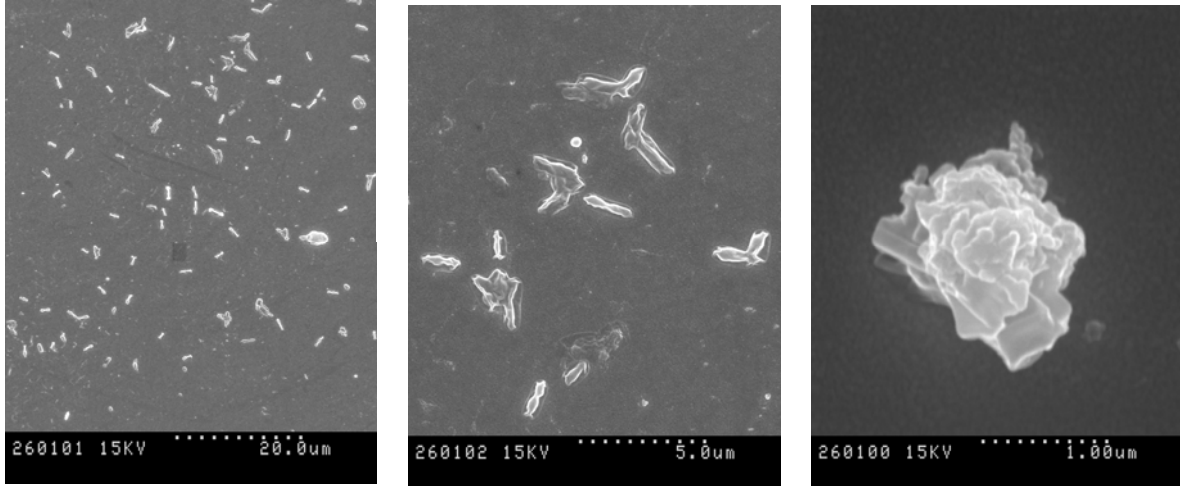
Fig. 5.8 Electronical Microscopy images of the surface of WE / CE chips in the initial steps of the biofilm formation. On the left, an overview of the particles attached to the electrode surface: cells (magnified in the middle), bacteria debris, precipitated compound (magnified on the right), etc.

On the other hand, the decrease in CPE_i could be associated to different processes, being the decrease in the area, A, of bare electrode the principal mechanism, since:

$$C = \frac{\varepsilon_o \varepsilon_r A}{d} \tag{5.1}$$

C is the capacitance magnitude (in F), ε_0 is the vacuum permittivity (in F m^{-1}), ε_r is the relative static permittivity and d is the distance between charged layers (in m). Following the discussion exposed in Chapter 4, the total measured CPE_i, C_i, capacitive in nature, can be considered to be the sum of the bare electrode capacitance, C_{Pt}, and the capacitance of the molecules composing the attached biofilm, C_{BC}, modulated by a time-dependent coverage factor, $\theta(t)$:

$$C_i = \theta(t) C_{BC} + (1 - \theta(t)) C_{Pt} \tag{5.2}$$

As shown in Fig. 5.9, bacteria biofilms attached to platinum and gold surfaces are heterogeneous structures basically composed of bacteria and exopolysaccharides, which generated capacitances of lower magnitude than C_{Pt}. For instance, the capacitance of bacteria commonly appeared to be smaller than pF[15], whereas the C_{Pt} was found experimentally to be of hundreds of μF. Thus, the CPE$_i$ would fall as bacteria and exopolysaccharides attached to the surface, as observed in Fig. 5.7.
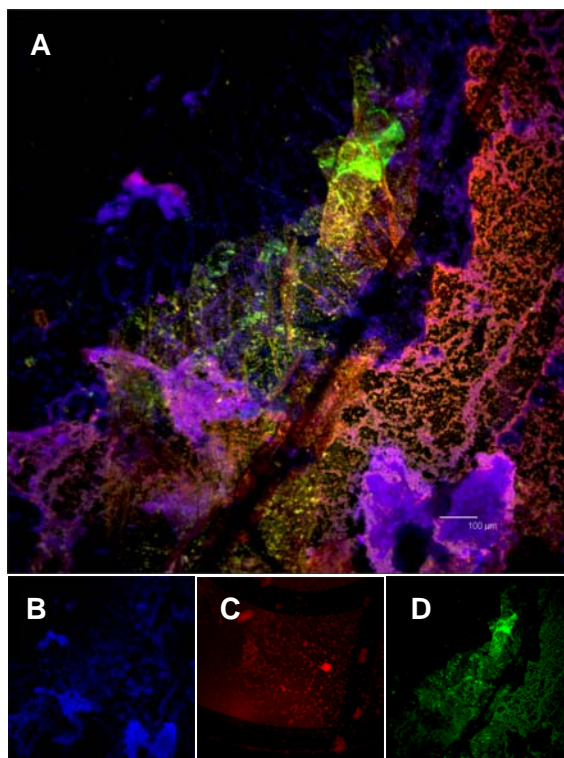
Fig. 5.9 (A) Confocal image of the heterogeneity of a mature biofilm growth on the surface of WE / CE chips. In this case, cells were stained with (B) 4'-6-DiAmidino-2-Phenylindole (DAPI) and the polysaccharides with (C) WGA and (D) concabalina A.

On the other hand, the magnitude of $C_{biofilm}$ increases with the biofilm growth, as shown in Fig. 5.10. Similarly, in a separate study focused on the optimization of the thickness of a polypyrrole coating for the measurement of the mixed response of sodium, potassium and ammonium using EIS and Artificial Neural Networks (ANNs), it was reported that the coating capacitance, C_C (here defined as $C_{biofilm}$) increased with the polymer growth[16]. The C_C (in F) was also found to be sensitive to the coating permittivity, ε_C, the coating area, A_C (in m^2) and the coating thickness, d_C (in m), as follows:

$$C_C = \frac{\varepsilon\,\varepsilon_C A_C}{d_C} \qquad\qquad (5.3)$$

According to Amidurin et al.[17], during the coating growth, the polymer capacitance was basically influenced by the amount of water or electrolyte solution retained inside the coating (that basically modified the coating permittivity), which mainly depended on the polymer porosity. Thus, the increase in C_C was attributed to the increase of the polymer porosity. Following the same reasoning, the increase in the biofilm porosity (or the increase of water inside the biofilm structure) during its growth appeared to be the responsible of the recorded increase in the $C_{biofilm}$ magnitude.
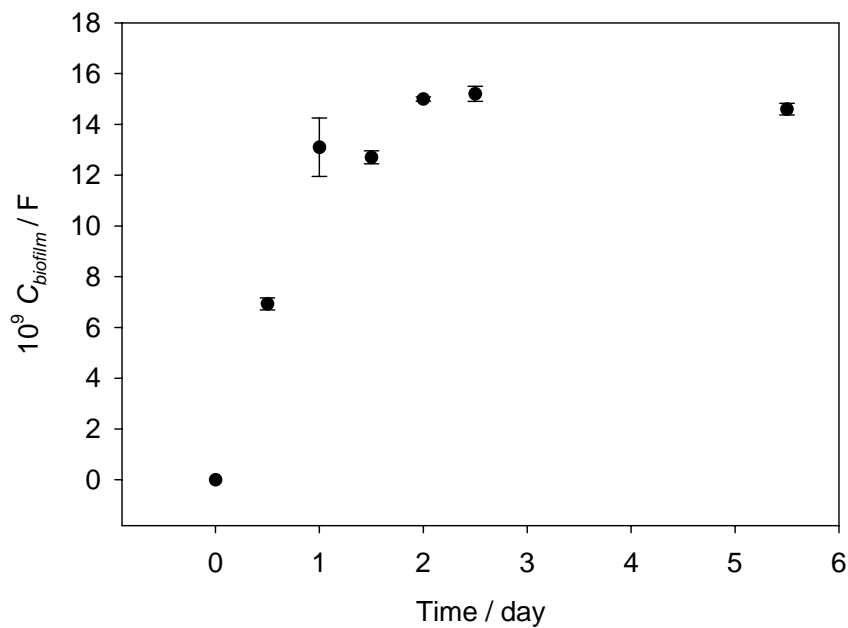
Fig. 5.10 Representation of the magnitude of the $C_{biofilm}$ versus the incubation time during the biofilm formation process on platinum WE / CE chips. This plot illustrates the changes caused by the biofilm formation in the $C_{biofilm}$.

The change in the $C_{biofilm}$ with the biofilm growth was compared with the average of the thickness of the biofilm at that time. The thickness of the biofilm was measured using CSLM as detailed in the Chapter 3 (Section 3.3.4). *P. putida* biofilms were found to progressively increase its thickness from 22 ± 5 μm, for a 2 days biofilm, to 58 ± 2 μm for a 7 days mature biofilm, when they stabilized. The initial steps of biofilm formation

showed correlation between impedance measurements and the biofilm thickness, probably because of the increase of water inside the biofilm structure, as previously exposed. When the thickness exceeded a value around 30 μm (after 3 days growing in a WE / CE chip), the $C_{biofilm}$ lost the correlation with the increase of the biofilm. Although this fact is currently under discussion, the equilibrium between the effect of the increasing thickness of the biofilm (which, regarding Eq. 5.3 should decrease the $C_{biofilm}$) and the increase of water inside the biofilm structure (which should increase the $C_{biofilm}$, considering Eq. 5.3) may be the most plausible cause.

5.3.3 Comparison between new and reused WE / CE chips when monitoring the biofilm formation using EIS

The effect of the biofilm formation on new (sensors not previously activated nor used) and reused chips (sensors used in other EIS assays or previously activated) was measured using EIS, as previously detailed. The most relevant results from the fitting are given in Fig. 5.11 and Fig. 5.12. The K_i changed as a function of the attachment time in both cases, although some differences between new and reused chips were registered, particularly at the initial steps of the biofilm formation.
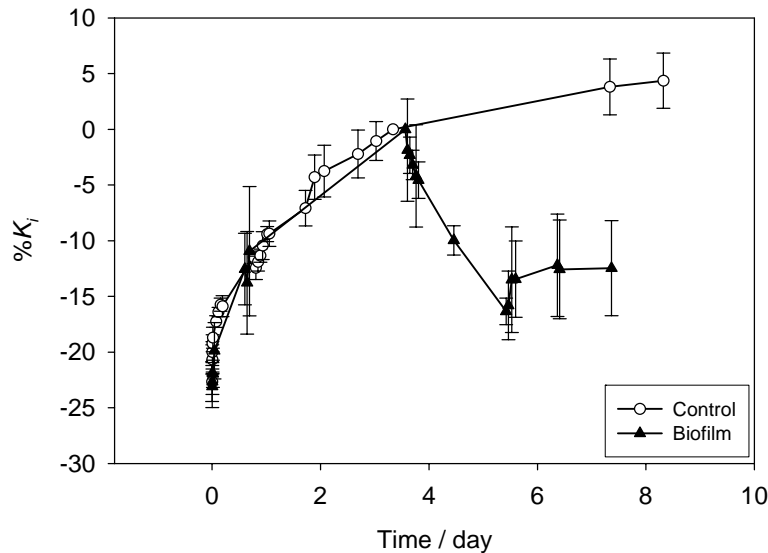
Fig. 5.11 Representation of the normalized K_i (%$K_i(t)$) versus the time of biofilm formation by new chips.

In Fig. 5.11 and Fig. 5.12, the change in K_i was normalized, as shown in Eq. 5.4. $K_i(t)$ is the value of the CPE at time t after the introduction of the WE / CE chip in the incubator and $K_i(3.5)$ is the value of the CPE after 3.5 days of biofilm formation. The %$K_i(t)$ was calculated using the following expression:

$$\% K_i(t) = \frac{\left(K_i(t) - K_i(3.5)\right)}{K_i(3.5)} \times 100 \qquad (5.4)$$

New chips immersed in culture media with or without bacteria showed an initial increase in the CPE_i magnitude for two days and a half. After this, the common decrease in CPE_i was recorded by chips immersed in bacterial cultures (Fig. 5.11). As shown in previous Sections, some compounds, basically salts which could not be eliminated by the cleaning process, were also found precipitated on the electrode surface during the initial biofilm formation steps (Fig. 5.8). This salt precipitation may involve an increase in the CPE_i magnitude.

Although the *real* cause is currently under discussion, another process may be the principal cause of this initial increase in CPE: a surface activation process. In general, new sensors were found to present debris parasitizing its surface and decreasing their active area. Activation through electrochemical cycling or certain EIS measurements were found to be enough to progressively remove these attached substances and to increase the electrode active area. In fact, chips immersed in non-bacterial solutions showed that the activation process may not finished after 2 days and a half but their impedance magnitude continued increasing.

On the other hand, reused chips showed a constant CPE_i value until the common decrease caused by the biofilm formation was recorded (Fig. 5.12). This means that any changes observed in the active area of reused chips (which had already undergone the activation process), reflected by their impedance, could be observed and related to the biofilm formation on the chip.

When immersed in bacterial cultures, both new and reused chips showed similar impedimetric responses to the biofilm growth. After 6 days of incubation, mature

biofilms were found grown in both chips with a comparable disposition of bacteria (Fig. 5.13).
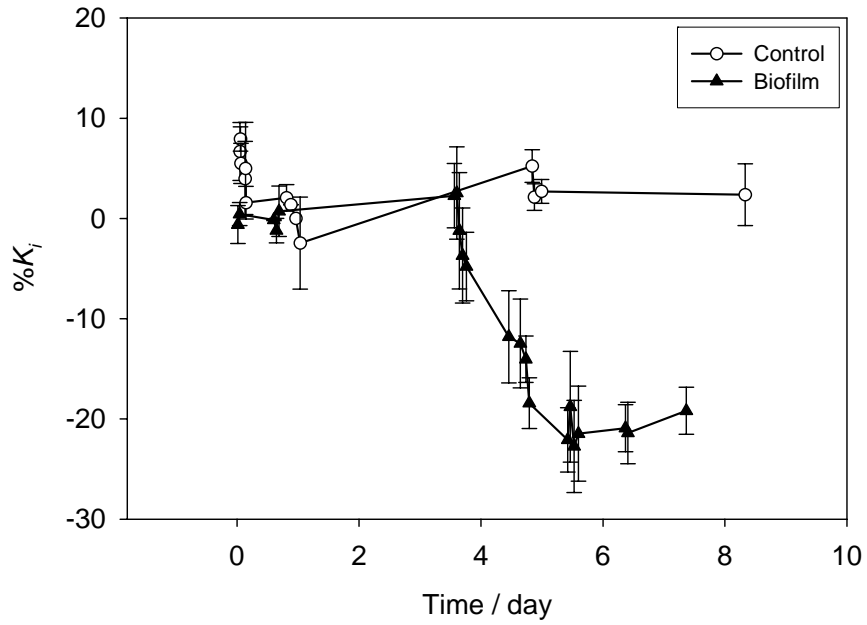
Fig. 5.12 Representation of the *%$K_i(t)$* versus the time of biofilm formation by reused chips.
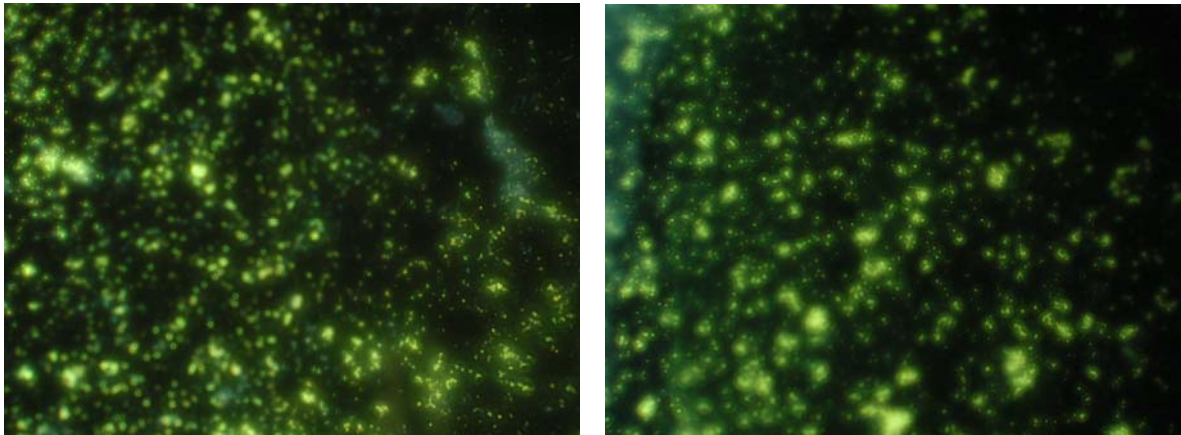
Fig. 5.13 Images of mature biofilms grown on the surface of new (left side) and reused (right side) WE / CE chips. The green points correspond to attached bacteria stained with DAPI.

5.3.4 Protocol for the elimination of mature biofilms attached to the WE / CE chips

The removal and detachment of mature biofilms from the surface of WE / CE chips was attempted using peroxide, strong acid and bases and alcoholic solutions. It has to be noted that after the cleaning process the electrodes did not completely recover their initial properties and their life-time was critically reduced. Each one of the previously enumerated solutions was found to be essential in the cleaning process for removing specific compounds attached to the electrode.

Peroxide solutions, particularly 30 % H_2O_2, were found to be the most effective solutions in the detachment of mature biofilms from the electrode surface. Experimental results showed that rinsing for 20 min was enough to remove the biofilm from gold WE / CE chips quantitatively. This time could be reduced to 10-15 min using platinum WE / CE chips. The irreversible attachment of bacteria and particles (especially proteins) containing thiol groups to the gold surface may be the principal cause of this difference in the removing time. This solution was always used in the first step of the cleaning protocol.

Strong acids and bases were used in the second step of the protocol to dissolve precipitated salts, when it was necessary. The combination of 3 M H_2SO_4 followed by 1 M NaOH removed this particles after 20 min of rinsing (10 min per solution).

As it was observed in Chapter 4 (Section 4.2.1), the hydrogen peroxide solution damaged the coating used for isolating the connection of the chip from the solution and coating fragments were found attached to the electrode surface. These fragments were eliminated by cleaning with 96 % v/v ethanol, which also sterilized the electrodes.

Next, the ethanol traces were eliminated by cleaning with distilled water. Electrodes were finally dried in a nitrogen stream and stored in suitable conditions.

5.4   CONCLUSIONS

In this Chapter, EIS has been used for the monitoring of biofilm formation on WE / CE chips. The $C_{biofilm}$ and the CPE_i have been found to be sensitive to the biofilm growth and maturation, especially in the initial stages of development. Impedance results have been well correlated with Electronic, Epifluorescence and Confocal Microscopy images. Also the biofilm thickness (from CSLM) in the initial steps of the growth has shown coincidence with impedance data. In terms of biofilm removal and detachment, peroxides have shown to be the most effective detaching solutions, although strong acid and basic and alcoholic solutions are also needed to remove specific particles which can be found attached to the WE / CE chips.

5.5 REFERENCES

[1] X. Muñoz-Berbel, F.J. Muñoz, N. Vigués, J. Mas, *Sensors and Actuators B: Chemical*, **118** (2006) 129-134

[2] X. Munoz-Berbel, C. García-Aljaro, F.X. Munoz, *Electrochimica Acta*, (Accepted)

[3] J.W. Costerton, P.S. Stewart, E.P. Greenberg, *Science*, **284** (1999) 1318-1322

[4] G. O'Toole, H.B. Kaplan, R. Kolter, *Annual Review of Microbiology*, **54** (2000) 49-79

[5] H.M. Lappin-Scott, J.W. Costerton, eds. *Microbial Biofilms*. Cambridge, Cambridge University Press (1995)

[6] C. Moser, M. van Gennip, T. Bjarnsholt, H. Calum, P.O. Jensen, B. Lee, O. Ciofu, M. Givskov, S. Molin, N. Hoiby, *International Journal of Antimicrobial Agents*, **29** (2007) S40-S41

[7] G. Reid, C. Tieszer, *International Biodeterioration & Biodegradation*, **34** (1994) 73-83

[8] E. van der Wende, W.G. Characklis, D.B. Smith, *Water Research*, **23** (1989) 1313-1322

[9] Y.H. An, R.J. Friedman, *Journal of Biomedical Materials Research*, **43** (1998) 338-348

[10] P.K. Singh, A.L. Schaefer, M.R. Parsek, T.O. Moninger, M.J. Welsh, E.P. Greenberg, *Nature*, **407** (2000) 762-764

[11] M.J. Kirisits, M.R. Parsek, *Cellular Microbiology*, **8** (2006) 1841-1849

[12] M. Klausen, A. Heydorn, P. Ragas, L. Lambertsen, A. Aaes-Jorgensen, S. Molin, T. Tolker-Nielsen, *Molecular Microbiology*, **48** (2003) 1511-1524

[13] A. Bressel, J.W. Schultze, W. Khan, G.M. Wolfaardt, H.-P. Rohns, R. Irmscher, M.J. Schoning, *Electrochimica Acta*, **48** (2003) 3363-3372

[14] C. Liu, Q. Bi, A. Leyland, A. Matthews, *Corrosion science*, **45** (2003) 1243-1256

[15] R. Holzel, *Biochimica et Biophysica Acta (BBA) - Molecular Cell Research*, **1450** (1999) 53-60

[16] M. Cortina-Puig, X. Munoz-Berbel, M. del Valle, F.J. Munoz, M.A. Alonso-Lomillo, *Analytica Chimica Acta*, **597** (2007) 231-237

[17] A. Amirudin, D. Thieny, *Progress in Organic Coatings*, **26** (1995) 1-28

CHAPTER 6: DETECTION OF BACTERIOPHAGES BY FOLLOWING THE DEGRADATION OF SPECIFIC BACTERIA BIOFILMS USING ELECTROCHEMICAL IMPEDANCE SPECTROSCOPY

CHAPTER 6: DETECTION OF BACTERIOPHAGES BY FOLLOWING THE DEGRADATION OF SPECIFIC BACTERIA BIOFILMS USING ELECTROCHEMICAL IMPEDANCE SPECTROSCOPY

This Chapter describes an impedimetric method for the indirect detection of bacteriophages by following the degradation of specific bacteria biofilms attached to platinum and gold working electrode / counter electrode (WE / CE) chips. *Pseudomonas putida (P. putida)* and *Escherichia coli (E. coli)* were chosen as model bacteria for biofilm formation and for the environmental interest of the detection of their bacteriophages, respectively. As a summary, the biofilm capacitance, $C_{biofilm}$, the parameter of the electrical circuit which modelled the biofilm, was found to be sensitive to the biofilm degradation as a consequence of the bacteriophage infection. Electrochemical Impedance Spectroscopy (EIS) data were discussed regarding traditional Optical and Confocal Microscopy measurements and the classical double layer agar method. This work has been partially accepted for publication in *Applied and Environmental Microbiology* (Annex V)[1] and in *Electrochimica Acta* (Annex IV)[2].

6.1   INTRODUCTION

Viruses are sub-microscopic and simple biological entities, composed of genetic material encased within a protein capsule called head or capsid. They strictly parasitize specific host cells using the machinery and metabolism of the cell to replicate themselves. Bacteriophages, viruses that infect bacteria, may have a lytic or lysogenic cycle of infection. In the lytic infection cycle, characteristic of virulent phages, bacterial cells are lysed (broken open) and destroyed after the replication of the phage. The lytic infection cycle mechanism is detailed in Fig. 6.1.

1. HOST CELL RECOGNITION   phage

1.1 Phage attachment to the bacteria surface   **1.2 Genome injection into the host**

host cell

2. ECLIPSE PERIOD

2.1 Replication of viral nucleic acid   **2.2 Late proteins biosyntesis**

3. INTRACELLULAR ACCUMULATION   **4. LYSIS AND RELEASE**

Infectious phages accumulation   **Phages release**
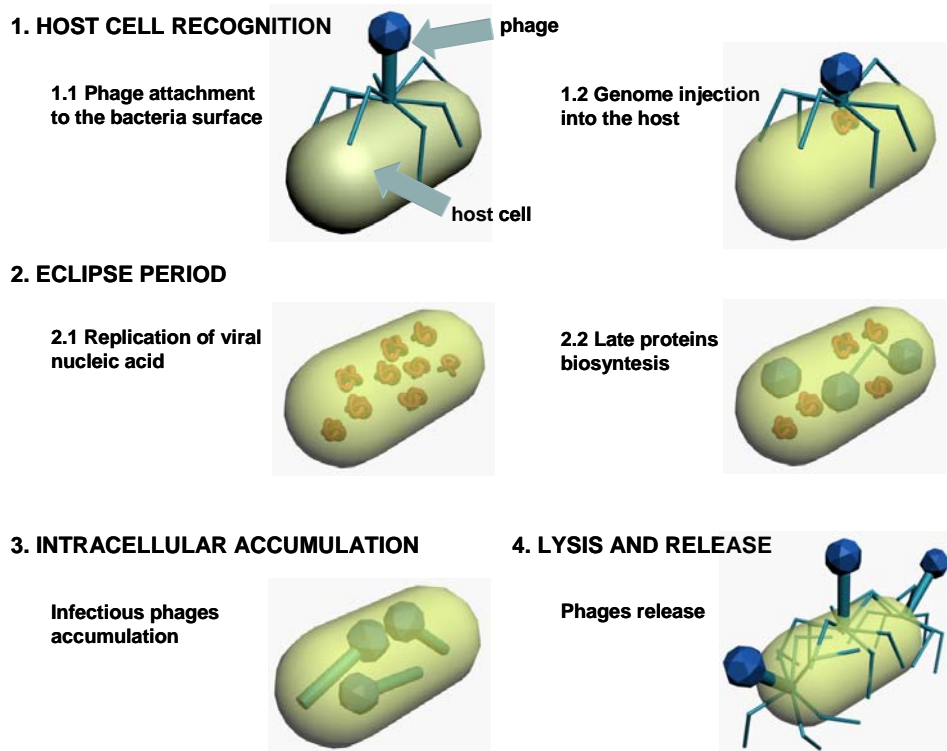
Fig. 6.1 Scheme of the typical life cycle for lytic bacteriophages.

The detection of bacteriophages is especially relevant in the environmental monitoring and food industries. On the one hand, the detection of somatic coliphages (e.g. phages infecting *E. coli*), F-RNA specific phages and bacteriophages infecting *Bacteroides* spp. has been suggested to be more reliable for predicting the contamination of viral pathogens than the typical bacterial indicator strains[3-8]. On the other hand, the detection of bacteriophages is also important because of the economic losses brought about by

them in the fermentation industry. In the fermented dairy products industry producing cheese and yoghurt, the infection and subsequent lysis of bacterial starter cultures can render a fermentation process inactive.

Rapid and real-time detection of bacteriophages is desirable in these areas, which can not be accomplished by the current available traditional methods. These methods consist basically in detecting bacteriophages by the double layer agar method where a host strain is seeded in a semi-solid agar layer. Exposure of the bacteria to bacteriophages results in the appearance of lysis zones that can be directly visualized after an appropriate incubation time, which is dependent on the bacteria, the number of which is related to the infective viral particles or viral aggregates in the original sample[9]. Despite of the emerging interest, bacteriophage detection has been given little attention and small progresses have been made during the last decades[10, 11].

The replication of bacteriophages within biofilms has been demonstrated causing biofilm degradation[12, 13]. Regarding this, the following Chapter describes an impedimetric approach based on the degradation of mature biofilms for the indirect detection of bacteriophages.

6.2   EXPERIMENTAL

This Section details the protocols and conditions used in the detection of bacteriophages following the degradation of mature biofilms. The experimental protocol for the EIS measurements is described in detail. In a microbiological viewpoint, collection and storage of the water samples containing bacteriophages is included. This Section also exposes the selection and enrichment of *P. putida* bacteriophages from raw sewage samples. The experimental conditions used for growing bacteria coincided with those previously exposed in Chapter 5 (Section 5.2.2). Optical and Confocal Microscopy imaging and bacterial quantification were made as detailed in Chapter 3 (Section 3.3).

6.2.1 Impedimetric detection of lytic bacteriophages infection following the biofilm degradation

Bacteria biofilms were grown on gold and platinum WE / CE chips and periodically monitored using EIS, as previously detailed in Chapter 5 (Section 5.2.1). Electrodes containing six days mature biofilms were transferred to 10 ml of fresh AB Minimal Medium (ABMM) or Modified Scholten's Broth (MSB)[14] culture media and inoculated with a bacteriophage stock or sewage sample 1/10 (v/v) prepared as indicated below. The electrodes were then impedimetrically measured in sterile Phosphate Buffered Saline (PBS) at 25 ºC after different incubation times, under the experimental conditions exposed in Chapter 3 (Section 3.3.1).

6.2.2 Sewage samples collection and processing

Raw sewage samples from an urban sewage treatment plant were collected and transported to the laboratory following the standard method recommended by the American Public Health Association (APHA)[15]. In the laboratory, samples were stored at -70 ºC to avoid inactivation of the bacteriophages until used[16]. Before using, frozen raw samples should be processed. In the processing stage, bacteriophages were isolated from other molecules which could interfere in the bacteriophages detection. The processing included a centrifugation step (10 min at 1000 g) and filtration with sterile 0.22 µm pore filter (Millipore Corporation, Barcelona, Spain). When detecting *P. putida* bacteriophages, an additional step was required. Viable *P. putida* bacteriophages were isolated from the filtered samples using the double layer plate method[17].

6.2.3 Bacteriophages enumeration and preparation of stock cultures

As detailed before, sewage samples from an urban wastewater treatment plant were used as source for *E. coli* and *P. putida* bacteriophages. The bacteriophages were quantified as Plaque Forming Units per mL (PFU mL) using the double layer agar plate method similar to that described by Adams[9]. The low concentration of *P. putida* bacteriophages in the samples recommended an enrichment step before the infection of

bacteria biofilms. The enrichment process was made in ABMM or MSB using the *P. putida* as host strain. All of the manipulations were performed under sterile conditions.

6.3   RESULTS AND DISCUSSION

6.3.1   *Fitting and interpretation of impedance spectra*

Z-View software was used to fit impedance data to the equivalent circuit previously described in Chapter 5 (Section 5.3.1).

6-days mature biofilm	24 hours of incubation with phages

Element	Freedom	Value	Error	Error %
Cref	Free(+)	6.2154E-10	5.2544E-11	8.4538
Rs	Free(+)	282.3	2.2169	0.7853
Cbiofilm	Free(+)	7.1278E-08	3.8285E-09	5.3712
Rbiofilm	Fixed(X)	79.03	N/A	N/A
Rct	Free(+)	72398	2655.4	3.6678
CPEi-T	Free(+)	1.8768E-06	3.7567E-08	2.0017
CPEi-P	Free(+)	0.73991	0.0042034	0.5681

Element	Freedom	Value	Error	Error %
Cref	Free(+)	7.02E-10	7.5626E-11	10.773
Rs	Free(+)	262.3	3.2416	1.2358
Cbiofilm	Free(+)	4.8414E-08	2.8621E-09	5.9117
Rbiofilm	Fixed(X)	114.4	N/A	N/A
Rct	Free(+)	3.4879E05	54797	15.711
CPEi-T	Free(+)	1.7155E-06	3.0304E-08	1.7665
CPEi-P	Free(+)	0.74272	0.0034107	0.45922

Fig. 6.2 Admittance complex plane plot before and after the incubation in phages suspensions. The experimental EIS spectra (points in the plot), the ideal EIS spectra from the fitting (line in the plot) are shown together with the initial value of the chip. Below, the calculated values and errors of each element from the fitting are shown.

Fig. 6.2 shows the changes in the EIS spectra associated to the biofilm degradation. The $C_{biofilm}$ was found to be very sensitive to the degradation of the biofilm caused by the bacteriophages infection.

6.3.2 *Evaluation of the degradation of mature biofilms by specific bacteriophages using EIS, Optical and Confocal Microscopy, and bacterial counts*

The effect of the degradation of biofilms grown on the WE / CE chips surfaces caused by specific bacteriophages was measured using EIS as previously detailed. The use of EIS for the detection of specific bacteriophages was assessed in parallel with both Optical Microscopy and CSLM, and microbial counts (in Colony Forming Units per unity of area, CFU cm^{-2}), in order to corroborate the obtained results. A six days mature *P. putida* biofilm, whose growth had been previously monitored impedimetrically, was used to elaborate a bacteriophage mediated biofilm infection model. Wastewater from the influent of an urban wastewater treatment plant was used as source of *P. putida* infecting bacteriophages. The concentration of these bacteriophages in the analysed sample was 40.5 ± 0.7 PFU mL^{-1}, which was increased up to 10^7 PFU mL^{-1} after a single enrichment step. Different concentrations of bacteriophages were assessed (10^6 and 10^7 PFU mL^{-1}) and the biofilm infection was monitored over 24 h.
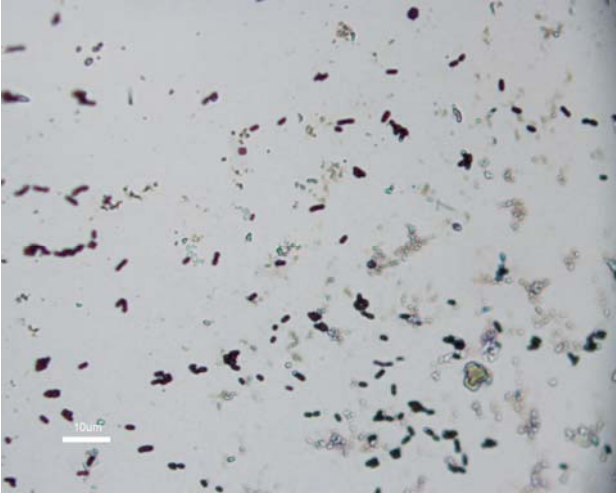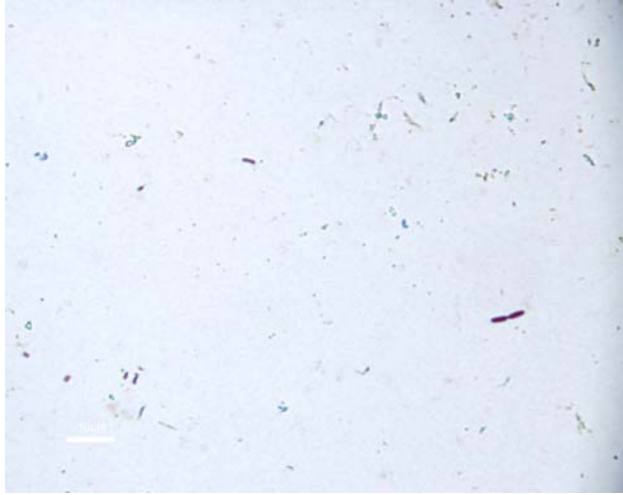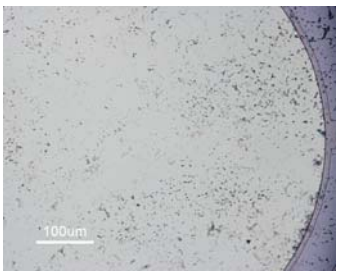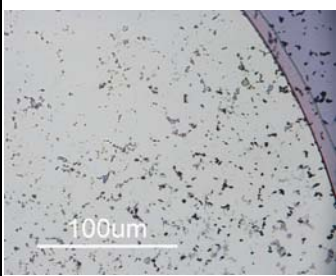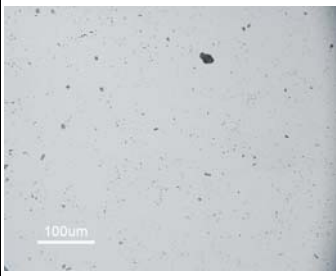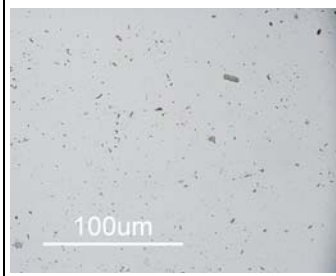
The most relevant results from the fitting are given in Fig. 6.3. In Fig. 6.3-B, the $C_{biofilm}$ changed as a consequence of the degradation of the biofilm by specific bacteriophages. On the other hand, the magnitude of the CPE$_i$ (K_i), which was also used for monitoring the biofilm formation, was found to be practically insensitive to the infection process (Fig. 6.3-A).

An explanation to this fact could be obtained by considering that the inner cells, especially those attached directly to the electrode, were more resistant to the bacteriophages infection than the superficial ones. Thus, inner cells remained attached and unaltered and the K_i did not change after the bacteriophages infection.
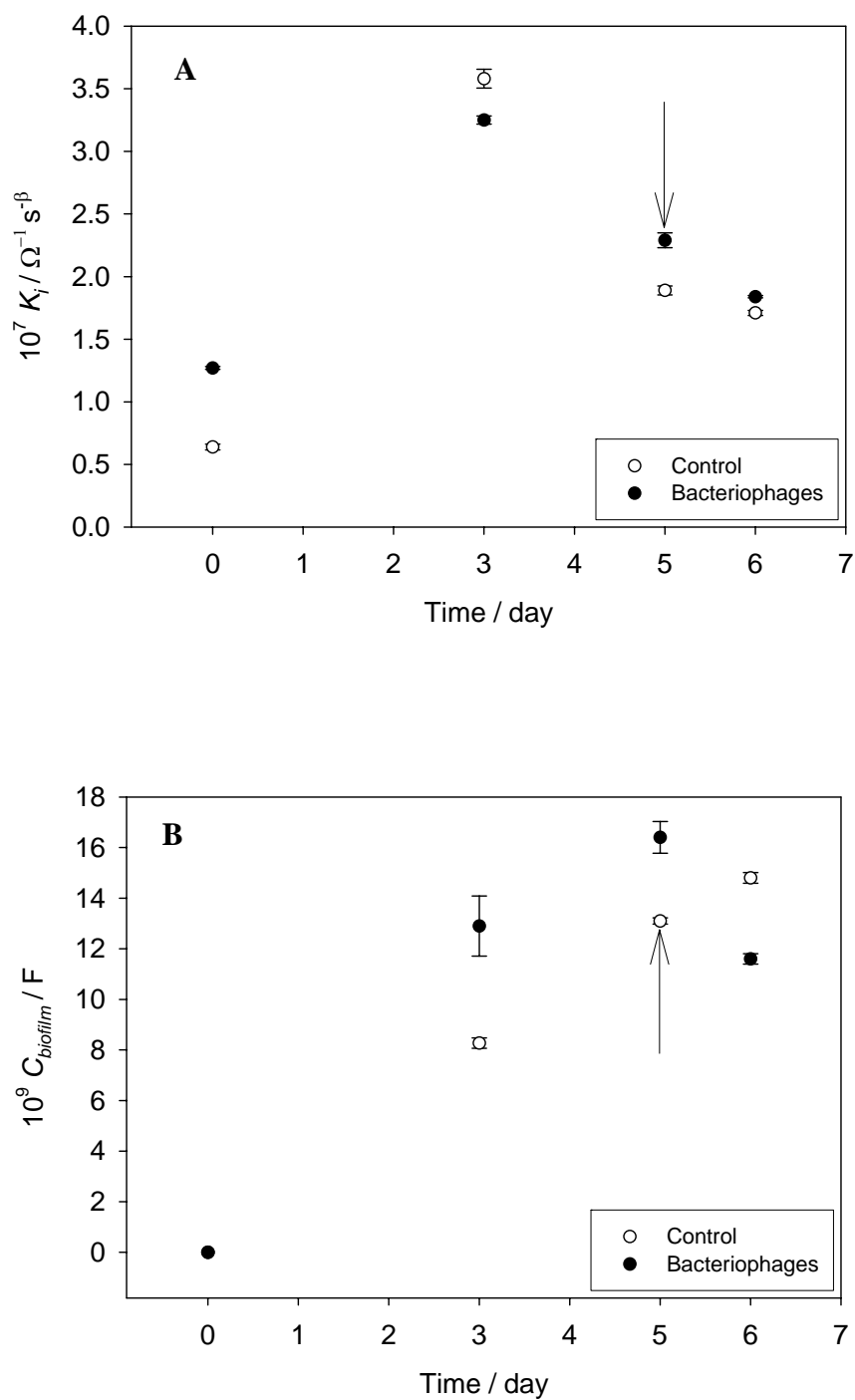
Fig. 6.3 Representation of (A) the K_i and (B) the $C_{biofilm}$ versus the time of incubation in the glass reactor (biofilm growth) and the subsequent exposure to bacteriophages (biofilm degradation). The moment when WE / CE chips were extracted from the incubator and introduced in the bacteriophages culture is indicated with a vertical arrow.

After the incubation in bacteriophages suspensions, WE / CE chips were stained and imaged using Optical Microscopy, as detailed in Chapter 3 (Section 3.3.3). Also the biofilm thickness (from CSLM) and the number of attached cells (from sonication and plating on agar) were determined and compared with control samples (the same culture media without the phages).

Control	**Bacteriophages**
31.65 ± 3.25 μm of thickness	15.94 ± 2.19 μm of thickness
4.08 ± 0.05 log (CFU mm^{-2})	3.37 ± 0.18 log (CFU mm^{-2})

Fig. 6.4 Optical Microscopy images at different magnification of WE / CE chips after overnight incubation in either ABMM with or without bacteriophages. The thickness of the biofilms and the number of attached cells per unit of area after the infection process is also included.

In Fig. 6.4, less attached bacteria were found on the chip after the incubation in bacteriophage suspensions, which could be associated to the infection process. The

biofilm thickness and the number of attached cells were also found to decrease after the bacteriophages infection by around 50 % and 20 %, respectively. The differences in the obtained percentages may be explained by considering the bacteriophages infection capacity: bacteriophages were thought to infect and lysis the most external bacteria of the biofilm easily, whereas those in the biofilm core, where cells are normally more densely grouped, became more resistant to the infection. Further, additional factors could modify the infection of biofilms by bacteriophages, for instance the presence of phage-borne polysaccharide depolymerases to degrade the extracellular matrix, in which the bacteria are immersed[18].

The decrease in $C_{biofilm}$ after 24 h of incubation was found sensitive to the initial concentration of bacteriophages. As shown in Fig. 6.5, the decrease in $C_{biofilm}$ was more pronounced when the initial concentration of bacteriophages increased.
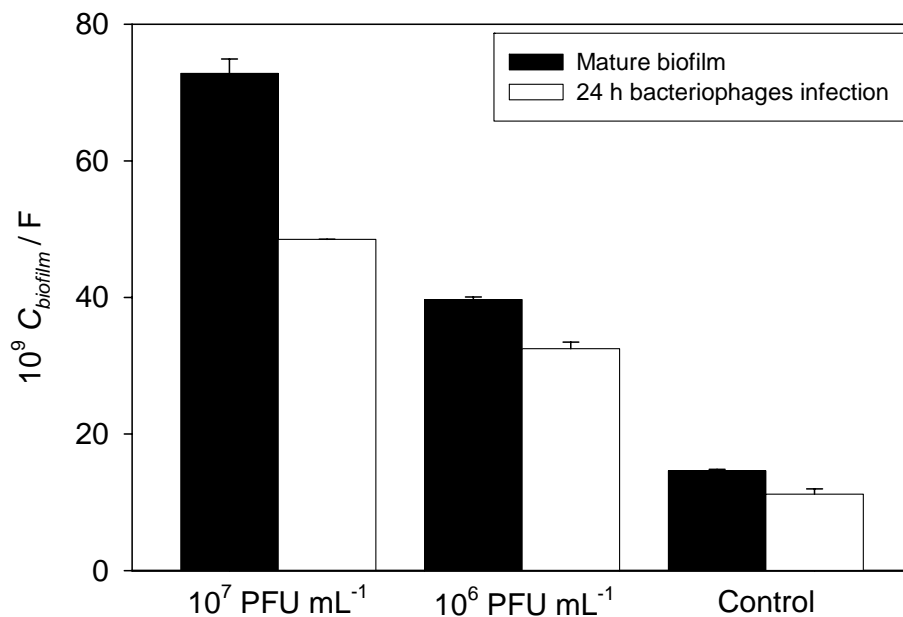
Fig. 6.5 Representation of the $C_{biofilm}$ before and after 24 h of incubation in 10^7 or 10^6 PFU mL^{-1} bacteriophages suspensions or medium without phages (control).

However, no differences were recorded in the $C_{biofilm}$ variation due to bacteriophages degradation when using a minimal (ABMM) or a rich medium (MSB) during the infection process (Fig. 6.6).
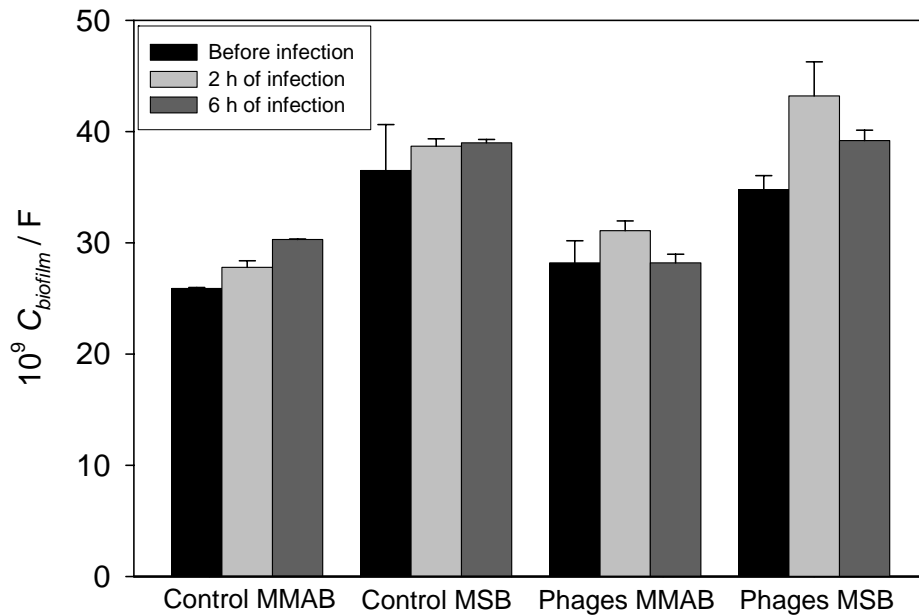
Fig. 6.6 Comparison of the initial value of $C_{biofilm}$ (before infection) with the corresponding magnitude after 2 and 6 h of bacteriophages infection in ABMM and MSB culture media. The control samples were incubated in the media without bacteriophages.

In Fig. 6.7, the variation in the $C_{biofilm}$ was monitored through the incubation time. This plot illustrates that the decrease in $C_{biofilm}$ was mainly recorded during the initial 6-8 h of infection, when the degradation of the biofilm seemed to be more intense.

In summary, the detection of changes in the $C_{biofilm}$ parameter in a mature biofilm was proved to be useful for the development of an indirect method for the detection of bacteriophages in liquid samples.
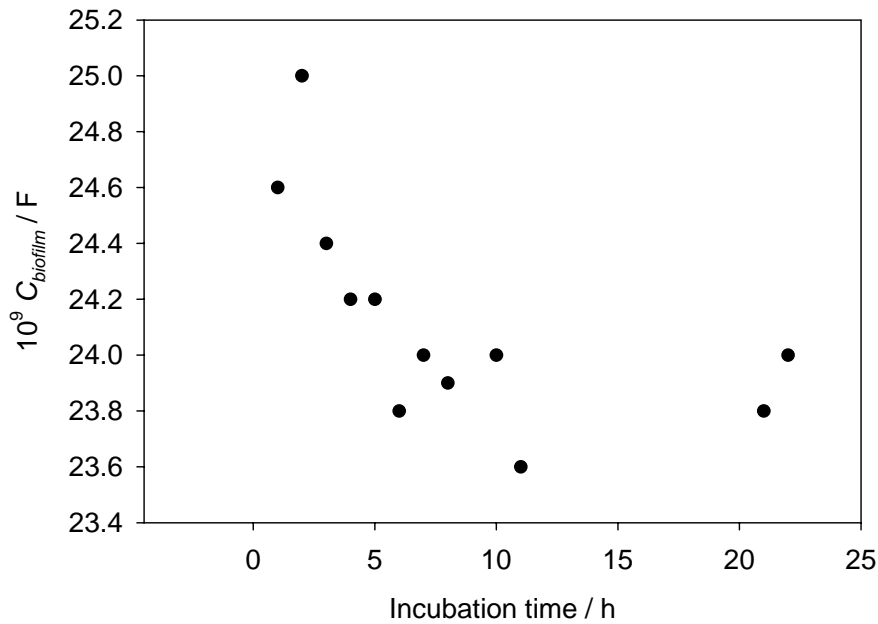
Fig. 6.7 Representation of the variation of the $C_{biofilm}$ versus the time of incubation in bacteriophage suspensions.

6.3.3 Application to real samples: detection of somatic coliphages from an urban sewage treatment plant

The impedimetric approach for detecting bacteriophages via the degradation of specific bacterial biofilms was applied to the detection of somatic coliphages from an urban sewage treatment plant. Five days mature biofilms of *E. coli* grown on WE / CE chips following the experimental conditions shown in Chapter 5 (Section 5.2.2) were used. In Fig. 6.8, the degradation of *E. coli* biofilms by specific bacteriophages from water samples was found to produce a similar response than that observed in the *P. putida* assay: the $C_{biofilm}$ significantly decreased in the sample containing bacteriophages with respect to the control sample, where no bacteriophages were present. Thus, this method, based on the degradation of mature bacteria biofilms by specific phages, was found to be sensitive to the detection of the viral contamination in water samples from a sewage treatment plant, which initially contained a concentration of somatic coliphages of around 10^4 PFU mL^{-1}.
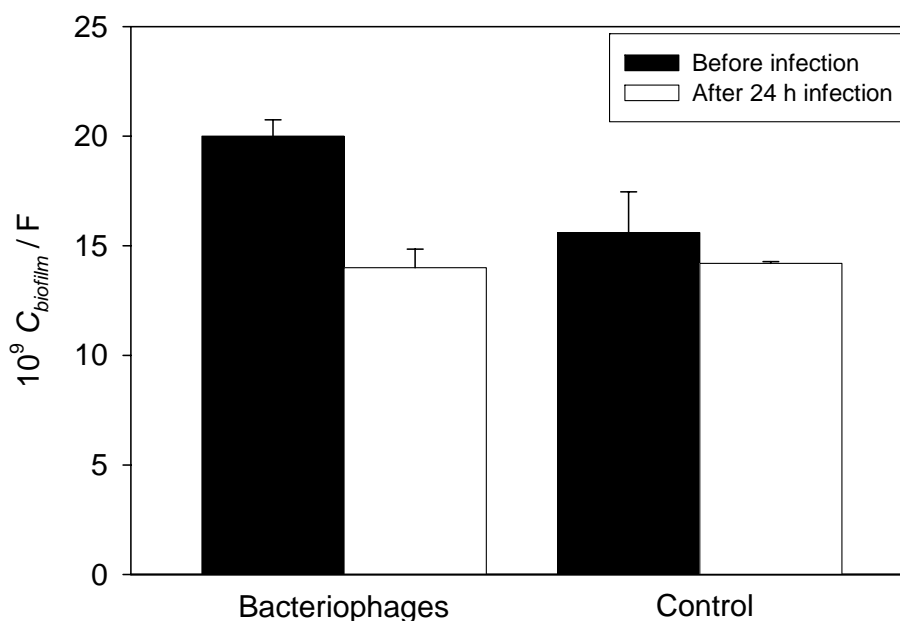
Fig. 6.8 Representation of the change in the $C_{biofilm}$ magnitude after 24 h of incubation in real samples from an urban sewage treatment plant. The control sample, water without bacteriophages, is also shown.

6.4   CONCLUSIONS

In this Chapter, EIS has been used for the detection of bacteriophages by following the degradation of mature biofilms grown on the surface of WE / CE chips. The $C_{biofilm}$ has been found to be particularly sensitive to the changes produced by the biofilm degradation. EIS measurements have shown correlation with Optical Microscopy images of mature biofilms before and after the infection process. Also the thickness of the biofilms (from CSLM) and the number of attached cells (from sonication and plating on agar) coincide with EIS data. The $C_{biofilm}$ has shown sensitivity both to the concentration of bacteriophages in the culture and to the time of incubation of the electrodes in the phages suspension. However, no differences have been obtained when using rich or minimal media during the infection process. This approach has been successfully applied to the detection of coliphages in real samples from an urban sewage treatment plant.

6.5 REFERENCES

[1] C. García-Aljaro, X.M. Berbel, A.T.A. Jenkins, A.R. Blanck, F.X. Muñoz, *Applied and Environment Microbiology*, (Accepted)

[2] X. Munoz-Berbel, C. García-Aljaro, F.X. Munoz, *Electrochimica Acta*, (Accepted)

[3] F. Traub, S.K. Spillmann, R. Wyler, *Applied and Environment Microbiology*, **52** (1986) 498-503

[4] J.J. Borrego, M.A. Morinigo, A. de Vicente, R. Cornax, P. Romero, *Water Research*, **21** (1987) 1473-1480

[5] A. Ketratanakul, S. Ohgaki, Y. K., *Water Science and Technology*, **24** (1991) 407-412

[6] J. Lasobras, J. Dellunde, J. Jofre, F. Lucena, *Journal of Applied Microbiology*, **86** (1999) 723-723

[7] W.O.W. Grabow, *Water SA*, **27** (2001) 251-268

[8] L. Moce-Llivina, F. Lucena, J. Jofre, *Applied and Environment Microbiology*, **71** (2005) 6838-6844

[9] M.H. Adams, *Bacteriophage*. New York, Interscience Publishers (1959)

[10] T. Neufeld, A.S. Mittelman, V. Buchner, J. Rishpon, *Analytical Chemistry*, **77** (2005) 652-657

[11] T. Neufeld, A. Schwartz-Mittelmann, D. Biran, E.Z. Ron, J. Rishpon, *Analytical Chemistry*, **75** (2003) 580-585

[12] M.M. Doolittle, J.J. Cooney, D.E. Caldwell, *Canadian Journal of Microbiology*, **41** (1995) 12-18

[13] B.D. Corbin, R.J.C. McLean, G.M. Aron, *Canadian Journal of Microbiology*, **47** (2001) 680-684

[14] Anonymous, "*Detection and enumeration of bacteriophages. Part 2: Enumeration of somatic coliphages"*. ISO 10705-2: Water quality. Geneva, Switzerland, International Organisation for Standardisation (2000)

[15] L.S. Clesceri, A.E. Greenberg, A.D. Eaton, eds. *Standard Method for the Examination of Water and Wastesater* Washington DC, American Public Health Association (1998)

[16] J. Mendez, J. Jofre, F. Lucena, N. Contreras, K. Mooijman, R. Araujo, *Journal of Virological Methods*, **106** (2002) 215-224

[17] T. Kieser, M.J. Bibb, K.F. Chater, M.J. Butter, D.A. Hopwood, *Practical Streptomyces genetics, a laboratory manual.* Norwich, United Kingdom, John Innes Foundation (2000)

[18] K.A. Hughes, I.W. Sutherland, M.V. Jones, *Microbiology*, **144** (1998) 3039-3047

CHAPTER 7: DEVELOPMENT OF AN IMPEDIMETRIC APPROACH FOR THE QUANTIFICATION OF SUSPENDED BACTERIA USING ELECTROCHEMICAL IMPEDANCE SPECTROSCOPY

CHAPTER 7: DEVELOPMENT OF AN IMPEDIMETRIC APPROACH FOR THE QUANTIFICATION OF SUSPENDED BACTERIA USING ELECTROCHEMICAL IMPEDANCE SPECTROSCOPY

This Chapter describes an impedimetric approach for bacterial quantification, especially at low concentration, based on the measurement of the initial attachment of bacteria to platinum surfaces. *Escherichia coli* (*E. coli*) were chosen as model bacteria for the development of the quantification method. In a few words, the value of the interface capacitance, modelled as a the interface Constant Phase Element (CPE_i), in the pre-attachment stage (before 2 min of attachment) showed correlation with suspended concentration of bacteria from 10^1 to 10^7 Colony Forming Units per mL (CFU mL^{-1}). This method was found to be sensitive to the attachment time, to the applied potential and to the size of the counter electrode. The sensor life-time was also evaluated. This work has been partially published in *Biosensors and Bioelectronics* (Annex II)[1].

7.1 INTRODUCTION

Bacteria are small prokaryotic and unicellular microorganisms with a huge variety of resources to adapt to any metabolic restriction and environmental condition. Thus, bacterial species can be found adapted to live elsewhere (air, water or soil) as free cells (planktonic cells) or in communities, such as biofilms[2]. The determination of the concentration of planktonic bacteria in liquids is important in different areas[3]. On the one hand, the monitoring of the concentration of suspended bacteria is especially relevant in the fermentation industries where a strict control of the concentration of cells in the incubator is necessary during the fermentation process. On the other hand, the presence of bacteria, even the non-pathogenic ones, is very restricted in other areas, namely the environmental monitoring, the food and the beverage industries and the clinical chemistry. For instance, the presence of non-pathogenic bacteria is limited to 10^2 CFU mL^{-1} in drinking waters[4]. Thus, these areas require fast and simple detection methods for the continuously quantification of planktonic bacteria in liquids, especially at low concentrations.

Conventional methods for the detection of viable bacteria typically rely on the culture-based assays. With the advent of modern molecular biological techniques, many new approaches have been investigated for this purpose, such as bioluminescent assays[5], Fluorescent In Situ Hybridization (FISH)[6], optical tweezers[7], nucleic acid amplification method (Polymerase Chain Reaction, PCR)[8], Reverse Transcription-Polymerase Chain Reaction (RT-PCR)[9, 10] and Nucleic Acid Sequence-Based Amplification (NASBA)[11]. Although these methods can offer high sensitivity, they are either time-consuming or relying on laboratory facilities, which limit their application for rapid operation and on-site analysis. In recent years a number of new methodologies have been applied to the detection of planktonic bacteria. These include Voltamperometry[3], Micromechanical Oscillators[12] and Quartz Crystal Microbalances (QCMs)[13]. These methods showed good sensitivities (around 10^2-10^3 CFU mL^{-1}) with short measurement times (between some minutes to hours depending on the method). However, their main drawback can be found by considering the complexity of the assay, which frequently requires the manipulation of fragile or biologically delicate materials.

This Chapter describes a simple and fast impedimetric approach for monitoring the concentration of suspended *E. coli* based on the changes produced in the electrode-solution interface by the early bacteria attachment. The effect of the counter electrode size in the measurement, the influence of the applied potential and the aging of the sensor are also investigated.

7.2   EXPERIMENTAL

This Section details the Electrochemical Impedance Spectroscopy (EIS) experimental protocol used for the determination of the suspended bacteria concentration. The biological samples were prepared as described in Chapter 4 (Section 4.2.3).

7.2.1   *Impedimetric quantification of suspended bacteria concentration*

Bacterial suspensions were introduced in the electrochemical cell, containing the working electrode / counter electrode (WE / CE) chip and an external Ag|AgCl reference electrode (RE), which was thermostatically kept at 4 ºC. EIS measurements were made 50 s after adding the bacterial suspension under the experimental conditions detailed in Chapter 3 (Section 3.3.1). After measuring, chips and the electrochemical cell were cleaned with distilled water and sterilized with ethanol.

7.3   RESULTS AND DISCUSSION

7.3.1   *Fitting and interpretation of impedance spectra*

Z-View software was used to fit EIS data to the equivalent circuit previously described in Chapter 4 (Section 4.3.1) and shown in Fig. 7.1.
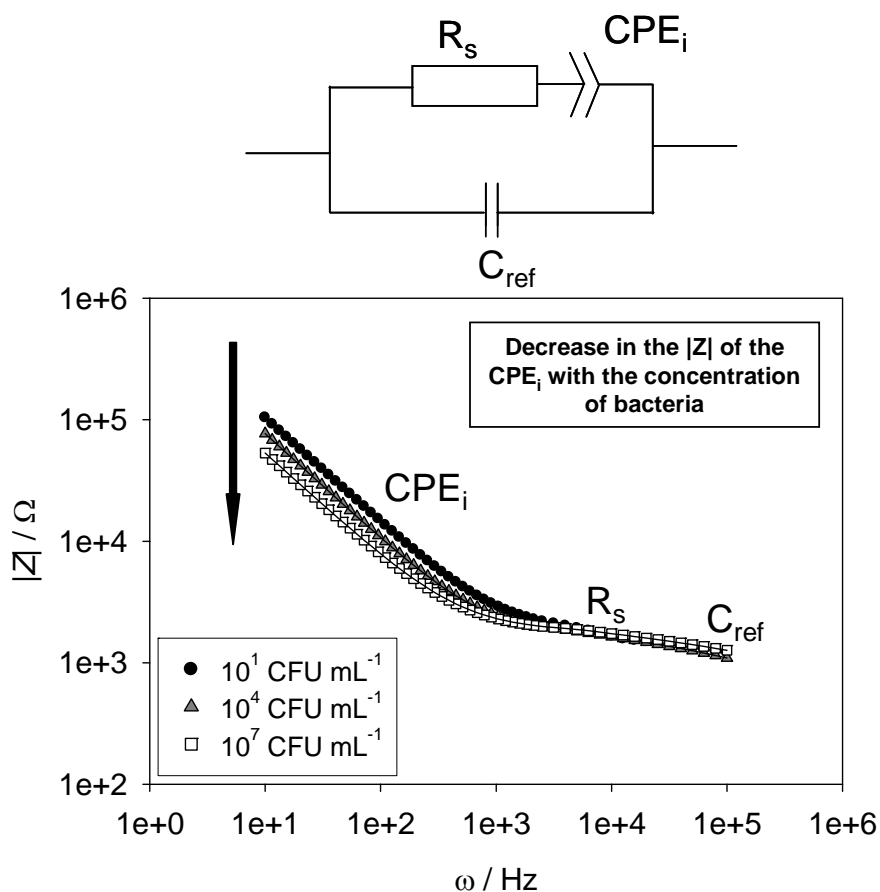
Fig. 7.1 Representation of the impedance modulus ($|Z|$) versus the frequency for *E. coli* at a concentration of 10^1, 10^4 and 10^7 CFU mL^{-1} after 50 s of attachment (points in the plot). The EIS spectra were fitted to the equivalent circuit shown inset (line in the plot), which contains the capacitor associated to the reference electrode (C_{ref}), the solution resistance (R_S) and the CPE$_i$. These parameters are included in the plot in the frequency range where they appear.

Fig. 7.1 shows EIS measurements for 10^1, 10^4 and 10^7 CFU mL^{-1} suspensions 50 s after adding these solutions to the electrochemical cell. The change in the impedance modulus in the region of the CPE$_i$ with bacterial concentration can be clearly seen.

7.3.2 *Effects of the very early stage attachment (at 50 s) on the CPE$_i$ magnitude (K$_i$): quantification of suspended bacteria*

The effect of the bacteria attachment to the surface of platinum WE / CE chips during the very early attachment stage (or pre-attachment step) was measured using EIS as previously detailed.

Fig. 7.2 shows the effect of the bacteria concentration on the CPE$_i$ after 50 s of attachment. At this point, the K_i increases with the concentration (rather than decreases as seen at longer times) with an evident correlation from 10^1 to 10^7 CFU mL^{-1}.
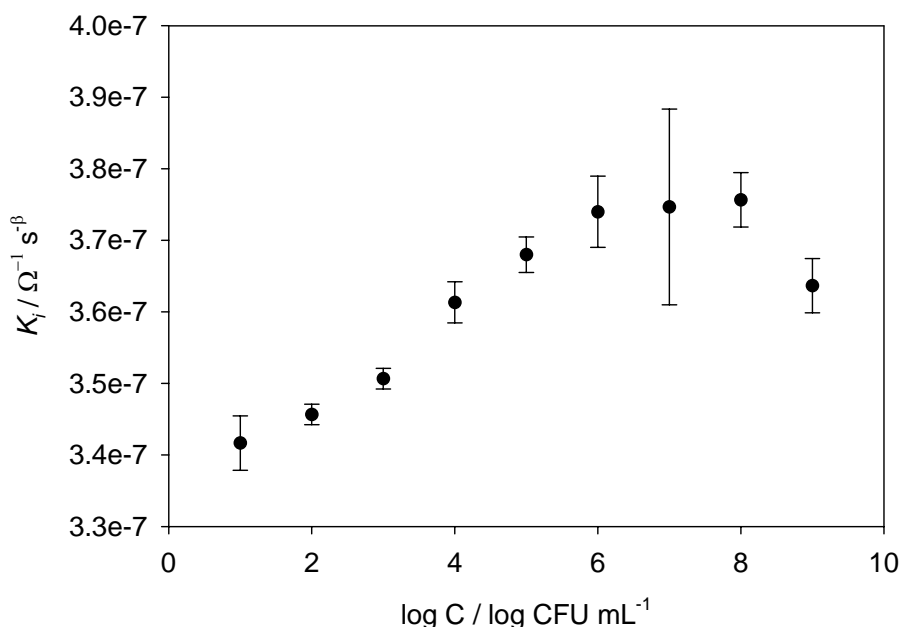
Fig. 7.2 Representation of the K_i versus the *E. coli* concentration after 50 s of incubation.

The changes produced in K_i by bacteria attachment and the differences with later steps have been discussed in Chapters 4 and 5. Briefly, at the pre-attachment stage, bacteria can be considered to be behaving as simple charged colloidal particles. The introduction of these charged particles, bacteria, and their associated counter-ions affects the double layer at the electrode interface, especially in terms of distance between layers: attached bacteria at the pre-attachment stage are thought to decrease the Debye length at the electrode double layer, causing an initial increase in CPE.

7.3.3 Analysis of the effect of the counter electrode size in the determination of the K_i at the pre-attachment stage

In this section, the effect of the CE size in the CPE magnitude at the pre-attachment stage was evaluated. Two platinum CEs of 1.4 mm^2, 3 times bigger than the WE (case A), and 117 mm^2, more than 200 times bigger (case B) were compared following the experimental conditions described above. The measured K_i was normalized using Eq. 7.1. In the equation, $K_i(c)$ is the value of CPE for any concentration of bacteria and $K_i(wb)$ is the value of CPE in absence of bacteria.

$$\Delta K_i = \frac{K_i(c) - K_i(wb)}{K_i(wb)} \cdot 100 \qquad (7.1)$$

As shown in the previous Section, the K_i increased at the pre-attachment stage as a consequence of a decrease in the Debye length at the electrode double layer. The double layer of both working and counter electrodes contributes to the CPE magnitude, as shown in Eq. 7.2 which considers the in series combination of both capacitances ($C_{dl(WE)}$ and $C_{dl(CE)}$, respectively for the WE and the CE)[14]:

$$CPE_i = \frac{C_{dl(WE)} \cdot C_{dl(CE)}}{C_{dl(WE)} + C_{dl(CE)}} \qquad (7.2)$$

The use of CEs of different area changes the value of the $C_{dl(CE)}$, whose magnitude increases with the size of the area, as follows:

$$C_{dl(CE)} = \varepsilon_0 \varepsilon_{dl(CE)} \frac{A_{CE}}{d_{dl(CE)}} \qquad (7.3)$$

ε_0 is the permittivity of the free space, $\varepsilon_{dl(CE)}$ is the permittivity of the CE double layer, A_{CE} is the CE area and $d_{dl(CE)}$ is the distance between layers of the CE double layer. Thus, the size of the CE area considerably modulates the value of $C_{dl(CE)}$ in the CPE, varying from approximately the 50 %, when WE and CE have a similar size (case A), to practically 0 % ($CPE_i \approx C_{dl(WE)}$), when a very large counter electrode is used (case B).

Experimentally, the normalized magnitude of the CPE was much bigger in the case B, when it only depended on the $C_{dl(WE)}$, than in the case A, especially at high concentrations, as shown in Fig. 7.3.
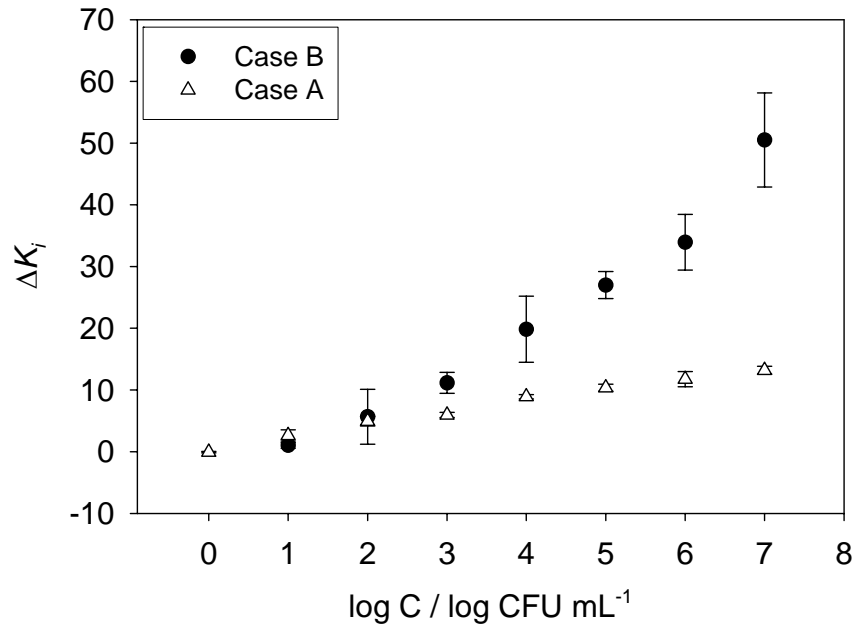
Fig. 7.3 Representation of the normalized K_i versus the logarithm of the suspended concentration using different CEs sizes. Case A: 1.4 mm^2. Case B: 117 mm^2.

In Chapter 4, bacteria were preferably attached to the WE and only a few cells were found attached to the CE, probably because of the fact that both CE and bacteria were negatively charged. The low level of attachment found on the CE suggests small changes in the $C_{dl(CE)}$ and coincides with the smaller magnitude of the CPE recorded when it is highly influenced by the $C_{dl(CE)}$ (case A).

7.3.4 *Influence of the magnitude of the potential applied on the WE during the pre-attachment stage*

The pre-attachment stage, mainly governed by electrostatic forces, can be modulated by applying a potential to the WE. In this Section, three applied potentials (0, +0.19 and +0.30 V vs. Ag|AgCl) were explored under the experimental conditions described

previously in order to determine the influence of the potential in the pre-attachment process.

Experimental data plotted in Fig. 7.4 showed that, for the same bacterial concentration, the normalized K_i increased when applying more positive potentials.
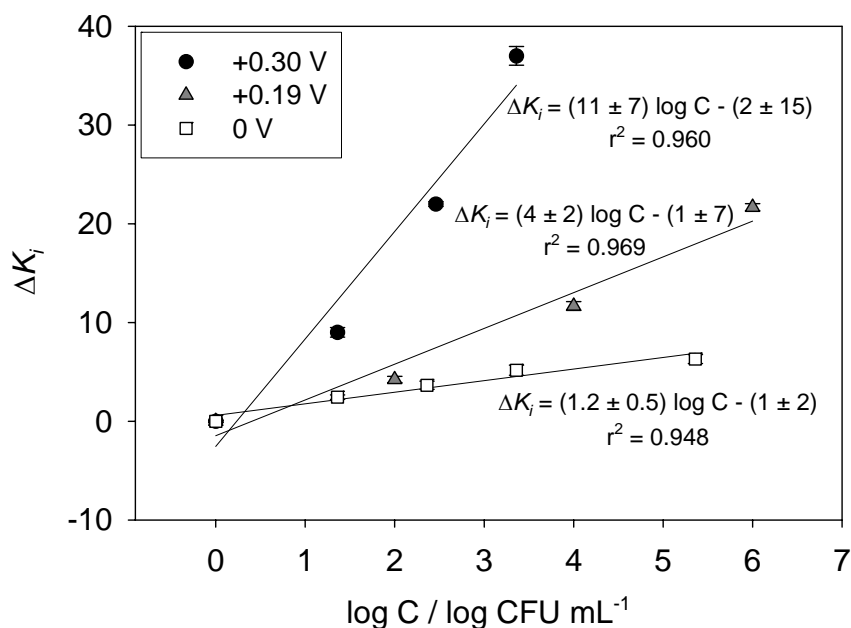
Fig. 7.4 Representation of the normalized K_i versus the suspended bacteria concentration after applying three different potentials, namely 0, +0.19 and +0.30 V vs. Ag|AgCl, over the WE surface.

The increase of the CPE, which can be thought to be caused by an increase in the number of attached cells, suggested that positive charges on the WE favoured the attachment of bacteria. Thus, the pre-attachment process, governed by electrostatic forces, can be understood as the attraction of positive surfaces and bacteria, which are negatively charged for the presence of ionized phosphate and carbonate groups in their outer membranes[2]. Potentials above + 0.6 V vs. Ag|AgCl could not be explored. These potentials showed a big variability in the recorded data, probably caused by the formation of non-stoichiometric platinum oxides of low stability[15].

7.3.5   Aging of the sensor

The sensors capacity to monitor bacteria attachment in the pre-attachment step was investigated. The aging of the sensors was determined by repeating the calibration process described in Section 7.3.2, which included 24 single EIS measurements (8 samples, including the medium without bacteria used as control, measured in triplicate), during consecutive days. Between assays, sensors were stored dry and clean in the optimum condition to preserve the superficial properties.
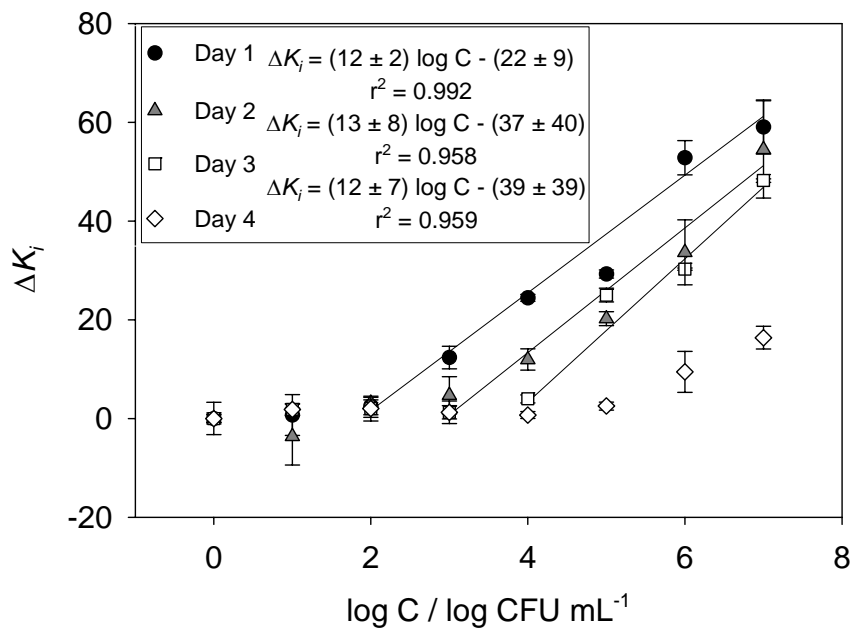
Fig. 7.5 Representation of the normalized K_i versus the logarithm of the suspended bacteria concentration for the same sensor during four consecutive days.

As shown in Fig. 7.5, sensors progressively lost their capacity to measure the changes produced in the magnitude of the CPE by bacteria attachment. Although the sensors sensitivity, in terms of slope of the calibration curve, remained practically constant after the three first days, the experimental limit of detection shifted to higher concentrations. The decrease in the sensor limit of detection with consecutive measurements is thought to be caused by the presence of membrane fragments, protein layers and exopolysaccharide layers, from death cells or secreted by bacteria, on the electrodes surface. The presence of these molecules would increase the distance between the electrode surface and the adhering bacteria thus decreasing the limit of detection of the

electrode. After 4 days, sensors completely lost their capacity to discriminate between different concentrations and a flat calibration curve was obtained. The maximum number of measurements *sensitive* to the changes produced by bacterial attachment was shown to be close to 80.

7.4   CONCLUSIONS

In this Chapter, EIS has been used for the quantification of suspended bacteria. The magnitude of the interface CPE has been correlated with the concentration of suspended bacteria at the pre-attachment stage (after 50 s of attachment). The sensitivity of the CPE_i has been enhanced by applying more positive potentials on the WE which favoured bacterial attachment. In terms of aging, sensors have been shown to lose the capacity to discriminate between concentrations with time, especially at low concentrations.

7.5 REFERENCES

[1] X. Munoz-Berbel, N. Vigués, A.T.A. Jenkins, J. Mas, F.J. Munoz, *Biosensors and Bioelectronics*, (Accepted)

[2] M.T. Madigan, J.M. Martinko, J. Parker, *Brock Biology of Microorganisms*. Hertfordshire, U.K., Prentice Hall International (1997)

[3] H. Tang, W. Zhang, P. Geng, Q. Wang, L. Jin, Z. Wu, M. Lou, *Analytica Chimica Acta*, **562** (2006) 190-196

[4] P. Lebaron, A. Henry, A.S. Lepeuple, G. Pena, P. Servais, *Marine Pollution Bulletin*, **50** (2005) 652-659

[5] J. Lee, R.A. Deininger, *Luminescence*, **19** (2004) 209-211

[6] T. Garcia-Armisen, P. Servais, *Journal of Microbiological Methods*, **58** (2004) 269-279

[7] M. Ericsson, D. Hanstorp, P. Hagberg, J. Enger, T. Nystrom, *Journal of Bacteriology*, **182** (2000) 5551-5555

[8] T.B. Tims, D.V. Lim, *Journal of Microbiological Methods*, **55** (2003) 141-147

[9] G. Bleve, L. Rizzotti, F. Dellaglio, S. Torriani, *Applied and Environment Microbiology*, **69** (2003) 4116-4122

[10] M. del Mar Lleo, S. Pierobon, M.C. Tafi, C. Signoretto, P. Canepari, *Applied and Environment Microbiology*, **66** (2000) 4564-4567

[11] S.A. Simpkins, A.B. Chan, J. Hays, B.P. opping, N. Cook, *Letters in Applied Microbiology*, **30** (2000) 75-79

[12] K.Y. Gfeller, N. Nugaeva, M. Hegner, *Biosensors and Bioelectronics*, **21** (2005) 528-533

[13] T.A. Camesano, Y. Liu, M. Datta, *Advances in Water Resources*, **30** (2007) 1470-1491

[14] E. Barsoukov, J.R. Macdonald, eds. *Impedance Spectroscopy: Theory, Experiment, and Applications*. New Jersey, John Wiley & Sons (2005)

[15] V.I. Birss, M. Chang, J. Segal, *Journal of Electroanalytical Chemistry*, **355** (1993) 181-191

CHAPTER 8: APPLICATION OF THE ELECTROCHEMICAL IMPEDANCE SPECTROSCOPY TO THE REAL-TIME MONITORING OF BACTERIA CULTURES

CHAPTER 8: APPLICATION OF THE ELECTROCHEMICAL IMPEDANCE SPECTROSCOPY TO THE REAL-TIME MONITORING OF BACTERIA CULTURES

This Chapter describes the application of the impedimetric approach previously described to the monitoring of the concentration of *real* bacterial suspensions using platinum electrodes. *Escherichia coli* (*E. coli*) was chosen as model bacteria again. Briefly, the interface Constant Phase Element (CPE$_i$), previously found to be very sensitive to the suspended concentration after short exposure times, was used for the quantification of bacteria samples directly extracted from the incubator. The effect of bacteria and metabolites in the CPE$_i$ magnitude was checked. Electrochemical Impedance Spectroscopy (EIS) measurements of *E. coli* cultures showed correlation with classical methods, namely plating onto agar, Optical Density and Epifluorescence Microscopy. Part of this work has been recently submitted for publication in *Applied and Environmental Microbiology* (Annex VI)[1].

8.1 INTRODUCTION

The control of the bacterial population is very important in different areas, particularly in the environmental monitoring and in the fermentation, the food and the beverage industries. These fields require simple, fast and real-time systems for the monitoring of planktonic bacteria, especially at low concentrations[2]. The classical method for the real-time monitoring of bacteria growth was based on the change in the Optical Density of the culture medium when bacteria grow[3]. Because of its experimental simplicity and fast response, some commercial instrumentation has been developed based on this. However, the low sensitivity, the detection limit [around 10^5 Colony Forming Units per mL (CFU mL^{-1})] and the interferences, particularly the air bubbles, extremely limits its application.

From an electrochemical viewpoint, EIS has become widely used for the study of biological systems and especially for the monitoring of suspended bacteria concentration. From the earlier 1950s, H. P. Schwan used the EIS to characterize the dielectric properties of cell suspensions and tissues[4]. EIS measurements show that the small conductivity of the cellular membranes, particularly at low frequencies (below 100 kHz), impedes the current to flow through the cells and thus, they behave as non-conducting particles. This decrease of conductivity was found proportional to the volume fraction of cells present in the sample and later studies used it to quantify biomass[5-7]. The linearity of the probe response extends from 2 to 100 mg dry weight per mL, nearly 10^3 CFU mL^{-1} in the case of bacteria.

In the 1970s-1980s, Cady and Firstenberg-Eden started to use EIS to measure the changes of conductivity caused by bacteria metabolism and used it to finally quantify biomass[8, 9]. Bacteria can be simplistically considered as units that convert uncharged particles into smaller and highly charged molecules, which excrete to the medium increasing its conductivity. They, and more recent authors, used this decrease in the magnitude of the impedance, due to this conductivity increase, to monitor bacterial metabolism[10-15]. However, the quantification was somewhat difficult to understand. The production of charged molecules depends on the number of active cells. Bacteria in

media are continuously duplicating thus increasing their concentration with time. When the concentration of bacteria exceeds 10^5 CFU mL^{-1}, the change of the conductivity due to bacteria metabolism can be detected using EIS. The time necessary to reach this boundary concentration depends both on the duplication time of the species and on the initial concentration of the sample. Hence, for the same specie, the measurement of this time was proportional to the bacteria concentration initially present in the sample. However, the time required to obtain a measurable change in the EIS magnitude was very long for low concentrations, expanding to more than 24 h for samples of 1 CFU mL^{-1}.

This Chapter describes a simple and fast impedimetric approach for monitoring the concentration of *real* bacteria samples from an incubator, based on the changes produced in the electrode-solution interface by the early bacteria attachment on platinum electrodes. The influence of the cells and the metabolites in the EIS measurement is also investigated.

8.2 EXPERIMENTAL

This Section details the bacterial strains and the experimental condition of the bacteria incubator. Also the protocol for the aseptic acquisition of bacteria suspensions from the incubator and the pre-treatment of the samples before measurement is included. EIS measurements were made as described in Chapter 7 (Section 7.2.1) under the experimental conditions exposed in Chapter 3 (Section 3.3.1). The protocols for the Optical Density and the Epifluorescence Microscopy measurements coincided with those detailed in Chapter 3 (Section 3.3.6 and Section 3.3.5, respectively).

8.2.1 Bacteria strains and culture conditions

E. coli (CGSC 5073 K12) was grown overnight at 37 ºC in AB Minimal Medium (ABMM) containing glucose as carbon source. The bacterial concentration was measured by plating in Luria-Bertani (LB) medium containing 1.5 % agar, with stock concentration at around 10^9 CFU mL^{-1}. The suspension was then serially diluted down to 10^6 CFU mL^{-1} in decade steps. Next, 1 mL of the 10^6 CFU mL^{-1} suspension was

sterilely inoculated into a 1.5 L water-jacketed glass reactor containing 1 L of ABMM. The initial concentration of bacteria in the incubator was thus of 10^3 CFU mL^{-1}. During the growth, the incubator was thermostatically kept at 37 ºC with constant agitation and aeration. After the inoculation, no nutrients were added into the reactor (batch process). Under these conditions, *E. coli* grew aerobically with a duplication time experimentally found to be close to 30 min.

Using the aseptic acquisition system of the reactor, aliquots of 20 mL were sterilely extracted every 30 min and directly measured using EIS, Optical Density and Epifluorescence Microscopy (after filtration, as specified in the experimental protocol for Epifluorescence Microscopy counting, shown in Chapter 3, Section 3.3.6). 5 mL were centrifuged for 15 min at 4388 *g* to separate the metabolites (supernatant liquid) from the bacteria cells (pelled). The pellet was cleaned with ABMM twice and finally re-suspended in sterile ABMM. Both metabolites and cells samples were then measured in separate using EIS. Biological samples were stored at 4 °C to slow growth until measurement. All of the manipulations were performed under sterile conditions.

8.3   RESULTS AND DISCUSSION

8.3.1   *Fitting and interpretation of impedance spectra*

Z-View software was used to fit EIS data to the equivalent circuit previously described (Chapter 4, Section 4.3.1). This equivalent circuit was composed of a resistance which modelled the behaviour of the electrolytic medium, R_S, the interface capacitance, which was modelled with a Constant Phase Element to improve the fitting, CPE$_i$, and an extra capacitance of small magnitude (experimentally found to be of some nF) associated with the presence of an external reference electrode, C_{ref}, which was not sensitive to the bacteria concentration.

Fig. 8.1 shows EIS measurements for bacterial suspensions extracted from the incubator 30 and 270 min after the inoculation of the stock bacterial suspension used as starter. Regarding the fitting, the magnitude of the CPE$_i$ (K_i-T in the figure) was found to change with time as a consequence of bacterial growth in the incubator.

30 min of incubation	270 min of incubation

Element	Freedom	Value	Error	Error %
Cref	Fixed(X)	1.568E-11	N/A	N/A
Rs	Free(+)	419.9	0.83279	0.19833
Ki-T	Free(+)	2.5424E-07	1.2384E-09	0.4871
Ki-P	Free(+)	0.87196	0.00064294	0.073735

Element	Freedom	Value	Error	Error %
Cref	Fixed(X)	1.568E-11	N/A	N/A
Rs	Free(+)	543.5	1.5331	0.28208
Ki-T	Free(+)	2.6407E-07	1.9497E-09	0.73833
Ki-P	Free(+)	0.87057	0.00099713	0.11454
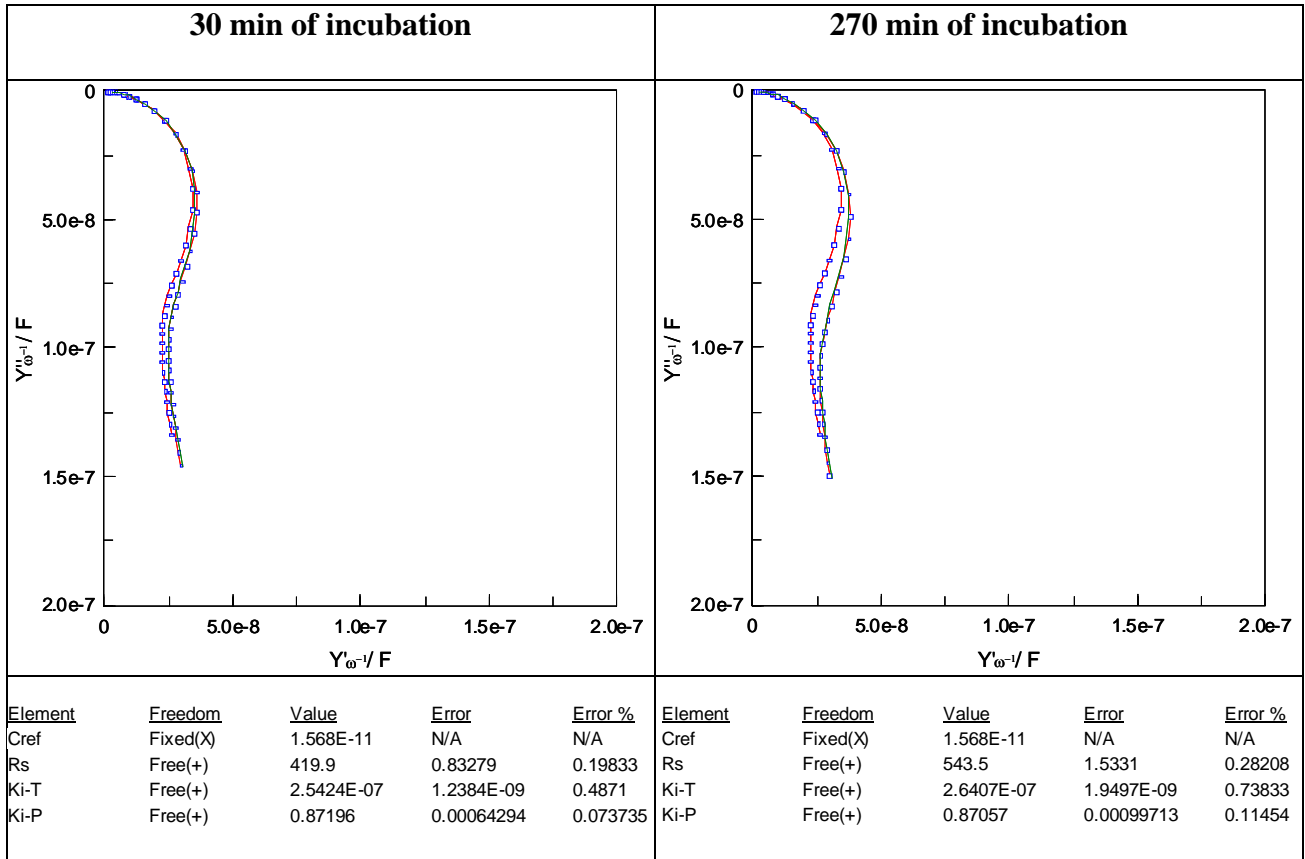
Fig. 8.1 Admittance complex plane plot for bacterial suspensions extracted from the incubator 30 and 270 min after the inoculation of the bacterial starter suspension. The experimental EIS spectra (points in the plot), the ideal EIS spectra from the fitting (line in the plot) are shown. Also the spectra corresponding to the culture medium without bacteria is added in each plot as control (red line). Below, the calculated values and errors of each element from the fitting are shown.

8.3.2 *Monitoring of the concentration of real bacterial samples extracted from an incubator using EIS: evaluation of the influence of the cells and metabolites in the EIS magnitude*

The impedimetric approach previously described in Chapter 7 for the quantification of suspended bacteria was applied to the monitoring of *real* samples extracted from a bacteria incubator. Bacterial growth was measured using EIS as described in Chapter 7 (Section 7.2.1) under the experimental conditions detailed in Chapter 3 (Section 3.3.1).

The most relevant results are shown in Fig. 8.2. It has to be noted that, after the fitting, the measured CPE magnitude (K_i) was normalized using Eq. 8.1. $K_i(it)$ is the value of

CPE at any incubation time and $K_i(m)$ is the value of CPE of the culture medium in absence of bacteria:

$$\Delta K_i = \frac{K_i(it) - K_i(m)}{K_i(m)} \cdot 100 \qquad\qquad (8.1)$$
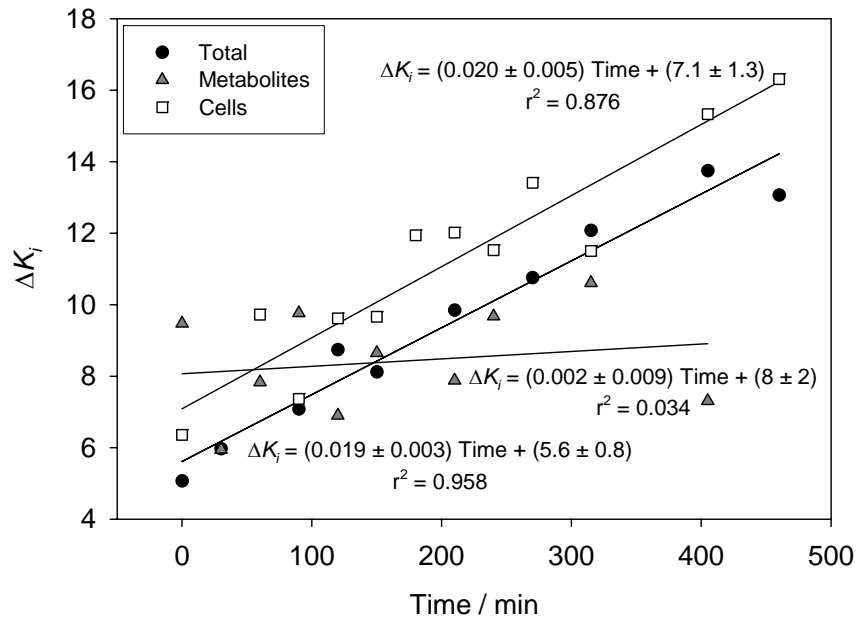
Fig. 8.2 Representation of the normalized K_i versus the incubation time for total samples containing both cells and metabolites (total samples), samples containing only metabolites (metabolites samples) and samples containing only cells (cells samples).

A constant R_S value was obtained with time for total samples (samples containing both suspended cells and metabolites), cells samples (samples containing re-suspended cells) and metabolites samples (samples mainly containing metabolites) with a magnitude of $445 \pm 19 \, \Omega$. Sample conductivity was measured separately with a conductance meter and found to be sample invariant, which confirmed that, under the experimental conditions previously exposed, the conductivity of the medium did not vary with the *E. coli* growth (or with the metabolites production).

However, the K_i changed with time by total and cells samples, although the correlation with time, and thus with bacteria concentration, was found to be better by total than cells samples, probably because of the centrifugation step. The increase in CPE

coincided with that reported in Chapters 4, 5 and 7. In those cases, the attachment of bacteria, considered to be behaving as simple charged colloidal particles during the very early attachment, was thought to modify the structure of the double layer at the electrode interface. Particularly, bacteria attachment to the electrode surface may decrease the Debye length at the electrode double layer, causing the initial increase in CPE.

In the case of metabolites samples, the random oscillation of the K_i was caused by the presence of bacteria since the variation disappeared after filtration in 2 μm pore size GTBP filters. Thus, the metabolites produced by *E. coli* during bacteria growth, under the experimental conditions here exposed, did not modify the CPE_i either.

Fig. 8.3 Representation of the normalized K_i with the logarithm of the suspended concentration of bacteria. This calibration curve was used for converting capacitance values into bacteria concentrations.

Using the calibration curve shown in Fig. 8.3, EIS data from total and cells samples were converted into concentration values. It has to be emphasized that both experiments (calibration curves and EIS data from total and cell samples) were comparable since both of them were made using the same bacteria, culture medium, equipment, experimental conditions and identical platinum electrodes.
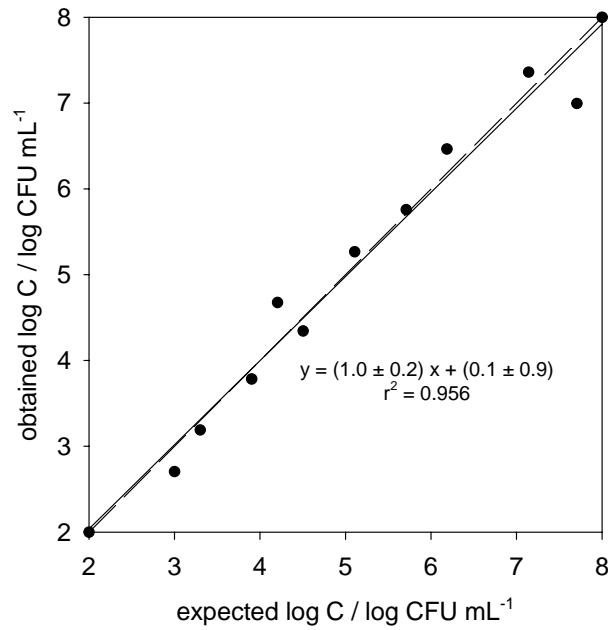
Fig. 8.4 Representation of the predicted bacteria concentration magnitude (obtained from total samples measured using EIS) against the expected ones (from plating on agar). The dotted line represents the theoretical comparison line y = x.
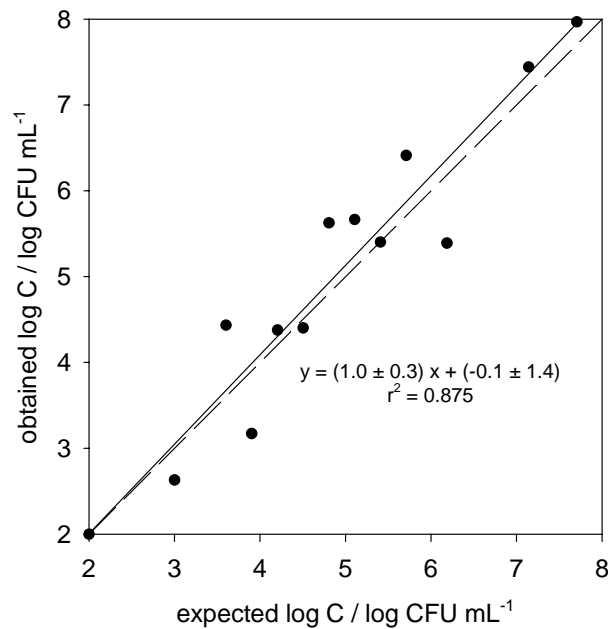
Fig. 8.5 Representation of the predicted bacteria concentration values (from cells samples measured using EIS) against the expected ones (from plating on agar). The dotted line represents the theoretical comparison line y = x.

The global behaviour of the new impedimetric approach in the determination of bacteria concentration for total and cells samples was evaluated by plotting the predicted values (from EIS) against the expected ones (from plating on agar) (see Fig. 8.4 and Fig. 8.5). A good method should display comparative lines with high correlation and a slope equal to one with zero intercept. As illustrated in Fig. 8.4 and Fig. 8.5, in both cases EIS measurements showed good correlation with comparison lines practically indistinguishable from the theoretical values. However, better results were obtained in the case of total samples directly extracted from the incubator. This fact was probed to be caused by the centrifugation process since, as previously shown, part of the cells remained in the supernatant after the centrifugation. Thus, the number of bacteria in both cells and total samples may not always be the same, which introduced a new variability factor in the EIS measurement.

Finally, the Student's t-test for paired samples was used for checking whether there were significant differences between the obtained and the expected values, significance being set at 95 %. The tabulated values of the t (t_{tab}), 2.26 and 2.20 for total and cells samples respectively, were always found to be bigger than the calculated ones (0.21 and 0.85 for total and cells samples, respectively). Thus, no significant differences between the predicted and the expected values were obtained. Again, better results were achieved when using total samples directly extracted from the incubator.

8.3.3 Comparison of the impedimetric approach with classical Optical Density measurements and Epifluorescence Microscopy counting

Bacteria concentration values from EIS were compared with those obtained from Optical Density and Epifluorescence Microscopy measurements. EIS, Optical Density and Epifluorescence Microscopy measurements were made as described above. Suspended concentration values from EIS data were obtained by interpolating in the calibration curve shown in Fig. 8.3, as previously detailed. The suspended concentration from Optical Density was also found after interpolation in the calibration curve shown in Fig. 8.6.
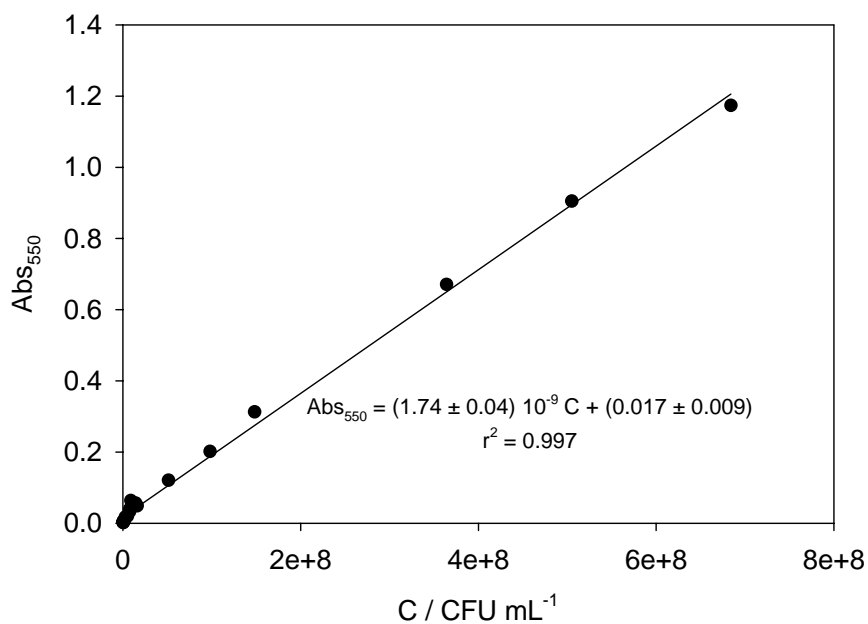
Fig. 8.6 Representation of the absorbance at 550 nm (Abs_{550}) with the suspended concentration of bacteria. This calibration curve was used for converting absorbance values into bacteria concentrations.
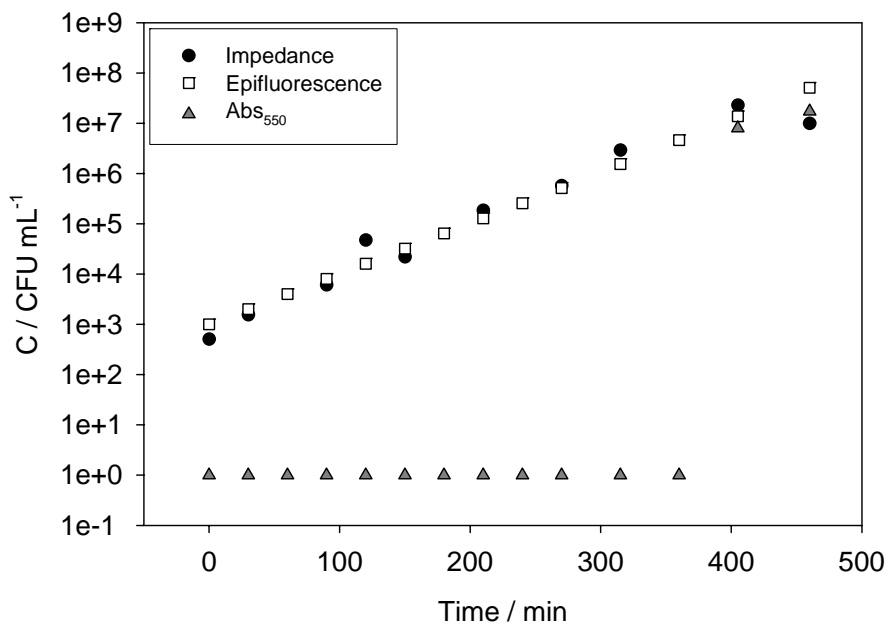
Fig. 8.7 Representation of the variation of the concentration values from EIS, Epifluorescence Microscopy and Optical Density measurements with the incubation time.

Fig. 8.7 illustrates the comparison between techniques. The experimental data showed that the concentration values from Epifluorescence Microscopy and EIS measurements were practically identical in the range of concentrations under study (which coincided with the linear response range for the impedimetric approach). However, the Optical Density was only found to be sensitive to the suspended concentration when exceeding 5×10^6 CFU mL^{-1}, at least three orders of magnitude more than the other techniques.

8.4   CONCLUSIONS

In this Chapter, the EIS has been used for monitoring the concentration of *real* bacteria samples directly extracted from an incubator. EIS measurements have been found to be insensitive to the presence of metabolites and only depended on bacteria concentration. After interpolation in a calibration curve, concentration values from EIS data have shown good correlation with classical methods, namely plating on agar and Epifluorescence Microscopy counting. The concentration values from EIS have also been found to be comparable with those obtained using Optical Density but with an improvement of at least three magnitude orders in the limit of detection.

8.5   REFERENCES

[1] X. Muñoz-Berbel, N. Vigués, R. Escudé, F.X. Muñoz, J. Mas, *Applied and Environment Microbiology*, (Submitted)

[2] H. Tang, W. Zhang, P. Geng, Q. Wang, L. Jin, Z. Wu, M. Lou, *Analytica Chimica Acta*, **562** (2006) 190-196

[3] M.T. Madigan, J.M. Martinko, J. Parker, *Brock Biology of Microorganisms*. Hertfordshire, U.K., Prentice Hall International (1997)

[4] H.P. Schwan, *Advances in Biological and Medical Physics*, **5** (1957) 147-209

[5] C.L. Davey, H.M. Davey, D.B. Kell, *Bioelectrochemistry and Bioenergetics*, **28** (1992) 319-340

[6] C.M. Harris, D.B. Kell, *Bioelectrochemistry and Bioenergetics*, **11** (1983) 15-28

[7] G.H. Markx, C.L. Davey, *Enzyme and Microbial Technology*, **25** (1999) 161-171

[8] R. Firstenberg-Eden, J. Zindulis, *Journal of Microbiological Methods*, **2** (1984) 103-115

[9] P. Cady, W. Dufour, J. Shaw, S.J. Kraeger, *Journal of Clinical Microbiology*, **7** (1977) 265-272

[10] L. Yang, Y. Li, C.L. Griffis, M.G. Johnson, *Biosensors and Bioelectronics*, **19** (2004) 1139-1147

[11] L. Yang, C. Ruan, Y. Li, *Biosensors and Bioelectronics*, **19** (2003) 495-502

[12] R. Fehrenbach, M. Comberbach, J.O. Petre, *Journal of Biotechnology*, **23** (1992) 303-314

[13] C.J. Felice, M.E. Valentinuzzi, *IEEE Transactions on Biomedical Engineering*, **46** (1999) 1483-1487

[14] C.J. Felice, M.E. Valentinuzzi, M.I. Vercellone, R.E. Madrid, *IEEE Transactions on Biomedical Engineering*, **39** (1992) 1310-1313

[15] K. Futschik, H. Pfützner. *Electrode and Media Impedance for Detection and Characterization of Microorganisms*. in *Proceedings of the RC IEEE-EMBS & 14th BMESI*. 1995

CHAPTER 9: DEVELOPMENT OF AN AUTOMATED FLOW SYSTEM FOR THE REAL-TIME MONITORING OF SUSPENDED BACTERIA USING ELECTROCHEMICAL IMPEDANCE SPECTROSCOPY

CHAPTER 9: DEVELOPMENT OF AN AUTOMATED FLOW SYSTEM FOR THE REAL-TIME MONITORING OF SUSPENDED BACTERIA USING ELECTROCHEMICAL IMPEDANCE SPECTROSCOPY

This Chapter describes the design and construction of new Virtual Instrumentation (VI) implemented in LabView 7.1 for the real-time monitoring of the suspended bacteria concentration using Electrochemical Impedance Spectroscopy (EIS) and platinum electrodes. As a summary, a home-made modification of a Sequential Injection Analysis (SIA) system was developed both for the transport of microbiological samples from the incubator to the electrochemical cell, where they were measured, and for the elimination of residues from the cell to a wasting recipient. This work has been recently submitted for publication in *Measurement Science and Technology* (Annex VII)[1].

9.1   INTRODUCTION

The use of flow methods in the field of chemical analysis started in the middle of the last century for mechanizing the collection of eluted fractions and the sampling step in industrial on-line processes[2]. At the end of the fifties, this objective was enlarged and the automation of all the steps of the analytical methodology was attempted by incorporating flow detectors in the system. In 1957, Skeegs developed the first practical application of flow measurements: the Segmented Flow Analysis (SFA). This approach, quickly accepted to perform clinical, environmental, agricultural and industrial analysis, used a fluid stream segmentation technique with air segments. In 1975, Ruzicka and Hansen developed a new flow analysis technique based on instant discrete sampling by injection into a carrier stream to the flow detector[3]. This approach, called Flow Injection Analysis (FIA) system, allowed continuous flow analysis to be performed in a fast, much simplified and robust way. The main drawback of this system was the high reagent and sample consumption (due to the continuous flow). In order to solve this problem, several methodologies have been established such as the fabrication of μFIA[4] or the immobilization of reagents or enzymes in adequate supports[5]. Although these variants solved several aspects, they caused the appearance of new inconveniences.

In 1990, Ruzicka and Marshal proposed a new approach: the Sequential Injection Analysis (SIA)[6]. This system did not use a continuous flow but a single-channel high precision bi-directional pump which could stop and revert the flow automatically[7]. The main advantages of the SIA system were the robustness, flexibility and the important saving on the consumption of reagents and samples, whereas the low analysis rate was its main disadvantage. SIA systems (illustrated in Fig. 9.1), always under the control of a Personal Computer (PC), can automate a huge variety of sample manipulation sequences without changing the physical characteristics or the configuration of the system[8]. The versatility of the system is basically provided by the multi-port Modular Valve Position (MVP). The MVP allows the access to different ports, containing samples, reagents, standards, cleaning solutions and the detector. The combination of items can be easily adapted to comply with the requirement of any specific analysis, which shows the vast potentiality of the SIA system in the on-line measurements[9].
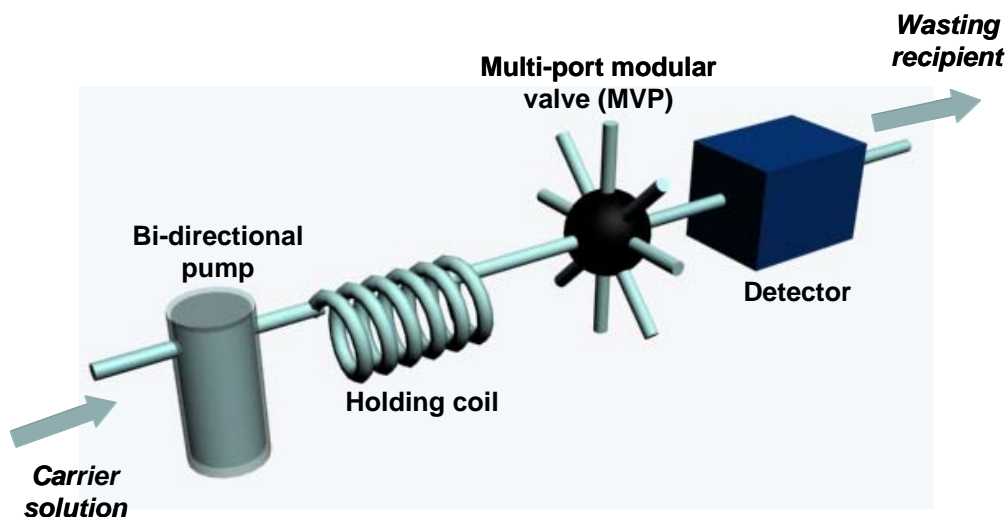
Fig. 9.1 Scheme of a basic SIA system.

Currently, SIA systems are well established in the field of chemical analysis and have been successfully applied to the beverage and food industries for the monitoring of bioprocesses and to immunologic, pharmaceutical and environmental assays[10]. However, new approaches have also appeared recently, such as the Multi-Commuted Flow Injection Analysis (MCFIA)[11], the All Injection Analysis (AIA)[12], the Multi-Syringe Flow Injection Analysis (MSFIA)[7] and the Multi-Pumped System (MPS)[13].

This Chapter describes the development of new VI for the real-time and automated monitoring of suspended bacteria concentration using both EIS and a flow system inspired in a SIA system.

9.2   EXPERIMENTAL

This Section describes the bacterial strains and the experimental conditions of the reactor. The instrumentation and the processing and programming tools for the control of the system and for the acquisition of data are exposed. The description of the experimental protocols for the automated sampling and cleaning processes is included. EIS measurements were made as described in Chapter 7 (Section 7.2.1) under the experimental conditions exposed in Chapter 3 (Section 3.3.1). The protocol for the

Epifluorescence Microscopy measurements coincided with that detailed in Chapter 3 (Section 3.3.5).

9.2.1 *Bacterial strains and experimental conditions*

As it has been detailed in Chapter 8 (Section 8.2.1), the water-jacketed glass incubator containing 1 L of AB Minimal Medium (ABMM) was sterilely inoculated with 1 mL of 10^6 Colony Forming Units per mL (CFU mL^{-1}) *E. coli* (CGSC 5073 K12) from an overnight culture. The initial concentration of bacteria in the incubator was thus of 10^3 CFU mL^{-1}. *E. coli* was grown in the incubator aerobically at 37 ºC in a batch process under the experimental conditions detailed in Chapter 8 (Section 8.2.1). On the other hand, a stock solution containing 10^4 CFU mL^{-1} in ABMM was prepared by serially diluting an overnight culture at around 10^9 CFU mL^{-1}. The stock solution, stored at 4 ºC in the fridge until measurement, was used for the checking of the electrodes as described below. All of the manipulations were performed under sterile conditions.

9.2.2 *Instrumentation for the real-time monitoring of bacteria concentration*

In terms of hardware, the modified SIA system and the measurement system are schematized in Fig. 9.2. The adaptation of the SIA system was composed of a PC controlled Burette 1S (Crison Instruments, Spain) containing a 10 mL syringe and an 8-way multi-port MVP (Hamilton, Switzerland). The MVP allowed the access to 8 different solutions, namely the incubator (port 1), the ABMM without bacteria (port 2), the stock bacterial suspension (port 3), distilled water (ports 4 and 5), 96% ethanol (Panreac, Spain) (port 6), air (port 7) and the wasting recipient (port 8). The bidirectional burette assures the accuracy in the management of liquids either to the electrochemical cell or to the wasting recipient to be removed. Solutions were transported through PolyTetraFluoro-Ethylene (PTFE) tubes (Hamilton, Switzerland) with an internal diameter of 0.5 mm.
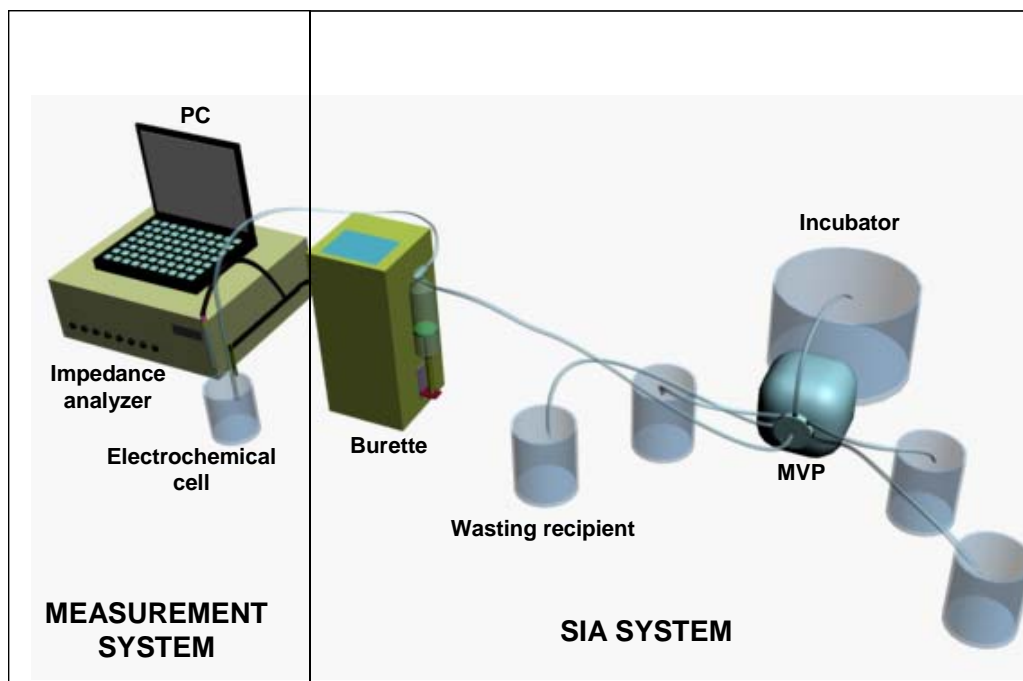
Fig. 9.2 Illustration of the most relevant elements composing the modification of the SIA and the measurement systems.

9.2.3   Control and data acquisition systems

The Data Acquisition (DAQ) DAQPad-6052E (National Instruments, Texas, USA) interface card was used in this application coupled with a 68 pin connector module SCB-68 (National Instruments, Texas, USA). The DAQ card, featuring 16 single-ended analogue inputs (Analogue-to-Digital Converter, ADC) and 2 analogue outputs (Digital-to-Analogue Converter, DAC) with 16 bits of resolution to 333 KS/s, 8 digital input/output (TTL/CMOS) and computer communication by FireWire (IEEE 1394), was interfaced to a 1.4 GHz Pentium III PC running LabView ver.7.1 under Windows XP. The DAQ card was integrated in the LabView environment by specific drivers. The PC sent orders to the bi-directional burette using the RS-232 serial protocol via the COM1 port. On the other hand, the MVP received TTL signals from the DAQ card to select one specific input.

The SIA and the measurement systems were synchronized using the *Project* application shown in Fig. 9.3 via trigger signals. This application remained the Impedance Analyzer in standby mode until receiving a trigger signal from the DAQ card. The trigger signal

was sent 15 s after the complete inoculation of the bacterial suspension to the electrochemical cell. At this moment, the Impedance Analyzer was activated and the EIS of the suspension was measured as detailed in Chapter 7 (Section 7.2.1).


```
Edit project                                   _ □ ✕
Edit  Check!  Wizard...

|
Procedure!Open("C:\Users\Xavi\Impedància\Continu_050406\general")
DIO!SetMode("P1","A","IN")
Dataset!AutoNum = 1
Dataset!AutoReplace("NNN")
Repeat(100)
   DIO!WaitBit("P1","A","0","ON")
Procedure!Start
Dataset!SaveAs("C:\Users\Xavi\demonstration\sample_NNN")
EndRepeat
```
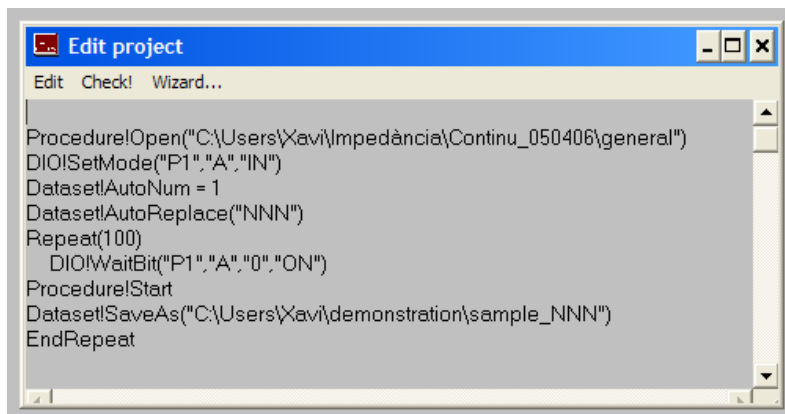
Fig. 9.3 Representation of the compendium of commands composing the *Project* application of the FRA-2 software for the synchronization of the SIA-IF and the measurement systems via trigger signals. The command DIO!WaitBit remained the FRA-2 module of the AUTOLAB in standby mode until receiving a trigger signal from the DAQ card to the port 1.

9.2.4 Software structure and hierarchy

The elements of the SIA system, namely the DAQ card, the MVP and the bi-directional burette, were controlled and synchronized with the measurement system with a home-made VI application implemented in LabView 7.1. This LabView application could be understood to be organized in three different levels of hierarchy (Fig. 9.4).

In the first level, the experiment was defined as a sequence of orders that the user declared as parameters using the interactive front panel shown in Fig. 9.5. For each input of the MVP, the content, the inoculated volume, the time remaining in the electrochemical cell and the position in the measurement sequence could be chosen. The time between sequences and the number of sequences could also be defined by the user. In the second level, each order previously declared was converted into a compendium of tasks involving a specific response of the burette and / or the MVP. Finally, in the third level, the sequence of commands describing a particular task was executed. Commands

are particular programming codes designed to change the status of specific devices, basically the burette and the MVP.

LEVEL 1: ORDERS

MVP port number	content	order sequence	features
1	Incubator	1	3 mL 3 min
2	ABMM medium	3	3 mL 3 min
3	Stock solution	4	3 mL 3 min
4	Distilled water	2	5 mL 15 min
5	…	…	…
6	…	…	…
7	…	…	…
8	…	…	…

LEVEL 2: TASKS

1. Collect the sample volume

2. Inject the volume into the cell

3. Wake up Autolab and measure

4. Move the liquid to the waste

LEVEL 3: COMMANDS

1. *BUR:* OP30000

2. *MVP:* INPUT 'WASTE'

3. *BUR:* IHOP 25000IH

Fig. 9.4 Scheme of the three levels of hierarchy of the LabView application during the sequence of experiments.
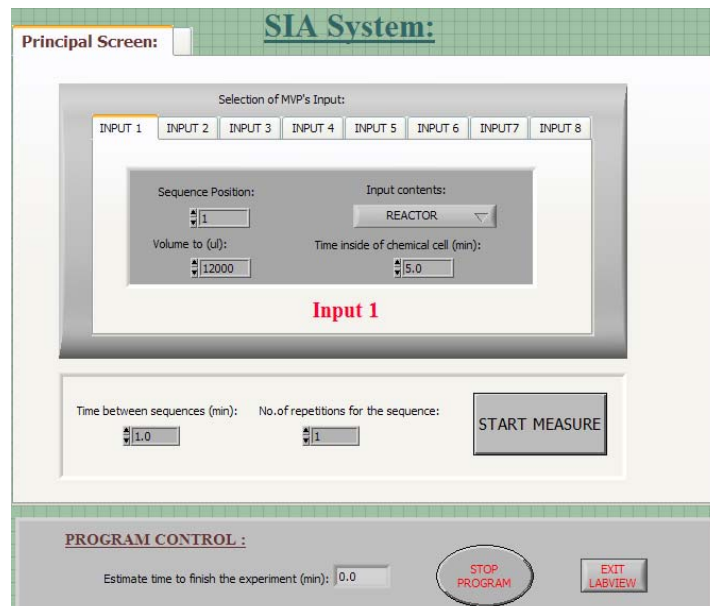
Fig. 9.5 Image of the front panel of the application containing the parameters declared by the experimental protocol in use.

As exposed above, the front panel showed the sequence of the experimental protocol in use. It has to be noted that the declared parameters could be changed by the user even when the experiment was running. However, these changes were not active in the experiment that was currently running but in next cycles.

9.2.5   Automated sampling and cleaning processes

Fig. 9.6 shows the automated system used in this application.
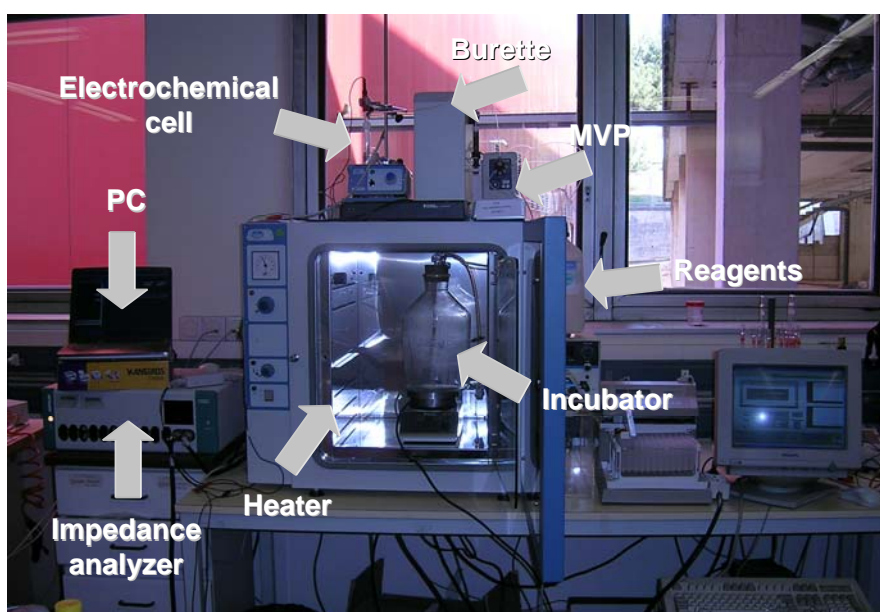
Fig. 9.6 Image of the elements composing the automatic system for the monitoring of bacteria concentration.

Tubes and mobile parts in contact with the microbiological samples were previously autoclaved to avoid contamination. In the sampling process, 2 mL culture aliquots were automatically extracted from the incubator (port 1) and transported to the electrochemical cell using the burette as a pump. This process was periodically repeated every 30 min. In the electrochemical cell, the aliquots were impedimetrically measured under the experimental conditions detailed in Chapter 3 (Section 3.3.1) 15 s after the complete inoculation of the sample. 1.5 min after the complete inoculation of the sample (when the EIS measurement were already made), the bacterial aliquot was automatically extracted from the electrochemical cell and removed to the wasting recipient (port 8).

The cleaning process was composed of two steps. In the first one, the electrochemical cell was sterilized with 3 mL of 96 % ethanol (port 6) for 3 min under constant stirring. After sterilization, the cell was cleaned twice with 3 mL of distilled water (ports 4 and 5) for 8 and 15 min, respectively. This process ensures the practically complete elimination of alcoholic traces from the electrochemical cell.

9.3 RESULTS AND DISCUSSION

9.3.1 Fitting and interpretation of impedance data

Z-View software was used to fit EIS data to the equivalent circuit shown in Fig. 9.7.
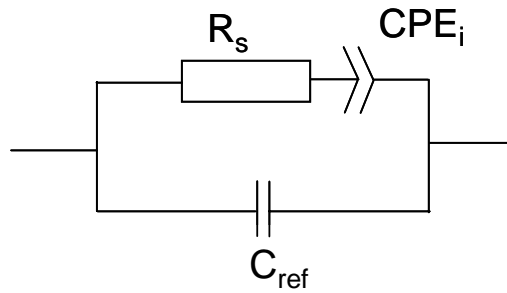
Fig. 9.7 Equivalent circuit used for the fitting of the EIS data, which contains the capacitance associated to the reference electrode (C_{ref}), the solution resistance (R_S) and the interface Constant Phase Element (CPE$_i$).

The CPE magnitude (K_i) from the fitting was then normalized using Eq. 9.1. $K_i(t)$ is the value of CPE at any time and $K_i(m)$ is the CPE value for the culture medium without bacteria:

$$\Delta K_i(t) = \frac{K_i(t) - K_i(m)}{K_i(m)} \cdot 100 \qquad (9.1)$$

The obtained $\Delta K_i(t)$ was finally interpolated in the calibration curve shown in Fig. 9.8. It has to be noted that both experiments (calibration curves and bacteria growth) were

comparable since both of them were made using the same bacteria, culture medium, equipment, experimental conditions and identical platinum electrodes.
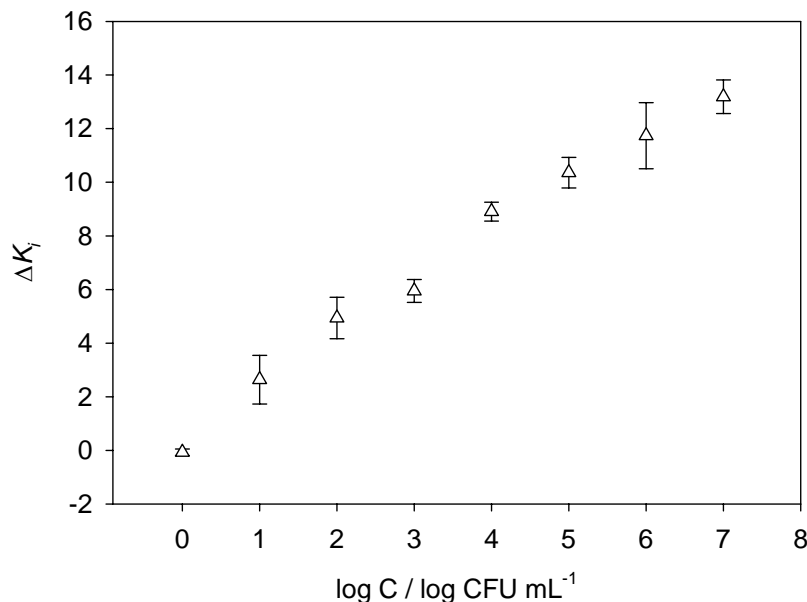
Fig. 9.8 Representation of the ΔK_i, with the suspended concentration of bacteria. This calibration curve was used for converting capacitance values into bacteria concentrations.

9.3.2 *Checking of the electrodes*

The checking of the electrode in use was absolutely necessary to keep the real-time system in good working order. With time, the *real* bacteria concentration in the incubator may differ from that value obtained from EIS data as a consequence of the aging of the sensor (see Chapter 7, Section 7.3.5). For this reason, at the beginning and sometimes in the middle of a sequence of experiments, the magnitude of the CPE_i of the electrode in use was adjusted to ensure the correct correlation of EIS data with the *real* concentration values. The checking process consisted in adjusting the calibration curve to the capacitance values given by the electrode.

Experimentally, 2 mL of culture medium without bacteria (port 2) were inoculated and measured in the electrochemical cell. After the cleaning process previously described, a stock suspension of 10^4 CFU mL^{-1} (port 3) was measured following the same experimental conditions and the normalized value for the 10^4 CFU mL^{-1} sample, called

$\Delta K_i(4)$, was next calculated. This value was compared with that introduced in the calibration curve and the curve was shifted and thus adjusted to the electrode in use.

It has to be noted that this adjusting process could be made since, regarding Chapter 7 (Section 7.3.5), the sensitivity of the electrode (slope of the calibration curve) remained invariant despite of the aging of the sensor.

9.3.3 Comparison of EIS data with bacteria concentration values from Epifluorescence Microscopy
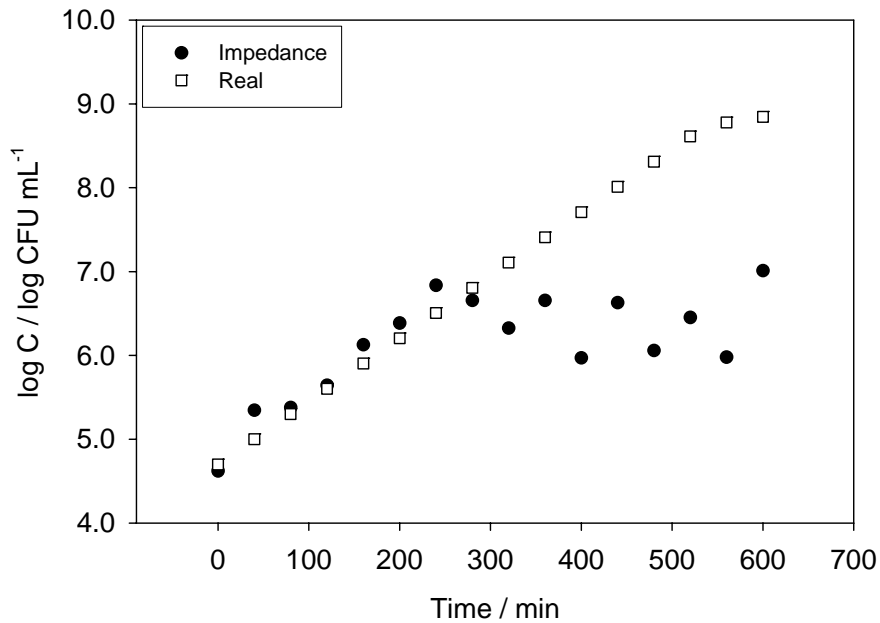
Fig. 9.9 Representation of the bacterial growth curve obtained using EIS and Epifluorescence Microscopy by *E. coli* aerobically growing at 37 ℃ with constant stirring.

The monitoring of the bacteria growth followed the experimental protocol previously detailed. EIS and Epifluorescence Microscopy measurements were made as described above. In Fig. 9.9, the bacteria concentration from the real-time impedimetric system was compared with the *real* concentration from Epifluorescence Microscopy. The bacteria concentration values recorded using both strategies were found to be practically

identical until 10^7 CFU mL^{-1}. Above this concentration, the impedimetric approach lost the linearity with bacteria concentration, as previously shown.

9.4 CONCLUSIONS

In this Chapter, new VI implemented in LabView environment has been applied to the real-time and automatic monitoring of bacteria growth. The VI has been used for the management of the adaptation of the SIA system and for the synchronization of both the flow and the EIS measurement systems. The concentration values from EIS have been found to show concordance with those obtained using Epifluorescence Microscopy until achieving a concentration around 10^7 CFU mL^{-1}.

9.5   REFERENCES

[1] R. Escudé-Pujol, X. Muñoz-Berbel, N. Vigués, J. Mas, F.X. Muñoz, *Measurement Science and Technology*, (Submitted)

[2] M. Trojanowick, *Flow injection analysis: Instrumentation and Applications*. Singapore, World Scientific Ltd. (2000)

[3] J. Ruzicka, E.H. Hansen, *Analytica Chimica Acta*, **78** (1975) 145-157

[4] A. Rainelli, R. Stratz, K. Schweizer, P.C. Hauser, *Talanta*, **61** (2003) 659-665

[5] E.H. Hansen, *Analytica Chimica Acta*, **216** (1989) 257-273

[6] J. Ruzicka, G.D. Marshall, *Analytica Chimica Acta*, **237** (1990) 329-343

[7] J.M. Estela, V. Cerda, *Talanta*, **66** (2005) 307-331

[8] G.D. Christian, *The Analyst*, **119** (1994) 2309-2314

[9] J.F. van Staden, *Analytica Chimica Acta*, **467** (2002) 61-73

[10] D. Balestrino, J.A.J. Haagensen, C. Rich, C. Forestier, *Journal of Bacteriology*, **187** (2005) 2870-2880

[11] F.R.P. Rocha, B.F. Reis, E.A.G. Zagatto, J.L.F.C. Lima, R.A.S. Lapa, J.L.M. Santos, *Analytica Chimica Acta*, **468** (2002) 119-131

[12] H. Itabashi, H. Kawamoto, T. Kawashima, *Analytical Sciences*, **17** (2001) 229

[13] R.A.S. Lapa, J.L.F.C. Lima, B.F. Reis, J.L.M. Santos, E.A.G. Zagatto, *Analytica Chimica Acta*, **466** (2002) 125-132

CHAPTER 10: RESOLUTION OF BINARY MIXTURES OF MICROORGANISMS USING ELECTROCHEMICAL IMPEDANCE SPECTROSCOPY AND ARTIFICIAL NEURAL NETWORKS

CHAPTER 10: RESOLUTION OF BINARY MIXTURES OF MICROORGANISMS USING ELECTROCHEMICAL IMPEDANCE SPECTROSCOPY AND ARTIFICIAL NEURAL NETWORKS

This Chapter describes the resolution of binary mixtures of microorganisms using Electrochemical Impedance Spectroscopy (EIS) and Artificial Neural Networks (ANNs) for the processing of data. *Pseudomonas aeruginosa* (*P. aeruginosa*), *Staphylococcus aureus* (*S. aureus*) and *Saccharomyces cerevisiae* (*S. cerevisiae*) were chosen as Gram-negative bacteria, Gram-positive bacteria and yeasts models, respectively. As overview, the magnitude of the interface Constant Phase Element (CPE$_i$) was found to correlate well with the suspended cells concentration when measuring samples that only contained single specie of microorganisms. In the resolution of binary mixed suspensions, best results were obtained by using back-propagation neural networks made up by two hidden layers. The optimal configuration of these layers respectively used the radial-basis (*radbas*) and the log-sigmoidal (*logsig*) transfer functions with 4 or 6 neurons in the first hidden layer and 10 neurons in the second one. In all cases, good prediction ability was obtained with correlation coefficients better than 0.989 when comparing the predicted and the expected values for a set of 6 external test samples not used for training. This work has been recently submitted for publication in *Biosensors and Bioelectronics* (Annex VIII)[1].

10.1 INTRODUCTION

Microbiological communities that inhabit in natural microenvironments (soil, water or air) are commonly composed of mixtures of microorganisms (e.g. bacteria, yeasts, fungi, etc.). Even, it is not surprising to find some microorganisms cohabiting together in biofilms (coopering or competing)[2-4]. The current microbiology pretends the development of new methods for the fast and simple discrimination, identification and quantification of microorganisms from complex and heterogeneous populations.

Quantification of microorganisms in mixed populations has been attempted using differential plating, nucleic acid techniques including oligonucleotides probes and genotyping[5, 6] or enzymatic methods[7]. Techniques using synthetic rRNA-targeted hybridization probes are particularly promising for detection, enumeration and identification in situ or after differential plating since their specificity can be adjusted[6]. However, although highly specific, the majority of these methods still require considerable experience as well as time and they are therefore less suitable for use in a routine laboratory.

The Infrared Spectroscopy, particularly after the development of the Fourier Transform Infrared (FTIR) Spectroscopy, has become one of the most widely used techniques for the identification, differentiation and classification of mixed microorganism samples[8-11]. With this method, the infrared spectrum of unknown species is compared with all spectra present in the spectral reference library and matched to the library strain whose spectrum is most similar[12]. Differences between spectra are generally not visible to the naked eye and powerful statistical methods, such as Principal Component Analysis (PCA)[13], Hierarchical Cluster Analysis (HCA)[14], Discriminant Analysis (DA)[15], Discriminant Function Analysis (DFA)[16], Canonical Variate Analysis (CVA)[17], *K*-Nearest Neighbour (KNN)[18], Soft Independent Modelling of Class Analogy (SIMCA)[18], Partial Least Square (PLC)[12] or ANNs[19], have to be applied. Although the quantitative differentiation of individual species present in a mixed population has been attempted using FTIR spectroscopy, the results have not been as good as expected. The main drawback was the fact that the quality of the obtained results was found to be especially

dependent on the characteristics of the microorganism involved in the quantification process[12].

ANNs are intelligent chemometric tools able to predict samples that have not been processed initially and then classify or quantify them, in much the same way as humans use the sense of taste[20]. An ANN is not based on an explicit algebraic model, but rather on a set of activation units, known as neurons or nodes, which are connected to each other in the form of a network[21]. Feedforward multilayer perceptron neural networks were used for modelling the sensors, which structure consists of an input layer (which feeds the input signals to the succeeding layer), a hidden layer (that receives, processes and sends the filtered signals to the next layer), and an output layer, which links the ANN to the outside world and supplies the processed information. The information is processed through a transfer function in each neuron. In the hidden layer the function is usually sigmoidal, such as *logsig* or tan-sigmoidal (*tansig*), while in the input and output layers it is typically linear[22]. In order to train the ANN it is necessary to determine the magnitude of interaction (weights) between neurons, that is, to establish how changes among the weights of one layer lead to variations in those of the succeeding one. This is achieved using back-propagation techniques, which aim to find the weights that minimise the error function. The calculation can be performed using training algorithms, such as Gradient Descent with Momentum (GDM) or Levenberg-Marquardt (LM). Further, chemometric tools, namely ANNs and PLC, were probed to be capable to resolve EIS data[23, 24].

This Chapter describes the resolution of binary mixtures of microorganisms (quantitative differentiation of individual microorganisms in mixed samples), using EIS and ANNs. In this case, the binary combinations of *P. aeruginosa* (Gram-negative bacteria model), *S. aureus* (Gram-positive bacteria model) and *S. cerevisiae* (yeasts model) were resolved.

10.2 EXPERIMENTAL

This Section describes the preparation of mixed microbiological samples. The modelling of EIS data using ANNs is also detailed. EIS measurements were made

following the protocol exposed in Chapter 7 (Section 7.2.1) under the experimental conditions exposed in Chapter 3 (Section 3.3.1).

10.2.1 Preparation of the microbiological mixed suspensions

Microorganisms were grown in separate under optimal experimental conditions in specific culture media, namely AB Minimal Medium (ABMM) for *P. aeruginosa*, Luria-Bertani (LB) medium for *S. aureus* (ATTC 6530) and the *universal medium for yeasts* DSMZ 186 (DSMZ, Germany) for *S. cerevisiae*. Bacteria were grown overnight at 37 ºC but yeasts, with a longer duplication time, required at least 48 h growing at 30 ºC to reach an initial concentration of around 10^9 Colony Forming Units per mL (CFU mL^{-1}). Cells were then isolated and cleaned. 10 mL of culture medium were centrifuged for 15 min at 1600 *g*. The supernatant liquid was removed and cells (the pellet) were re-suspended in 5 x 10^{-3} M KCl. The process was repeated twice in order to remove metabolic products, membrane fragments and cytoplasmatic proteins. The final pellet was re-suspended in 10 mL of 5 x 10^{-3} M KCl and then counted using plating on agar containing LB medium. The suspension was then serially diluted down to 1 CFU mL^{-1} in decade steps.

The mixed response to *P. aeruginosa* and *S. aureus*, to *P. aeruginosa* and *S. cerevisiae* and to *S. aureus* and *S. cerevisiae* was evaluated. A total amount of 22 mixed suspensions were manually prepared, with values selected randomly that completely covered the linear range of response of each microorganism. Before measurement, biological samples were stored at 4 °C to slow growth. All of the manipulations were performed under sterile conditions.

10.2.2 ANN modelling

ANNs were used to model the combined response of three binary mixtures of microorganism and the response to these cells was modelled with 22 manually prepared mixed suspensions, whose values were selected randomly, as previously detailed. 22 samples were proved to be enough to model correctly the combined response of two species and considered sufficient examples of interactions among them[25].

The whole EIS spectrum, recorded after 50 s of attachment (see Chapter 7, Section 7.2.1), was treated with ANNs as a calibration tool. The total set of samples was randomly divided into two subsets: (1) the training set (75 % of EIS spectra), which served to determine the model's parameters, and (2) the test set (25 % of EIS spectra), which enabled the model's predictive ability to be evaluated[26].

Calculations were made by developing the corresponding programs in MATLAB (MATLAB 6.1, Mathworks, USA) which employed its Neural Network Toolbox (Neural Network Toolbox 4.0.2, Mathworks, USA). In all cases, the ANNs used were feedforward networks and were trained using back-propagation algorithms, viz. Bayesian Regularization (BR), specially efficient with small data sets, given it does not employ an internal validation subset[27].

10.3 RESULTS AND DISCUSSION

10.3.1 Determination of the calibration curves for each microorganism using EIS

EIS data for each individual microorganism in a range of concentrations from 10^1 to 10^9 CFU mL^{-1} were fitted using the *Z-View* software to the equivalent circuit shown in Fig. 10.1.
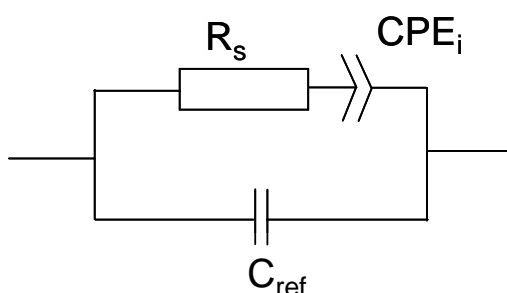
Fig. 10.1 Equivalent circuit used for the fitting of the EIS data, which contains the capacitance associated to the reference electrode (C_{ref}), the solution resistance (R_S) and the CPE$_i$.
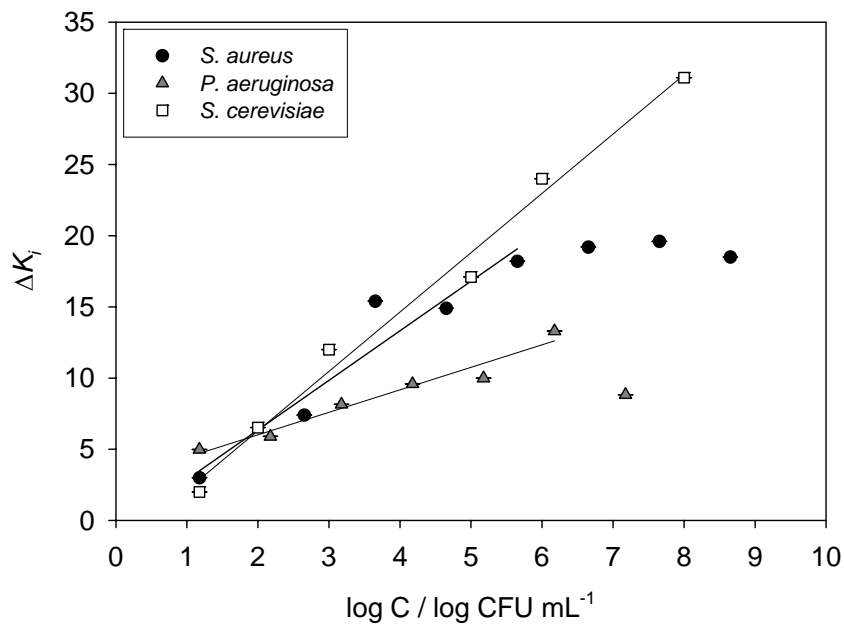
Fig. 10.2 Representation of the normalized magnitude of the interface capacitance, ΔK_i, with the suspended concentration of *S. aureus*, *P. aeruginosa* and *S. cerevisiae*. This calibration curve was used for obtaining the linear range of response of each microorganism.

The CPE magnitude from the fitting was then normalized using Eq. 10.1. K_i is the value of CPE at any concentration and $K_i(m)$ is the value of CPE of the culture medium in absence of bacteria:

$$\Delta K_i = \frac{K_i - K_i(m)}{K_i(m)} \cdot 100 \qquad (10.1)$$

Fig. 10.2 shows the correlation of the normalized CPE_i magnitude with the suspended concentration of each individual microorganism.

Following the discussion exposed in Chapters 4 and 7, all of these microorganisms showed capacity to attach to the platinum electrode surface and thus modifying the structure of the electrode-solution interface. However, the magnitude of the response differed between microorganisms. EIS was found to be extremely sensitive to the changes produced in the interface structure by *S. cerevisiae* attachment in a vast range

of concentrations, from 10^1 to 10^8 CFU mL^{-1}. This may be associated to the fact that yeasts are much bigger than bacteria and may produce deeper changes in the interface structure when attaching. Regarding to bacteria, the impedimetric approach was more sensitive (in terms of slope of the calibration curve) to the changes caused by *S. aureus* than those caused by *P. aeruginosa*. An explanation of this fact could be obtained by considering the composition of the external membranes of these bacteria: the presence of teichoic acids, highly charged molecules, in the external layers of *S. aureus* may be thought to cause deeper changes in the interface structure than the lipopolysaccharides that surround *P. aeruginosa*.

Although experimental data showed differences between microorganisms, they were not visible to the naked eye and powerful statistical methods were applied, specifically ANNs.

10.3.2 *Building of the response models and interpretation of ANNs results*

As stated above, three sets of 22 mixed suspensions were prepared in order to build the response models. The concentration range was chosen to practically coincide with the linear response range of each microorganism to the impedimetric method in use, commonly avoiding the boundary values. Thus, regarding the previous calibration curves, the ranges from 10^1 to 10^6 CFU mL^{-1}, 10^2 to 10^6 CFU mL^{-1} and 10^1 to 10^7 CFU mL^{-1} were respectively selected for *S. aureus*, *P. aeruginosa*, and *S. cerevisiae*. Each set of samples was then randomly subdivided into two different subsets, namely training and test, which comprised 16 and 6 points, respectively. It has to be noted that the extreme values were reserved for the training subset to avoid the adjusted ANN to extrapolate these points out of the obtained model.

In the impedimetric approach here described, the CPE$_i$ was found to correlate with the concentration of microorganism, whereas resistive elements, such as the R_S, remained invariant. Thus, the imaginary component of the 22 impedance spectra (Z'') corresponding to each binary mixture of microorganisms was considered as the input vector in the ANN (a total of 30 values, corresponding to the 30 scanned frequencies),

being the corresponding concentrations the targets that the modelling should reach. Fig. 10.3 shows the schematic way of action of the proposed ANN modelling.
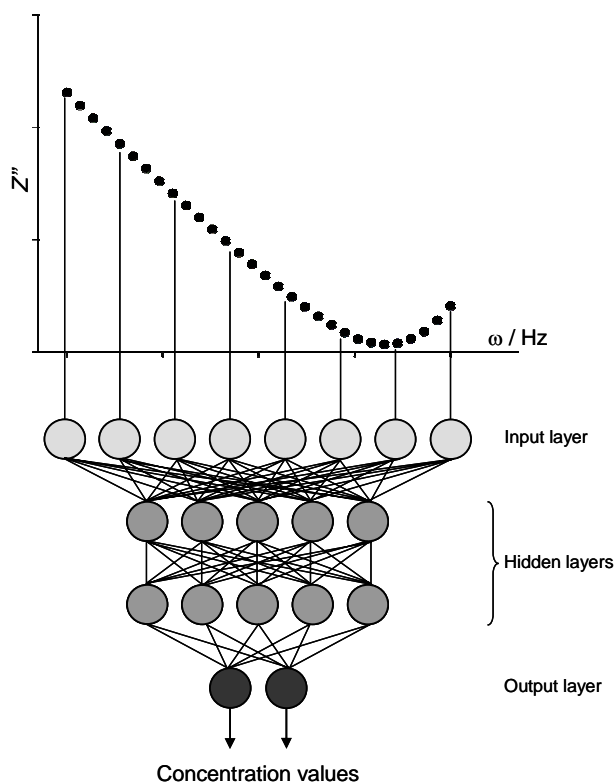
Fig. 10.3 Scheme of the approach used in the study. Each Z'' was taken as input in the ANN. Appropriate training was made until the targets were reached within the established errors.

In order to choose the ANN that best fulfilled this purpose, different structures with supervised learning were considered. In all cases, some features of the structure were established in advance: 30 neurons in the input layer (one for each Z''), two neurons in the output layer (one for each microorganism to be quantified in the binary mixture) and linear transfer functions in both input and output layers. The use of two hidden layers was found to be necessary when modelling EIS data[24]. Thus, the evaluated structures always had two hidden layers with a variable number of neurons (from 3 to 6 in the first hidden layer and from 3 to 20 in the second one). Finally, all possible combinations of transfer functions (*tansig*, *logsig* and *radbas*) in both hidden layers were tested.

The modelling capacity of the ANN was evaluated in terms of the Root Mean Squared Error (RMSE):

$$RMSE = \sqrt{\frac{\sum_{ij}\left(c_{ij} - \hat{c}_{ij}\right)^2}{2n - 1}} \qquad (10.2)$$

where n is the number of samples ($2n$, as many as two species were determined) and c_{ij} and $\hat{c}_{ij}$ are the expected concentration value and that provided by the ANN, respectively, for each compound, with i denoting samples and j species.

Table 10.1 shows the magnitude of the RMSE for some relevant tested combinations. It has to be emphasized that, for each tested combination, the RMSE magnitude was an average from three reinitialisations of the ANN. Before reinitializing, the weight values were reset and fixed to random values. Thus, the ANN was retrained to see if the model converged in similar situations or whether it reached local minima.

Table 10.1 Obtained RMSE values for different combinations of transfer functions in the hidden layers and number of neurons in these layers.

Neurons number (hidden layer 1-hidden layer 2)	Transfer function (hidden layer 1-hidden layer 2)	RMSE (log CFU mL^{-1})
S. aureus – P. Aeruginosa **mixed samples**		
4-10	*radbas-logsig*	0.8196
5-10	*radbas-tansig*	1.1871
3-15	*radbas-logsig*	1.1605
6-20	*logsig-tansig*	2.2085
S. aureus – S. cerevisiae **mixed samples**		
3-5	*radbas-tansig*	2.0050
4-10	*radbas-logsig*	1.2530
5-15	*tansig-radbas*	1.9926
6-10	*logsig-radbas*	2.1557
P. aeruginosa – S. cerevisiae **mixed samples**		
3-10	*tansig-logsig*	2.0553
4-15	*tansig-radbas*	2.2239
5-5	*radbas-tansig*	1.7902
6-10	*radbas-logsig*	1.4337

In all cases, lower RMSEs were found when using the *radbas* and the *logsig* transfer functions in the first and the second hidden layers, respectively. However, the optimum number of neurons depended on the case, being 4 and 10 for the first and second hidden layers when resolving binary mixtures containing *S. aureus* (*S. aureus - P. aeruginosa* or *S. aureus - S. cerevisiae*) or 6 and 10 by binary mixtures of *P. aeruginosa* and *S. cerevisiae*.

The global behaviour of the modelling system for the external test set was also evaluated by plotting the predicted values (from the ANN) against the expected ones (from plating on agar). Good models should display comparative lines with high correlation, a slope equal to one with zero intercept. Best models were found to coincide with those that previously showed low RMSEs.

The regression parameters of the comparative lines between predicted and expected values for the optimal ANN configurations are shown in Table 10.2.

Table 10.2 Correlation between obtained and expected values in training (n = 16) and external test (n = 6) sets using the final ANN configuration.

		Slope	Intercept (log CFU mL^{-1})
***S. aureus – P. Aeruginosa* mixed samples**			
Training	*S. aureus*, *r* = 0.996	0.96 ± 0.05	0.10 ± 0.15
	P. aeruginosa, *r* = 0.998	0.97 ± 0.03	0.12 ± 0.13
Test	*S. aureus*, *r* = 994	1.0 ± 0.2	-0.2 ± 0.5
	P. aeruginosa, *r* = 0.996	0.89 ± 0.11	0.1 ± 0.4
***S. aureus – S. cerevisiae* mixed samples**			
Training	*S. aureus*, *r* = 0.999	0.996 ± 0.012	0.02 ± 0.05
	S. cerevisiae, *r* = 0.999	0.998 ± 0.005	0.02 ± 0.02
Test	*S. aureus*, *r* = 977	1.0 ± 0.3	-0.2 ± 1.3
	S. cerevisiae, *r* = 0.997	1.03 ± 0.11	-0.1 ± 0.5
***P. aeruginosa – S. cerevisiae* mixed samples**			
Training	*P. aeruginosa*, *r* = 0.996	0.94 ± 0.06	0.2 ± 0.2
	S. cerevisiae, *r* = 0.988	0.94 ± 0.10	0.2 ± 0.5
Test	*P. aeruginosa*, *r* = 994	0.87 ± 0.14	0.3 ± 0.6
	S. cerevisiae, *r* = 0.989	1.0 ± 0.2	-0.2 ± 0.8

In all cases, very good correlation was obtained with comparison lines indistinguishable from the theoretical values.

10.4 CONCLUSIONS

In this Chapter, the combination of EIS and ANNs has been demonstrated to be able to quantitatively solve three binary mixtures of microorganisms, namely *P. aeruginosa*, *S. aureus* and *S. cerevisiae*. In all cases, best models have been found to be made up by two hidden layers, using the *radbas* transfer function in the first one and the *logsig* in the second one. Configurations with lowest RMSEs have been always found to use 10 neurons in the second hidden layer. However, the optimal number of neurons in the first hidden layer varied depending on the case: 4 when resolving binary mixtures containing *S. aureus* (*S. aureus - P. aeruginosa* or *S. aureus - S. cerevisiae*) or 6 by binary mixtures of *P. aeruginosa* and *S. cerevisiae*. Finally, the predictive ability of the final modelling system has been evaluated by comparing the predicted values (from the ANN) against the expected ones (from plating on agar). In this case, very good correlation has obtained with comparison lines indistinguishable from the theoretical values (slope equal to one with zero intercept in the three cases under study).

10.5 REFERENCES

[1] X. Muñoz-Berbel, N. Vigués, J. Mas, M.d. Valle, F.X. Muñoz, M. Cortina, *Biosensors and Bioelectronics*, (Submitted)

[2] P. Stoodley, K. Sauer, D.G. Davies, J.W. Costerton, *Annual Review of Microbiology*, **56** (2002) 187-209

[3] J. Wiley. *Wiley series in ecological and applied microbiology*. W.G. Characklis, K.C. Marshall, eds. *Biofilms*. New York, John Wiley (1990)

[4] H.M. Lappin-Scott, J.W. Costerton, eds. *Microbial Biofilms*. Cambridge, Cambridge University Press (1995)

[5] R.I. Amann, B.J. Binder, R.J. Olson, S.W. Chisholm, R. Devereux, D.A. Stahl, *Applied and Environment Microbiology*, **56** (1990) 1919-1925

[6] W.P. Charteris, P.M. Kelly, L. Morelli, J.K. Collins, *International Journal of Food Microbiology*, **35** (1997) 1-27

[7] C.Y. Boquien, G. Corrieu, M.J. Desmazeaud, *Applied Microbiology and Biotechnology*, **30** (1989) 402-407

[8] L. Mariey, J.P. Signolle, C. Amiel, J. Travert, *Vibrational Spectroscopy*, **26** (2001) 151-159

[9] L.C. Thomas, J.E.S. Greenstreet, *Spectrochimica Acta*, **6** (1954) 302-319

[10] D. Naumann, V. Fijala, H. Labischinski, P. Giesbrecht, *Journal of Molecular Structure*, **174** (1988) 165-170

[11] I. Horbach, D. Naumann, F.J. Fehrenbach, *Journal of Clinical Microbiology*, **26** (1988) 1106-1110

[12] H. Oberreuter, F. Mertens, H. Seiler, S. Scherer, *Letters in Applied Microbiology*, **30** (2000) 85-89

[13] G.D. Sockalingum, W. Bouhedja, P. Pina, P. Allouch, C. Mandray, R. Labia, J.M. Millot, M. Manfait, *Biochemical and Biophysical Research Communications*, **232** (1997) 240-246

[14] J. Bastert, H.C. Korting, P. Traenkle, A.F. Schmalreck, *Mycoses*, **42** (1999) 525-528

[15] C. Amiel, L. Mariey, M.-C. Curk-Daubié, P. Pichon, J. Travert, *Lait*, **80** (2000) 445-459

[16] É.M. Timmins, D.E. Quain, R. Goodacre, *Yeast*, **14** (1998) 885-893

[17] S.H. Beattie, C. Holt, D. Hirst, A.G. Williams, *FEMS Microbiology Letters*, **164** (1998) 201-206

[18] M. Kansiz, P. Heraud, B. Wood, F. Burden, J. Beardall, D. McNaughton, *Phytochemistry*, **52** (1999) 407-417

[19] T. Udelhoven, D. Naumann, J. Schmitt, *Applied Spectroscopy*, **54** (2000) 1471-1479

[20] M. Cortina, A. Gutes, S. Alegret, M. del Valle, *Talanta*, **66** (2005) 1197-1206

[21] M. Ramis, M.C. García, *Quimiometría*. Madrid, Síntesis (2001)

[22] J.A. Freeman, D.M. Skapura, *Neural Networks: Algorithms, Applications and Programming Techniques*. Reading, MA, USA, Addison-Wesley (1991)

[23] M. Cortina-Puig, X. Munoz-Berbel, M.A. Alonso-Lomillo, F.J. Munoz-Pascual, M. del Valle, *Talanta*, **72** (2007) 774-779

[24] M. Cortina-Puig, X. Munoz-Berbel, M. del Valle, F.J. Munoz, M.A. Alonso-Lomillo, *Analytica Chimica Acta*, **597** (2007) 231-237

[25] M. Cortina, C. Ecker, D. Calvo, M. del Valle, *Journal of Pharmaceutical and Biomedical Analysis*, **46** (2008) 213-218

[26] J.C. Mackay, *Network: Computation in Neural Systems*, **6** (1995) 469-505

[27] H. Demuth, M. Beale, *Neural Network Toolbox, for Use with MATLAB*. Natick, MA, USA, Mathworks Inc (1992)

CHAPTER 11: DETERMINATION OF THE ROLE OF SEVERAL PROTEINS FROM PHOTORHABDUS LUMINESCENS IN THE FORMATION OF BIOFILMS, EARLY ATTACHMENT, MOTILITY AND VIRULENCE

CHAPTER 11: DETERMINATION OF THE ROLE OF SEVERAL PROTEINS FROM *PHOTORHABDUS LUMINESCENS* IN THE FORMATION OF BIOFILMS, EARLY ATTACHMENT, MOTILITY AND VIRULENCE

This Chapter describes the determination of the role of some proteins in the formation of biofilms, early attachment, motility and virulence using traditional microbiological methods and Surface Plasmon Resonance (SPR) for the characterization of the attachment capacity. In a few words, the biofilm formation, attachment capacity, motility and virulence of some mutants from a *Photorhabdus luminescens* TT01 (*P. luminescens* TT01) library was determined and compared with the wild-type (non-mutated strains), whose characteristics were taken as reference. The combination of experimental data and DNA-sequence information (when it was possible) were used for a tentative prediction of the protein function. This work was carried out at University of Bath under the supervision of Dr. A.T.A. Jenkins and Dr. Nick Waterfield during a 4-month academic visit.

11.1 INTRODUCTION

The bacterial mechanism of surface colonization is known to be a multi-step process which entails at least five stages from the initial preconditioning of the surface until the biofilm maturation and stabilization. However, the exact mechanism of colonization varies depending on the specific bacterium involved[1]. Although the mechanism of biofilm formation of some model bacteria, such as *Escherichia coli*[2] or *Pseudomonas putida or aeruginosa*[3-5], has been vastly studied, at the present time it is practically unknown for most of other microbe species.

Recently, there is an increasing interest in the colonization process of several bacteria species. One of them is *P. luminescens*, a rod and motile Gram-negative gamma proteobacterium that forms mutualistic symbiosis with insect-pathogenic nematodes of the family *Heterorhabditidae*[6]. Until now, *P. luminescens* was only the subject of intensive study by agricultural scientists because of the role that these bacteria play in controlling insects[7]. However, one specie of *Photorhabdus* has been identified in some human infections and even considered an emerging human pathogen[8, 9].

The external structure of pathogenic bacteria plays an important role in their lifecycle and infection since the attachment to host tissues, which is mediated by cell surface structures, may promote the initial stage of infection in many different organisms[10]. The lifecycle of *P. luminescens*, illustrated in Fig. 11.1, comprises both symbiotic and pathogenic stages and has been extensively described in the literature[6, 11]. Briefly, the free-living infective forms of the nematode, called infective juveniles, seek out and physically penetrate insect hosts. Upon reaching the insect blood system (hemocoel), bacteria, initially found within the gut of the nematode, are regurgitated. Bacteria start releasing a wide variety of virulence factors and toxins and rapidly kill the insect. Within the larval carcass, bacteria grow to stationary-phase conditions while nematodes develop and reproduce. Next, nematodes and bacteria re-associate and the infective juvenile, carrying the bacteria in their intestinal tracts, emerge from the insect carcass in search of a new insect host.
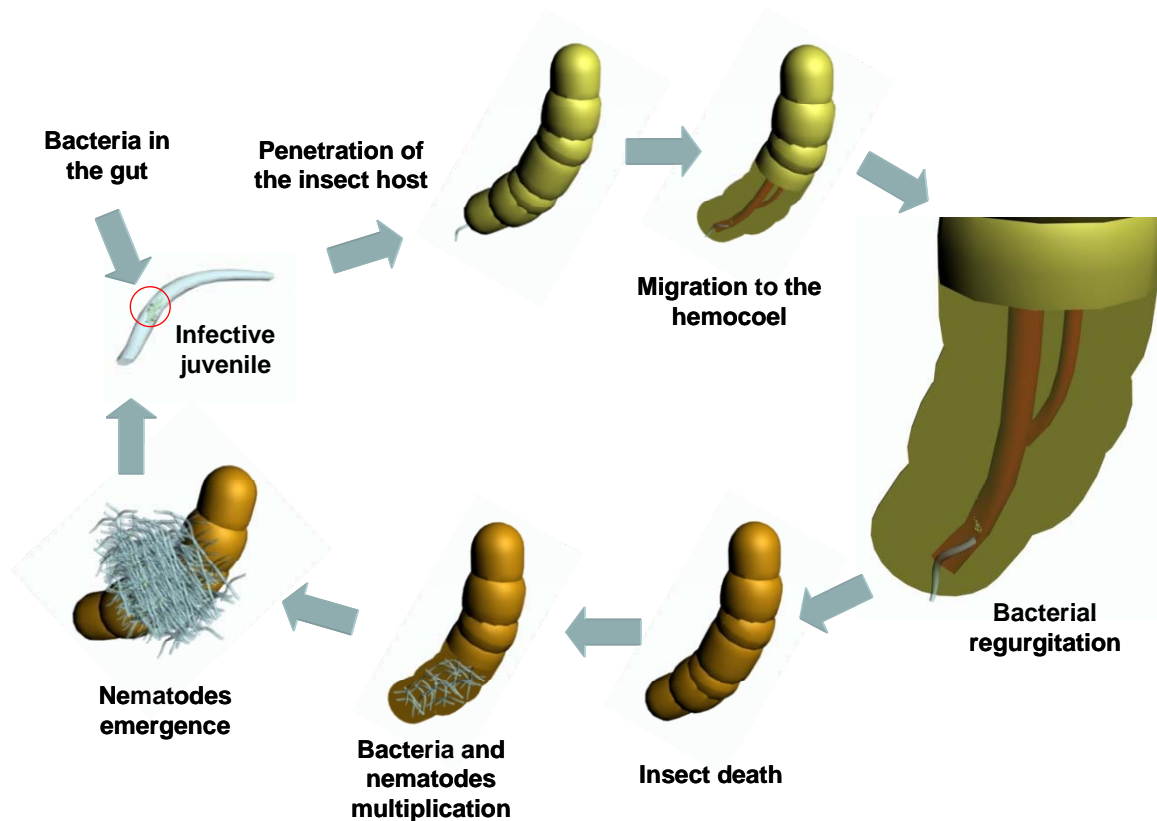
Fig. 11.1 Representation of the lifecycle of the entomopathogenic nematode *Heterorhabditis* and its bacterial symbiont *P. luminescens*.

Only few studies have been focused on the characterization of the structures involved in the attachment of *Photorhabdus* and its relationship with other important features such as motility and virulence, although they obtained important results. In the closely related *Xenorhabdus* species, fimbriae are thought to be involved in the establishment of the specific association between the bacterium and the nematode gut. Actually, their main protein has been only found expressed when the bacteria inhabit the gut of the nematode (Phase-I form of the bacteria), whereas it has not been found at detectable levels in free Phase-II bacteria[12]. The fimbriae did not either appear in Scanning Electron Microscopy images of negatively stained Phase-II cells. Phase I cells were found motile in liquid culture and semisolid agar for the presence of flagella[13]. In contrast, Phase-II bacteria were found to lack both swimming and swarming ability and did not produce flagella. Finally, *Photorhabdus* showed differences in the thickness and probably in the composition of the glycocalyx layer depending on the phase-form: Phase-I cells possessed a thicker glycocalyx layer than Phase-II cells[14]. The thickness

and the composition of the glycocalyx may be the cause of the different ability of both forms of the same bacteria to adhere to the intestinal cells of the nematode.

Mutant libraries are frequently used in molecular biology for the functional analysis of proteins[15-21]. These libraries of mutants can be generated using different methods. For example, the transposon mutagenesis, where mutants are generated by introducing vectors containing transposons (small sequences of DNA that can move around and insert at random sites within the genome of a single cell) into the organism of interest[22-25]. In this process, the transposon sequence is randomly inserted in the cell genome disrupting one gene which will result the lack of the encoded protein or in a truncated (non functional) protein. Classically, the transposon carries an antibiotic marker which confers antibiotic resistance, allowing the selection of the appropriate mutants by adding specific antibiotics in the medium, although currently other strategies can be chosen[26].

This Chapter describes the analysis of the role of several proteins of *P. luminescens* in the mechanisms of biofilm formation, early attachment, motility and virulence using SPR and microbiological methods. This study required the use of a mutant library of *P. luminescens* TT01 previously generated.

11.2 EXPERIMENTAL

This Section describes the microbiological protocols used both in the generation of the *P. luminescens* TT01 mutant library and in the preparation of the microbiological samples for their subsequent measurement. The microbiological methods used for the evaluation of the biofilm formation, the motility and the virulence of each mutant under study are also detailed. The early attachment capacity of each mutant was determined using SPR as detailed in Chapter 3 (Section 3.3.2) and following the experimental protocol exposed in Chapter 4 (Section 4.2.2).

11.2.1 Generation of the P. luminescens mutant library

P. luminescens TT01 mutants used in the development of the present Chapter were kindly supplied by Dr. Nick Waterfield from the University of Bath. These mutants were generated using random transposon mutagenesis, following the experimental protocol previously detailed by Herrero et al[26]. The exact position of the transposon insertion causing the disruption in the bacterial DNA sequence was localized using sequencing techniques, although accurate sequences could not be obtained for all of the mutants. Bacterial mutants were stored in the freezer at -80 ºC in 20 % glycerol.

11.2.2 P. luminescens TT01 cultures

P. luminescens TT01 mutants were grown overnight in Luria-Bertani (LB) medium at 30 ºC with constant stirring at 250 *rpm*. 2 mL of each culture were centrifuged for 3 min at 3500 *g*. The supernatant liquid was removed and cells (the pellet) were re-suspended in Phosphate Buffered Saline (PBS). This process was repeated twice to ensure the complete cleaning of the cells and the elimination of metabolites, membrane fragments and debris from the final sample. Next, the pellet was finally re-suspended in PBS and cell growth was estimated by measuring the Optical Density of the suspension at 600 nm. From the calibration curve, 1 Unity of Absorbance (UA) at this wavelength was found to be equivalent to a concentration of 10^9 Colony Forming Units per mL^{-1} (CFU mL^{-1}) of *P. luminescens*. Regarding this equivalency, bacteria suspensions were then diluted down to 10^8 CFU mL^{-1}. All manipulations were performed under sterile conditions.

11.2.3 Determination of the biofilm formation ability of different P. luminescens TT01 mutants

Experimentally, the biofilm formation was induced by introducing 1 mL of the overnight culture of each *P. luminescens* TT01 mutant in a vial containing 20 mL of a culture medium poor in nutrients. As shown in Fig. 11.2, under these experimental conditions, bacteria made up thick and stable biofilms in the air-liquid interface.

The biofilm formation ability was evaluated by comparing some interesting features of the mutant biofilms under study with those shown by the wild-type biofilm. Thus, the colour, the thickness and the porosity of the mutant biofilms were monitored with time and compared with the properties of the wild-type biofilm, which were taken as a reference.
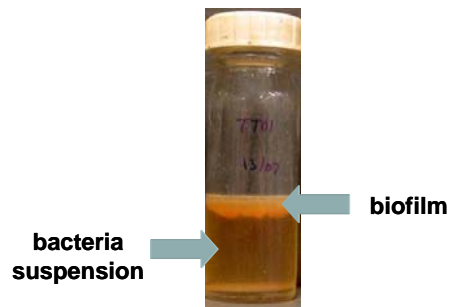
Fig. 11.2 Image of the vial where the wild-type biofilm was grown in the air-liquid interface.

11.2.4 Evaluation of swimming motility in the P. luminescens TT01 mutants

The motility of the mutants under study was evaluated using the swimming process. Experimentally, 2 µL of the overnight suspension of each mutant were inoculated in the middle of a Petri plate containing diluted Luria-Bertani (LB) nutrient medium and 0.3 % agar.
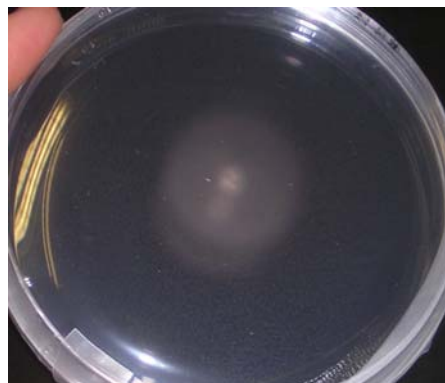
Fig. 11.3 Image of a motility assay where bacteria were moving from the inoculation point to the edges of the Petri plate.

Initially, bacteria grew in the region of the inoculation eating the nutrients that they had closer. When nutrients were insufficient, bacteria moved to richer regions expanding from the centre to the edges of the plate. This movement generated concentric circles which are illustrated in Fig. 11.3. The diameter of the circle was used to follow the motility capacity of each mutant by monitoring its magnitude with time. This value was compared with that obtained for the wild-type after the same time growing (mm diameter at 6 days post inoculation), which was taken as a reference.

For data interpretation, it has to be noted that the huge number of porous and channels in the structure of this low density agar allowed bacteria to swim through the almost-liquid medium. Although other elements, such as fimbriae, may be though to be involved in the swimming motion, this is basically produced by the flagella.

11.2.5 Determination of the virulence of the P. luminescens TT01 mutants

The virulence of the mutants under study was evaluated by injecting ten *Galleria mellonella* (larvae of the wax moth) with 10 μL of overnight culture of the mutant of interest.
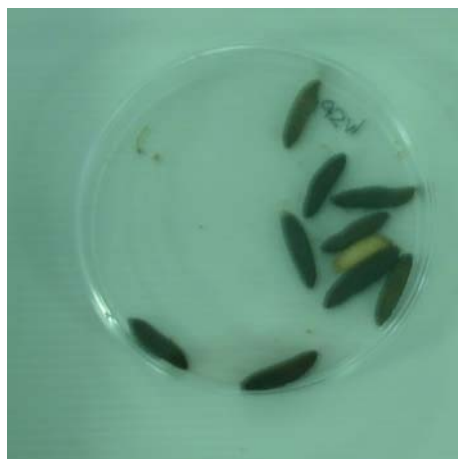
Fig. 11.4 Image of death (black) and intact (yellow) *Galleria mellonella* larvae after performing the virulence test.

The virulence of each mutant was determined by counting the number of death larvae and was expressed in percentage terms. The virulence was also compared with the wild-

type bacterium, which was taken as a reference. The counting process was easy since death larvae became black because of the necrosis of the tissues, as shown in Fig. 11.4.

11.3 RESULTS AND DISCUSSION

11.3.1 Evaluation of initial attachment capacity of the P. luminescens TT01 mutants using SPR

The initial attachment capacity of the mutants under study was evaluated using SPR as described in Chapter 3 (Section 3.3.2) by following the experimental protocol detailed in Chapter 4 (Section 4.2.2). Fig. 11.5 shows the change of the SPR differential angle when monitoring the initial attachment of some *P. luminescens* TT01 mutants.
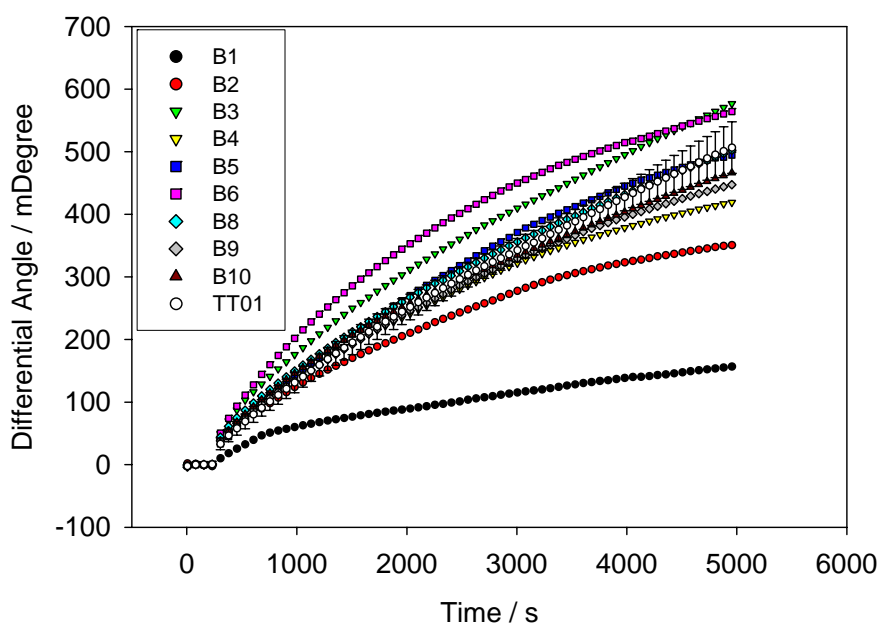
Fig. 11.5 Representation of the differential angle (from SPR measurements) versus time for nine *P. luminescens* TT01mutants and the TT01 wild-type, which was taken as a reference.

Fig. 11.5 shows that the differential angle measured using SPR changed as a function of the attachment time. However, the variation of the angle was found to be very similar in most of the mutants and comparable to that obtained when measuring the initial attachment of the wild-type. Only B1 and B2 mutants showed an important decrease in

the attachment capacity of the bacteria. Small differences in comparison with the wild-type could also be found in B3 and B6 mutants, with a slightly more attachment capacity, and in B4 and B9, with slightly less attachment capacity.

11.3.2 Interpretation of experimental data for the determination of the role of specific *P. luminescens* proteins

Biofilm formation, motility and virulence assays were made as detailed in Sections 11.2.3, 11.2.4 and 11.2.5, respectively. Table 11.1 summarizes some relevant features of nine interesting *P. luminescens* TT01 mutants in terms of biofilm formation, initial attachment, motility and virulence.

Table 11.1 Summary table containing some relevant features of the mutants under study, namely the gene disrupted by the mutation, the capacity to build biofilm, the initial attachment, the motility and the virulence.

Sample name	Mutant number	Gene disrupted by transposon insertion	Biofilm formation	Initial attachment	Motility (mm diameter)	Virulence (% dead larvae)
B1	TTO1:30	phosphoheptose isomerase domain	no	lower	0.3	lower
B2	H7	unknown	pale pigmentation	lower	1.0	not tested
B3	H4	homologue to *tcaC*-tail	no	slightly higher	0.9	not tested
B4	E3	unknown	no	slightly lower	0.2	70 %
B5	A2	small ORF	no	normal	1.1	not tested
B6	G3	enterochelin gene	no	slightly higher	1.2	not tested
B8	E11	unknown	thin	normal	0.9	not tested
B9	A4	unknown	no	slightly lower	0.9	not tested
B10	G1 / G2	inositol-1-monophosphatase	no or very thin	normal	1.0	not tested
TT01	**wild type**	**no**	**yes**	**normal**	**2.0**	**90 %**

This table shows the *P. luminescens* TT01 mutants and the name of the gene disrupted by the transposon insertion. In terms of biofilm formation, all of them built abnormal biofilms (thinner and / or differently pigmented than the wild-type) or could not even form mature biofilms in the air-liquid interface. Despite of the fact that biofilm formation is always thought to be linked to the initial attachment of bacteria, the

capacity of attachment of most mutants remained practically unaltered (only small changes were recorded). This fact implied that, for the mutants under study, the impossibility to build biofilms may not be caused exclusively by the lack of adhesion capacity but by another reason. This reason may be, for instance, their low capacity of movement since all of them showed an important decrease in the motility. However, this should be tested for each case under study. Finally, the virulence has been only tested on two mutants and in both cases it was lower than the wild-type which may suggest a relationship between biofilm formation, motility and virulence.

11.3.3 Analysis of the role of a specific protein when knowing the position of the mutation: B1 mutant

In the determination of the role of the protein suppressed by the mutagenesis process in the mutant B1, the experimental data shown in Table 11.1 was considered. As a summary, B1 mutant has the transposon insertion in the *gmhA* gene (plu4004: gene name in the fully sequence *P. luminescens* TT01 genome, see http://genolist.pasteur.fr/PhotoList/), encoding a phosphoheptose isomerase. B1 could not grow biofilm in the air-liquid interface and its initial attachment, swimming motility and virulence were found to be lower than the wild-type.

Phosphoheptose isomerase is a bacterial enzyme involved in the biosynthesis of LipoPolySaccharide (LPS), particularly in the synthesis of the inner core domain[27, 28]. LPS, an integral component of the outer membrane of Gram-negative bacteria, consists of lipid A attached to a core oligosaccharide, and in some microorganisms, contains an *O*-specific surface polysaccharide which is subsequently attached to the terminal residues of the core[29, 30]. LPS plays an important role in maintaining the structural integrity of the outer membrane by interacting with other components of the external membrane and providing a physical barrier against the entry of deleterious compounds and some bacteriophages.

A clear correlation between the putative function of this protein and the experimental data could be established by considering how the modification of the outer membrane structure in bacteria could change their ability to form biofilms, to attach or even to

move. Regarding experimental data, the changes produced by the mutation in the outer layers practically impaired bacterial movement (in terms of swimming). Other structural changes in the outer bacteria membranes not directly linked with flagella and currently unknown may be the responsible of the decrease in the attachment capacity. Finally, the lack of motility and attachment of this mutant would be enough reasons to justify the impossibility to perform mature biofilms, although it should be experimentally probed. In terms of virulence, LPS have been demonstrated to have a direct relationship with virulence[31, 32]. For this reason, it is not surprising to find that after modifying the biosynthesis of LPS, the bacteria virulence also changed. On the other hand, the decrease in the bacteria virulence may also be attributed to the previously mentioned loss of attachment capacity, which could decrease both bacteria colonization and infection capacity. Also other processes may be the responsible of the decrease of virulence, such as the modification of the toxins secretion capacity of the bacteria.

11.3.4 Analysis of the role of a specific protein when the position of the mutation is unknown: B4 mutant

As illustrated in Table 11.1, the B4 mutant has not been sequenced yet and the position of its mutation is currently unknown. Experimentally, the B4 mutant could not build mature biofilms, although it was found attached around the vial glass in the air-liquid interface. Further, the attachment capacity measured using SPR was again found practically the same than that obtained by the wild-type (only slightly lower), which could suggest that the mutation has not changed the adhesion capacity of the bacteria. However, the motility and the virulence of the B4 mutant were lower than that recorded for the wild type.

From the experimental data it could be stated that: (1) this mutation did not change the bacteria adhesion capacity since it was found practically unaltered when attaching to glass or to metallic surfaces and (2) the mutation impaired swimming motility in the bacteria possibly by modifying the structure and / or function of the flagella. Thus, the other changes recorded, namely inability to form mature biofilms in the air-liquid interface and decrease virulence, may be a consequence of the previously exposed decrease of movement capacity which may prevent bacteria from both organizing in a

complex structure such as biofilm and infecting host cells. The DNA-sequencing of the mutation and additional data concerning the structure or the function of the flagella is absolutely essential for an accurate prediction of the function of this protein.

11.4 CONCLUSIONS

In this Chapter, biofilm formation (in the air-liquid interface) data, attachment capacity information (from SPR), motility results (from the swimming process) and virulence assays (using *Galleria mellonella* larvae) of some *P. luminescens* TT01 mutants have been combined for the prediction of the function of some proteins. Although characterization of the role of these proteins has been only achieved at a very basic level, the combination of techniques used, and particularly SPR, is capable of supplying relevant information rapidly and easily. The sequencing of the transposon insertion point is essential to find out the mutated gene, and to predict accurately the role of the protein under study.

11.5 REFERENCES

[1] Y.H. An, R.J. Friedman, *Journal of Biomedical Materials Research*, **43** (1998) 338-348

[2] R. Van Houdt, C.W. Michiels, *Research in Microbiology*, **156** (2005) 626-633

[3] J.W. Costerton, P.S. Stewart, E.P. Greenberg, *Science*, **284** (1999) 1318-1322

[4] M.J. Kirisits, M.R. Parsek, *Cellular Microbiology*, **8** (2006) 1841-1849

[5] M. Klausen, A. Heydorn, P. Ragas, L. Lambertsen, A. Aaes-Jorgensen, S. Molin, T. Tolker-Nielsen, *Molecular Microbiology*, **48** (2003) 1511-1524

[6] R. Ffrench-Constant, N. Waterfield, P. Daborn, S. Joyce, H. Bennett, C. Au, A. Dowling, S. Boundy, S. Reynolds, D. Clarke, *FEMS Microbiology Reviews*, **26** (2003) 433-456

[7] N. Boemare, A. Givaudan, M. Brehelin, C. Laumond, *Symbiosis*, **22** (1997) 21-45

[8] M.M. Peel, D.A. Alfredson, J.G. Gerrard, J.M. Davis, J.M. Robson, R.J. McDougall, B.L. Scullie, R.J. Akhurst, *Journal of Clinical Microbiology*, **37** (1999) 3647-3653

[9] J.G. Gerrard, S. McNevin, D.A. Alfredson, R. Forgan-Smith, N. Fraser, *Emerging infectious diseases*, **9** (2003) 251-254

[10] G. Massad, C.V. Lockatell, D.E. Johnson, H.L. Mobley, *Infection and Immunity*, **62** (1994) 536-542

[11] S. Forst, K. Nealson, *Microbiological Reviews*, **60** (1996) 21-43

[12] K. Binnington, L. Brooks, "*Fimbrial attachment of Xenorhabdus nematophilus to the intestine of Steinernema carpocapsae"*. R. Bedding, R. Akhurst, H. Kaya (Eds). Nematodes and the biological control of insect pests. Melbourne, CSIRO Publications (1993)

[13] A. Givaudan, S. Baghdiguian, A. Lanois, N. Boemare, *Applied and Environment Microbiology*, **61** (1995) 1408-1413

[14] M. Brehelin, A. Cherqui, L. Drif, J. Luciani, R. Akhurst, N. Boemare, *Journal of Invertebrate Pathology*, **61** (1993) 188-191

[15] A. Aertsen, I.V. Opstal, S.C. Vanmuysen, E.Y. Wuytack, C.W. Michiels, *FEMS Microbiology Letters*, **243** (2005) 385-391

[16] L.R. Camacho, D. Ensergueix, E. Perez, B. Gicquel, C. Guilhot, *Molecular Microbiology*, **34** (1999) 257-267

[17] M. Ito, T. Baba, H. Mori, H. Mori, *Metabolic Engineering*, **7** (2005) 318-327

[18] X. Jian, X. Pang, Y. Yu, X. Zhou, Z. Deng, *Antonie van Leeuwenhoek*, **90** (2006) 29-39

[19] J.M. Mei, F. Nourbakhsh, C.W. Ford, D.W. Holden, *Molecular Microbiology*, **26** (1997) 399-407

[20] V. Pelicic, M. Jackson, J.-M. Reyrat, W.R. Jacobs, B. Gicquel, C. Guilhot, *Proceedings of the National Academy of Sciences*, **94** (1997) 10955-10960

[21] S. Zotchev, K. Haugan, O. Sekurova, H. Sletta, T.E. Ellingsen, S. Valla, *Microbiology*, **146** (2000) 611-619

[22] R. Simon, U. Priefer, A. Puhler, *Nat Biotech*, **1** (1983) 784-791

[23] H. Vilen, J.-M. Aalto, A. Kassinen, L. Paulin, H. Savilahti, *Journal of Virology*, **77** (2003) 123-134

[24] S.B. Snapper, R.E. Melton, S. Mustafa, T. Kieser, W.R. Jacobs, *Molecular Microbiology*, **4** (1990) 1911-1919

[25] C.A. Hutchison, S.N. Peterson, S.R. Gill, R.T. Cline, O. White, C.M. Fraser, H.O. Smith, J. Craig-Venter, *Science*, **286** (1999) 2165-2169

[26] M. Herrero, V. de Lorenzo, K.N. Timmis, *Journal of Bacteriology*, **172** (1990) 6557-6567

[27] J.S. Brooke, M.A. Valvano, *Journal of Biological Chemistry*, **271** (1996) 3608-3614

[28] S. Tamaki, T. Sato, M. Matsuhashi, *Journal of Bacteriology*, **105** (1971) 968-975

[29] C.A. Schnaitman, J.D. Klena, *Microbiol. Mol. Biol. Rev.*, **57** (1993) 655-682

[30] C. Whitfield, M.A. Valvano, *Advances in Microbial Physiology*, **35** (1993) 135-246

[31] R. ffrench-Constant, D. Bowent, *Current Opinion in Microbiology*, **2** (1999) 284-288

[32] B.A. Bauer, M.K. Stevens, E.J. Hansen, *Infection and Immunity*, **66** (1998) 4290-4298

CHAPTER 12: CONCLUSIONS

CHAPTER 12: CONCLUSIONS

This Chapter describes the most relevant goals achieved during the development of the present thesis to cover the necessities previously exposed in Chapter 2.

The most important aims accomplished during the realization of this thesis have been:

1. Electrochemical Impedance Spectroscopy (EIS) and Surface Plasmon Resonance (SPR) have been found to be sensitive methods for the real-time monitoring of bacteria attachment, particularly during the very early attachment, and showed good correlation with traditional methods.

2. EIS has been demonstrated capable to monitor the formation of biofilms on gold or platinum working electrode / counter electrode (WE/CE) chips, especially in the initial stages of development, and again with good correlation with classical microbiological methods. In terms of biofilm removal, peroxides have been found to be the most effective detaching solutions.

3. The detection of bacteriophages has been probed to be possible using EIS when following the degradation of mature biofilms grown on the surface of WE/CE chips, which data correlated well with Optical and Confocal Microscopy measurements.

4. The change in the EIS magnitude due to bacteria attachment has been shown to correlate well with suspended bacteria in a wide range of concentrations [from 10 to 10^7 Colony Forming Units per mL (CFU mL^{-1})] when measuring at the pre-attachment stage, concretely measuring after 50 s of attachment.

5. The impedimetric approach previously developed has been demonstrated to be capable to monitor *real* bacteria samples directly extracted from an incubator, with good correlation with classical microbiological methods. Further, this impedimetric approach has shown an improvement in the detection limit of some orders of magnitude in comparison with traditional on-line methods, such as Optical Density.

6. New Virtual Instrumentation (VI) implemented in LabView environment, managing the modification of the Sequential Injection Analysis (SIA) system and the measurement systems, has been developed and applied to the real-time and automatic monitoring of bacteria growth. The concentration values from EIS data showed good concordance with those obtained by using Epifluorescence Microscopy until 10^7 CFU mL^{-1}.

7. The combination of EIS and Artificial Neural Networks (ANNs) has been probed to solve three binary mixtures of microorganisms, namely *Pseudomonas aeruginosa*, *Staphylococcus aureus* and *Saccharomyces cerevisiae* with good concordance with classical microbiological methods.

8. The combination of biofilm formation data (in the air-water interface), attachment capacity information (from SPR), motility results (from the swimming process) and virulence assays (using *Galleria mellonella*) of some *Photorhabdus luminescens* TT01 mutants has been shown capable to predict the function of some proteins, although at a very basic level.

ANNEX

I. **Impedimetric characterization of the changes produced in the electrode–solution interface by bacterial attachment**

Electrochemical Communications, 9 (2007) 2654-2660

X. Muñoz-Berbel, N. Vigués, J. Mas, A.T.A. Jenkins, F.J. Muñoz

II. **Impedimetric approach for quantifying low bacteria concentrations based on the changes produced in the electrode-solution interface during the pre-attachment stage**

Biosensors and Bioelectronics, Accepted manuscript

X. Muñoz-Berbel, N. Vigués, A.T.A. Jenkins, J. Mas, F.J. Muñoz

III. **On-chip impedance measurements to monitor biofilm formation in the drinking water distribution network**

Sensors and Actuators, 118 (2006) 129-134

X. Muñoz-Berbel, F.J. Muñoz, N. Vigués, J. Mas

IV. **Impedimetric approach for monitoring the formation of biofilms on metallic surfaces and the subsequent application to the detection of bacteriophages**

Electrochimica Acta, Accepted manuscript

X. Muñoz-Berbel, C. García-Aljaro, F.J. Muñoz

Impedimetric characterization of the changes produced in the electrode–solution interface by bacterial attachment

Xavier Muñoz-Berbel [a,*], Núria Vigués [b], Jordi Mas [b], A. Toby A. Jenkins [c], Francisco J. Muñoz [a]

[a] *Centre Nacional de Microelectrònica (IMB-CSIC), Esfera UAB, Campus Univ., Autónoma de Barcelona, 08193 Bellaterra, Barcelona, Spain*
[b] *Grup de Microbiologia Ambiental, Universitat Autònoma de Barcelona, Campus UAB, E-08193 Bellaterra, Spain*
[c] *Department of Chemistry, University of Bath, Bath BA27AY, United Kingdom*

Abstract

This paper describes a new method for measuring the attachment of bacteria, specifically *Escherichia coli* on platinum electrodes using impedance spectroscopy. Impedance spectroscopy measurements showed that the double layer capacitance of the electrode was very sensitive both to the concentration of bacteria in the solution and to the attachment time. Impedance measurements of *E. coli* were compared with classical measurements of bacterial attachment on identical electrodes such as staining/microscopy and bacterial removal by sonication and plating onto agar. The relationship between the measured impedance of the electrode during attachment and the biophysical processes involved is discussed.
© 2007 Elsevier B.V. All rights reserved.

Keywords: Impedance spectroscopy; Bacterial attachment; Fluorescence microscopy; Bacterial quantification; Platinum chips

1. Introduction

Electrochemical measurements of biological systems have in general focused on the detection and study of the enzymatic production or consumption of small molecules, such as glucose or NADH [1,2] or the direct electrochemical behaviour of proteins that contain redox active sites, such as cytochrome P450 [3]. Relative few studies have looked at larger and more complex biological systems such as bacteria. For example, in the early 1950s, Schwan studied the dielectric properties of the cell suspensions and tissues using impedance spectroscopy [4]. Other scientists related changes in the conductivity of the medium, in which the bacteria are dispersed, to bacteria metabolism. Bacteria can be simplistically considered as units that convert uncharged particles into smaller and highly charged molecules [5–7]. Immunosensors for whole cell detection and quantification have been recently developed [8–11]. The study of bacterial attachment on solid surfaces is important, as many pathogenic bacteria attach and colonise them, forming highly antibiotic resistant biofilms. For example, a serious human pathogen, *Pseudomonas aeruginosa* colonises the lungs of persons with Cystic Fibrosis, often leading to their premature death, and Gram-positive bacteria such as *Staphylococcus aureus* are known to infect medical devices such as urinary catheters leading to infection [12,13].

The attachment of bacteria to surfaces is generally thought to be a two stage process: Stage 1 is a fast initial adsorption phase, governed by physical forces such as electrostatic charges, Brownian motion and van der Waals forces and it is likely that bacterial swimming, which requires flagella, is required for initial attachment to allow the bacteria to overcome these physical forces and come into close proximity to the surface. Stage 2 of attachment is a slower cellular phase whereby bacteria tightly adhere to the surface via pili, binding proteins, polysaccharides

---

and fimbriae. The exact adhesion process depends on the specific bacteria [14].

In this paper, the initial attachment of *Escherichia coli* bacteria at a range of concentrations is investigated on platinum electrodes using impedance spectroscopy. Attachment is the first stage in bacterial colonisation, is relatively poorly understood since its study requires very sensitive and preferably real-time instrumentation and methods. The classical method for studying attached bacteria was pioneered by Robert Koch, back in the 19th century, where attached bacteria are stained with a dye and then studied by optical microscopy. This method is still one of the principal bacteriological methods used today. The disadvantage of staining is however that it can be difficult to accurately quantify the response, especially at low bacterial concentrations and is an 'end point' method. In recent years a number of new methodologies have been employed to study bacterial attachment. These include cyclic voltammetry [15], surface plasmon resonance [16] and quartz crystal microbalance with dispersion (QCM-D) [17]. Impedance spectroscopy has been previously used to study bacterial colonisation and biofilm formation [18] but has not to date, been used to study real-time initial attachment.

2. Experimental

2.1. Electrodes

A platinum disc working electrode (WE) with an area of $0.5 \, mm^2$ surrounded by a platinum counter electrode (CE) of $1.4 \, mm^2$ were integrated on a silicon nitride substrate using sputtering. Electrode production was carried out in-house at the IMB-CSIC Barcelona. The electrodes were 0.08 mm apart, ensuring near-homogeneous polarization of the working electrode [19].

2.2. Microbiological preparation

E. coli (CGSC 5073 K12) was grown at 37 °C in Minimal Medium AB (MMAB) [20] containing glucose. An overnight aliquot was centrifuged for 10 min at 3500*g*. Bacteria were re-suspended in MMAB and centrifuged again in order to remove metabolic products. After the washing process, bacteria were finally re-suspended in 10 mL of MMAB. The bacterial concentration was measured using plating on LB medium in 1.5% agar, with stock concentration at around 10^9 colony forming units per mL (CFU mL^{-1}). These measurements were replicated three times. The suspension was then serially diluted down to 1 CFU mL^{-1} in decade steps. Before measurements, biological samples were stored in the fridge at 4 °C to slow growth. All of the manipulations were performed under sterile conditions.

2.3. Impedance measurements

An external Ag|AgCl electrode, 5240 (Crison, Barcelona, Spain), was used as a reference electrode in a 10 mL electrochemical cell together with the WE/CE chip. The electrodes were connected to a potentiostat (Solartron 1287 (Solartron Analytical, Hampshire, UK)) which itself was connected to an impedance analyzer (Solartron SI 1260A). Electrochemical impedance spectroscopy (EIS) spectra were recorded using the Z-Plot software (Scribner Associates Inc., North Carolina, USA). A 25 mV AC potential was applied at the cell open circuit potential ($+0.26 \pm 0.5$ V vs. Ag|AgCl) over a frequency range between 100 kHz and 10 Hz.

Bacterial suspensions were introduced in the electrochemical cell which was thermostatically kept at 4 °C. Impedance measurements were made immediately and at periodic interval for 40 min. After each sequence of measurements chips were washed with 30% v/v hydrogen peroxide (Sigma–Aldrich, Switzerland) for 2 min. This was used to remove proteins irreversibly attached on the electrode surface and help regenerate the chip for future use [18]. Chips and the electrochemical cell were sterilized with 96% v/v ethanol (Panreac, Spain). After cleaning, chips were checked by measuring the MMAB without bacteria. Similar data were obtained in all cases (data not shown).

2.4. Fluorescence microscopy

Bacteria attached to the chip surface were imaged using epifluorescence microscopy after different attachment times and concentrations for correlation with the impedance measurements. An Olympus BH Fluorescence Microscope (Olympus, California, USA) was used. Bacteria were stained with 20 µg mL^{-1} 4′-6-diamidino-2-phenylindole (DAPI) (Merck, Germany) for 5 min and then rinsed in phosphate buffered saline (PBS) immediately prior to imaging.

2.5. Quantification of attached bacteria

Following attachment, chips were sonicated for 3 min to remove the attached bacteria from the surface in 5 mL of PBS. An aliquot of 100 µL of the supernatant liquid was then added to an agar plate containing LB medium and bacteria allowed to grow for 16 h. Bacteria were then counted to quantify the relative degree of attachment onto the chips.

3. Results and discussion

3.1. Fitting and interpretation of impedance spectra

Z-View software was used to fit the measured impedance data spectra were fitted to a simplified Randles equivalent circuit (Fig. 1) [21]. No electroactive species were present in the electrolyte solution, hence the impedance was dominated by non-Faradaic processes (as seen in the equivalent circuit) [22]. The inclusion of a reference electrode gave an extra capacitance associated with it C_{ref} (Fig. 1). This par-
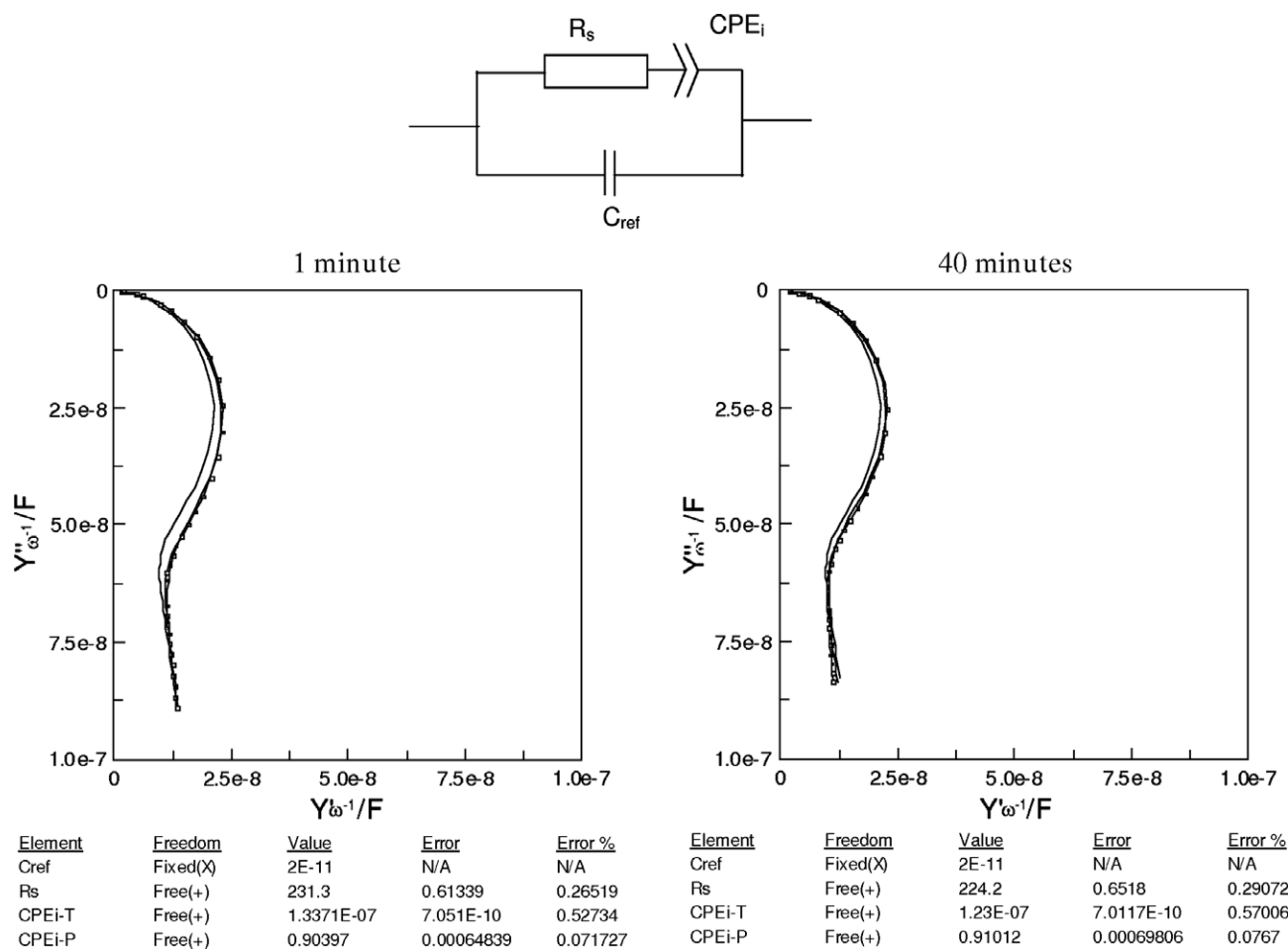
Fig. 1. Admittance complex plane plot for *E. coli* at a concentration of 10^7 CFU mL^{-1} after 1 and 40 min of attachment. The spectrum corresponding to the control (MMAB medium without bacteria) is also included in each plot (black line). The impedance spectra (points in the plot) were fitted to the equivalent circuit shown inset, which contains the capacitor associated to the reference electrode (C_{ref}), the solution resistance (R_s) and the interface constant phase element (CPE$_i$). The ideal impedance spectra obtained from the fitting (line in the plot), the calculated values and errors using the Z-View software for each element of the equivalent circuit are also shown.

asitic element was of small magnitude (approx. 10^{-9} F) and did not vary with time or with the bacterial concentration. Comparable equivalent circuits have been employed in similar applications [5]. On most solid electrodes, the double layer does not behave as a pure capacitance. Usually its phase angle is slightly smaller than 90° [23], the reasons for this are subject to continuing discussion, however a roughness factor appears to be one important cause of this effect. As a consequence, a constant phase element (CPE) is very frequently used to fit the double layer capacitance of the electrode. While this approach may be controversial, in the work reported here, variation of the CPE parameters are important and used in themselves as parameters for following bacterial attachment. The impedance of most interfacial CPEs in non-electroactive electrolyte is described by the expression [24]

$$Z = \frac{1}{K(j\omega)^\beta}. \tag{1}$$

Z is the magnitude of the impedance (in Ω), K is the CPE magnitude (in Ω s$^{-\beta}$), ω is the angular frequency (in s^{-1})

and β is a parameter linked with the phase angle which oscillates from 1 for planar surfaces to 0.5 for very rough ones [25]. In these experiments, where charged bacteria become part of the interfacial region, and in doing, modify the dielectric properties of the electrode, the CPE obtained will contain more parameters than those linked simply to roughness, such as bacterial density and the nature of the attached bacteria. For this reason, Fig. 1 shows a CPE labelled CPE$_i$ as a generic element which accounts for many complex processes which cannot, themselves, be deconvoluted.

Fig. 1 shows impedance measurements. The change in the interfacial CPE with bacterial attachment can be clearly seen.

3.2. Effect of bacterial concentration on attachment when measured by impedance spectroscopy

The effect of bacterial concentration on the measured impedance response of the electrodes was measured as described in Section 2.3. Impedance spectra were recorded

and fitted as detailed above. The results from the fitting are given in Fig. 2. A constant R_s value was obtained with time for each measurement regardless of concentration ($230 \pm 17\ \Omega$). Sample conductivity was measured separately with a conductance meter and found also to be sample invariant. However, the CPE_i magnitude (K_i) changed both as a function of attachment time and with concentrations (Fig. 2a). The effect on K_i is most pronounced with the higher concentration ($10^5\ CFU\ mL^{-1}$ and above) of bacterial samples. After a small initial increase (for around 1 min), K_i decreases. In Fig. 2b, the change in K_i was normalised, as shown in Eq. (2). $K_i(t)$ is the value of the CPE at time t after the introduction of bacteria and $K_i(1)$ the value of the CPE after 1 min attachment

$$\%K_i(t) = \frac{(K_i(t) - Ki(1))}{K_i(1)} \times 100. \tag{2}$$

It can be seen that the relative change in K_i is proportional to the concentration of the bacteria: higher concentration suspensions gave the greatest decrease after 40 min attachment.
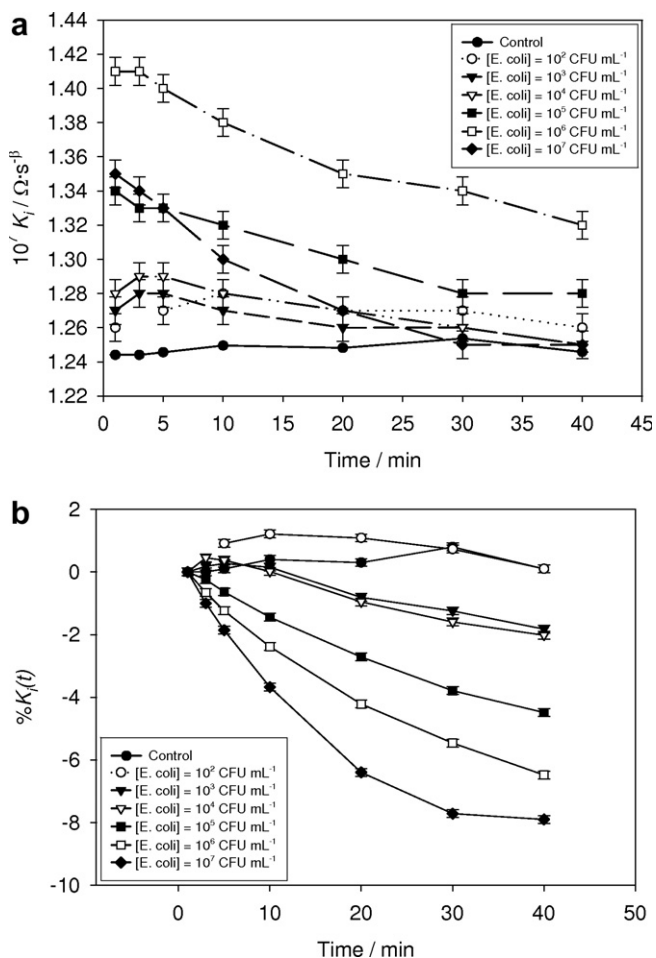

Fig. 2. Representation of (a) the variation of the K_i and (b) the $\%K_i(t)$ with time by six bacterial concentrations and the control sample (MMAB medium without bacteria). Changes recorded were due to bacterial attachment to the electrode surface. Confidence intervals were calculated at the 95% confidence level.

In all cases, K_i mainly decreased with time. In a separate study of impedance measurements of antibody–antigen binding, Katz reported that on antigen binding to an electrode immobilised antibody a decrease in the interfacial capacitance was measured [9]. This was ascribed to changes in the dielectric separation in the interfacial double layer. In this study of bacterial attachment, similar results were obtained. At frequencies below 100 MHz, current cannot cross the cell membranes and bacteria behave as isolating particles [4,26]. Gingell reported that cell attachment did not affect the double layer capacitance since the lipid bilayer was not deposited directly onto the electrode surface, but bacterial cells attached to the electrode usually being separated by a gap of 10–20 nm [27]. Thus, it is supposed that the aqueous gap between the cell membrane and the electrode would prevent a direct influence of the cell membrane on the interface impedance of the electrode [28]. However, the attachment of bacteria to the electrode may change the microstructure of the double layer, thus may result in a change in the double layer capacitance.

A more important mechanism may be the principal cause of this large decrease in CPE. Adhesion process can also be understood in terms of a decrease in the area, A, of bare electrode which causes a decrease in the double layer capacitance of the bare electrode since

$$C = \frac{\varepsilon_o \varepsilon_r A}{d}. \tag{3}$$

A reasonable, if simplistic model of the CPEs pertaining to the measured interfacial CPE can be understood if, for the sake of simplicity, we consider the measured CPE to be primarily capacitive in nature. In this case, the total measured capacitance, C_i is the sum of the bare electrode capacitance (C_{Pt}) and the capacitance of the bacteria, $C_{bacteria}$, *modified by the coverage of bacteria, given by* $\theta(t)$,

$$C_i = \theta(t)C_{bacteria} + (1 - \theta(t))C_{Pt}. \tag{4}$$

The magnitude of the capacitance of the plasmatic membrane has been reported in the literature to be nearly $1\ \mu F\ cm^{-2}$ [29]. Providing $C_{bacteria}$ (below the pF when considering an area of the cell close to several μm^2) is lower in magnitude than C_{Pt} (experimentally found higher than $100\ \mu F$), the measured interfacial capacitance C_i will fall as bacteria attach, which is what is observed in Fig. 2a and b. These results correlate well with measurement of attached bacteria and percentage of coverage (calculated regarding that each attached bacterium covered an area of $3.5\ \mu m^2$) made by sonication/removal and growth on agar plates (Table 1). This showed higher concentrations of attached bacteria (or larger covered areas) correlated with larger changes in K_i and with higher concentrations of bacteria in suspension. However, the percentage of attached cells decreased with the concentration and hence, higher concentrations of bacteria in suspension showed lower percentages of attachment. It is important to note, that at the time period used for these measurements only reversible, early stage attachment is taking place. Colonisa-

Table 1
Summary table of the amount of attached bacteria, percentage of attached bacteria, percentage of coverage of the electrode after sonication and the corresponding K_i value from impedance measurements

Bacterial concentration (CFU mL^{-1})	Attachment time (min)	Adhered bacteria[a] (CFU mL^{-1})	Percentage of attached cells[a]	Percentage of coverage of bacteria[a/b]	$10^7 K_i$ ($\Omega\,s^{-\beta}$)
3.6×10^3	3	$(5.0 \pm 0.3) \times 10^1$	1.4 ± 0.8	0.015 ± 0.009	1.28 ± 0.08
1.5×10^4	1	$(1.9 \pm 0.5) \times 10^3$	1.1 ± 0.3	0.55 ± 0.16	1.34 ± 0.12
1.5×10^4	3	$(1.0 \pm 0.3) \times 10^3$	0.59 ± 0.17	0.29 ± 0.08	1.33 ± 0.07
1.5×10^4	5	$(3.8 \pm 0.9) \times 10^2$	0.23 ± 0.05	0.11 ± 0.03	1.33 ± 0.08
1.5×10^4	10	$(6.5 \pm 2.1) \times 10^2$	0.38 ± 0.12	0.19 ± 0.06	1.32 ± 0.08
1.5×10^4	20	$(5.8 \pm 1.8) \times 10^2$	0.34 ± 0.10	0.17 ± 0.05	1.30 ± 0.05
1.5×10^4	40	$(8.5 \pm 0.7) \times 10^2$	0.50 ± 0.04	0.25 ± 0.02	1.28 ± 0.06
5×10^7	3	$(5.4 \pm 0.6) \times 10^3$	0.0108 ± 0.0012	1.56 ± 0.18	1.34 ± 0.08

Suspended concentrations and exposure times are included in the table.
[a] From sonication.
[b] Area of the *E. coli K12*: 3.5 μm^2; area of the WE/CE chip: 6 mm^2.

tion and associated growth of any extra polysaccharide matrix takes several hours or days and was not measured here [30].

The change in impedance on attachment of lower concentrations of bacteria (below 10^4 CFU mL^{-1}) is less easy to understand. It is clear from Table 1 that the number of attached bacteria at these concentrations is relatively low. It can also be seen that on addition of bacteria to the chip at these low concentrations, different behaviour is observed. The CPE initially increases, by around 1%, before slightly decreasing. A large decrease in CPE is not observed. The reason for the initial increase in the CPE is unclear, but we speculate on the basis of reports in the literature [5–7] that this may be due to a decrease in the Debye length caused by increase in charge at the interface associated with weakly attached bacteria (since bacteria are themselves charged and therefore have their own double layer charge region around them).

3.3. Verification of impedimetric data by fluorescence microscopy

After impedance measurements were made, chips were rinsed with distilled water, dried under a nitrogen stream and subsequently stained with 4′-6-diamidino-2-phenylindole (DAPI). DAPI is a small molecule which can penetrate inside the cell and stains DNA sequences. Fluorescent images of cells adhered on the chip surface were obtained (Fig. 3). The line crossing the pictures was taken as a spatial reference of the chip, to aid identification of electrodes. The working electrode was on the left side in A.1, B.2 and B.3 pictures, and on the right side in A.2, A.3 and B.1. These images show bacterial distribution on the chip. A rough estimation of the number of attached cells was made, but aggregation made bacterial counting difficult. These results were compared with the results shown in Table 1. Experimentally, 20 different objective fields were used for quantification of bacterial attachment.
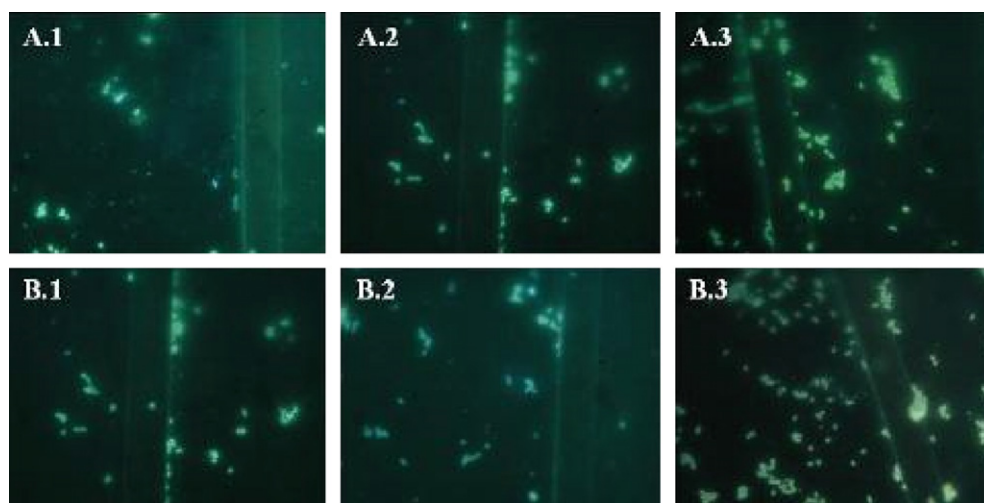

Fig. 3. Fluorescent images at 400× of bacteria attached to platinum surfaces. (A) Chips immersed 2 min in (1) 10^2 CFU mL^{-1}, (2) 10^5 CFU mL^{-1} and (3) 10^7 CFU mL^{-1} bacterial samples. (B) Chips immersed in a 10^5 CFU mL^{-1} sample for (1) 2, (2) 5 and (3) 10 min.

The images show that the bacteria adhered to any surface. Attached bacteria were found on the platinum electrodes or the silicon nitride area. Bacteria actually adhered better on the silicon nitride area. Fig. 3A illustrates attached bacteria on the chip after 3 min of exposure to 10^2, 10^5 and 10^7 CFU mL^{-1} samples, respectively. With increasing concentration, the number of adhered cells increased (Table 1). However, the level of aggregation also increased. After 2 min attachment, bacteria were mainly found attached around the edges of the working electrode. This may be due to two reasons. Firstly, the electric field lines around the edges are more densely packed and the electric field is more intense (although this will be still low in AC measurements without an applied DC bias potential), favouring bacterial adhesion [22]. Moreover, bacteria quickly attached to the silicon nitride area, which surrounds the working electrode. Thus, for proximity, the edges would be the first covered region. The fast adhesion induced aggregation, especially in concentrated samples. Due to aggregation, bacteria covered less area. However, bacterial count showed proportionality between the number of attached cells and the logarithm of the concentration. This agreed with impedance data. K_i plots shifted to higher values with the concentration after very short attachment times, before decreasing.

In Fig. 3b, chips were immersed in a 10^5 CFU mL^{-1} sample for 2, 5 and 10 min, respectively. The number of attached cells remained almost constant with time (Table 1) probably because of the fact that the flux of attaching cells was balanced with the flux of cells which, due to their weak attachment by physical forces, left the surface of the electrode. However, bacterial distribution changed significantly. Initially, bacteria attached around the electrode edges. With time, they expanded across the entire electrode area, although a higher bacterial density was found on the edges. This corroborated impedance measurements, which showed that bacterial adhesion on non-polarized electrode (an electrode at its OCP) is a spontaneous process and confirmed the time-dependence of the coverage of bacteria ($\theta(t)$) since the amount of covered area is shown to increase with time.

3.4. Comparison of very early stage attachment (at 50 s) and later attachment effects on K_i

The discussion until now has largely focussed on measurement of attachment at between 2 min up to 40 min. However, the very early stage attachment, at the point where bacteria can be considered to be behaving as simple charged colloidal particles is interesting, and quite a different effect on the CPE$_i$ is seen compared with later time measurements.

Fig. 4a shows the effect on the CPE of concentration and time of attachment. The general effect seen in Fig. 2 is observed. However, in Fig. 4b, the very early stage change in CPE at 50 s attachment is plotted against concentration of bacteria. A quite different effect is seen. Here the CPE
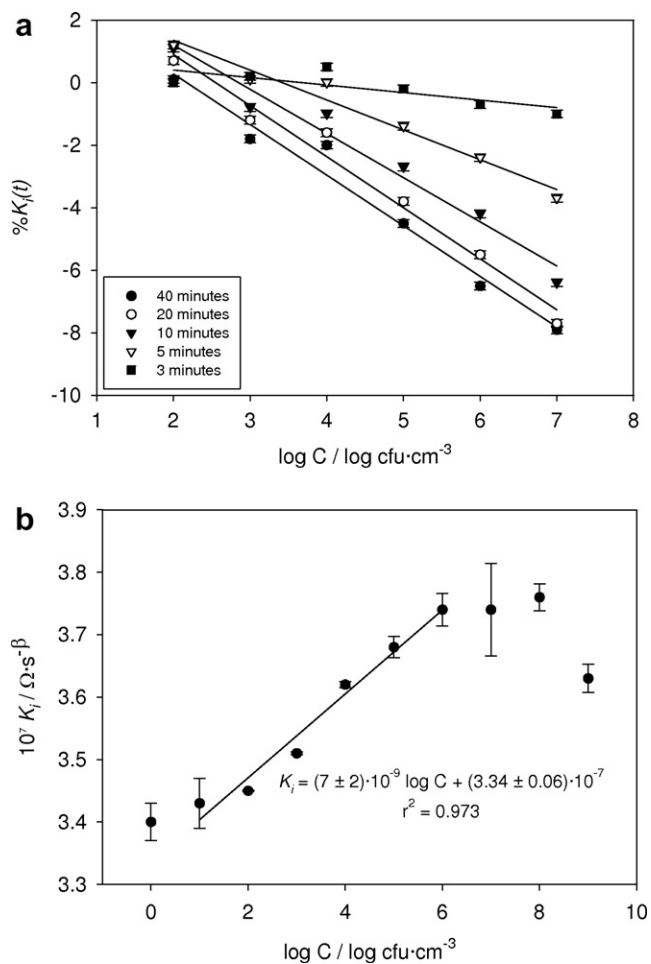
Fig. 4. Representation of (a) the %$K_i(t)$ (after 3, 5, 10, 20 and 40 min of attachment) and (b) K_i (after 50 s of attachment) versus bacterial concentration. Confidence intervals were calculated at the 95% confidence level.

actually *increases* with concentration of bacteria (rather than decreases as seen at longer times). Moreover, a correlation between concentration and increase in CPE is evident. An explanation for this very early stage behaviour is probably provided by again considering how the introduction of charged bacterial particles, with their associated counter-ions, affects the double layer at the electrode interface. In fact, the behaviour is perhaps the same as was observed in Fig. 2a for very low bacterial concentrations, where a pronounced early increase in CPE was also observed: that is a decrease in Debye length at the electrode double layer causes an initial increase in CPE, prior to the actual attachment of bacteria at later times. This early stage (at times lower than 2 min) could be termed as pre-attachment phase.

4. Conclusions

We have shown that impedance spectroscopy can be used as a real-time method for following bacterial attachment to metallic surfaces. The most useful parameter,

which relates to coverage of bacteria on the electrode surface is electrode CPE_i, approximately the electrode double layer capacitance, which decreased during early stage attachment. The change in CPE showed dependence on both the attachment time and the concentration of bacteria. Impedance measurements correlated with traditional methods such as staining/microscopy and bacterial removal by sonication and plating onto agar.

Acknowledgements

References

[1] M.A. Alonso Lomillo, J.G. Ruiz, F.J.M. Pascual, Anal. Chim. Acta 547 (2005) 209.
[2] C. Lau, G.-U. Flechsig, P. Grundler, J. Wang, Anal. Chim. Acta 554 (2005) 74.
[3] V.V. Shumyantseva, T.V. Bulko, S.A. Usanov, R.D. Schmid, C. Nicolini, A.I. Archakov, J. Inorg. Biochem. 87 (2001) 185.
[4] H.P. Schwan, Adv. Biol. Med. Phys. 5 (1957) 147.
[5] L. Yang, Y. Li, C.L. Griffis, M.G. Johnson, Biosens. Bioelectron. 19 (2004) 1139.
[6] R. Firstenberg-Eden, J. Zindulis, J. Microbiol. Methods 2 (1984) 103.
[7] K. Futschik, H. Pfützner. Electrode and Media Impedance for Detection and Characterization of Microorganisms, in: Proceedings of the RC IEEE-EMBS and 14th BMESI, 1995.
[8] L. Yang, Y. Li, G.F. Erf, Anal. Chem. 76 (2004) 1107.
[9] E. Katz, I. Willner, Electroanalysis 15 (2003) 913.
[10] C. Hao, F. Yan, L. Ding, Y. Xue, H. Ju, Electrochem. Commun. 9 (2007) 1359.
[11] G.-H. Kim, A.G. Rand, S.V. Letcher, Biosens. Bioelectron. 18 (2003) 91.
[12] C. Moser, M. van Gennip, T. Bjarnsholt, H. Calum, P.O. Jensen, B. Lee, O. Ciofu, M. Givskov, S. Molin, N. Hoiby, Int. J. Antimicrob. Agents 29 (2007) S40.
[13] G. Reid, C. Tieszer, Int. Biodeter. Biodegr. 34 (1994) 73.
[14] Y.H. An, R.J. Friedman, J. Biomed. Mater. Res., Part B 43 (1998) 338.
[15] M.J. Vieira, I.A. Pinho, S. Giao, M.I. Montenegro, Biofouling 19 (2003) 215.
[16] A.T.A. Jenkins, R. ffrench-constant, A. Buckling, D.J. Clarke, K. Jarvis, Biotechnol. Prog. 20 (2004) 1233.
[17] T.A. Camesano, Y. Liu, M. Datta, Adv. Water Resour. 30 (2007) 1470.
[18] X. Muñoz-Berbel, F.J. Muñoz, N. Vigués, J. Mas, Sensor. Actuat. B 118 (2006) 129.
[19] J.E. Harrar, I. Shain, Anal. Chem. 38 (1966) 1148.
[20] D. Balestrino, J.A.J. Haagensen, C. Rich, C. Forestier, J. Bacteriol. 187 (2005) 2870.
[21] J.E.B. Randles, Faraday Discuss. Chem. Soc. 1 (1947) 11.
[22] A.J. Bard, L.R. Faulkner, Electrochemical Methods: Fundamentals and Applications, John Wiley & Sons, New York, 2001.
[23] E. Barsoukov, J.R. Macdonald (Eds.), Impedance Spectroscopy: Theory Experiment and Applications, John Wiley & Sons, New Jersey, 2005.
[24] H. Fricke, Philos. Mag. 7 (1932) 310.
[25] W.H. Mulder, J.H. Sluyters, T. Pajkossy, L. Nyikos, J. Electroanal. Chem. 285 (1990) 103.
[26] C.L. Davey, H.M. Davey, D.B. Kell, Bioeletrochem. Bioenerg. 28 (1992) 319.
[27] D. Gingell, in: R. Glaser, D. Gingell (Eds.), Biophysics of the Cell Surface, Springer, New York, 1990.
[28] R. Ehret, W. Baumann, M. Brischwein, A. Schwinde, K. Stegbauer, B. Wolf, Biosens. Bioelectron. 12 (1997) 29.
[29] R. Holzel, BBA-Mol. Cell. Res. 1450 (1999) 53.
[30] M.T. Madigan, J.M. Martinko, J. Parker, Brock Biology of Microorganisms, Prentice Hall International, Hertfordshire, UK, 1997.

Impedimetric approach for quantifying low bacteria concentrations based on the changes produced in the electrode–solution interface during the pre-attachment stage

X. Muñoz-Berbel [a,*], N. Vigués [b], A.T.A. Jenkins [c], J. Mas [b], F.J. Muñoz [a]

[a] *Centro Nacional de Microelectrónica (IMB-CSIC), Esfera UAB, Campus Univ. Autónoma de Barcelona, 08193 Bellaterra, Barcelona, Spain*
[b] *Grup de Microbiologia Ambiental, Universitat Autònoma de Barcelona, Campus UAB, E-08193 Bellaterra, Spain*
[c] *Department of Chemistry, University of Bath, Bath BA2 7AY, UK*

Abstract

This paper describes an approach for quantifying low concentrations of bacteria, particularly *Escherichia coli*, based on the measurement of the initial attachment of bacteria to platinum surfaces, using impedance spectroscopy. The value of the interface capacitance in the pre-attachment stage (before 1 min of attachment) showed correlation with suspended concentration of bacteria from 10^1 to 10^7 CFU mL^{-1} (colony forming units per mL). This method was found to be sensitive to the attachment time, to the applied potential and to the size of the counter electrode. The sensor lifetime was also evaluated.
© 2008 Elsevier B.V. All rights reserved.

Keywords: Platinum electrodes; Biomass quantification; Impedance spectroscopy; Bacterial attachment; Surface plasmon resonance

1. Introduction

Environmental monitoring and food and the beverage industries require simple, fast and real-time systems to monitor the attachment and colonization of bacteria on surfaces and concentrations of planktonic bacteria in liquids, especially at low concentrations (Tang et al., 2006). From an electrochemical viewpoint, impedance spectroscopy has become widely used for the study of biological systems—from lipid membrane to medical imaging (Ireland et al., 2004; Jenkins et al., 2000). From the early 1950s, Schwan used the impedance spectroscopy to characterize the dielectric properties of the cell suspensions and tissues (Schwan, 1957). Impedance measurements show that the small conductivity of the cellular membranes, particularly at low frequencies (below 100 kHz) impedes the current to flow through the cells and thus, they behave as non-conducting particles. This decrease of conductivity was found proportional to the volume fraction of cells present in the sample and later studies used it to quantify biomass (Davey et al., 1992;

Harris and Kell, 1983; Markx and Davey, 1999). The linearity of the probe response extends from 2 to 100 mg dry weight mL^{-1}, nearly 10^3 CFU mL^{-1} (colony forming units per mL) in the case of bacteria.

In the 1970–1980s, Cady and Firstenberg-Eden started to use impedance spectroscopy to measure the changes of conductivity caused for bacteria metabolism and used it to finally quantify biomass (Firstenberg-Eden and Zindulis, 1984; Cady et al., 1977). Bacteria can be simplistically considered as units that convert uncharged particles into smaller and highly charged molecules, which excrete to the medium increasing its conductivity. They, and more recent authors used this decrease in the magnitude of the impedance due to this conductivity increase, to monitor bacterial metabolism (Yang et al., 2004; Yang et al., 2003; Fehrenbach et al., 1992; Felice and Valentinuzzi, 1999; Felice et al., 1992; Futschik and Pfützner, 1995), however, the quantification was somewhat difficult to understand. The production of charged molecules depends on the number of active cells. Bacteria in media are continuously duplicating thus increasing their concentration with time. When the concentration of bacteria exceeds 10^5 CFU mL^{-1}, the change of the conductivity due to bacteria metabolism can be detected using impedance spectroscopy. The time necessary to reach this boundary concen-

* Corresponding author. Tel.: +34 93 594 77 00; fax: +34 93 580 14 96.
  E-mail address: xavier.munoz@cnm.es (X. Muñoz-Berbel).

tration depends both on the duplication time of the specie and on the initial concentration of the sample. Hence, for the same species, the measure of this time was proportional to the bacteria concentration initially present in the sample. However, the time required to obtain a measurable change in the value of impedance was very long for low concentrations, expanding to more than 24 h for samples of 1 CFU mL^{-1}.

In this paper, the impedance measurements of the attachment of *Escherichia coli* on platinum electrodes are used to quantify bacteria. The effect of the size of the counter electrode, the influence of the applied potential and the aging of the sensor are also investigated. Bacteria colonize solid surfaces in a multi-step mechanism, where the initial step is reversible attachment. Previous works showed that the early bacterial attachment could be impedimetrically monitored, especially in the very early attachment stage (from 1 min following addition of bacteria) (Muñoz-Berbel et al., 2007). When attachment time was controlled, the value of the electrode–solution interface capacitance correlated with the initial concentration of bacteria in the sample. This approach was particularly sensitive at low bacterial concentrations (with a limit of detection of 10^1 CFU mL^{-1} using the 3 sigma method), provides a rapid (1 min of measurement) and a simple quantification method.

2. Materials and methods

2.1. Electrochemical cell

A platinum disc working electrode (WE) with an area of 0.5 mm^2 surrounded by a platinum counter electrode (CE) of 1.4 mm^2 were integrated on a silicon nitride substrate of 9 mm^2 (3 mm length per 3 mm width). Electrode production was carried out in-house at the IMB-CSIC Barcelona (Alonso Lomillo et al., 2005). The electrodes were 0.08 mm apart, ensuring near-homogeneous polarization of the working electrode (Harrar and Shain, 1966). These WE/CE chips were introduced in a 100 mL electrochemical cell together with an external Ag|AgCl electrode, 5240 (Crison, Barcelona, Spain).

2.2. Microbiological preparation

E. coli (CGSC 5073 K12) was grown overnight in Minimal Medium AB (MMAB) (Balestrino et al., 2005) at 37 °C. An aliquot of 10 mL of culture was centrifuged for 10 min at $3500 \times g$ [Sigma 4–10 centrifuge (Sigma, Switzerland)]. The supernatant liquid was removed and cells (the pellet) were resuspended in 5×10^{-3} M KCl or in phosphate buffer saline (PBS) at pH 7.4, depending on whether they would be measured by impedance spectroscopy or surface plasmon resonance (SPR), respectively. The process was repeated twice in order to remove metabolic products, membrane fragments and cytoplasmatic proteins. The final bacterial pellet was resuspended in 10 mL of 5×10^{-3} M KCl or PBS and then counted using plating on agar containing LB medium, in both cases. The suspension was then serially diluted down to 1 CFU mL^{-1} in decade steps. Before measurements, biological samples were stored in the fridge at 4 °C to

slow growth. All of the manipulations were performed under sterile conditions.

2.3. Impedance measurements

The impedance analyser, a Solartron SI 1260A (Solartron Analytical, Hampshire, UK), was coupled to a potientiostatic interface Solartron 1287. Impedance spectroscopy spectra were recorded using the Z-Plot software (Scribner Associates Inc., NC, US). A 25 mV AC potential was applied at the cell open circuit potential (+0.26 ± 0.05 V vs. Ag|AgCl) over a frequency range between 100 kHz and 10 Hz. The measurement time was around 55 s after recording 17 points per frequency decade. All measurements given in this work are in relation to the Ag|AgCl reference electrode.

Bacterial suspensions were introduced in the electrochemical cell which was thermostatically kept at 4 °C. Impedance measurements were made either at periodic intervals for 40 min when monitoring the initial attachment of bacteria or after 50 s of attachment when quantifying suspended bacteria. It should be noted that these times were the time before for measurement of the impedance spectrum—which itself took 55 s. The cleaning process depended on the specific experiment: when monitoring the initial attachment, electrodes were in contact with bacteria suspensions for long periods of time. Cleaning with 30% hydrogen peroxide (Sigma–Aldrich, Switzerland) for 2 min was proved to detached molecules and whole cells irreversibly attached to the electrode during the measurement (Muñoz-Berbel et al., 2006). However, the hydrogen peroxide solution also damaged the coating used for isolating the connection of the chip from the solution and critically reduced the sensor lifetime (data not shown). Coating fragments attached to the electrode surface were eliminated by cleaning with 96% (v/v) ethanol (Panreac, Spain). Quantification measurements, where most bacteria were reversibly attached, did not require the use of aggressive reagents which could compromise the electrodes viability. In this case, the electrodes and the electrochemical cell were cleaned with water and sterilized with ethanol.

2.4. Surface plasmon resonance measurements

SPR data were acquired using the Autolab ESPRIT (Eco Chemie, BV, The Netherlands). Measurements were made by following the change in the reflected light minimum angle with time, which is indicative of the change in optical properties of the interface as bacteria attach. The instrument has two independent channels allowing two experiments to be carried out simultaneously. In these experiments, one of the channels was used as an internal control to subtract artefacts such as changes in bulk refractive index. Bacterial suspensions in PBS and buffer without bacteria were measured in channel 1 (CH1) and channel 2 (CH2), respectively. Hence, the difference between the angles recorded in CH1 and CH2, called differential angle, was indicative of the change produced in the refractive index by bacterial attachment. Glass disks with a thin gold coating (50 nm thick) were placed on a hemispherical prism using index match fluid (RI = 1.518, Cargille), which ensured optical continuity.

The system was allowed to stabilise for four minutes before addition of the corresponding sample in each channel. The difference in angle of SPR was thus recorded. Measurements were made every three seconds for the duration of the experiment.

2.5. Optical microscopy measurements

Bacteria attached to the chip surface were imaged using optical microscopy (without staining) after different attachment times and concentrations for correlation with the impedance measurements using a Nikon Eclipse ME-600 microscope (Nikon Corporation, Japan).

3. Results and discussion

3.1. Fitting and interpretation of impedance data

Z-View software was used to fit impedance data to the equivalent circuit shown in Fig. 1. The circuit included a resistor modelling the solution resistance (R_S), a double layer capacitance, which appears as the interface constant phase element (CPE_i), and an extra capacitance of small magnitude (nF) associated with the presence of an external reference (C_{ref}), whose value did not vary with the concentration of bacteria. The use of the CPE_i instead of a conventional double layer capacitance was discussed in previous works (Muñoz-Berbel et al., 2007). In this work, as on most solid electrodes, the double layer impedance did not behave as a pure capacitance since its phase angle was slightly smaller than 90°. Although this is currently under study, a roughness factor appears to be one important cause of this
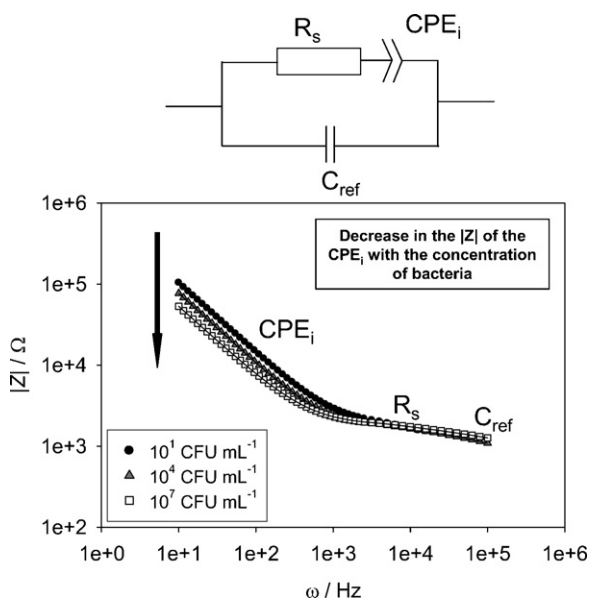

Fig. 1. Representation of the measured impedance magnitude (|Z|) vs. the frequency for *E. coli* at a concentration of 10^1, 10^4 and 10^7 CFU mL^{-1} after 50 s of attachment (points in the plot). The impedance spectra were fitted to the equivalent circuit shown inset (line in the plot), which contains the capacitor associated to the reference electrode (C_{ref}), the solution resistance (R_S) and the interface constant phase element (CPE_i). These parameters are included in the plot in the frequency range where they appear.

effect. For this reason, the double layer capacitance is frequently fitted using a constant phase element (CPE). In absence of electroactive electrolytes in the medium, the impedance of most interfacial CPEs is described by the expression below (Fricke, 1932)

$$Z = \frac{1}{K(j\omega)^\beta} \qquad (1)$$

Z is the magnitude of the impedance (in Ω), K is the CPE magnitude (in $\Omega^{-1}\,s^{-\beta}$), ω is the angular frequency (in s^{-1}), $j = \sqrt{-1}$ and β is a parameter linked with the phase angle which oscillates from 1 for planar surfaces to 0.5 for very rough ones (Mulder et al., 1990). In these experiments, attached bacteria become part of the interfacial region, thus modifying the dielectric properties of the electrode. Hence, the CPE contains more parameters than simply the surface roughness or the charge separation, such as bacterial density and the nature of the attached bacteria. For this reason, Fig. 1 shows a CPE labelled CPE_i as a generic element which accounts for many complex processes which cannot, themselves, be deconvoluted. Fig. 1 shows impedance measurements for 10^1, 10^4 and 10^7 CFU mL^{-1} suspensions 50 s after adding these solutions to the electrode. The change in the magnitude of the impedance (|Z|) in the region of the interfacial CPE with bacterial concentration can be clearly seen.

3.2. Determination of the effect of the initial bacterial concentration on the attachment of bacteria when using impedance spectroscopy, SPR and optical microscopy

The effect of bacterial concentration on impedance spectroscopy, SPR and optical microscopy measurements was determined as described in Sections 2.3–2.5, respectively. Impedance spectra were recorded and fitted as detailed above. Fig. 2 shows the change of the magnitude of the CPE and the differential angle measured using SPR with time at three different bacteria concentrations.

Fig. 2a shows that the magnitude of the CPE_i, K_i, changed both as a function of attachment time and with concentration. With time, decreases in K_i were recorded. The changes were proportional to the concentration of bacteria. The effect of the bacteria attachment to the electrode on K_i was discussed in previous works (Muñoz-Berbel et al., 2006, 2007). In the early attachment (below 40 min), the change in the CPE magnitude follows Eq. (2).

$$C_i = \theta(t)C_{bacteria} + (1 - \theta(t))C_{Pt} \qquad (2)$$

C_i is the total measured capacitance, C_{Pt} is the bare electrode capacitance, $C_{bacteria}$ is the capacitance of the bacteria and $\theta(t)$ is the coverage of bacteria. $C_{bacteria}$ (below the pF (Holzel, 1999)) is lower in magnitude than C_{Pt} (experimentally, hundreds of μF) and thus, the measured interfacial capacitance should fall as bacteria attach, as in Fig. 2a. Similar results were obtained using gold working electrodes with identical areas. However, the cleaning process was more difficult using gold electrodes, which was associated with the presence of external or transmem-
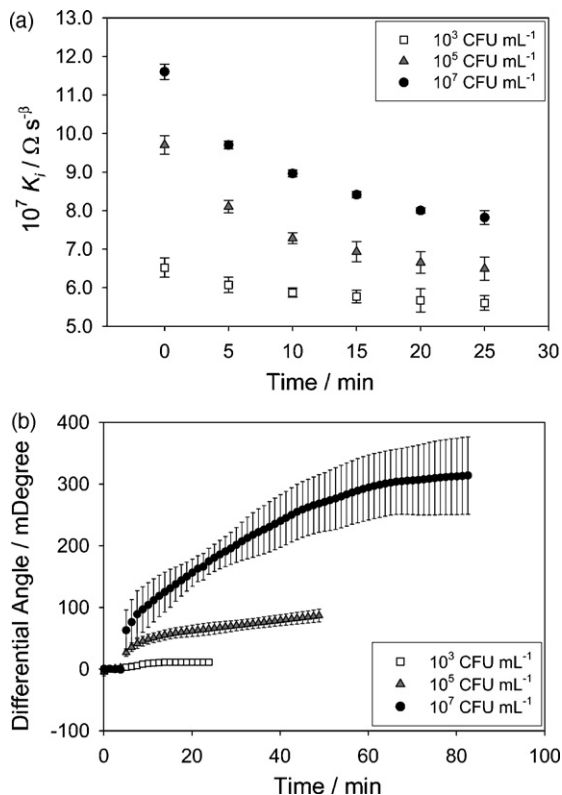
Fig. 2. Representation of (a) the magnitude of the interface CPE, K_i, and (b) the differential angle measured using SPR vs. time for *E. coli* at a concentration of 10^3, 10^5 and 10^7 CFU mL^{-1}.

brane proteins with thiol groups that may attach covalently to the electrode surface.

Fig. 2b shows that the differential angle measured using SPR also changed both as a function of attachment time and with concentration. Increases in the differential angle, proportional to the bacteria concentration, were recorded. The SPR measurement principle is based on the fact that the recorded angle (the angle of surface plasmon resonance) is highly sensitive to changes in the refractive index of the dielectric layer above the gold. Previous works show that bacterial attachment to the gold changed the refractive index of the dielectric, which is observed in Fig. 2b (Jenkins et al., 2004).

After the impedance measurements, chips were rinsed with distilled water, dried under nitrogen stream and imaged as described in Section 2.5. Fig. 3 shows that the number of attached bacteria also changed as a function of attachment time and with concentration. The number of attached cells was proportional to the concentration of the bacteria in suspension. With time, the number of attached cells increased until stabilization after 20 min attachment, which coincide with impedance spectroscopy data.

3.3. Effects of the very early stage attachment (at 50 s) on K_i: quantification of suspended bacteria

Impedance spectroscopy measurements were made as described in Section 2.3 and fitted using the equivalent circuit shown in Fig. 1. Here, we focus on the very early attachment stage or
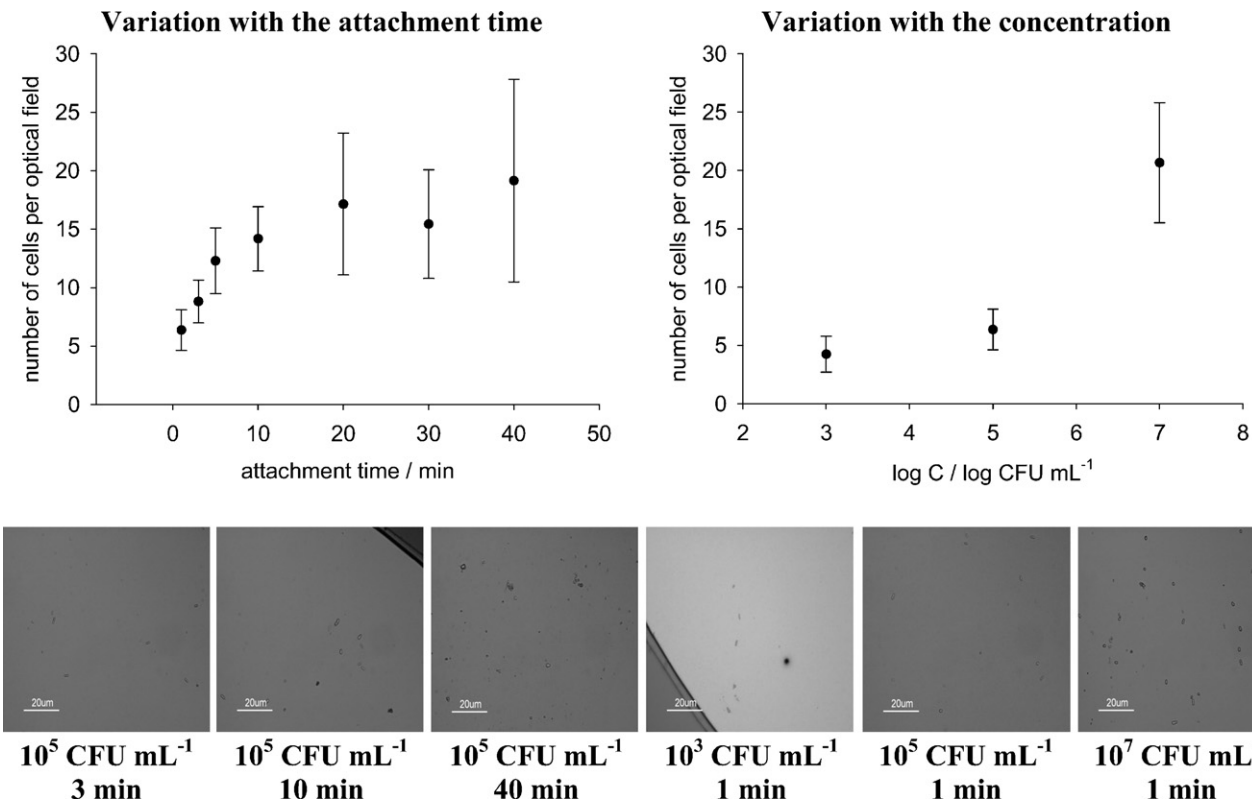
Fig. 3. (a) Variation of the number of attached cells for a 10^5 CFU mL^{-1} sample vs. the time. (b) Variation of the number of attached cells after 1 min of exposure for bacteria concentrations of 10^3, 10^5 and 10^7 CFU mL^{-1}. Also relevant images of the attachment process are included. The number of attached cells was found after counting 20 different optical fields.

Fig. 4. Representation of the normalized K_i vs. the suspended concentration for different sizes of the counter electrode area. Case A: $1.4\,mm^2$ and Case B: $117\,mm^2$.

pre-attachment of bacteria to the electrode. In Fig. 4, the measured CPE magnitude was normalized using Eq. (3). K_i is the value of CPE for any concentration of bacteria and K_i(wb) is the value of CPE in absence of bacteria.
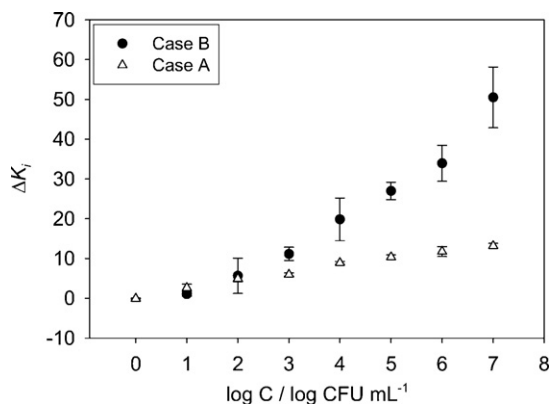
$$\Delta K_i = \frac{K_i - K_i(\text{wb})}{K_i(\text{wb})} \cdot 100 \qquad (3)$$

Fig. 4 shows the effect of concentration on the CPE at the pre-attachment stage (at times lower than 2 min). At this point, the CPE magnitude increases with the concentration of bacteria (rather than decreases as seen at longer times) with an evident correlation from 10^1 to $10^7\,CFU\,mL^{-1}$.

The changes produced by bacteria attachment to the magnitude of the CPE and the differences with later steps have been discussed in previous works (Muñoz-Berbel et al., 2007). At the pre-attachment stage, bacteria can be considered to be behaving as simple charged colloidal particles. The introduction of these charged particles, bacteria, and their associated counter-ions affects the double layer at the electrode interface, especially in terms of distance between layers: attached bacteria at the pre-attachment stage are thought to decrease the Debye length at the electrode double layer, causing an initial increase in CPE.

3.4. Analysis of the effect of the counter electrode (CE) size in the determination of the CPE magnitude at the pre-attachment stage

In this section, the effect of the counter electrode size in the CPE magnitude at the pre-attachment stage was analyzed. Two platinum CEs of $1.4\,mm^2$, 3 times bigger than the WE (case A), and $117\,mm^2$, more than 200 times bigger (case B) were compared following the experimental conditions described in Section 2.3. At the pre-attachment stage, the magnitude of the CPE was shown to increase as a consequence of a decrease in the Debye length at the electrode double layer. The double layer of both working and counter electrodes contributes to the CPE magnitude, as shown in Eq. (4) which considers the in series combination of both capacitances ($C_{dl(WE)}$ and $C_{dl(CE)}$, respectively, for the WE and the CE) (Barsoukov and Macdonald, 2005).

$$\text{CPE}_i = \frac{C_{dl(WE)} \cdot C_{dl(CE)}}{C_{dl(WE)} + C_{dl(CE)}} \qquad (4)$$

The use of CEs of different area changes the value of the $C_{dl(CE)}$, whose magnitude increases with the size of the area as follows:

$$C_{dl(CE)} = \varepsilon_0 \varepsilon_{dl} \frac{A}{d} \qquad (5)$$

Thus, the size of the CE area considerably modulates the value of $C_{dl(CE)}$ in the CPE, varying from approximately the 50%, when WE and CE have a similar size (case A), to practically 0% ($\text{CPE}_i \approx C_{dl(WE)}$), when a very large counter electrode was used (case B).

Experimentally, the normalized magnitude of the CPE is much bigger in the case B, when it only depends on the $C_{dl(WE)}$, than in the case A, especially at high concentrations (Fig. 4). Previous works showed that bacteria preferably attached to the WE and only a few cells were found attached to the CE (Muñoz-Berbel et al., 2007), probably because of the fact that both CE and bacteria were negatively charged. The low level of attachment found on the CE suggests small changes in the $C_{dl(CE)}$ and coincides with the smaller magnitude of the CPE recorded when it is highly influenced by the $C_{dl(CE)}$ (case A).

3.5. Influence of the magnitude of the potential applied on the working electrode during the pre-attachment stage

The pre-attachment stage, mainly governed by electrostatic forces, can be modulated by applying a potential to the working electrode. In this section, three applied potentials (0, +0.19 and +0.30 V vs. Ag|AgCl) were explored under the experimental conditions described in Section 2.3 in order to determine the influence of the potential in the pre-attachment process.

Experimental data showed that, for the same bacterial concentration, the normalized magnitude of the CPE increased when applying more positive potentials (Fig. 5). The increase of the CPE, which can be thought to be caused by an increase in the number of attached cells, suggested that the positive charge of the electrode favoured the attachment of bacteria. Thus, the pre-attachment process, governed by electrostatic forces, can be
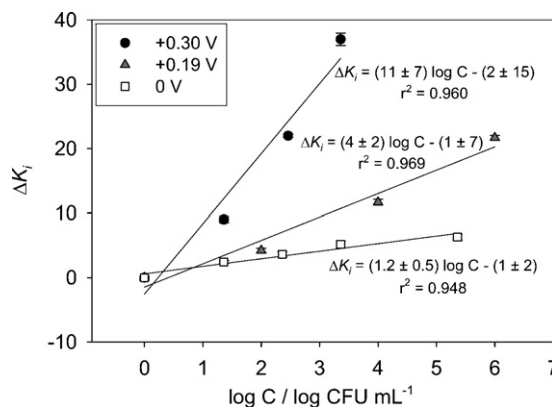

Fig. 5. Representation of the normalized K_i vs. the suspended bacteria concentration after applying three different potentials, namely 0, +0.19 and +0.30 V vs. Ag|AgCl, over the working electrode surface.
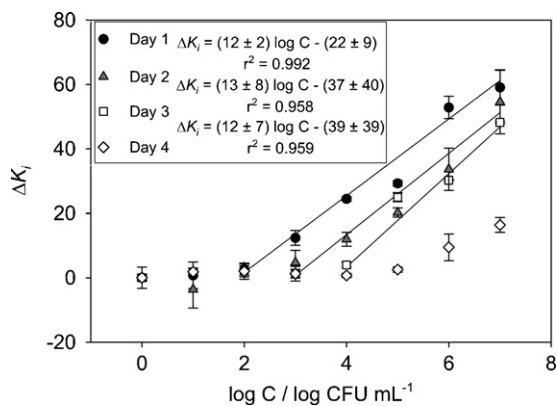
Fig. 6. Representation of the normalized K_i vs. suspended bacteria concentration for the same sensor during four consecutive days.

understood as the attraction of positive surfaces and bacteria, which are negatively charged for the presence of ionized phosphate and carbonate groups in their outer membranes (Madigan et al., 1997). Potentials above +0.6 V vs. Ag|AgCl could not be explored. These potentials showed a big variability in the recorded data probably caused by the formation of non-stoichiometric platinum oxides of low stability (data not shown) (Birss et al., 1993).

3.6. Aging of the sensor

The sensors capacity to monitor bacteria attachment in the pre-attachment step was investigated. The aging of the sensors was determined by repeating the calibration process described in Section 2.3, which included 24 single impedance measurements (8 samples, including the medium without bacteria used as control, measured in triplicate), during consecutive days. Between assays, sensors were stored dry and clean in the optimum condition to preserve the superficial properties.

As shown in Fig. 6, sensors progressively lost their capacity to measure the changes produced in the magnitude of the CPE by bacteria attachment. Although the sensors sensitivity, in terms of slope of the calibration curve, remained practically constant after the three first days, the experimental limit of detection shifted to higher concentrations. The decrease in the sensor sensitivity with consecutive measurements is thought to be caused by the presence of membrane fragments, protein layer and exopolysaccharide layers, from death cells or secreted by bacteria, on the electrodes surface. The presence of these molecules would increase the distance between the electrode surface and the adhering bacteria thus decreasing the electrode sensitivity. After 4 days, sensors completely lost their capacity to discriminate between different concentrations and a flat calibration curve was obtained. The maximum number of measurements sensitive to the changes produced by bacterial attachment was shown to be close to 80.

4. Conclusions

We have shown that SPR and impedance spectroscopy can be used as real-time methods for following bacterial attach-

ment to metallic surfaces, and these measurements showed good correlation with the traditional optical microscopy. Impedance spectroscopy was found to be particularly sensitive to the very early attachment/pre-attachment. The magnitude of the interface capacitance could be correlated with the concentration of suspended bacteria. The sensitivity of the interface capacitance could be enhanced by applying more positive potentials on the working electrode which favoured bacterial attachment. In terms of aging, sensors lost the capacity to discriminate between concentrations with time, especially at low concentrations.

Future work will be focused on the optimization of the measurement system which includes the exploration of better cleaning processes for decreasing the aging of the sensor and the development of on-line systems for the real-time monitoring of bacterial concentration. In terms of equipment, we are developing an automatic integrated flow system containing a bi-directional burette and a modular multi-port valve (MVP) for the suitable manipulation of liquids. The flow system will be integrated and synchronized with the measurement system containing a portable homemade impedance analyzer and the electrochemical cell.

Acknowledgements

References

Alonso Lomillo, M.A., Ruiz, J.G., Pascual, F.J.M., 2005. Anal. Chim. Acta 547 (2), 209–214.

Balestrino, D., Haagensen, J.A.J., Rich, C., Forestier, C., 2005. J. Bacteriol. 187 (8), 2870–2880.

Barsoukov, E., Macdonald, J.R. (Eds.), 2005. Impedance Spectroscopy: Theory, Experiment, and Applications. John Wiley & Sons, New Jersey.

Birss, V.I., Chang, M., Segal, J., 1993. J. Electroanal. Chem. 355 (1–2), 181–191.

Cady, P., Dufour, W., Shaw, J., Kraeger, S.J., 1977. J. Clin. Microbiol. 7 (3), 265–272.

Davey, C.L., Davey, H.M., Kell, D.B., 1992. Bioelectrochem. Bioenerget. 28 (1–2), 319–340.

Fehrenbach, R., Comberbach, M., Petre, J.O., 1992. J. Biotechnol. 23 (3), 303–314.

Felice, C.J., Valentinuzzi, M.E., 1999. IEEE Trans. Biomed. Eng. 46 (12), 1483–1487.

Felice, C.J., Valentinuzzi, M.E., Vercellone, M.I., Madrid, R.E., 1992. IEEE Trans. Biomed. Eng. 39 (12), 1310–1313.

Firstenberg-Eden, R., Zindulis, J., 1984. J. Microbiol. Methods 2 (2), 103–115.

Fricke, H., 1932. Philos. Magaz. 7, 310–318.

Futschik, K., Pfützner, H., 1995. Proceedings of the RC IEEE-EMBS & 14th BMESI.

Harrar, J.E., Shain, I., 1966. Anal. Chem. 38 (9), 1148–1158.

Harris, C.M., Kell, D.B., 1983. Bioelectrochem. Bioenerget. 11 (1), 15–28.

Holzel, R., 1999. Biochim. Biophys. Acta (BBA): Mol. Cell Res. 1450 (1), 53–60.

Ireland, R.H., Tozer, J.C., Barker, A.T., Barber, D.C., 2004. Physiol. Measure. 25 (3), 775–796.

Jenkins, A.T.A., Ffrench-Constant, R., Buckling, A., Clarke, D.J., Jarvis, K., 2004. Biotechnol. Progr. 20 (4), 1233–1236.

Jenkins, A.T.A., Hu, J., Wang, Y.Z., Schiller, S., Foerch, R., Knoll, W., 2000. Langmuir 16 (16), 6381–6384.

Madigan, M.T., Martinko, J.M., Parker, J., 1997. Brock Biology of Microorganisms. Prentice Hall International, Hertfordshire, UK.

Markx, G.H., Davey, C.L., 1999. Enzyme Microb. Technol. 25 (3–5), 161–171.

Mulder, W.H., Sluyters, J.H., Pajkossy, T., Nyikos, L., 1990. J. Electroanal. Chem. 285 (1–2), 103–115.

Muñoz-Berbel, X., Muñoz, F.J., Vigués, N., Mas, J., 2006. Sens. Actuators B: Chem. 118 (1–2), 129–134.

Muñoz-Berbel, X., Vigués, N., Mas, J., Jenkins, A.T.A., Muñoz, F.J., 2007. Electrochem. Commun. 9 (11), 2654–2660.

Schwan, H.P., 1957. Adv. Biol. Med. Phys. 5, 147–209.

Tang, H., Zhang, W., Geng, P., Wang, Q., Jin, L., Wu, Z., Lou, M., 2006. Anal. Chim. Acta 562 (2), 190–196.

Yang, L., Li, Y., Griffis, C.L., Johnson, M.G., 2004. Biosens. Bioelectron. 19 (10), 1139–1147.

Yang, L., Ruan, C., Li, Y., 2003. Biosens. Bioelectron. 19 (5), 495–502.

On-chip impedance measurements to monitor biofilm formation in the drinking water distribution network

X. Muñoz-Berbel [a,*], F.J. Muñoz [a], N. Vigués [b], J. Mas [b]

[a] Centro Nacional de Microelectrónica (IMB-CSIC), Campus University Autónoma de Barcelona, 08193 Bellaterra, Barcelona, Spain
[b] Grup de Microbiologia Ambiental, Universitat Autònoma de Barcelona, Campus UAB, E-08193 Bellaterra, Spain

Abstract

Aquatic microorganisms have the ability to adhere onto any solid surface. They are able to re-organise as biofilms when environmental conditions change and put their life at risk. Biofilms allow bacteria to remain inside water pipes without being eliminated by biocides. Among other properties, biofilms are electrically insulating. Because of this, as they grow on a metal transducer surface, biofilms produce changes in the electrode–solution interface properties. These changes have been monitored using impedance measurements and microchips as electrical transducers. Biofilm formation has been characterised using on-chip gold working electrodes and the various growth phases have been related to specific impedance changes.

Measurements employing new and reused chips of bacterial and non-bacterial solutions have been performed. Although differences between new and reused chips have been found, both kinds of electrodes can be used to evaluate biofilm formation.

The effect of several biocides on biofilms has also been studied. The disinfecting properties of peroxides, strong acid/bases and alcohols have been compared as well as their ability to remove adhered substances from chip surfaces.
© 2006 Elsevier B.V. All rights reserved.

Keywords: Impedance measurements; Biofilm monitoring; On-chip measurements; Biofilm elimination

1. Introduction

In order to guarantee strict organoleptic and sanitary standards in drinking water, purification treatments are needed which also modify other physicochemical properties. Biocides, such as chlorine, are added to the water as part of these purification processes. However, the concentration of chlorine decreases as it diffuses through the water distribution network [1,2]. Chlorine levels below a certain threshold do not prevent the growth of bacteria, which modifies the biological and chemical characteristics of the stream.

Biofilms are heterogeneous bacterial formations, which grow on the inner surface of water distribution network pipes. They consist of a great variety of cellular communities cross-linked in an organic matrix by a bacterial polymer [3,4]. This arrangement provides several advantages to bacteria. It: (1) facilitates nutrient uptake, (2) improves bacterial activity, (3) stimulates microbial interactions and (4) offers better protection against toxic agents [4].

Indeed, bacterial concentration increases are due to biofilm formation [5] and not to free bacteria suspended in the water, since division time is smaller than their residence time in the distribution networks [5]. Although, it is the latter parameter that water companies monitor nowadays, controlling the formation and activity of adhered bacterial communities is a much more critical issue.

Several optical and electrochemical techniques may be used to monitor biofilm formation [6]. In this research work, the use of on-chip impedance measurements is proposed to evaluate the biofilm formation, because of the low-cost, reduced size and high sensitivity involved.

Biofilm formation on gold surfaces modifies the interfacial electrical properties of the system [7]. These changes can be characterized using bipolar impedance measurements, which provide information about both the solution and the electrode–solution interface. Following the impedance changes taking place, it is possible to monitor the biofilm formation process.

Exposing biofilms to disinfectant solutions allowed the evaluation of the disinfectant's capacity to eliminate these complex structures. Strong acids and bases, ethanol and peroxide solutions were used as disinfectants. Hydrogen peroxide

---

* Corresponding author. Tel.: +34 93 594 77 00; fax: +34 93 580 14 96.
E-mail address: xavier.munoz@cnm.es (X. Muñoz-Berbel).

proved itself as an effective disinfectant with great capacity to remove bacterial biofilms [8]. However, strong acids and bases were needed to eliminate other substances, such as precipitated salts.

A very effective cleaning protocol to remove biofilm formations on-chip surfaces was achieved and is described below. Impedance measurements were employed to monitor the cleaning ability of each product.

2. Materials and methods

2.1. Biological material

Biofilms containing only *Pseudomonas aeruginosa* have been used in this work. Biofilm formation is best achieved under conditions of turbulent stirring and lack of nutrients [4]. Gold chips were immersed in a bioreactor containing a *P. aeruginosa* solution under biofilm favouring conditions as described above. These aquatic bacteria formed very large biofilms easily and quickly.

2.2. Measurement system

2.2.1. Equipment
Impedance data were obtained using the Impedance Analyzer SI1260A (Solartron Analytical, Cambridge, UK). Other devices integrating the measurement system were an electrochemical cell with a Teflon lid and a refrigeration system (Frigiterm-10. J.P. Selecta, Barcelona, Spain) which allowed to perform the measurements at 25 ($\pm$0.1)°C.

The impedance data were recorded using D-Plot (Solartron Analytical) and data analysis was done with the help of Z-View (Solartron Analytical).

In this experimental mode, a commercial platinum electrode, M241PT (Radiometer Analytical S.A., France) was employed as counter electrode and an in-house built gold chip electrode [9], of much smaller area, served as working electrode. No reference electrodes were used.

2.2.2. Biofilm monitoring
The chip surface was regularly washed to eliminate weakly adhered compounds. As it is shown in Fig. 1, the presence of weakly adsorbed compounds on the chip surface is responsible for the impedance changes registered during cleaning process. After 10 min of electrochemical cleaning, most of these particles were eliminated and the impedance module value, |Z|, reached a constant value. Therefore, subsequent rinses (using sterile physiological serum) were performed for at least 10 min.

After the washing process, impedance measurements of chip surface modification were carried out. Typically, the working chip was placed inside an electrochemical cell containing physiological serum at 25 °C (the measurements were performed at constant temperature).

The sterile physiological serum solution provided a constant salinity medium for impedance measurements, which avoided osmotic problems in biofilm cells during measurements and washing.
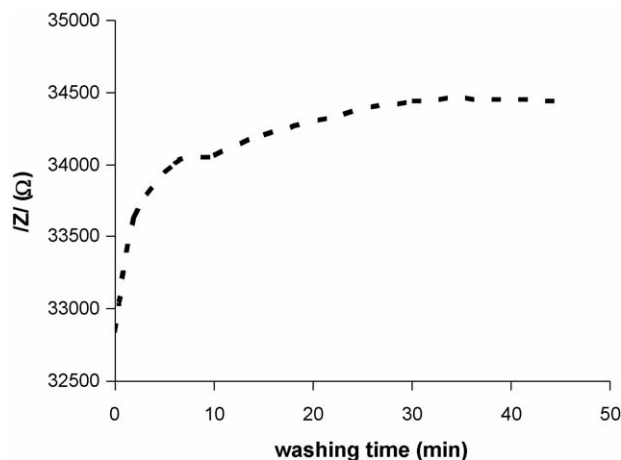
Fig. 1. Impedance value variation vs. washing time.

Next, bipolar impedance measurements were carried out. Impedance spectra were recorded over a frequency range from 10 Hz to 10 kHz, applying a zero DC potential between electrodes and an AC signal of 25 mV amplitude. These DC potential and AC amplitude used ensured working in the system linear region [10–13]. Current densities close to 3 mA/cm^2 were typically recorded.

In spite of the fact that the DC potential difference between working and counter electrode was set to zero, the system applied an effective potential close to +0.8 V versus Ag/AgCl (3 M KCl) over the working electrode. This brought about the oxidation of the chip [14], which increased its surface roughness and turned out to be beneficial to bacterial adhesion.

2.2.3. Biofilm removal
When the biofilm was completely built up, several solutions were employed to remove it. Rinses in H_2O_2 30%, H_2SO_4 3 and NaOH 1 mol dm^{-3} or ethanol 96% were tried to evaluate the ability of peroxides, acids, bases and alcohols to eliminate each compound of this bacterial structure.

3. Results and discussion

Impedance data were fitted to the equivalent circuit shown in Fig. 2 using Z-View. In this model, R_s represents the solution resistance and the CPE_{dl} the double layer constant phase element. The use of a CPE instead of a capacitor deserves some explanation. Although, the double layer capacitance is commonly represented as a capacitor, the fact of the matter is that the superficial roughness of the chip causes this electrical element to turn into a constant phase element, CPE [15]. A CPE is an electrical parameter composed by two parts: K, which is a measure of the impedance magnitude, and β a constant value parameter. In this research work, the K_{dl} value has been shown to be the only electrical parameter able to give information about the biofilm formation.

Fig. 2. Equivalent circuit.

Fig. 3. K_{dl} in percentage terms vs. contact time using new gold chips: (A) in bacterial culture medium and (B and C) in saline medium.

Fig. 4. K_{dl} change (in percentage) versus contact time by using reused gold chips: (A and B) in bacterial culture medium and (C and D) in saline medium.

3.1. Biofilm monitoring

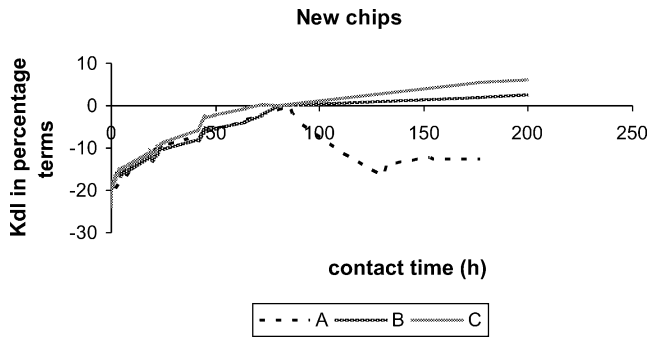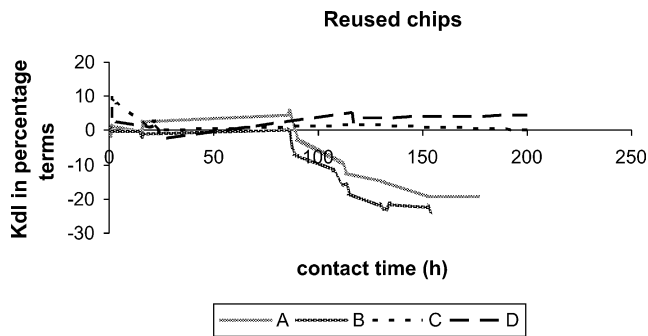The changes produced by the formation of the biofilm on the chip surface were related to the CPE_{dl} through its K_{dl} value. Figs. 3 and 4 show how K_{dl} changes over time while the chip remains in the reactor. This time is referred to as contact time.

The performance of new chips (Fig. 3) (sensors not previously activated nor used) and reused chips (Fig. 4) (sensors employed in other impedance experiments or previously activated) was studied in these measurements. Different behaviours were observed before and after 80 h of contact time, depending on the initial electrode characteristics and the solution they were immersed.

During the first 80 h, an increase of the K_{dl} value could be seen for the new chips. This is thought to be due to the surface activation process (Fig. 3). In general, new sensors were found to present debris parasitizing its surface and decreasing their active area.

Activation through electrochemical cycling or certain impedance measurements applying a DC potential of +0,8 V versus Ag/AgCl (3 M KCl) were enough to remove these substances and increase the electrode active area. As shown in Fig. 3 some impedance measurements could be enough to activate sensor surface increasing K_{dl} a 20% of its initial value. In fact, chips immersed in non-bacterial solutions showed that the activation process did not finished at 80 h and their impedance value continued increasing.

In the case of reused chips, a constant K_{dl} value was recorded (Fig. 4). These electrodes had already undergone the activation process. This means that any changes observed in their active area, reflected by their impedance, could be observed and related to before biofilm formation on the chip.

In addition, although during the first 80 h certain compounds, which could not be eliminated by washing, precipitated on the chip surface (Fig. 5A.1) as can be seen in Fig. 4 this precipitation process did not change the impedance value. Actually, the medium salts could precipitate due to the experimental conditions. A very fast change of AC potential (25 mV) in a very high value of DC potential [+0,8 V versus Ag/AgCl (3 M KCl)] has been found to produce the precipitation of certain salts on-chip surface.

Then, although these compounds did not seem to modify the electrical properties of the electrode–solution interface, their opaque nature did modify the optical properties of the chip surface as can be shown in Fig. 5A and B. Therefore, the relation between surface pollution and biofilm formation is quite difficult or even impossible to establish.

In the initial stages, few bacteria adhere on the electrode surface (Fig. 5A.2). The change they bring on interfacial properties was so small that they were invisible to impedance measurements too. The obvious implication is that any impedance
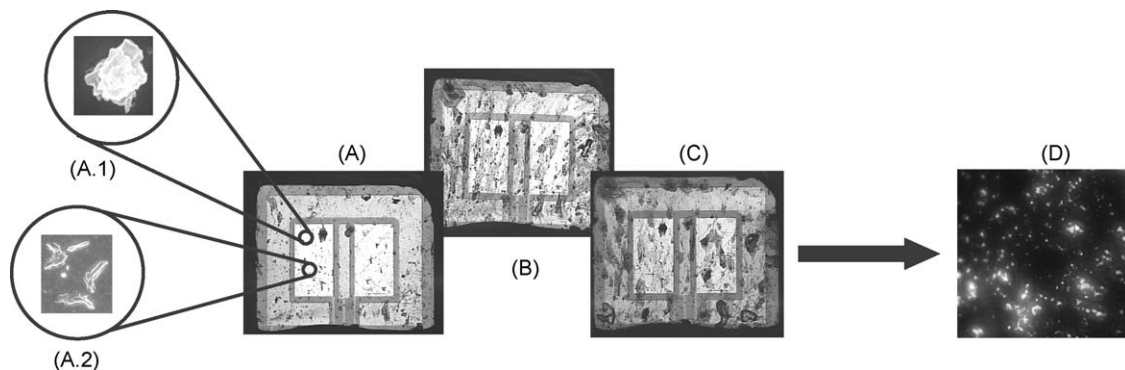
Fig. 5. Chip surface pollution process. (A) Optical microscopy (25×) chip surface image before 80 h (25 h). Electrical microscopy image of the high level of precipitated salts (A.1) and a few bacteria placed at the electrode surface (A.2) in the initial step (25 h). (B) Optical microscopy (25×) chip surface image at 80 h. (C) Optical microscopy (25×) chip surface image after 80 h (150 h). (D) Fluorescent microscopy (40×) chip surface image after 80 h (150 h).

$$Kdl \approx \varepsilon_0 \cdot \varepsilon_{dl} \cdot \frac{A}{d}$$

Fig. 6. Capacitor expression, where ε_0 is the vacuum permittivity, ε_{dl} the double layer permittivity, A the active area of electrode and d is the distance between layers.

changes measured will be due to the presence of structures more complex than a simple cell.

After 80 h, K_{dl} decreased exponentially in the case of culture-immersed chips (Figs. 3A and 4A and B) while it practically remained constant for those chips immersed in non-bacterial solution (Figs. 3B and C, and 4C and D).

Despite the tendency of some salts from the saline medium to precipitate on the sensor surface under measurement conditions, as shown for chips immersed in non-bacterial solution, it never influenced the interfacial properties enough to change impedance value appreciably.

On the other hand, Figs. 3 and 4 show the variation percentage of K_{dl} was almost 20% for chips immersed in bacterial solutions, regardless of whether they were new or reused. This suggested that measurement capacity did not depend on the superficial activity of the sensor.

As K_{dl} decreases could only be seen in culture-immersed chips and always measuring in the same solution, this reduction was associated with the changes produced on electrode surface by the presence of bacteria in solution.

The change in interfacial parameter values could be related to the adhesion capacity of bacteria, specifically their predisposition to make up biofilms on solid structures. Fluorescent microscopy images of the chip surface stained with DAPI after 80 h of experiment (150 h to be precise) confirmed bacterial presence and biofilm formation (Fig. 5C). On the other hand, the change produced by biofilm formation on opacity was so small than it seemed to be very difficult to characterize biofilm though optical observations (Fig. 5A and B).

Initially, bacteria showed little adherence to the sensor surface and little ability to change its superficial characteristics. When environmental conditions got worse (lack of nutrients and oxygen, excess of toxins, etc.), microorganisms changed their metabolism to produce polymers, which enabled them to adhere and build a favourable structure, as biofilms [16].

After 80 h, most *Escherichia coli* bacteria produced enough amount of polymer to adhere irreversibly onto the electrode, thus modifying its interfacial characteristics. These changes were monitored by impedance measurements and thus the first stages in the creation of a biofilm were identified.

The equivalent CPE reduced its magnitude following an exponential curve for almost 50 h before its value reached a plateau. These results suggest that *P. aeruginosa* needed approximately, 50 h to build a stable biofilm on rough gold oxide surfaces.

The insulating properties given by the biofilm could be responsible for the apparent decrease in the magnitude of K_{dl}. In a smooth surface, CPE_{dl} become a capacitor and its value could be approached such as a capacitor. As can be seen in Fig. 6, its magnitude depends on several variable parameters, such as the medium conductivity and the active area of the electrode.

On account of the experimental conditions where medium conductivity was constant, only the A value is a real variable. In fact, this variable was the responsible of all the observations shown in both activation process and biofilm formation.

Fig. 7 shows an intuitive model of the biofilm formation process. Initially the electrode surface is clean and the K_{dl} value remains constant over time. At some stage, a few bacteria adhere onto the chip surface, resulting in a decrease of the active area, which is so small that the resulting change in K_{dl} is unnoticed through impedance measurements.

Once the biofilm has grown to cover the entire sensor surface, K_{dl} changes abruptly and the development of the biofilm can be followed impedimetrically.

As the results show, bacterial adhesion was so great after 80 h that the electrode active area is drastically reduced, which increase the impedance value as K_{dl} also decreases.

As can be shown by the exponential form of impedance data (Figs. 3 and 4), adhesion of bacteria could be produced by a cooperative process favoured after adhesion of other microorganisms. Indeed; bacteria can adhere more easily onto biofilm structures than onto gold surfaces.

Once the biofilm was completely formed, both K_{dl} and impedance values remained constant. At this point, the electrode area was completely covered by the biofilm, which cannot modify interface properties of the sensor further.

3.2. Biofilm elimination

The cleaning process was constituted by four steps. In the initial one, the chip was rinsed inside a H_2O_2 30% solution. Peroxide solutions were the most effective in the removal of
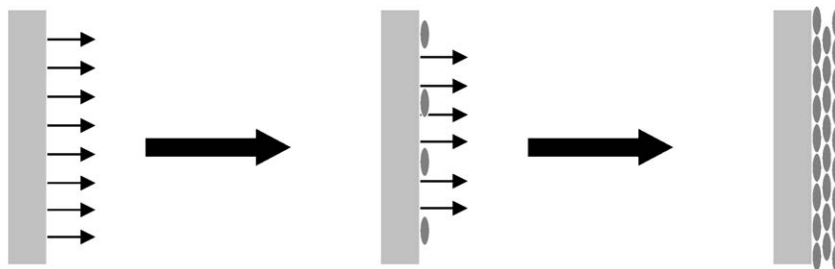

Fig. 7. Scheme of bacterial adhesion process. Initially bacteria could not adhere on-chip surface but changing their protein expression enables them to grow into a biofilm. The arrow represents the electron flux.
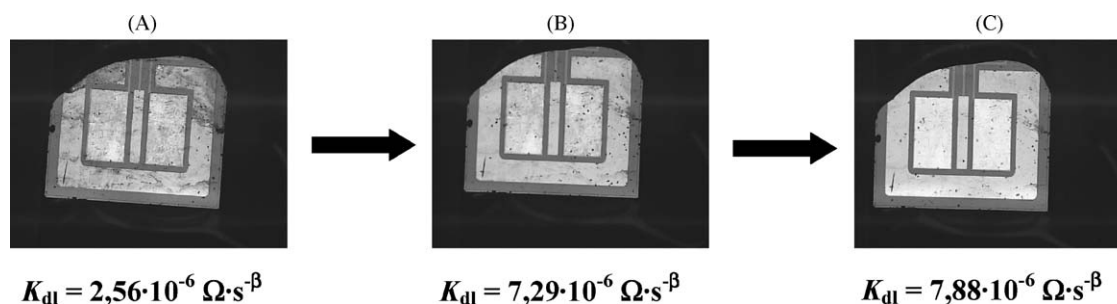
(A)   (B)   (C)

$K_{dl} = 2,56 \cdot 10^{-6} \ \Omega \cdot s^{-\beta}$ $K_{dl} = 7,29 \cdot 10^{-6} \ \Omega \cdot s^{-\beta}$ $K_{dl} = 7,88 \cdot 10^{-6} \ \Omega \cdot s^{-\beta}$

Fig. 8. Cleaning processes. Optical microscopy (25×) chip surface image and K_{dl} value (A) before the cleaning process, (B) after 20 min of cleaning with H_2O_2 30% and (C) after 20 min of cleaning with H_2SO_4 3 mol dm^{-3} and NaOH 1 mol dm^{-3}.

biofilms from chip surfaces. Experimental results showed that rinsing for 20 min was enough to remove the biofilm quantitatively. In fact, the increase of K_{dl} value showed after this washing process could be related with an increase of conductivity and, therefore with a biofilm removing procedure (Fig. 8).

Next, the chip was rinsed in 3 mol dm^{-3} H_2SO_4 followed by 1 mol dm^{-3} NaOH to eliminate precipitated salts for 20 min. This was necessary because the capacity of peroxide to eliminate precipitated salts was rather low and acid/base solutions had to be employed to dissolve them. The effect of this washing process was checked by optical microscopy, since the impedance value kept constant (Fig. 8).

The main drawback of this cleaning process is the resulting attack of the encapsulating polymer, debris of which was then adsorbed onto the chip surface. Therefore, a new step should be added to this process. To eliminate the unwanted encapsulating polymer, the electrode was gently rinsed using 96% ethanol.

This cleaning process gradually eliminated the encapsulating polymer, thus decreasing the chip lifetime. However, the chip could be employed for 3 months without suffering any changes in its original electrical properties. Work is currently being done to study different sensor packaging alternatives.

4. Conclusions

On-chip impedance measurements provide an easy, reproducible, economic and miniaturized way to follow biofilm formation in drinking water pipes. In addition, impedance measurements can be really useful to monitor bacterial elimination from chip surfaces.

This allows free chlorine levels to be properly adjusted throughout the entire water distribution network, thus optimising the amount of disinfectant used along the drinking water pipes.

Peroxides have shown to be the most effective products to remove biofilms. However, acid and basic solutions are also needed to dissolve precipitated salts.

For microchips, which are usually encapsulated, further washing step with alcohols is necessary.

References

[1] A. Maul, et al., Heterotrophic bacteria in water distribution systems. I. Spatial and temporal variation, Sci. Total Environ. 44 (3) (1985) 201–214.

[2] A. Maul, et al., Heterotrophic bacteria in water distribution systems. II. Sampling design for monitoring, Sci. Total Environ. 44 (3) (1985) 215–224.

[3] W.G. Characklis, K.C. Mashall (Eds.), Biofilms, John Wiley and Sons Inc., New York, 1990.

[4] H.M. Lappin-Scott, J.W. Costerton (Eds.), Microbial Biofilms, Cambridge University Press, 1995.

[5] E. van der Wende, et al., Biofilms and bacterial drinking water quality, Water Res. 23 (10) (1989) 1313–1322.

[6] A. Bressel, et al., High resolution gravimetric, optical and electrochemical investigations of microbial biofilm formation in aqueous systems, Electrochim. Acta 48 (20–22) (2003) 3363–3372.

[7] C. Davis, V. Birss, D. Cramb, Electrochemical characterization of biofilm growth on platinum surfaces, in: 204th Meeting of the Electrochemical Society, 2003.

[8] G. Wirtanen, S. Salo, I.M. Helander, T. Mattila-Sandholm, Microbiological methods for testing disinfectant efficiency on Pseudomonas biofilm, Colloids Surf. B: Biointerfaces 20 (2001) 37–50.

[9] C. de Haro, et al., Electrochemical platinum coatings for improving performance of implantable microelectrode arrays, Biomaterials 23 (23) (2002) 4515–4521.

[10] L.A. Geddes, Electrodes and the measurement of bioelectric events, 1972.

[11] H.P. Schwan, Linear and nonlinear electrode polarization and biological materials, Ann. Biomed. Eng. 20 (1992) 269–288.

[12] E.T. McAdams, J. Jossinet, The detection of the onset of electrode-electrolyte interface impedance nonlinearity: a theoretical study, IEEE Trans. Biomed. Eng. 41 (5) (1994) 498–500.

[13] C.D. Ferris, Introduction to bioelectrodes, 1974.

[14] C.B. Berggren, B. Bjarnason, G. Johansson, Capacitive biosensors, Electroanalysis 13 (3) (2001) 173–180.

[15] E.T. McAdams, Effect of surface topography on the electrode-electrolyte interface impedance, Surf. Topogr. 2 (1989) 107–122.

[16] D.G. Davies, G.G. Geesey, Regulation of the alginate biosynthesis gene algC in Pseudomonas aeruginosa during biofilm development in continuous culture, Appl. Environ. Microbiol. 61 (3) (1995) 860–867.

Biographies

Xavier Muñoz Berbel received the MSc degree in biotechnology in September of 2002 from the University Autonomous of Barcelona (UAB), where he is at the moment pursuing his PhD in biotechnology. His research has been done in the National Centre of Microelectronics in the UAB campus. His main research topics are bioimpediemtric microchips by several applications, such as bacterial quantification, biofilms characterization and ion selective and enzymatic sensors development.

Fco. Javier Muñoz received the PhD degree in physical chemistry from the University Autonomous of Barcelona in 1990. During 1990 to 1992 he performed postdoctoral research work in the Biosensors Group of the MESA Institute at the University of Twente. In 1992 he joined the Centro Nacional de Microelectronica of Barcelona (CNM-CSIC), where he has been working in the development of new chemical and biochemical microsensors. In 1997 he joined the CNM's Department of Microsystems as an associated researcher scientist. His areas

of interest are silicon micromachining technologies, polymer micro-fabrication and their application to integrated chemical microsensors and biosensors. He has participated and has been project leader of different national and European projects in this field. Currently he is responsible at CNM of several FP6 projects based on the application of biosensors and BioMEMs to the detection of special pathogen bacteria, as well as national projects and contracts focused on the integration of Microfluidics and Bio-Micro/Nanotechnology.

Nuria Vigués received the MSc degree in Microbiology in 2005 from the Autonomous University of Barcelona, where she is at the moment pursuing her doctorate in Microbiology. Her main research topics are biofilm formation in different species and materials, transport and survival of microorganisms in soil.

Jordi Mas received the PhD in biology in 1985 from the Autonomous University of Barcelona, and got his full professor position of microbiology at Autonomous University of Barcelona in 1989. He is a member of the Ambiental Microbiology group in the Genetics and Microbiology Department. He is involved in the concept and development of micro organism biofilms, ecology and bacterial physiology, development and characterization of toxicity sensors.

Accepted Manuscript

Title: Impedimetric approach for monitoring the formation of biofilms on metallic surfaces and the subsequent application to the detection of bacteriophages

Authors: X. Muñoz-Berbel, Cristina García-Aljaro, F.J. Muñoz
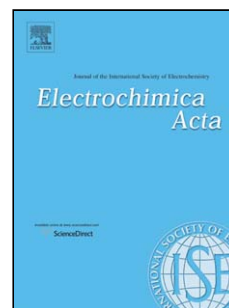
Please cite this article as: X. Muñoz-Berbel, C. García-Aljaro, F.J. Muñoz, Impedimetric approach for monitoring the formation of biofilms on metallic surfaces and the subsequent application to the detection of bacteriophages, *Electrochimica Acta* (2007), doi:10.1016/j.electacta.2008.03.050

Impedimetric approach for monitoring the formation of biofilms on metallic surfaces and the subsequent application to the detection of bacteriophages

X. Muñoz-Berbel[1*], Cristina García-Aljaro[1], F. J. Muñoz[1]

[1]*Centro Nacional de Microelectrónica (IMB-CSIC), Esfera UAB, Campus Univ. Autónoma de Barcelona, 08193 Bellaterra, Barcelona, Spain.*

Abstract

This paper describes an impedimetric method for monitoring the formation of bacterial biofilms on the surface of platinum and gold electrodes and its application for the indirect detection of bacteriophages. Impedance measurements showed that the biofilm capacitance, $C_{biofilm}$, the parameter of the electrical circuit which modelled the biofilm, was sensitive both to the biofilm growth and to its degradation as a consequence of the bacteriophage infection. Impedance results were compared with optical and confocal microscopy studies showing a good correlation with the data obtained from the impedance analysis. These results guarantee further work in this area to develop portable devices for the detection of bacteriophages.

Keywords: platinum chips, biofilm growth monitoring, impedance spectroscopy, bacteriophages infection, confocal microscopy.

1. Introduction

Bacteria have the ability to colonize solid surfaces forming biofilms [1]. Biofilms are complex heterogeneous structures of cells grouped in a hydrated extracellular matrix mostly composed of polysaccharides, proteins and lipids [2]. Biofilm formation includes different steps, starting with an initial pre-attachment of molecules to the surface, a reversible attachment of cells followed by growth until maturation of the biofilm is reached. This process of biofilm formation has been monitored using several optical and electrochemical techniques [3]. Among other characteristics, biofilms become electrically insulating as they grow, modifying the electrode-solution interface properties and even inducing the appearance of new electrical parameter in the equivalent circuit. In previous works, the interface capacitance, the parameter of the equivalent circuit which monitors the electrode-solution interface, has been shown to be sensitive to the bacteria attachment and colonization of metallic surfaces from the early attachment until the formation of mature biofilms [4, 5].

The replication of bacteriophages, i.e. viruses that infect bacteria, within biofilms has been demonstrated causing biofilm degradation [6, 7]. However, no studies have been performed to assess the change in the electrochemical parameters that model biofilm formation after bacteriophage infection. Detection of bacteriophages is especially relevant in the environmental monitoring and food industries. On the one hand, detection of somatic coliphages (i.e. phages infecting *E. coli*), F-RNA specific phages and bacteriophages infecting *Bacteroides* spp. has been suggested to be more reliable for predicting the contamination of viral pathogens than the typical bacterial indicator strains [8-13]. On the other hand, detection of bacteriophages is also important because of the economic losses brought about by them in the fermentation industry. In the fermented dairy products industry producing cheese and yoghurt, the infection and subsequent lysis of bacterial starter cultures can render a fermentation process inactive.

Rapid and real time detection of bacteriophages is desirable in these areas, which can not be accomplished by the current available traditional methods. These methods consist basically in detecting bacteriophages by the double layer agar method where a host strain is seeded in a semi-solid agar layer. Exposure of the bacteria to bacteriophages results in the appearance of lysis zones that can be directly visualized after an appropriate incubation time, which is dependent on the bacteria, the number of which is related to the infective viral particles or viral aggregates in the original sample [14]. Despite of the emerging interest, bacteriophage detection has been given little attention and small progresses have been made during the last decades [15, 16].

In this study, the formation of *Pseudomonas putida* biofilms on gold and platinum electrodes and the subsequent degradation process after bacteriophage infection was impedimetrically monitored. The biofilm capacitance, $C_{biofilm}$, the electrical parameter of the equivalent circuit

related to the biofilm growth was found more sensitive to the biofilm degradation than the interface capacitance. The results obtained here proved that the degradation of mature biofilms grown on electrodes could be used as an indirect method for the detection of bacteriophages, using impedance spectroscopy. It has to be noted that the present method, developed with *P. putida* because of their huge capacity to build thick and stable biofilms, may be applied for the detection of any bacteriophage of interest, e.g. somatic coliphages, as long as a host bacterium for this bacteriophage is available and capable of biofilm forming.

2. Experimental

2.1 Bacterial strains and culture conditions

Pseudomonas putida DSM 291 and *Escherichia coli* ATCC 700078 (also known as *E. coli* WG5 by Grabow and Couborough [17]) were used in this study. Bacteria cultures were grown overnight in AB minimal medium (ABMM) [18] at room temperature (approximately 22 ºC). An overnight aliquot of 25 mL was inoculated into a 500 mL glass reactor containing ABMM. Bacteria were grown under constant agitation, *MR 2000* (Heidolph, Germany), and aeration, *BioFlo* (New Brunswick Scientific, New Jersey, USA). After the inoculation, no nutrients were added into the reactor (batch process). The electrodes used in this study were aseptically introduced into the reactor to avoid contamination. All manipulations were performed under sterile conditions.

2.2 Electrochemical cell

Electrode production was carried out in-house at the IMB-CSIC Barcelona under microfabrication technology [19]. A gold or platinum disc working electrode with an area of 0.5 mm^2 surrounded by a platinum counter electrode of 1.4 mm^2 were integrated on a silicon nitride substrate of 9 mm^2 (3 mm length per 3 mm width). The electrodes were 0.08 mm apart, ensuring near-homogeneous polarization of the working electrode [20]. These working electrode/counter electrode (WE/CE) chips were introduced in a 25 mL electrochemical cell in PBS thermostatically kept at 37 ºC together with an external Ag|AgCl electrode, 5240 (Crison, Barcelona, Spain).

2.3 Impedance analysis set up

A 25 mV AC potential was applied at the cell open circuit potential (+0.26 ± 0.05 V vs. Ag|AgCl) over a frequency range between 100 kHz and 10 Hz. An AUTOLAB PGSTAT 12 (EcoChemie, BV, The Netherlands) containing a FRA-2 module was used. Impedance spectroscopy spectra were recorded using the FRA-2 software (EcoChemie, BV, The Netherlands). The measurement time was around 1 minute after recording 17 points per frequency decade. All measurements given in this work are in relation to the Ag|AgCl reference electrode.

2.4 Impedimetric assay for biofilm formation monitoring

An impedimetric assay was performed in order to characterise the initial bacteria attachment and the subsequent formation of mature biofilms on the WE/CE chips. For that purpose, the WE/CE chips were introduced into a glass reactor containing a fresh bacterial culture prepared as indicated in the section 2.1. The electrodes were kept there to allow bacterial colonization during a period of 6 days, in which the chips were impedimetrically measured every 24 h, as described above. Before the measurement, electrodes were previously washed with sterile ABMM to remove weakly surface-attached compounds (Muñoz-Berbel et al., 2006).

2.5 Impedimetric assay for bacteriophage detection

For the detection of bacteriophages, the WE/CE chips containing six days mature biofilms were transferred to 10 ml of fresh ABMM or Modified Scholtens Broth (MSB) [21] culture media and inoculated with a bacteriophage stock or sewage sample 1/10 (v/v) prepared as indicated below. The electrodes were then impedimetrically measured in sterile PBS after different incubation times, as previously detailed.

2.6 Sewage samples collection and processing

Raw sewage samples from an urban sewage treatment plant were collected and transported to the laboratory according to standard methods [22]. Samples were stored at -70 ºC to avoid inactivation of the bacteriophages [23] until used. Processing of the samples included a centrifugation step of 10 min at 1000 *g* and filtration with sterile 0.22 µm pore filter (Millipore Corporation, Barcelona, Spain).
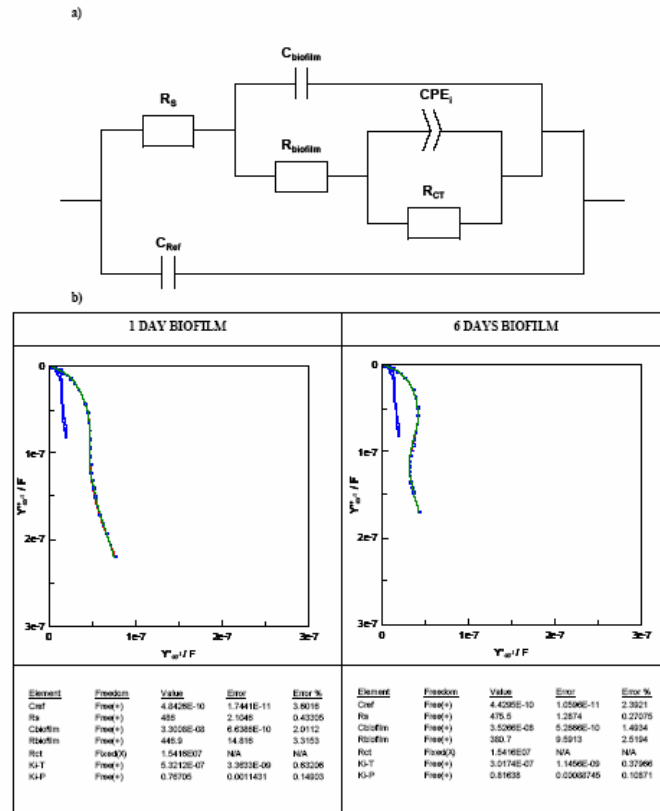
Figure 1. (a) Equivalent circuit and (b) admittance complex plane plot for *Pseudomonas putida* biofilms after 1 and 6 days of incubation. The impedance spectra (points in the plot) were fitted to the equivalent circuit shown inset, which contains the capacitor associated to the reference electrode (C_{ref}), the solution resistance (R_S), the biofilm capacitance ($C_{biofilm}$), the resistance of the biofilm pores ($R_{biofilm}$), the interface Constant Phase Element (CPE_i) and the charge-tranfer resistance (R_{CT}). The ideal impedance spectra obtained from the fitting (line in the plot), the calculated values and errors using the ZView software for each element of the equivalent circuit are also shown. The spectrum corresponding to the electrode before the introduction in the bacterial incubator is also included in each plot (black line).

2.7 Bacteriophage enumeration and preparation of stock cultures

Sewage samples from an urban wastewater treatment plant were used as source for *P. putida* and *E. coli* WG5 (somatic coliphages) bacteriophages. Enumeration of the bacteriophages was performed by the double layer agar method [14]. *P. putida* bacteriophages present in the sewage samples were enriched in ABMM using *P. putida* as host strain to increase their concentration because of the low number detected in the samples.

2.8 Sample preparation and imaging by confocal laser microscopy (CLM)

Briefly, biofilm-coated platinum chips were removed from the reactor and washed in PBS as explained above for the impedance measurements. The biofilm was stained with DAPI and WGA and then observed by CLM. Measurement of the biofilm thickness was expressed as the mean of 10 independent measurements conducted on each chip. The microscope used was a Laser Confocal Leica TCS SP2 AOBS (Leica, Heidelberg, Germany).

2.9 Optical microscopy measurements

Bacterial biofilms were Gram stained and imaged using a Nikon Eclipse ME-600 optical microscope (Nikon Corporation, Japan) to complement the impedance measurements.

2.10 Quantification of attached bacteria

Attached bacteria were quantified by sonication and plating on agar. Briefly, WE/CE chips were sonicated for 3 minutes to remove the attached bacteria from the surface of the electrodes in 5 mL of PBS. The supernatant was 1/10 serially diluted in PBS and 100 µL of the corresponding dilutions were then inoculated on an agar plate containing Luria Bertani (LB) medium. After growing overnight at 37 ℃, bacteria were counted and the number of attached bacteria onto the chips was estimated.

3. Results and discussion

3.1 Fitting and interpretation of impedance data

Z-View software was used to fit impedance data to the equivalent circuit shown in Figure 1a [24]. This circuit was composed of the solution resistance (R_S), the biofilm capacitance ($C_{biofilm}$), the resistance of the biofilm pores ($R_{biofilm}$), the double layer capacitance, which appears as the interface constant phase element (CPE_i), the charge-tranfer resistance (R_{CT}) and an extra capacitance of small magnitude (some nF) associated with the presence of an external reference (C_{Ref}), whose value did not vary with the biofilm growth. The use of the CPE_i instead of a conventional double layer capacitance has been discussed in previous works. Thus, on platinum electrodes, as on most solid-state electrodes, the double layer does not behave as a pure capacitance [5]. Although this is currently under study, a roughness factor appears to be one important cause for that. In absence of electroactive electrolytes in the medium, the impedance of most interfacial CPEs can be described by the following expression [25]:

$$Z = \frac{1}{K(j\omega)^{\beta}} \qquad (1)$$

Z is the magnitude of the impedance (in Ω), K is the CPE magnitude (in $\Omega^{-1}s^{-\beta}$), ω is the angular frequency (in s^{-1}) and β is a parameter linked with the phase angle, which oscillates from 1 for planar surfaces to 0.5 for very rough ones [26]. In this study, the biofilm became part of the interfacial region, thus modifying the dielectric properties of the electrode. Hence, the CPE_i represented in the equivalent circuit (Figure 1a) can be described as a generic element, which accounts for many complex processes which cannot, themselves, be deconvoluted.

Figure 1b shows the changes in the impedance spectra associated to biofilm formation. The magnitude of the CPE_i (shown in the figure as K_i-T), and the $C_{biofilm}$ were found very sensitive to the growth and maturation of biofilms.

3.2 Effect of the biofilm formation when measured by impedance spectroscopy

Pseudomonas made thick biofilms on the electrode surface quickly and easily. The effect of the biofilm formation on the electrode surface was measured using impedance spectroscopy as described in section 2.3. Impedance data were recorded and fitted as detailed above. The most relevant results from the fitting are given in Figure 2. The CPE_i magnitude (K_i-T) and the

$C_{biofilm}$ changed as a function of the attachment time.
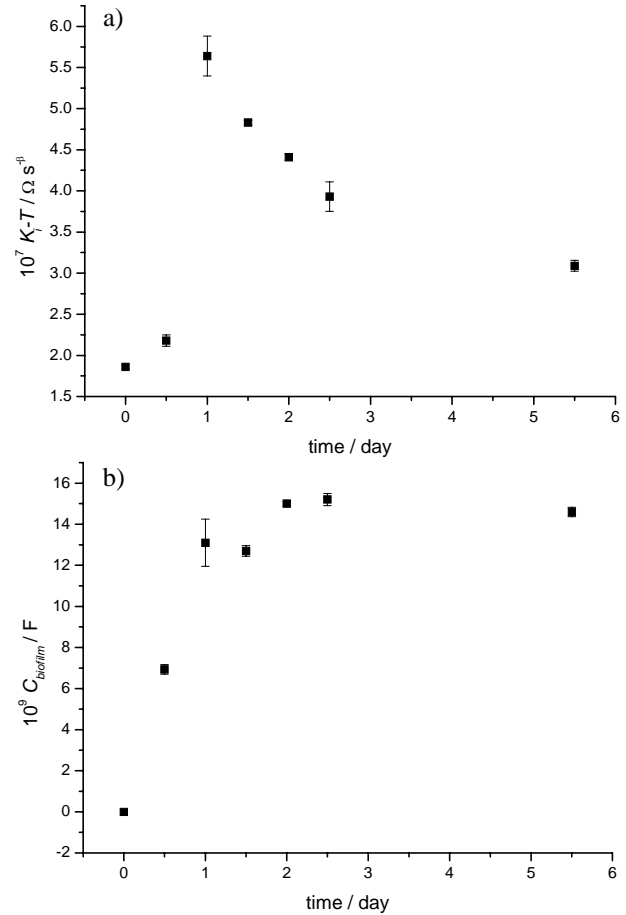
Figure 2. Representation of (a) the magnitude of the CPE_i (K_i-T), and (b) the $C_{biofilm}$ versus incubation time during the *P. putida* biofilm formation process on the platinum WE/CE chips. These plots illustrate the changes caused by the biofilm formation in both parameters.

In Figure 2a, the magnitude of the CPE_i shows a pronounced early increase followed by a deep decrease. This behaviour is the same as was observed in previous works for *E. coli* attached to platinum electrodes [5], where a pronounced early increase in CPE_i was also observed prior to the massive attachment of bacteria, which decreased the CPE_i later. The cause of the initial increase in CPE_i was associated to the decrease in the Debye length at the electrode double layer for the attachment of single bacteria, behaving as simple charged colloidal particles, with their counter-ions. The decrease in CPE_i, also found during the formation of *Pseudomonas aeruginosa* biofilms on gold surfaces [4], could be associated to different processes, being the decrease in the area, A, of bare electrode the principal mechanism, since:

$$K_i - T = \frac{\varepsilon_o \varepsilon_{dl} A}{d} \quad (2)$$

K_i-T is the double layer capacitance magnitude, ε_0 is the vacuum permittivity, ε_{dl} is the permittivity of the double layer, A is the area of the bare electrode and d is the distance between layers. Regarding previous works, the total measured CPE_i, capacitive in nature, can be considered to be the sum of the bare electrode capacitance, C_{Pt}, and the capacitance of the molecules composing the attached biofilm, C_{BC}, modulated by a time-dependent coverage factor, $\theta(t)$.

$$CPE_i = \theta(t) C_{BC} + (1 - \theta(t)) C_{Pt} \quad (3)$$

Bacteria biofilms are basically composed of bacteria and exopolysaccharides, which generate capacitances of lower magnitude than C_{Pt}. For instance, the capacitance of bacteria is commonly below pF [27], whereas the C_{Pt} has been found experimentally of hundreds of μF. Thus, the CPE_i would fall as bacteria and exopolysaccharides attached to the surface, as observed in Figure 2a.

Figure 2b shows that the magnitude of the $C_{biofilm}$ increases with the biofilm growth. Similarly, in a separate study conducted for the optimization of the thickness of a polypyrrole coating, it was reported that the coating capacitance, C_C, increased with the polymer growth [28]. The C_C was found to be sensitive to the coating permittivity, ε_C, the coating area, A_C and the coating thickness, d_C, as follows:

$$C_C = \frac{\varepsilon \varepsilon_C A_C}{d_C} \quad (4)$$

According to Amidurin et al. [29], during the coating growth, the polymer capacitance is basically influenced by the coating permittivity, which mainly depends on the polymer porosity. Thus, the increase in C_C was attributed to the increase of the polymer porosity. Following the same reasoning, the increase in the biofilm porosity during its growth appears to be the responsible of the recorded increase in the $C_{biofilm}$ magnitude.

3.3 Evaluation of the degradation of mature biofilms by specific bacteriophages using impedance spectroscopy, optical and confocal microscopy, and microbial counts

The use of impedance spectroscopy for the detection of specific bacteriophages was assessed in parallel with both optical and laser confocal microscopy, and microbial counts (CFU cm^{-2}), in order to corroborate the obtained results. A 6 days mature *P. putida* biofilm, whose growth had been previously impedimetrically monitored, was used to elaborate a bacteriophage mediated biofilm infection model. Wastewater from the influent of an urban wastewater treatment plant was used as source of *P. putida* infecting bacteriophages. The concentration of these bacteriophages in the analysed sample was 40.5 (±0.7) PFU mL^{-1}, which was increased up to 10^7 PFU mL^{-1} after a single enrichment step.
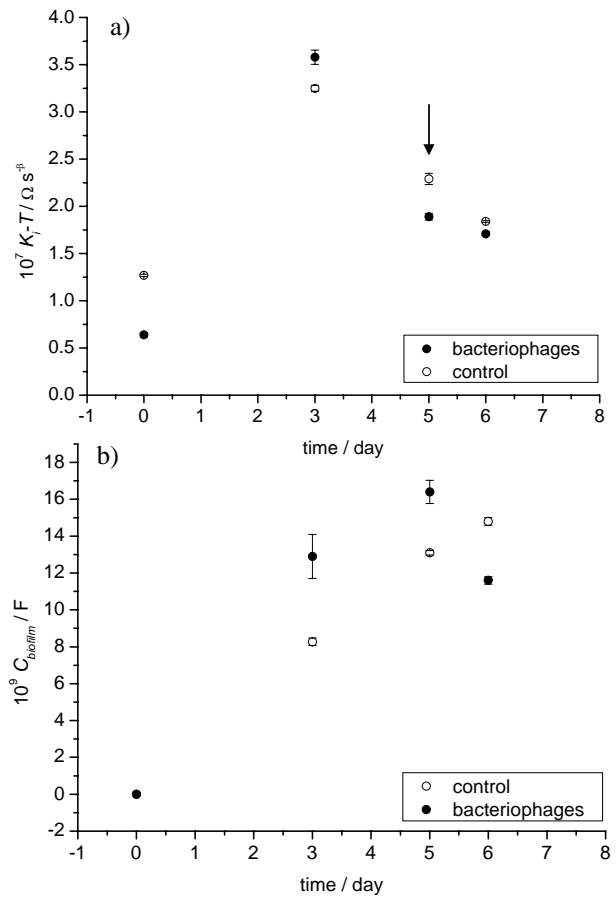
Figure 3. Representation of (a) the K_i-T, and (b) the $C_{biofilm}$ versus the time of incubation in the *P. putida* incubator (biofilm growth) and the subsequent exposure to bacteriophages (biofilm degradation). The moment when WE/CE chips were extracted from the incubator and introduced in the bacteriophages culture is shown with a vertical arrow.

Different concentrations of bacteriophages were assessed (10^6 and 10^7 PFU mL^{-1}) and the biofilm infection monitored over 24 h. Figure 3 shows the changes produced in the CPE_i and the $C_{biofilm}$ during the biofilm growth and the subsequent degradation by bacteriophages. The magnitude of the CPE did not change with the infection process whereas the $C_{biofilm}$ decreased as a consequence of the bacteriophages degradation of the biofilm. Thus, bacteriophages

CONTROL	BACTERIOPHAGES
31.65 (±3.25) μm of thickness	15.94 (±2.19) μm of thickness
4.08 (±0.05) log (CFU mm^{-2})	3.37 (±0.18) log (CFU mm^{-2})

Figure 4. Optical microscopy images at different magnification of WE/CE chips after overnight incubation in either ABMM with or without bacteriophages. The thickness of the biofilms and the number of attached cells per unit area after the infection process is also shown.

infected and lysed superficial cells modifying the biofilm structure but inner cells, especially those attached directly to the electrode, were more resistant to the infection.

As shown in Figure 4, after incubation of the WE/CE chips in the bacteriophage suspensions, less attached bacteria were found in these chips compared to the ones exposed to control suspensions (i.e. the same culture media without the phages), which could be associated to the infection process. Also the biofilm thickness and the number of attached cells decreased with the bacteriophages infection process in around 50% and 20%, respectiv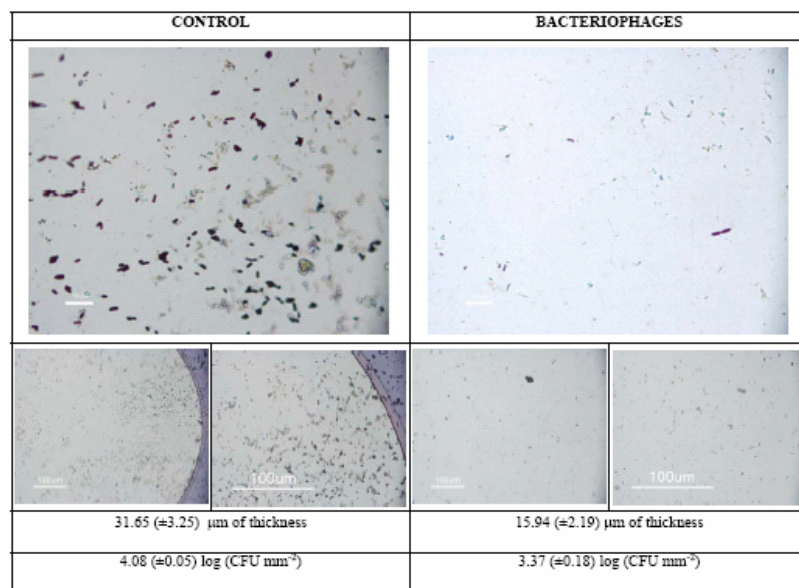ely. The differences in the obtained percentages could be probably explained because only the most distant bacteria in the biofilm would have been infected and lysed with the bacteriophages, while the core of the biofilm, where the bacteria are normally more densely grouped, would have not been reached by these bacteriophages. Infection of biofilms by bacteriophages is indeed a complex process dependent on different factors such us the presence of phage-borne polysaccharide depolymerases to degrade the extracellular matrix, in which the bacteria are immersed [30]. The decrease in $C_{biofilm}$ after 24 hours of incubation was found sensitive to the initial concentration of bacteriophages, being more pronounced as the concentration of bacteriophages increased. It was also observed a variation in the $C_{biofilm}$ value through the incubation time. Thus, the decrease in $C_{biofilm}$ was mainly recorded during the initial 6-8 hours when the degradation of the biofilm seemed to be more intense (data not shown).

In summary, the detection of changes in the $C_{biofilm}$ parameter in a mature biofilm proved useful for the development of an indirect method for the detection of bacteriophages in liquid samples.

3.4 Application to real samples: detection of somatic coliphages from an urban sewage treatment plant
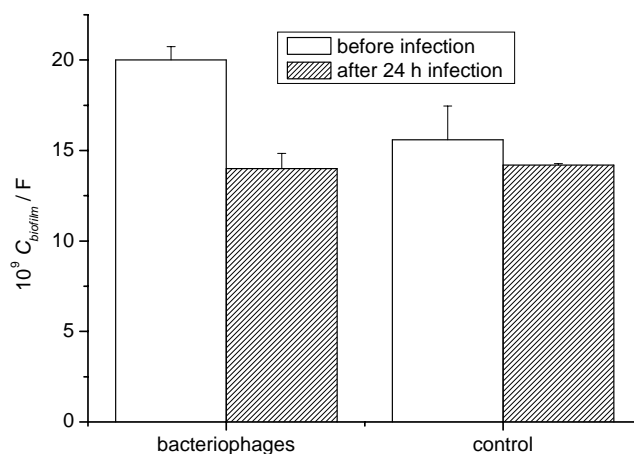
Figure 5. Representation of the change in the Cbiofilm magnitude after 24 hours of incubation in real samples from an urban sewage treatment plant. The control sample, water without bacteriophages, is also shown.

The impedimetric approach for detecting bacteriophages via the degradation of specific bacterial biofilms was applied to the detection of somatic coliphages from an urban sewage treatment plant. Five days mature biofilms of *E. coli* grown on WE/CE chips following the

experimental condition shown in section 2.1 were used. As shown in Figure 5, this method was sensitive enough to detect the viral contamination in water samples from a sewage treatment plant, which contained a concentration of around 10^4 PFU mL^{-1} of somatic coliphages. A similar response to the *P. putida* assay was observed, with a significant decrease in the $C_{biofilm}$ in the sample containing bacteriophages with respect to the control sample, where no bacteriophages were present.

4. Conclusions

We have shown that impedance spectroscopy can be used for following both bacterial biofilm growth on metallic surfaces and the subsequent degradation caused by the infection of specific bacteriophages. The biofilm capacitance, $C_{biofilm}$, the parameter of the equivalent circuit related to the biofilm growth, has been found to be sensitive to the biofilm formation and degradation. Impedance results are well correlated with optical microscopy images. Also the thickness of the biofilms (from laser confocal microscopy) and the number of attached cells coincide with impedance data. The $C_{biofilm}$ has been shown sensitive both to the concentration of bacteriophages in the culture and to the incubation time. This approach has been applied to the detection of coliphages in real samples from an urban sewage treatment plant.

Future work will be focused on the optimization of the sensitivity and the variability of the impedimetric approach. Also some effort will be done in the development of automatic devices for the real-time detection of bacteriophages.

References

[1] J.W. Costerton, P.S. Stewart, E.P. Greenberg, Science 284 (1999) 1318.
[2] G. O'Toole, H.B. Kaplan, R. Kolter, Annu. Rev. Microbiol. 54 (2000) 49.
[3] A. Bressel, J.W. Schultze, W. Khan, G.M. Wolfaardt, H.-P. Rohns, R. Irmscher, M.J. Schoning, Electrochimica Acta 48 (2003) 3363.
[4] X. Muñoz-Berbel, F.J. Muñoz, N. Vigués, J. Mas, Sens. Actuators B 118 (2006) 129.
[5] X. Muñoz-Berbel, N. Vigués, J. Mas, A.T.A. Jenkins, F.J. Muñoz, Electrochem. Commun. 9 (2007) 2654.
[6] M.M. Doolittle, J.J. Cooney, D.E. Caldwell, Can. J. Microbiol. 41 (1995) 12.
[7] B.D. Corbin, R.J.C. McLean, G.M. Aron, Can. J. Microbiol. 47 (2001) 680.
[8] F. Traub, S.K. Spillmann, R. Wyler, Appl. Environ. Microbiol. 52 (1986) 498.
[9] J.J. Borrego, M.A. Morinigo, A. de Vicente, R. Cornax, P. Romero, Water Res. 21 (1987) 1473.
[10] A. Ketratanakul, S. Ohgaki, Y. K., Water Sci. Technol. 24 (1991) 407.
[11] J. Lasobras, J. Dellunde, J. Jofre, F. Lucena, J. Appl. Microbiol. 86 (1999) 723.
[12] W.O.W. Grabow, Water SA 27 (2001) 251.
[13] L. Moce-Llivina, F. Lucena, J. Jofre, Appl. Environ. Microbiol. 71 (2005) 6838.
[14] M.H. Adams, Bacteriophage, Interscience Publishers, New York, 1959.
[15] T. Neufeld, A.S. Mittelman, V. Buchner, J. Rishpon, Anal. Chem. 77 (2005) 652.
[16] T. Neufeld, A. Schwartz-Mittelmann, D. Biran, E.Z. Ron, J. Rishpon, Anal. Chem. 75 (2003) 580.
[17] W.O.W. Grabow, P. Coubrough, Appl. Environ. Microbiol. 52 (1986) 430.
[18] D. Balestrino, J.A.J. Haagensen, C. Rich, C. Forestier, J. Bacteriol. 187 (2005) 2870.
[19] M.A. Alonso Lomillo, J.G. Ruiz, F.J.M. Pascual, Anal. Chim. Acta 547 (2005) 209.
[20] J.E. Harrar, I. Shain, Anal. Chem. 38 (1966) 1148.
[21] Anonymous, in, International Organisation for Standardisation, Geneva, Switzerland, 2000.
[22] L.S. Clesceri, A.E. Greenberg, A.D. Eaton, in, American Public Health Association, Washington DC, 1998.
[23] J. Mendez, J. Jofre, F. Lucena, N. Contreras, K. Mooijman, R. Araujo, J. Virol. Methods 106 (2002) 215.
[24] C. Liu, Q. Bi, A. Leyland, A. Matthews, Corrosion science 45 (2003) 1243.
[25] H. Fricke, Philosophical Magazine 7 (1932) 310.
[26] W.H. Mulder, J.H. Sluyters, T. Pajkossy, L. Nyikos, J. Electroanal. Chem. 285 (1990) 103.
[27] R. Holzel, Biochimica et Biophysica Acta (BBA) - Molecular Cell Research 1450 (1999) 53.
[28] M. Cortina-Puig, X. Munoz-Berbel, M. del Valle, F.J. Munoz, M.A. Alonso-Lomillo, Anal. Chim. Acta 597 (2007) 231.
[29] A. Amirudin, D. Thieny, Prog. Org. Coat. 26 (1995) 1.
[30] K.A. Hughes, I.W. Sutherland, M.V. Jones, Microbiology 144 (1998) 3039.

Surface plasmon resonance assay for real time monitoring of somatic coliphages in surface waters

Cristina García-Aljaro [a,*], Xavier Muñoz-Berbel [a], A.T.A. Jenkins [b], Anicet R. Blanch [c] and Francesc Xavier Muñoz [a]

[a] *Centre Nacional de Microelectrònica de Barcelona (CNM- IMB), CSIC. Campus UAB, 08193 Bellaterra, Spain*
[b] *Department of Chemistry, University of Bath, BA2 7AY, Bath, United Kingdom*
[c] *Departament de Microbiologia, Facultat de Biologia, Universitat de Barcelona, 08028 Barcelona, Spain*

Abstract

Surface plasmon resonance (SPR) technique has been proved to be a very sensitive method for detecting bio-molecular interactions. In this study, a two-channel microfluidic SPR sensor device was used to detect the presence of somatic coliphages, a group of bacteriophages that have been proposed as faecal pollution indicators in waters, using their host, *Escherichia coli* WG5, as a target for their selective detection. *E. coli* WG5 was immobilized onto gold films through avidin-biotin interactions and was allowed to be lysed by the bacteriophages present in the water samples. Exposure of the immobilized host strain to the bacteriophages resulted in a shift of SPR response angle of at least 150 m° after a period of time that was dependent on the concentration of the bacteriophages in the sample. As few as 1 PFU mL^{-1} injected into the chamber could be detected after a phage incubation period of 120 min, which means that a minimum concentration of around 10^2 PFU mL^{-1} in the original sample can be detected. These results are very promising for the construction of portable biosensors for bacteriophage detection and enumeration in the future based on this technique.

Keywords: Surface plasmon resonance; Biosensor; Somatic coliphages; *E. coli*; Surface water

1. Introduction

In the last two decades, a wide variety of biosensors including electrochemical (amperometric and impedimetric), piezoelectric (quartz crystal microbalance) and optical (surface plasmon resonance, SPR) devices have been developed for the detection of viral and bacterial pathogens (Gau et al. 2001; Kurosawa et al., 2006). Among them, biosensors based on the surface plasmon resonance technique (SPR) have received increasing interest because of the power and easiness of this technique. The first theories that now explain the SPR phenomenon were presented in 1873 by James Clark Maxwell but it was not until nearly two decades ago that the first SPR-based biosensor was developed (Jönsson et al., 1991). It relies on the detection of changes in the refractive index close to the sensor surface, which is related to the amount of macromolecules bound to the sensor surface. As shown in Fig. 1, there is an incident light (*P* polarized light) that is coupled to the electron field (plasmon wave) through a glass prism that create an energy wave (surface plasmon resonance) that can extend through the dielectric material deposited onto the gold surface. The maximum coupling of the light with the surface plasmon occurs at an angle θ (angle of resonance), which depends on the dielectric material deposited above the gold surface (Kretschmann, 1971). Hence, this technique is useful for the study of bimolecular interactions that occur at no more than 300-400 nm from the gold surface. In last years this technique has been improved and a wide variety of SPR-based biosensors have been developed (see Hoa et al., 2007 for review of advances in SPR technology). SPR has proved useful for the monitoring of several compound among which, we can find hormones (Habauzit et al., 2007), pesticides (Mauriz et al., 2007) […] with very important applications, which traditionally had been studied by immunoassays, spectroscopic techniques or chromatographic methods. One important advantage of the SPR method over the rest is that the measure is taken nearly continuously so it offers nearly real time responses of the process that is being measured. It has other advantages over electrochemical systems, like its high sensitivity.

In the last years some SPR detection protocols have been described for the detection of certain virus (Baac et al., 2006; Bolovets et al., 2004). However, they focus mostly in the detection of animal virus particles than in the intact form of the virus (Wittekindt et al., 2000), while bacteriophage detection, *i.e.* virus that infect bacteria, remains an unexplored subject. Recent work by Jenkins has shown that SPR is sensitive to bacterial attachment, despite the fact that bacteria are larger than the evanescent decay length of the resonant surface plasmons. Moreover, SPR could accurately discriminate

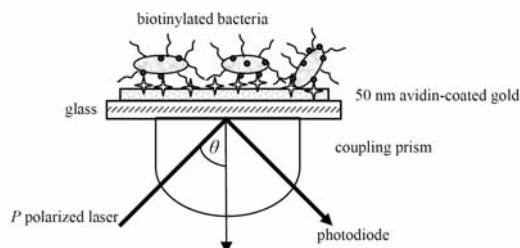between pili mutants of *P. aeruginosa* vs. wildtype in early stage attachment (Jenkins et al., 2005).

Fig. 1. Schematic representation of the SPR setup used in this study (adapted from Jenkins et al., 2005). P polarized light is reflected forming an energy wave at the gold surface. The angle θ of incident light which forms maximum excitation is sensitive to changes in the dielectric properties of the molecules attached to the gold film surface.

The monitoring of faecal pollution in surface waters has become a growing concern in the last century. Every day is more frequent the reutilisation of water worldwide for diverse purposes, and therefore to diminish the risk of pathogens, reasonably good faecal indicators are needed. Traditionally, *Escherichia coli* and/or *Enterococcus* sp have been used as microbial indicators to monitor faecal pollution in waters. However, it has been suggested that these bacterial strains are not good for predicting contamination of faecal-oral transmitted virus. In last decades great advance has been made and bacteriophages have been proposed as indicators of the presence of virus (Traub et al., 1986; Borrego et al., 1987; Lasobras et al.1999; Grabow, 2001; Mocé-Llivina et al., 2005). Moreover, in the last report from the United States Environmental Protection Agency somatic coliphages have been included as faecal indicators of viral origin (USEPA, 2006). Somatic coliphages are virus that infect *E. coli* and are highly related to the faecal contamination because they can only infect faecal bacteria.

Traditional methods to detect bacteriophages include the double layer assay method, which is based on the deposition of a semi-solid agar layer containing the host strain of the bacteriophage to be detected and the sample which is object of study on the top of an agar plate. Enumeration of the lysis zones that are visualized after an appropriate incubation time is related to the number of bacteriophages present in the original sample (Adams, 1959). The standardized method used for the enumeration of somatic coliphages can be reviewed in the ISO 10705 part 2 (Anonymous, 2000, Anonymous, 2001).

In this study, the use of SPR to detect somatic bacteriophages in water samples was analysed. The sensitivity of the method was also investigated with the type phage PhiX174.

2. Materials and methods

2.1. Bacterial strains and culture conditions

The *Escherichia coli* ATCC 700078 also known as WG5 (Grabow and Couborough, 1986) was grown at 37 ºC with constant agitation at 100 rpm in modified Scholten's broth (MSB) supplemented with nalidixic acid (250 µg mL^{-1}) (Anonymous, 2000) to prepare an ON culture. This culture was diluted 1:100 into fresh MSB and incubated again until an OD_{600nm} of 0.3 was reached to proceed with either the enumeration of somatic coliphages or the preparation of stock cultures for bacteria immobilization.

2.2. Bacteriophage enumeration and preparation of stock cultures

Bacteriophage PhiX174 (ATCC 13706-B1) was used as reference bacteriophage for somatic coliphages. Enumeration of this bacteriophage was performed by the double layer agar method (Adams, 1959). Enrichment cultures of this bacteriophage were prepared according to the ISO 10705-2 (Anonymous, 2000). Briefly, 25 mL of an *E. coli* WG5 culture prepared as indicated above was diluted 1:100 in 25 mL of fresh MSB and incubated with a stock of 10^2 plaque forming units (PFU) mL^{-1} for 5 hours at 37 ºC. Then 2.5 mL of chloroform was added and the mixture was placed ON at 4 ºC. The aqueous phase was centrifuged at 3000 *g* for 20 min and the supernatant was stored at 4 ºC. The supernatant was 1:10 serially diluted into Phosphate Buffered Saline (PBS) and enumerated with the double layer method as indicated above before performing the SPR test.

2.3. Preparation of stock cultures of biotinylated bacteria

E. coli WG5 culture prepared as previously described (OD_{600nm}= 0.3) was used to prepare stock cultures to be used for the immobilization of bacteria onto gold-coated-glass disks (Windsor Scientific Ltd, Slough, United Kingdom). Bacteria were immobilized to the gold film through avidin-biotin interactions. Biotinylation of bacteria was performed as follows: 10 mL of *E. coli* culture was centrifuged at 16000 *g* for 5 min and washed 3 times with chilled PBS (pH: 8.0) to remove the culture media and incubated 1 h in ice with 1 mg mL^{-1} of Sulfo-NHS-XX-Biotin (Invitrogen,

Barcelona, Spain). The biotinylated cells were then washed 3 more times with chilled PBS to remove residual biotin. Finally, the cells were recovered and resuspended in PBS with 10 % sterile glycerol and preserved in 200 µL aliquots at -20 ºC until used. Bacterial counts were performed in triplicate by 1:10 serially diluting the aliquot in PBS and incubating the lowest dilutions in MSB agar at 37 ºC for 24 h, giving a final concentration of 8.37($\pm$0.25) log (CFU mL^{-1}).

2.4. Immobilization of biotinylated bacteria onto gold-coated glass disks

Different concentrations of avidin (Sigma Aldrich, Barcelona, Spain) in PBS ranging from 0.01 to 1 mg mL^{-1} were assayed by direct adsorption onto the gold surface of the disk and evaluated by SPR measurements as indicated below. Then biotinylated bacteria were incubated onto the avidin-coated gold film for 1 h at 37 ºC to allow the coupling reaction between avidin and biotin. These results were compared to direct adsorption of non-biotinylated bacteria onto the bare gold surface.

2.5. Assay protocol for SPR measurements

Detection of reference bacteriophage PhiX174 and natural occurring bacteriophages in wastewaters from urban treatment plants was conducted using the two chamber SPR Autolab SPRIT® system (Eco Chemie, Utrecht, Netherlands). The two chambers allowed us to carry out two assays at the same time with what one could be used as negative control to suppress the residual noise generated by injection of buffers and the other one could be loaded with the same sample but containing bacteriophages. Briefly, to begin the measurement the device was allowed to settle down by injecting into the chamber 50 µL of PBS. Then 50 µL of avidin (0.5 mg mL^{-1}) was injected and was allowed to be adsorbed onto the gold film for 10 min. After washing with PBS, 50 µL of biotinylated cells were incubated in the chamber for 1 hour to allow the coupling between biotin from the bacteria and avidin from the gold film. Then a wash step with PBS was performed to remove unadhered bacteria. The environmental samples containing bacteriophages were diluted 1:10 into MSB and 50 µL of the mixture were injected into the chamber to allow the bacteriophages to replicate within their host *E. coli* WG5. The SPR response produced was monitored during at

least 100 minutes taking a measure every 3 seconds. All steps were realised at 37 ºC. The gold disks used for the immobilization were re-used for several times. They were cleaned before performing the experiment with ethanol and distilled water. After drying an ozonisation cycle of 30 minutes was performed and they were washed again with sterile distilled water before their use.

2.6. Electrochemical impedance spectroscopy

In addition, detection of bacterial attachment through electrochemical impedance spectroscopy (EIS) was made to compare the results obtained with the SPR method. This technique has been previously reported to be useful for detection of bacterial adhesion (Muñoz-Berbel et al., 2007). However, the sensitivity of this technique was not high enough to detect a single layer of bacteria, and therefore IES was discarded for this approach.

2.7. Wastewater sample collection and processing

Three samples from different urban wastewater treatment plants were collected (Table 1) and transported to the laboratory according to Standard methods (Eaton et al., 2005). Samples were stored at -70 ºC to avoid inactivation of the bacteriophages (Mendez et al., 2002) until used. Processing of the samples included a centrifugation step of 10 min at 1000 *g* and filtration with sterile 0.22 µm pore filter (Millipore Corporation, Barcelona, Spain). The filtered suspension was used for the enumeration and detection of somatic coliphages with the double layer method and SPR, respectively.

Table 1
Samples analysed in this study

Samples	Origin	Bacteriophage counts log (PFU mL^{-1}) $\pm$ sd
GA2007	Wastewater treatment plant 1	4.90 $\pm$ 0.01
HM2001	Wastewater treatment plant 2	3.81 $\pm$ 0.01
HM1402	Wastewater treatment plant 3	3.84 $\pm$ 0.02
PhiX174 stock	laboratory enrichment	9.79 $\pm$ 0.02

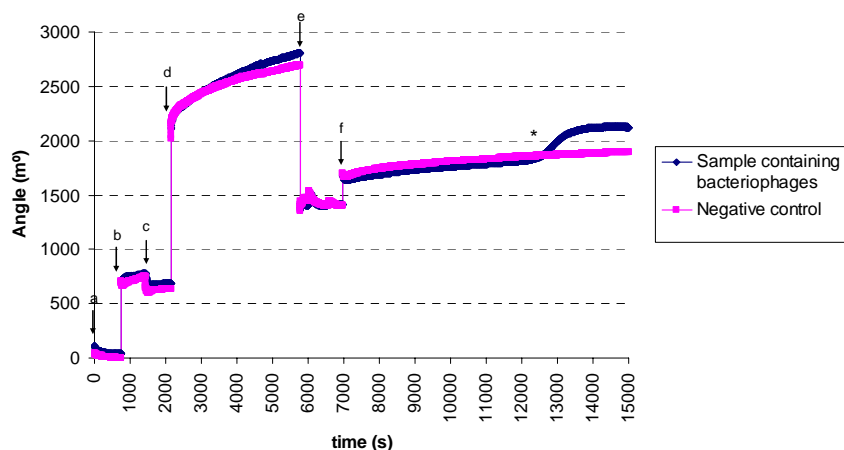PFU, plaque forming units; sd, standard deviation

Fig. 2. Representation of a typical SPR cycle used for the detection of bacteriophage PhiX174 and other somatic coliphages present in the wastewater samples. Arrows indicate the different steps from the cycle that were described in the "materials and methods" section: *a*, initialization of the system by rinsing the gold disk with 50 µL of PBS; *b*, addition of 50 µL of avidin solution (0.5 mg mL^{-1}); *c*, PBS washing; *d*, incubation of the host strain *E. coli* WG5; *e*, PBS washing; *f*, addition of the sample to be analysed in one chamber (and negative control in the other chamber).

3. Results and discussion

3.1 Bacteriophage PhiX174 and wastewater sample coliphages enumeration by the double layer agar method

The bacteriophage PhiX174 stock culture prepared for the calibration of the SPR assay was enumerated by the double layer agar method giving rise to a final bacteriophage concentration of 9.79 log (PFU mL^{-1}) units (Table 1). Additionally, somatic coliphages present in three different raw wastewater samples were also enumerated presenting values among 3.8 and 4.9 log (PFU ml^{-1}) units. These values are consistent with other previous reports of somatic coliphages in wastewater samples of similar characteristics (Mocé-Llivina et al., 2003).

3.2 Optimization of avidin adsorption onto the gold film and bacteria immobilization

Direct adsorption of different concentrations of avidin ranging from 0.001 to 1 mg mL^{-1} were assayed and analysed by SPR. The adsorption of avidin onto the gold film could be followed by an increase of more than 500 mº of the SPR angle (Fig. 2.). The maximal response, as measured by the SPR angle shift after avidin addition, was already reached with a concentration of 0.5 mg avidin mL^{-1}, indicating from this concentration on the gold film was immediately saturated (Fig. 2d).
Functionalisation of the gold disk with avidin allowed adsorption of biotinylated *E. coli* to avidin through avidin-biotin interactions (Fig. 3). Direct adsorption of *E. coli* to avidin has been previously documented (Korpela et al., 1984). However, in this study direct adsorption

of bacteria to avidin-coated-gold disk was not strong enough to carry out the protocol inside the SPR cell and therefore biotinylation of the surface proteins of the bacterial envelope was necessary. The results obtained here suggest that biotinylation of the surface proteins did not alter the functionality of the bacteriophage receptor of the host strain. In relation to this, it has been reported that avidin-biotin immobilisation generally maintains biomolecule activity than other used methods (Da Silva et al., 2004). Moreover, avidin-biotin affinity interaction has been shown to be extremely high with an association constant (K_a) of 10^{15} M^{-1} (Wilchek and Bayer, 1988) and the binding of both molecules can be regarded nearly as a covalent bound.
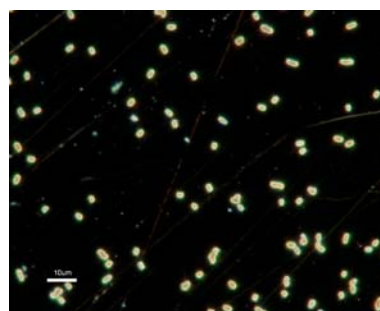

Fig.3. Adsorption of *E. coli*, onto the gold through avidin-biotin interactions. Optical micrograph in dark field, 1000X.

3.3 SPR measurements

The whole process, attachment and lysis of bacteria, was monitored continuously "real-time" giving a curve shape that was repeated in all samples tested that contained bacteriophages showing an increase of the resonance angle of at
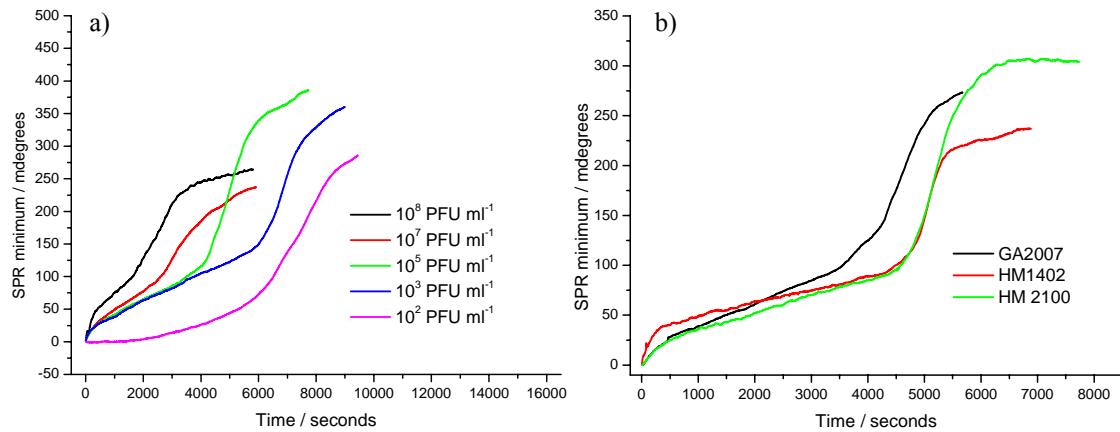
Fig. 4. Variation of the angle of resonance in response time detection to different concentration of bacteriophages: a) detection of bacteriophage PhiX174 as measured by the difference angle among the sample and the control; b) detection of somatic coliphages in wastewater samples.

least 150 mº with respect to the control sample that did not contain bacteriophages (Fig. 2). The time lapse before this increase could be detected varied according to the concentration of bacteriophages present in the sample being longer as the bacteriophage concentration decreased (Fig. 4). As few as 10^2 PFU mL^{-1} in the initial sample could be detected after an incubation time of 120 min. Taking into consideration that a single bacteriophage can give rise to 20-50 new bacteriophages per infected host cell in a lapse time of around 20 min (Kokjohn et al., 1991; Anonymous, 2000), it can be estimated that more than 10^6 bacteriophages can easily be produced in 120 min from a single bacteriophage. The shift in the resonance angle detected is theoretically hypothesized to be caused by the attachment of released phage particles, and bacterial lysates (especially, fragments of the bacterial membranes and intracellular proteins) that might adhere to the gold film. According to this observation, an increase in the resonance angle has been previously reported in a study for determining toxicity in waters by SPR in an *E. coli* assay, in which an increase of 60 mº was observed after exposure to different phenol concentrations due to bacterial membrane damage (Choi et al., 2005). To test this hypothesis phospholipase A (1 µg mL^{-1}) was added to a control sample that did not contain bacteriophages and again an increase in the resonance angle was observed (data not shown).

3.4 Detection of somatic coliphages in wastewater samples

Three samples from different wastewater treatment plants were evaluated for the presence of bacteriophages by both SPR method and the traditional double layer agar method. The curves shape obtained after the addition of the wastewater samples were similar to those of bacteriophage PhiX174. Moreover, the time lapse before the increase of the resonance angle was similar to that one expected according to the calibration of bacteriophage PhiX174 and concentration (PFU mL^{-1}) of bacteriophages in the samples as estimated by the double layer agar method.

As far as we know this is the first attempt to real time monitoring of the presence of somatic coliphages in wastewater samples through SPR measurements. Moreover, the method described here possesses the two characteristics which are desired for the development of an optimal biosensor, which are a high specificity, which relies on the specificity of the host-phage interaction and the high sensitivity of the SPR technique. This new approach can therefore be applied and extended to the development of miniaturized and portable SPR biosensors to detect other bacteriophages of interest in industry, which need to be detected in a short period of time to prevent the lysis of starter cultures, by just adapting the host strain to the bacteriophage to be detected.

4. Conclusions

In this study, we have shown that the presence of bacteriophages in water samples can be real-time monitored by the use of SPR technique using their host bacteria adsorbed to gold films as a bio-recognition element. The detection limit of the method was estimated to be around 10^2 PFU mL^{-1}, requiring a minimum incubation time of 120 min for the detection. All the experiments were performed in a closed, non-flowing system in a semi automated process. However, automation of the whole process could be achieved in most SPR machines. These results are very encouraging for the future development of portable biosensors for bacteriophage and other faecal indicators detection, because it offers the possibility to

make automated and real time measurements in the field.

Acknowledgements

References

Adams, M.H., 1959. Bacteriophages. Interscience Publishers, Inc., New York.

Anonymous, 2000. ISO 10705-2: Water quality. Detection and enumeration of bacteriophages-part 2: Enumeration of somatic coliphages. International Organisation for Standardisation. Geneva, Switzerland.

Anonymous. 2001. Method 1602: Male-specific (F+) and Somatic Coliphage in Water by Single Agar Layer (SAL) Procedure. EPA 821-R-01-029. April 2001. Office of Water. United States Environmental Protection Agency, Washington, DC.

Baac, H., Hajos, J.P., Lee, J., Kim, D., Kim, S.J., Shuler, M.L., 2006. Biotechnol. Bioeng. 94, 815-819.

Boltovets, P.M., Snopok, B.A., Boyko, V.R., Shevchenko, T.P., Dyachenko, N.S., Shirshov, Y.M., 2004. J. Virol. Methods 121, 101-106.

Borrego, J., Moriñigo, M., De Vicente, A., Córnax, R., Romero, P., 1987. Wat. Res. 21, 1473-1480.

Choi, J.W., Park, K.W., Lee, D.B., Lee. W., Lee, W.H., 2005. Biosens. Bioelectron. 20, 2300-2305.

Da Silva S., Grosjean L., Ternan N., Mailley P., Livache T., Cosnier S., 2004. Bioelectrochemistry 63, 297-301

Eaton, A.D., Clesceri, L.S., Rice, E.W., Greenberg, E., 2005. Standard Methods for the Examination of Water & Wastewater. American Public Health Association, American Water Works Association & Water Environment Federation. Washington DC.

Gau, J.J., Lan, E.H., Dunn, B., Ho, C.M., Woo, J.C., 2001. Biosens. Bioelectron. 16, 745-55.

Grabow, W.O.K, Coubrough, P., 1986. Appl. Environ. Microbiol. 52, 430-433.

Grabow, W.O.K., 2001. Water SA. 27, 251-268.

Habauzit, D., Chopineau, J., Roig, B., 2007. Anal. Bioanal. Chem. 387, 1215-1223.

Hoa, X.D., Kirk, A.G., Tabrizian, M. 2007. Biosens. Bioelectron. 23, 151-160.

Jenkins, A.T.A, Buckling, A., McGhee, M., ffrench-Constant, R.H., 2005. J. R. Soc. Interface. 22, 255-259.

Jönsson, U., Fägerstam L, Ivarsson, B., Johnsson, B., Karlsson, R., Lundh, K., Löfas, S., Persson, B., Roos, H., Rönnberg, I., et al., 1991. Biotechniques 11, 620-627.

Kokjohn, T.A., Sayler, G.S., Miller, R.V., 1991. J. Gen. Microbiol. 137, 661–666.

Korpela, J., Salonen, E.M., Kuusela, P., Sarvas, M., Vaheri, A., 1984. FEMS Microbial. Lett. 22, 3-10

Kretschmann, E.Z., 1971. Physics 241, 313–324.

Kurosawa, S., Park, J.W., Aizawa, H., Wakida, S., Tao, H., Ishihara, K., 2006. Biosens. Bioelectron. 22, 473-481.

Lasobras J, Dellunde J, Jofre J, Lucena F., 1999. J. Appl. Microbiol. 86, 723-729.

Mauriz, E., Calle, A., Manclús, J.J., Montoya, A., Lechuga, L.M., 2007. Anal. Bioanal. Chem. 387, 1449-1458.

Mendez, J., Jofre, J., Lucena, F., Contreras, N., Mooijman, K., Araujo, R., 2002. J. Virol. Methods 106, 215–224.

Mocé-Llivina, L., Muniesa M., Pimenta-Vale, H., Lucena, F., Jofre, J., 2003. Appl. Environ. Microbiol. 69, 1452-1456.

Mocé-Llivina, L., Muniesa M., Pimenta-Vale, H., Lucena, F., Jofre, J., 2005. Appl. Environ. Microbiol. 71, 6838-6844.

Muñoz-Berbel, X., Muñoz, F.J., Vigués N., Mas, J., 2006. Sens. Actuators B: Chem. 118, 129-134.

Traub, F., Spillmann, S.K., Wyler, R., 1986. Appl. Environ. Microbiol. 52, 498-503.

U.S.E.P.A., 2006. National Primary Drinking Water Regulations; Ground Water Rule; Final Rule (40 CFR Parts 9, 141, 142). Federal Registration, 71: 65573-65660.

Wilchek, M., Bayer, E.A., 1988. Anal. Biochem. 171, 1-32.

Wittekindt, C., Fleckenstein, B., Wiesmuller, K., Eing, B.R., Kuhn, J.E., 2000. J. Virol. Methods 87, 133-144.

Impedimetric approach for monitoring bacterial cultures based on the changes in the magnitude of the interface capacitance

X. Muñoz-Berbel[1*], N. Vigués[2], R. Escudé[1], J. Mas[2], F. J. Muñoz[1]

[1]*Centro Nacional de Microelectrónica (IMB-CSIC), Campus Univ. Autónoma de Barcelona, Esfera UAB, 08193 Bellaterra, Barcelona, Spain.*
[2]*Grup de Microbiologia Ambiental, Universitat Autònoma de Barcelona, Campus UAB, E-08193 Bellaterra, Spain*

Abstract

This paper describes a new approach for monitoring the concentration of *real* bacterial suspensions from an incubator using impedance spectroscopy and platinum electrodes. The interface capacitance, commonly fitted as a constant phase element, CPE_i, was found sensitive to the suspended concentration after short exposure times. The effect of the metabolites in the CPE_i magnitude was checked. Impedance measurements of *E. coli* cultures showed correlation with classical measurements of bacteria concentration such as plating onto agar, optical density and fluorescence microscopy.

Keywords: platinum electrodes, impedance spectroscopy, bacteria monitoring, metabolites effect.

1. Introduction

Bacteria are small prokaryotic and unicellular microorganisms with a huge variety of resources to adapt to any metabolic restriction and environmental condition. Thus, bacterial species can be found adapted to live elsewhere (air, water or soil) as free cells (planktonic cells) or in communities, such as biofilms (Madigan et al., 1997). The determination of the concentration of planktonic bacteria in liquids is important in different areas (Tang et al., 2006). On the one hand, the monitoring of the concentration of suspended bacteria is especially relevant in the fermentation industries where a strict control of the concentration of cells in the incubator is necessary during the fermentation process. On the other hand, the presence of bacteria, even the non-pathogenic ones, is very restricted in other areas, namely the environmental monitoring, the food and the beverage industries and the clinical chemistry. For instance, the presence of non-pathogenic bacteria is limited to 10^2 CFU mL^{-1} in drinking waters (Lebaron et al., 2005). Thus, these areas require fast and simple detection methods for the continuously quantification of planktonic bacteria in liquids, especially at low concentrations.

Conventional methods for the detection of viable bacteria typically rely on the culture-based assays. With the advent of modern molecular biological techniques, many new approaches have been investigated for this purpose, such as bioluminescent assays (Lee et al., 2004), Fluorescent In Situ Hybridization (FISH) (Garcia-Armisen et al., 2004), optical tweezers (Ericsson et al., 2000), nucleic acid amplification method (Polymerase Chain Reaction, PCR) (Tims et al., 2003), Reverse Transcription-Polymerase Chain Reaction (RT-PCR) (Bleve et al., 2003; del Mar Lleo et al., 2000) and Nucleic Acid Sequence-Based Amplification (NASBA) (Simpkins et al., 2000). Although these methods can offer high sensitivity, they are either time-consuming or relying on laboratory facilities, which limit their application for rapid operation and on-site analysis. In recent years a number of new methodologies have been applied to the detection of planktonic bacteria. These include Voltamperometry (Tang et al., 2006), Micromechanical Oscillators (Gfeller et al., 2005) and Quartz Crystal Microbalances (QCMs). These methods showed good sensitivities (around 10^2-10^3 CFU mL^{-1}) with short measurement times (between some minutes to hours depending on the method). However, their main drawback can be found by considering the complexity of the assay, which frequently requires the manipulation of fragile or biologically delicate materials.

This article describes a simple and fast impedimetric approach for monitoring *real* bacteria samples from an incubator, based on the changes produced in the electrode-solution interface by the early bacteria attachment on platinum electrodes. Previous works showed that bacterial attachment to platinum electrodes could be used for suspended bacteria quantification (Munoz-Berbel et al., Accepted; Muñoz-Berbel et al., 2007). In this paper, the influence of the cells and the metabolites in the impedimetric measurement is also investigated.
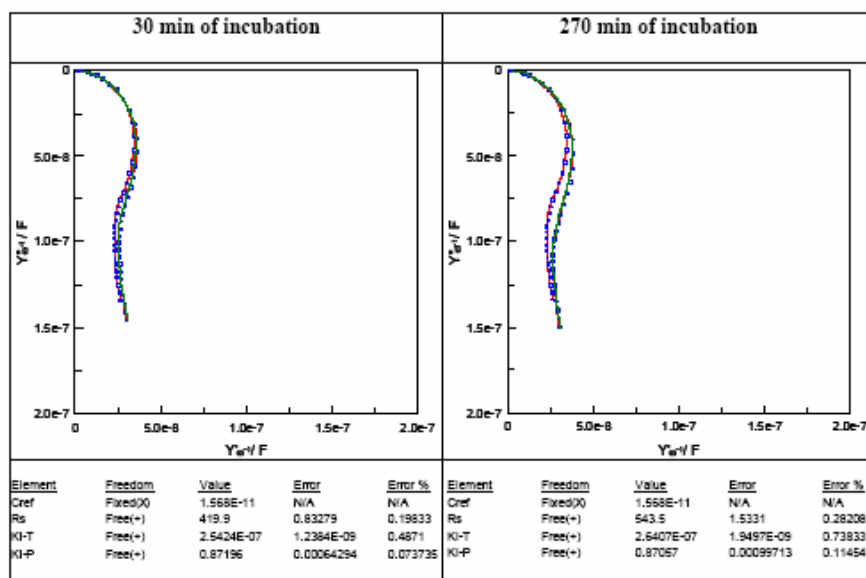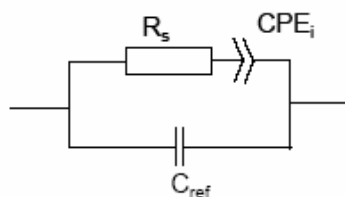
Fig. 1. Admittance complex plane plot for bacterial suspensions extracted from the incubator 30 and 270 minutes after the inoculation of the bacterial starter suspension. Impedance data were fitted using the equivalent circuit shown inset. The experimental impedance spectra (points in the plot), the ideal impedance spectra from the fitting (line in the plot) are shown. Also the spectra corresponding to the culture medium without bacteria is added in each plot as control (red line). Below, the calculated values and errors of each element from the fitting are shown.

30 min of incubation

Element	Freedom	Value	Error	Error %
Cref	Fixed(X0)	1.568E-11	N/A	N/A
Rs	Free(+)	419.9	0.83279	0.19833
KI-T	Free(+)	2.5424E-07	1.2384E-09	0.4871
KI-P	Free(+)	0.87196	0.00064294	0.073735

270 min of incubation

Element	Freedom	Value	Error	Error %
Cref	Fixed(X0)	1.568E-11	N/A	N/A
Rs	Free(+)	543.5	1.5331	0.28208
KI-T	Free(+)	2.6407E-07	1.9497E-09	0.73833
KI-P	Free(+)	0.87057	0.00099713	0.11454

2. Materials and methods

2.1 Electrochemical cell

The measurement systems comprised the working electrode / counter electrode (WE / CE) chip and an external Ag|AgCl reference electrode, 5240 (Crison, Barcelona, Spain) both introduced in a 10 mL electrochemical cell. The WE / CE production was carried out in-house at the IMB-CSIC Barcelona (Alonso Lomillo et al., 2005) where a platinum disc working electrode with an area of 0.5 mm^2 surrounded by a platinum counter electrode of 1.4 mm^2 were integrated on a silicon nitride substrate of 9 mm^2 (3 mm length per 3 mm width). The electrodes were 0.08 mm apart, ensuring near-homogeneous polarization of the working electrode (Harrar et al., 1966).

2.2 Microbiological preparation

Escherichia coli (CGSC 5073 K12) was grown overnight at 37 ℃ in Minimal Medium AB (MMAB) containing glucose (Balestrino et al., 2005). The bacterial concentration was measured using plating in LB medium containing 1.5 % agar, with stock concentration at around 10^9 colony forming units per mL (CFU mL^{-1}). The suspension was then serially diluted down to 10^6 CFU mL^{-1} in decade steps. For the monitoring of the bacterial growth, 1 mL of either the 10^8 CFU mL^{-1} or the 10^6 CFU mL^{-1} suspensions were sterilely inoculated into a 1.5 L water-jacketed glass reactor to achieve an initial concentration inside of 10^5 or 10^3 CFU mL^{-1}, respectively. During the growth, the incubator was thermostatically kept at 37 ℃ with constant agitation, *MR 2000* (Heidolph, Germany), and aeration, *BioFlo* (New Brunswick Scientific, New Jersey, USA). Under these conditions, *E. coli* grew aerobically with a duplication time experimentally found to be close to 40 minutes (data not shown). After the inoculation, no nutrients were added into the reactor (batch process). All of the manipulations were performed under sterile conditions.

Using the aseptic acquisition system, aliquots of 20 mL were sterilely extracted from the incubator in periodic intervals of 30 minutes and directly measured using impedance spectroscopy, optical density and fluorescence microscopy. After 20 minutes of centrifugation at 4388 g, Sigma 4-10 centrifuge (Sigma,

Switzerland), the metabolites (supernatant) and the suspended cells (pelled cleaned and resuspended in sterile MMAB) were also measured in separate using impedance spectroscopy. Biological samples were stored in the fridge at 4 °C to slow growth until measurement.

2.3 Impedance Measurements

The impedance analyser Solartron SI 1260A (Solartron Analytical, Hampshire, UK) was coupled to a potientiostatic interface Solartron 1287. Impedance spectroscopy spectra were recorded using the *Z-Plot* software (Scribner Associates Inc., North Carolina, US). A 25 mV AC potential was applied at the cell open circuit potential (+0.26 ± 0.05 V vs. Ag|AgCl) over a frequency range between 100 kHz and 10 Hz. All measurements given in this work are in relation to the Ag|AgCl reference electrode. Bacterial suspensions were introduced to the electrochemical cell which was thermostatically kept at 4 ℃. Impedance measurements were made after 50 seconds of exposure for direct (non-centrifuged samples), metabolites or suspended cells samples. After the measurement, the electrochemical cell, including electrodes, was sterilized with 96% v/v ethanol (Panreac, Spain).

2.4 Optical density measurements

The magnitude of the optical density at 550 nm was used to follow the bacterial concentration of the culture. Optical density measurements were made with the spectrophotometer Ultrospec 1100 pro (Biochrom, Cambridge, UK). Optical density values were interpolated in a calibration curve previously obtained for E. coli growing under the same experimental conditions, which was used as a calibration curve (data not shown).

2.5 Fluorescence microscopy measurements

The bacteria concentration in the incubator was monitored with time using fluorescence microscopy for correlation with impedance measurements. The cells of each aliquot were fixed with formaldehyde (CH_2O, Sigma) and retained in 2 μm pore size GTBP filters (Millipore, Billerica, Massachusets, USA). Bacteria were stained with 20 μg mL^{-1} 4'-6-diamidino-2-phenylindole (DAPI) (Merk, Germany) for 5 minutes and then rinsed in phosphate buffer saline (PBS) immediately prior to imaging. An Olympus BH Fluorescence Microscope (Olympus, California, USA) was used.

3. Results and discussion

3.1 Fitting and interpretation of impedance spectra

Impedance spectra were fitted using the *Z-View* software to the equivalent circuit shown in Figure 1. This circuit was composed of the solution resistance (R_S), the interface capacitance, which was modelled with a Constant Phase Element to improve the fitting, CPE_i, and an extra capacitance of small magnitude (experimentally found to be of some nF) associated with the presence of an external reference electrode, C_{ref}, which was not sensitive to the bacteria concentration. In all cases, errors never exceeded the 5 %. The use of the CPE_i instead of a conventional double layer capacitance was discussed in previous works (Muñoz-Berbel et al., 2007). The reason of this change is currently under study but the roughness of the electrode appears to play a relevant role on it.

Figure 1 shows impedance measurements for bacterial suspensions extracted from the incubator 30 and 270 minutes after the inoculation of the stock bacterial suspension used as starter. Regarding the fitting, the magnitude of the CPE_i (K_i-T in the figure) was found to change with time as a consequence of bacterial growth in the incubator.

3.2 Monitoring of the concentration of real bacterial samples extracted from an incubator using impedance spectroscopy: evaluation of the influence of the cells and metabolites in the impedance magnitude

Impedance measurements were made and fitted as previously shown. The most relevant results are shown in Figure 2. It has to be noted that, after the fitting, the measured CPE magnitude (K_i) was normalized using Eq. 1. $K_i(it)$ is the value of CPE at any incubation time and $K_i(m)$ is the value of CPE of the culture medium in absence of bacteria:

$$\Delta K_i = \frac{K_i(it) - K_i(m)}{K_i(m)} \cdot 100 \qquad (1)$$

A constant R_S value was obtained with time for total samples (samples containing both suspended cells and metabolites), cells samples (samples containing re-suspended cells) and metabolites samples (samples mainly containing metabolites) with a magnitude of 445 ± 19 Ω. Sample conductivity was measured separately with a conductance meter and found to be sample invariant, which confirmed that, under

3

the experimental conditions previously exposed, the conductivity of the medium did not vary with the *E. coli* growth (or with the metabolites production).

However, the K_i changed with time by total and cells samples, although the correlation with time, and thus with bacteria growth, was found to be better by total than cells samples, probably because of the centrifugation step. The increase in CPE coincided with that reported in previous works (Munoz-Berbel et al., Accepted; Muñoz-Berbel et al., 2007). In those cases, the attachment of bacteria, considered to be behaving as simple charged colloidal particles, during the very early attachment was thought to modify the structure of the double layer at the electrode interface. Particularly, bacteria attachment to the electrode surface may decrease the Debye length at the electrode double layer, causing the initial increase in CPE. In the case of metabolites samples, the random oscillation of the K_i was caused by the presence of bacteria since the variation disappeared after filtration in 2 μm pore size GTBP filters. Thus, the metabolites produced by *E. coli* during bacteria growth, under the experimental conditions here exposed, did not modify the CPE_i either.
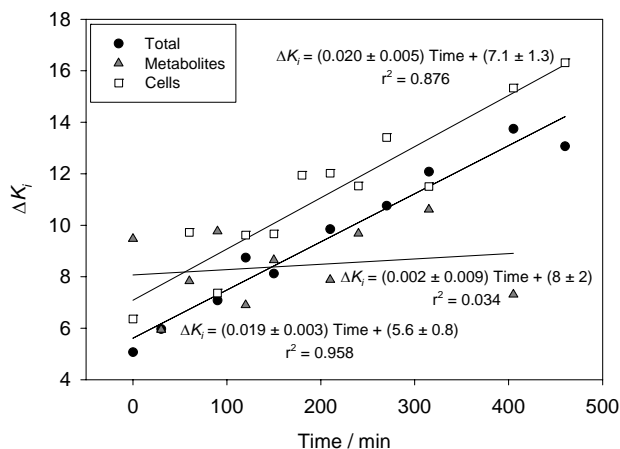

Fig. 2. Representation of the normalized K_i versus the incubation time for total samples containing both cells and metabolites (total samples), samples containing only metabolites (metabolites samples) and samples containing only cells (cells samples).

Using the calibration curve shown in Figure 3, impedance data from total and cells samples were converted into concentration values. It has to be emphasized that both experiments (calibration curves and impedance data from total and cell samples) were comparable since both of them were made using the same bacteria, culture medium, equipment, experimental conditions and identical platinum electrodes.
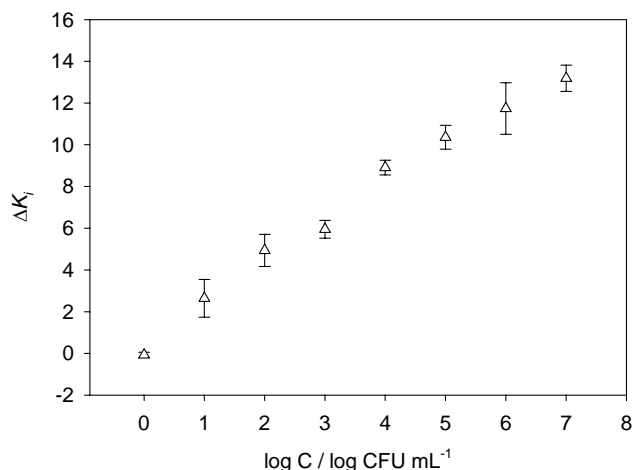

Fig. 3. Representation of the normalized K_i versus the logarithm of the suspended concentration of bacteria. This calibration curve was used for converting capacitance values into bacteria concentrations.

The global behaviour of the new impedimetric approach in the determination of bacteria concentration for total and cells samples was evaluated by plotting the predicted values (from impedance spectroscopy) against the expected ones (from plating on agar) (Figure 4). A good method should display comparative lines with high correlation and a slope equal to one with zero intercept. As illustrated in Figure 4, in both cases impedance spectroscopy measurements showed good correlation with comparison lines practically indistinguishable from the theoretical values. However, better results were obtained in the case of total samples directly extracted from the incubator. This fact was probed to be caused by the centrifugation process since, as previously shown, part of the cells remained in the supernatant after the centrifugation. Thus, the number of bacteria in both cells and total samples may not always be the same, which introduced a new variability factor in the EIS measurement.

Finally, the Student's *t*-test for paired samples was used for checking whether there were significant differences between the obtained and the expected values, significance being set at 95 %. The tabulated values of the *t* (t_{tab}), 2.26 and 2.20 for total and cells samples respectively, were always found to be bigger than the calculated ones (0.21 and 0.85 for total and cells samples, respectively). Thus, no significant differences between the predicted and the expected values were obtained. Again, better results were achieved when using total samples directly extracted from the incubator.
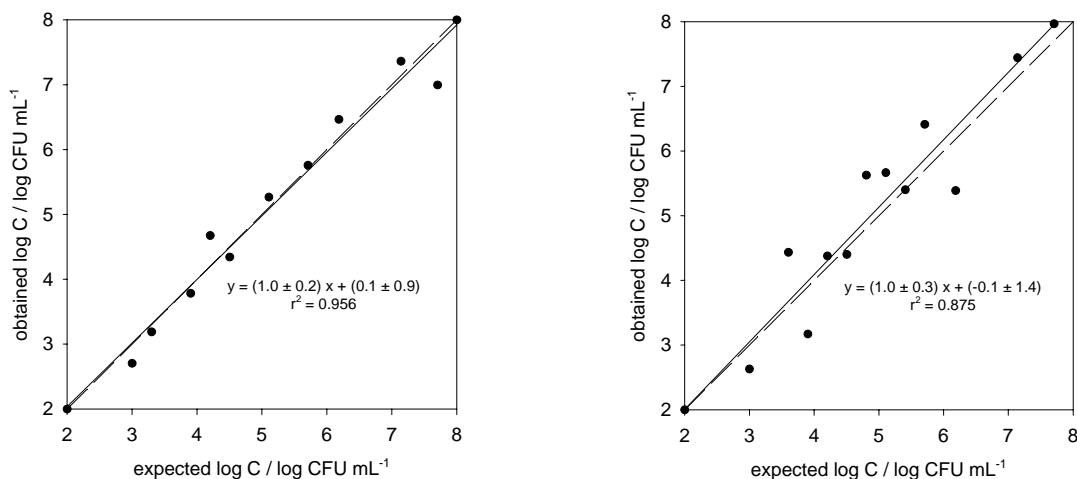
4

Fig. 4. Representation of the predicted bacteria concentration magnitude (obtained from total and cells samples respectively after measuring using impedance spectroscopy) against the expected ones (from plating on agar). The dotted line represents the theoretical comparison line y = x.

3.3. Comparison of the impedimetric approach with classical optical density measurements and epifluorescence microscopy counting

Bacteria concentration values from impedance spectroscopy were compared with those obtained from optical density and epifluorescence microscopy measurements. Impedance, optical density and epifluorescence microscopy measurements were made as described above. Suspended concentration values from impedance spectrosocpy data were obtained by interpolating in the calibration curve shown in Figure 3, as previously detailed. The suspended concentration from optical density was also found after interpolation in the calibration curve (data not shown).
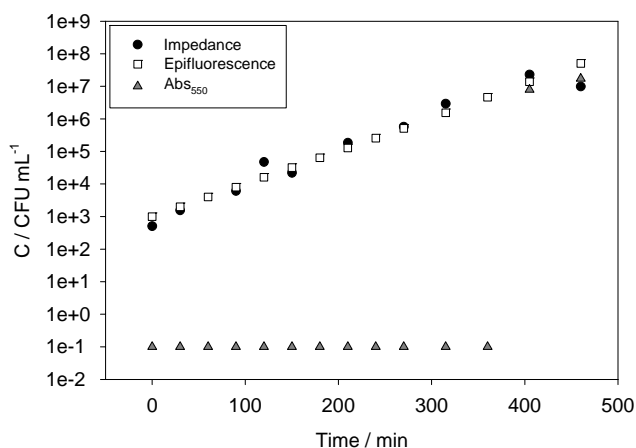

Fig. 5. Representation of the variation of the concentration values from impedance spectroscopy, epifluorescence microscopy and optical density measurements with the incubation time.

Figure 5 illustrates the comparison between techniques. The experimental data showed that the concentration values from epifluorescence microscopy and impedance spectroscopy

measurements were practically identical in the range of concentrations under study (which coincided with the linear response range for the impedimetric approach). However, the optical density was only found to be sensitive to the suspended concentration when exceeding 5 x 10^6 CFU mL^{-1}, at least three orders of magnitude more than the other techniques.

4. Conclusions

In this paper, impedance spectroscopy measurements have been used for monitoring the concentration of *real* bacteria samples directly extracted from an incubator. The interface capacitance has been found to be insensitive to the presence of metabolites and only depended on bacteria concentration. After interpolation of this parameter in a calibration curve, concentration values from impedance data have shown good correlation with classical methods, namely plating on agar and epifluorescence microscopy counting. The concentration values from impedance spectroscopy have also been found to be comparable with those obtained using optical density but with an improvement of at least three magnitude orders in the limit of detection.

References

Alonso Lomillo, M.A., Ruiz, J.G., Pascual, F.J.M., 2005. Analytica Chimica Acta 547(2), 209-214.

Balestrino, D., Haagensen, J.A.J., Rich, C., Forestier, C., 2005. Journal of Bacteriology 187(8), 2870-2880.

Bleve, G., Rizzotti, L., Dellaglio, F., Torriani, S., 2003. Appl. Environ. Microbiol. 69(7), 4116-4122.

Del Mar Lleo, M., Pierobon, S., Tafi, M.C., Signoretto, C., Canepari, P., 2000. Appl. Environ. Microbiol. 66(10), 4564-4567.

Ericsson, M., Hanstorp, D., Hagberg, P., Enger, J., Nystrom, T., 2000. J. Bacteriol. 182(19), 5551-5555.

Garcia-Armisen, T., Servais, P., 2004. Journal of Microbiological Methods 58(2), 269-279.

Gfeller, K.Y., Nugaeva, N., Hegner, M., 2005. Biosensors and Bioelectronics 21(3), 528-533.

Harrar, J.E., Shain, I., 1966. Analytical Chemistry 38(9), 1148-1158.

Lebaron, P., Henry, A., Lepeuple, A.S., Pena, G., Servais, P., 2005. Marine Pollution Bulletin 50(6), 652-659.

Lee, J., Deininger, R.A., 2004. Luminescence 19(4), 209-211.

Madigan, M.T., Martinko, J.M., Parker, J., 1997. Brock Biology of Microorganisms, Prentice Hall International, Hertfordshire, U.K.

Munoz-Berbel, X., Vigués, N., Jenkins, A.T.A., Mas, J., Munoz, F.J., Accepted. Biosensors and Bioelectronics.

Muñoz-Berbel, X., Vigués, N., Mas, J., Jenkins, A.T.A., Muñoz, F.J., 2007. Electrochemistry Communications 9(11), 2654-2660.

Simpkins, S.A., Chan, A.B., Hays, J., Opping, B.P., Cook, N., 2000. Letters in Applied Microbiology 30(1), 75-79.

Tang, H., Zhang, W., Geng, P., Wang, Q., Jin, L., Wu, Z., Lou, M., 2006. Analytica Chimica Acta 562(2), 190-196.

Tims, T.B., Lim, D.V., 2003. Journal of Microbiological Methods 55(1), 141-147.

Real time automatic system for the impedimetric monitoring of bacterial growth

Roger Escudé-Pujol[1], X. Muñoz-Berbel[1*], N. Vigués[2], J. Mas[2], F. J. Muñoz[1]

[1]*Centro Nacional de Microelectrónica (IMB-CSIC), Campus Univ. Autónoma de Barcelona, Esfera UAB, 08193 Bellaterra, Barcelona, Spain.*
[2]*Grup de Microbiologia Ambiental, Universitat Autònoma de Barcelona, Campus UAB, E-08193 Bellaterra, Spain*

Abstract

This note describes the design and construction of new Virtual Instrumentation implemented in LabView 7.1 for the real time monitoring of the bacteria concentration of *Escherichia coli* cultures using impedance spectroscopy and platinum electrodes. A home-made Sequential Injection Analysis (SIA) system was used both for the transport of microbiological samples from the incubator to the electrochemical cell, where they were measured, and for the elimination of residues from the cell to a wasting recipient.

Keywords: Impedance measurements, bacteria concentration, platinum electrodes, Sequential Injection Analysis, Virtual Instrument.

---

1. Introduction

The use of flow analysis methods in the field of chemical analysis started in the middle of the last century for mechanizing the collection of eluted fractions and the sampling step in industrial on-line processes (Trojanowick, 2000). At the end of the fifties, this objective was enlarged and the automation of all the steps of the analytical methodology was attempted by incorporating flow detectors in the system. In 1957, Skeegs developed the first practical application of flow measurements: the Segmented Flow Analysis (SFA). This approach, quickly accepted to perform clinical, environmental, agricultural and industrial analysis, used a fluid stream segmentation technique with air segments. In 1975, Ruzicka and Hansen developed a new flow analysis technique based on instant discrete sampling by injection into a carrier stream to the flow detector (Ruzicka et al., 1975). This approach, called Flow Injection Analysis (FIA) system, allowed continuous flow analysis to be performed in a fast, much simplified and robust way. The main drawback of this system was the high reagent and sample consumption (due to the continuous flow). In order to solve this problem, several methodologies have been established such as the fabrication of μFIA (Rainelli et al., 2003) or the immobilization of reagents or enzymes in adequate supports (Hansen, 1989). Although these variants solved several aspects, they caused the appearance of new inconveniences.

In 1990, Ruzicka and Marshal proposed a new approach: the Sequential Injection Analysis (SIA) (Ruzicka et al., 1990). This system did not use a continuous flow but a single-channel high precision bi-directional pump which could stop and revert the flow automatically (Estela et al., 2005). The main advantages of the SIA system were the robustness, flexibility and the important saving on the consumption of reagents and samples, whereas the low analysis rate was its main disadvantage. SIA systems, always under the control of a Personal Computer (PC), can automate a huge variety of sample manipulation sequences without changing the physical characteristics or the configuration of the system (Christian, 1994). The versatility of the system is basically provided by the multi-port Modular Valve Position (MVP). The MVP allows the access to different ports, containing samples, reagents, standards, cleaning solutions and the detector. The combination of items can be easily adapted to comply with the requirement of any specific analysis, which shows the vast potentiality of the SIA system in the on-line measurements (van Staden, 2002).

Previous works showed that bacteria attachment to the electrode surface could be used for bacterial quantification using impedance spectroscopy (Munoz-Berbel et al., Accepted; Muñoz-Berbel et al., 2007). In this article, the combination of the impedimetric approach and a flow system inspired in a SIA system have been applied to the real-time and automatic monitoring of bacterial growth. This combination required the development of new Virtual Instrumentation which is detailed in this article.
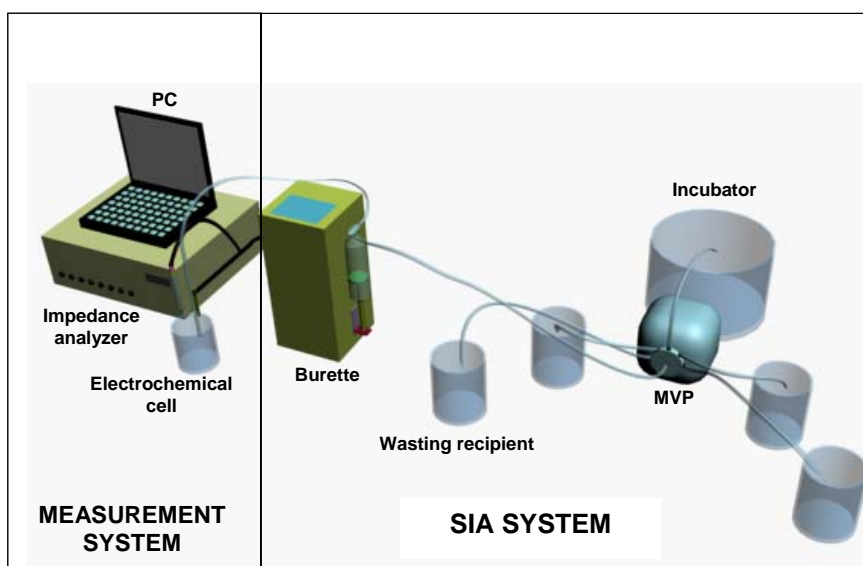
Figure 1. Scheme of the sequential injection analysis (SIA) system, composed of a PC controlled Burette 1S containing a 10 mL syringe and an 8-way multi-port modular valve position (MVP), and the measurement systems composed of the electrochemical cell and the impedance analyzer. All of them were governed by a Virtual Instrument implemented in LabView and installed in the PC.

2. Material and Methods

2.1 Electrochemical cell

A platinum disc working electrode with an area of 0.5 mm^2 surrounded by a platinum counter electrode of 1.4 mm^2 were integrated on a silicon nitride substrate of 9 mm^2 (3 mm length per 3 mm width). Electrode production was carried out in-house at the IMB-CSIC Barcelona (Alonso Lomillo et al., 2005). The electrodes were 0.08 mm apart, ensuring near-homogeneous polarization of the working electrode (Harrar et al., 1966). These working electrode / counter electrode (WE / CE) chips were introduced in a 5 mL electrochemical cell together with an external Ag|AgCl reference electrode, 5240 (Crison, Barcelona, Spain).

2.2 Microbiological preparations

Escherichia coli (CGSC 5073 K12) was grown at 37 ºC in Minimal Medium AB (MMAB) (Balestrino et al., 2005) containing glucose. The bacterial concentration was measured using plating in LB medium containing 1.5 % agar, with stock concentration at around 10^9 colony forming units per mL (CFU mL^{-1}). The suspension was then serially diluted down to 10^4 CFU mL^{-1} in decade steps. The 10^4 CFU mL^{-1} sample was used as stock for the checking of the electrodes (see section 2.7.1). For the real time monitoring of the bacterial growth, 1 mL of the 10^7 CFU mL^{-1} suspension were inoculated into a 1.5 L water-jacketed glass reactor which was thermostatically kept at 37 ºC, with constant agitation, *MR 2000* (Heidolph, Germany), and

aeration, *BioFlo* (New Brunswick Scientific, New Jersey, USA). Under these conditions, *E. coli* grew aerobically with a duplication time experimentally found to be of 40 minutes (data not shown). After the inoculation, no nutrients were added into the reactor (batch process). Before inoculation, biological samples were stored in the fridge at 4 °C to slow growth. All of the manipulations were performed under sterile conditions.

2.3 Instrumentation

Fig. 1 schematizes the SIA system and the measurement systems where impedance spectroscopy was measured using an AUTOLAB PGSTAT 12 (EcoChemie, BV, The Netherlands) containing a FRA-2 module. The SIA system was composed of a PC controlled Burette 1S (Crison Instruments, Spain) containing a 10 mL syringe and an 8-way multi-port modular valve position (MVP) (Hamilton, Switzerland). The multi-port valve allows the access to 8 different ports (solutions), namely the incubator (port 1), the MMAB without bacteria (port 2), the stock bacterial suspension, 10^4 CFU mL^{-1} (port 3), distilled water (port 4 and 5), 96% ethanol (Panreac, Barcelona, Spain) (port 6), air (port 7) and the wasting recipient (port 8). The bidirectional burette assures the accuracy in the management of liquids either to the electrochemical cell or to the wasting recipient to be removed. Solutions were transported through polytetrafluoro-ethylene (PTFE) tubes (Hamilton, Switzerland) with an internal diameter of 0.5 mm.
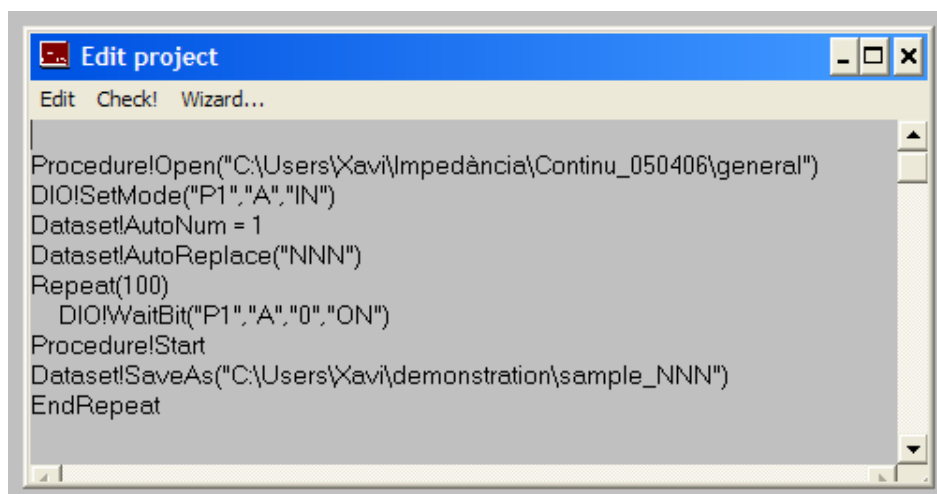
Figure 2. Representation of the compendium of commands composing the *Project* application of the FRA-2 software for the synchronization of the SIA and the measurement systems via trigger signals. The command *DIO!WaitBit* remained the FRA-2 module of the AUTOLAB in standby mode until receiving a trigger signal from DAQ card to the port 1.

2.4 Impedance measurements

A 25 mV AC potential was applied at the cell open circuit potential (+0.26 ± 0.05 V vs. Ag|AgCl) over a frequency range between 100 kHz and 10 Hz. Impedance spectroscopy spectra were recorded using the FRA-2 software (Eco Chemie, The Netherlands).

2.5 Control and acquisition system

The DAQPad-6052E (National Instruments, Texas, U.S.) interface card was used in this application coupled with a 68 pin connector module SCB-68 (National Instruments, Texas, U.S.). The DAQ card, featuring 16 single-ended analogue inputs (ADC) and 2 analogue outputs (DAC) with 16 bits of resolution to 333KS/s, 8 digital input/output (TTL/CMOS) and computer communication by FireWire (IEEE 1394), was interfaced to a 1.4GHz Pentium III Portable Computer (PC) running LabView ver.7.1. under Windows XP. The DAQ card was integrated in the LabView environment by specific drivers. The PC sent orders to the microburette using the RS-232 serial protocol via the COM1 port. On the other hand, the MVP received TTL signals from the DAQ to select a specific input.

The SIA and the measurement systems were synchronized using the *Project* application of the FRA-2 software via trigger signals. Fig. 2 shows the application used in this work. This application remained the impedance analyzer in standby mode until receiving a trigger signal from DAQ card which was sent 15 seconds after the complete inoculation of the bacterial suspension to the electrochemical cell.

2.6 Software structure and hierarchy
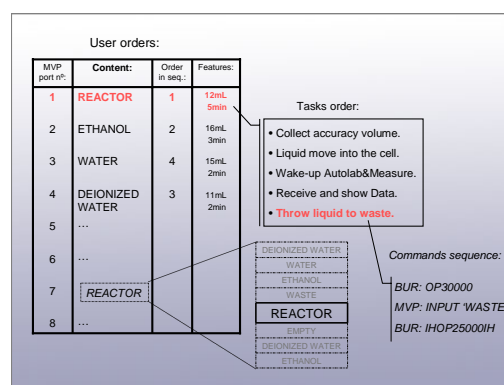
Figure 3. Illustration of the three levels of hierarchy of the LabView application during the sequence of experiments.

The Virtual Instrument application used in this work controlled the SIA System (DAQ, MVP, Burette and Autolab) and directly displayed the bacteria concentration values. The LabView applications could be understood to be organized in three levels of hierarchy (Fig. 3). In the first level, the experiment was defined as a sequence of orders that the user declared as parameters using the interactive front panel shown in Fig. 4. For each input of the MVP, the content, the inoculated volume, the time remaining in the electrochemical cell and the position in the measurement sequence could be chosen. The time between sequences and the number of sequences could also be defined by the user. In the second level, each order previously declared was converted into a compendium of tasks involving a specific response of the burette and/ or the MVP. Finally, in the third level, the sequence of

commands describing a particular task was executed. Commands are particular programming codes designed to change the status of specific devices, basically the burette or the MVP.
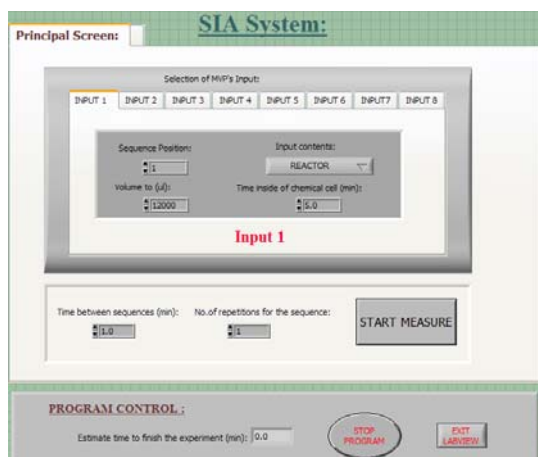
Figure 4. Image of the front panel of the application containing the parameters declared by the experimental protocol in use.

2.7 Sampling and cleaning processes

Tubes and mobile parts in contact with the microbiological samples were autoclaved. During the sampling, 2 mL aliquots were transported in regular intervals of 30 minutes from the incubator (port 1) to the electrochemical cell, where it was impedimetrically measured, using the burette as a pump. 1.5 minutes after the complete inoculation of the suspension, the aliquot was extracted and removed to the wasting recipient (port 8). The cleaning process was composed of three steps. In the first stage, the electrochemical cell was cleaned with 3 mL of 96 % ethanol (port 6) for 3 minutes under constant agitation to sterilize the electrochemical cell. After sterilization, the cell was cleaned twice with 3 mL of distilled water (port 4 and 5) for 8 and 15 minutes respectively. This process ensures the practically complete elimination of alcoholic traces from the electrochemical cell.

2.7.1 Checking of the WE / CE chips

The checking of the electrode in use was absolutely necessary to keep the real-time system in good working order. With time, the *real* bacteria concentration in the incubator may differ from that value obtained from EIS data as a consequence of the aging of the sensor (Munoz-Berbel et al., Accepted). For this reason, at the beginning and sometimes in the middle of a sequence of experiments, the magnitude of the interface Constant Phase

element (CPE$_i$) of the electrode in use was adjusted to ensure the correct correlation of EIS data with the *real* concentration values. The checking process consisted in adjusting the calibration curve to the capacitance values given by the electrode.

Experimentally, 2 mL of culture medium without bacteria (port 2) were inoculated and measured in the electrochemical cell. After the cleaning process previously described, a stock suspension of 10^4 CFU mL^{-1} (port 3) was measured following the same experimental conditions and the normalized value for the 10^4 CFU mL^{-1} sample, called $\Delta K_i(4)$, was next calculated. This value was compared with that introduced in the calibration curve and the curve was shifted and thus adjusted to the electrode in use.

It has to be noted that this adjusting process could be made since, regarding previous works (Munoz-Berbel et al., Accepted), the sensitivity of the electrode (slope of the calibration curve) remained invariant despite of the aging of the sensor.

2.8 Fluorescence microscopy

The bacteria concentration in the incubator was monitored with time using fluorescence microscopy for correlation with impedance measurements. The cells of each aliquot were fixed with formaldehyde (CH$_2$O, Sigma) and retained in 2 μm pore size GTBP filters (Millipore, Billerica, Massachusets, USA). Bacteria were stained with 20 μg mL^{-1} 4'-6-diamidino-2-phenylindole (DAPI) (Merk, Germany) for 5 minutes and then rinsed in phosphate buffer saline (PBS) immediately prior to imaging. An Olympus BH Fluorescence Microscope (Olympus, California, USA) was used.

3. Results and discussion

3.1 Fitting and interpretation of impedance data

Z-View software was used to fit EIS data to the equivalent circuit shown in Fig. 5, containing the resistance of the solution (R_S), the interface capacitance modelled as a Constant Phase Element (CPE$_i$) and an extra capacitance associated to the reference electrode (C_{ref}) which did not change with bacteria concentration. The CPE magnitude (K_i) from the fitting was normalized using Eq. 1. $K_i(t)$ is the value of CPE at any time and $K_i(m)$ is the value of CPE of the culture medium in absence of bacteria:

$$\Delta K_i(t) = \frac{K_i(t) - K_i(m)}{K_i(m)} \cdot 100$$

$$(1)$$

The obtained $\Delta K_i(t)$ was finally interpolated in the calibration curve shown in Fig. 5. It has to be noted that both experiments (calibration curves and bacteria growth) were comparable since both of them were made using the same bacteria, culture medium, equipment, experimental conditions and identical platinum electrodes.
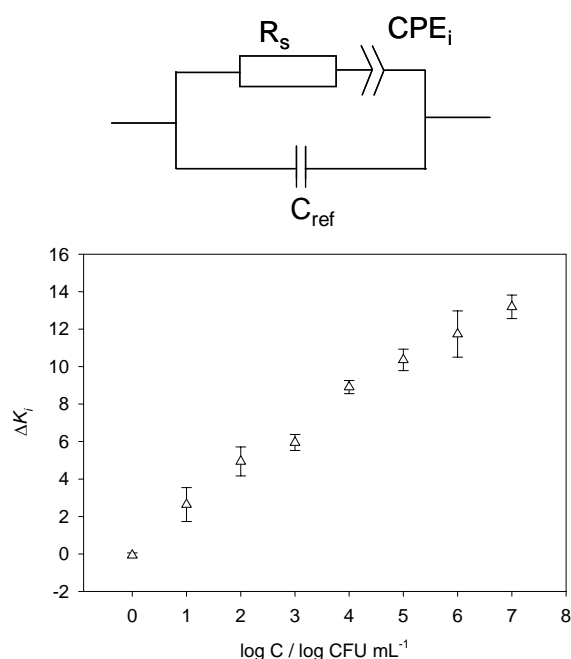

Figure 5. Equivalent circuit used for the fitting of the EIS data, which contains the capacitance associated to the reference electrode (C_{ref}), the solution resistance (R_S) and the CPE_i. Also the representation of the ΔKi with the suspended concentration of bacteria is shown. This calibration curve was used for converting capacitance values into bacteria concentrations.

3.2 Comparison of bacteria concentration values obtained from impedance and epifluorescence microscopy measurements

E. coli was grown under the experimental conditions exposed in section 2.2. The monitoring of the bacteria growth followed the experimental protocol detailed in section 2.7. Impedance and fluorescence microscopy measurements were made as described in sections 2.4 and 2.8, respectively. The front panel shows the sequence of the experimental protocol in use. The declared parameters could be changed by the user even when the experiment was running. However, these

changes were not active in the experiment that was currently running but in next cycles.
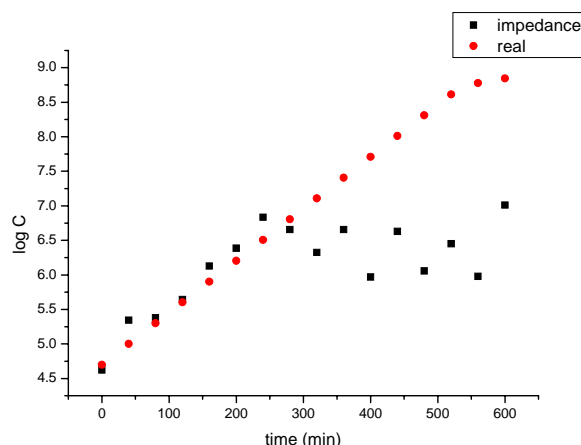
Figure 6. Representation of the bacterial growth curve obtained using impedance spectroscopy and fluorescence microscopy by *E. coli* aerobically growing at 37ºC with constant agitation.

In Fig. 6, the bacteria concentration displayed by the real-time impedimetric system was compared with the *real* concentration of the culture obtained with time using fluorescence microscopy. The concentration values recorded by both strategies were found practically identical until 10^7 CFU mL^{-1}.

4. Conclusions

We have developed new Virtual Instrumentation (VI) implemented in LabView environment for the real-time and automatic monitoring of bacterial growth using impedance spectroscopy and a Sequential Injection Analysis (SIA) system for the transport of samples, reagents and residues. The VI synchronized the SIA and the measurement system. In the front panel this application displayed the value of the bacteria concentration with time, after adjusting the calibration curve previously introduced in the software to the platinum electrode in use. The concentration values from impedance spectroscopy measurements showed concordance with those obtained using fluorescence microscopy until 10^7 CFU mL^{-1}.

5. Future work

Future work includes the substitution of the commercial impedance analyzer for a home-made impedance equipment of similar features but smaller in size. This new equipment favored the integration of the measurement and the SIA systems in a miniaturized and compacted device.

REFERENCES

Alonso Lomillo, M.A., Ruiz, J.G., Pascual, F.J.M., 2005. Analytica Chimica Acta 547(2), 209-214.

Balestrino, D., Haagensen, J.A.J., Rich, C., Forestier, C., 2005. Journal of Bacteriology 187(8), 2870-2880.

Christian, G.D., 1994. The Analyst 119(2309-2314.

Estela, J.M., Cerda, V., 2005. Talanta 66(2), 307-331.

Hansen, E.H., 1989. Analytica Chimica Acta 216(257-273.

Harrar, J.E., Shain, I., 1966. Analytical Chemistry 38(9), 1148-1158.

Munoz-Berbel, X., Vigués, N., Jenkins, A.T.A., Mas, J., Munoz, F.J., Accepted. Biosensors and Bioelectronics.

Muñoz-Berbel, X., Vigués, N., Mas, J., Jenkins, A.T.A., Muñoz, F.J., 2007. Electrochemistry Communications 9(11), 2654-2660.

Rainelli, A., Stratz, R., Schweizer, K., Hauser, P.C., 2003. Talanta 61(5), 659-665.

Ruzicka, J., Hansen, E.H., 1975. Analytica Chimica Acta 78(1), 145-157.

Ruzicka, J., Marshall, G.D., 1990. Analytica Chimica Acta 237(329-343.

Trojanowick, M., 2000. Flow injection analysis: Instrumentation and Applications, World Scientific Ltd., Singapore.

Van Staden, J.F., 2002. Analytica Chimica Acta 467(1-2), 61-73.

Resolution of binary mixtures of microorganism using impedance spectroscopy and artificial neural networks

X. Muñoz-Berbel[1], N. Vigués[2], J. Mas[2], M. del Valle[3], F. J. Muñoz[1], M. Cortina[4*]

[1]*Centro Nacional de Microelectrónica (IMB-CSIC), Campus UAB, E-08193, Bellaterra, Barcelona, Spain.*
[2]*Grup de Microbiologia Ambiental, Universitat Autònoma de Barcelona, Campus UAB, E-08193, Bellaterra, Barcelona. Spain.*
[3]*Grup de Sensors i Biosensors, Universitat Autònoma de Barcelona, Campus UAB, E-08193, Bellaterra, Barcelona. Spain.*
[4]*BIOMEM group, Université de Perpignan, 52 Avenue Paul Alduy, 66860 Perpignan Cedex, France*

Abstract

This work describes the resolution of binary mixtures of microorganism using electrochemical impedance spectroscopy (EIS) and artificial neural networks (ANNs) for the processing of data. *Pseudomonas aeruginosa*, *Staphylococcus aureus* and *Saccharomyces cerevisiae* were chosen as Gram-negative bacteria, Gram-positive bacteria and yeasts models, respectively. Best results were obtained by using backpropagation neural networks made up by two hidden layers. The optimal configuration of these layers respectively used the *radbas* and the *logsig* transfer functions with 4 or 6 neurons in the first hidden layer and 10 neurons in the second one. In all cases, good prediction ability was obtained with correlation coefficients better than 0.989 when comparing the predicted and the expected values for a set of 6 external test samples not used for training.

Keywords: Microbial binary mixtures resolution, electrochemical impedance spectroscopy, artificial neural networks

1. Introduction

Microbiological communities that inhabit in natural microenvironments (soil, water or air) are commonly composed of mixtures of microorganism (e.g. bacteria, yeasts, fungi, etc.). Even though, it is not surprising to find some microorganism cohabiting together in biofilms (coopering or competing) [1-3]. The current microbiology pretends the development of new methods for the fast and simple discrimination, identification and quantification of microorganism from complex and heterogeneous populations.

Quantification of microorganism in mixed populations has been attempted using differential plating, nucleic acid techniques including oligonucleotides probes and genotyping [4, 5] or enzymatic methods [6]. Techniques using synthetic rRNA-targeted hybridization probes are particularly promising for detection, enumeration and identification in situ or after differential plating since their specificity can be adjusted [5]. However, although highly specific, the majority of these methods still require considerable experience as well as time and they are therefore less suitable for use in a routine laboratory.

The infrared spectroscopy, particularly after the development of the Fourier transform infrared spectroscopy (FTIR), has become one of the most widely used techniques for the identification, differentiation and classification of mixed microorganism samples [7-10]. With this method, the infrared spectrum of unknown species is compared with all spectra present in the spectral reference library and matched to the library strain whose spectrum is most similar [11]. Differences between spectra are generally not visible to the naked eye and powerful statistical methods, such as principal component analysis (PCA) [12], hierarchical cluster analysis (HCA) [13], discriminant analysis (DA) [14], discriminant function analysis (DFA) [15], canonical variate analysis (CVA) [16], K-nearest neighbour (KNN) [17], soft independent modelling of class analogy (SIMCA) [17], partial least square (PLC) [11] or artificial neural networks (ANNs) [18], have to be applied. Although the quantitative differentiation of individual species present in a mixed population has been attempted using FTIR spectroscopy, the results have not been as good as expected. The main drawback was the fact that the quality of the obtained results was found to be especially dependent on the characteristics of the microorganism involved in the quantification process [11].

ANNs are intelligent chemometric tools able to predict samples that have not been processed initially and then classify or quantify them, in much the same way as humans use the sense of

taste [19]. An ANN is not based on an explicit algebraic model, but rather on a set of activation units, known as neurons or nodes, which are connected to each other in the form of a network [20]. Feedforward multilayer perceptron neural networks were used for modelling the sensors, which structure consists of an input layer (which feeds the input signals to the succeeding layer), a hidden layer (that receives, processes and sends the filtered signals to the next layer), and an output layer, which links the ANN to the outside world and supplies the processed information. The information is processed through a transfer function in each neuron. In the hidden layer the function is usually sigmoidal, such as log-sigmoidal (*logsig*) or tan-sigmoidal (*tansig*), while in the input and output layers it is typically linear [21]. In order to train the ANN it is necessary to determine the magnitude of interaction (weights) between neurons, that is, to establish how changes among the weights of one layer lead to variations in those of the succeeding one. This is achieved using back-propagation techniques, which aim to find the weights that minimise the error function. The calculation can be performed using training algorithms, such as Gradient Descent with Momentum (GDM) or Levenberg-Marquardt (LM). Further, chemometric tools, namely ANNs and PLC, were probed to be capable to resolve EIS data [22, 23].

This work describes the resolution of binary mixtures of microorganism (quantitative differentiation of individual microorganism in mixed samples), using electrochemical impedance spectroscopy (EIS) and ANNs. In this case, the binary combinations of *Pseudomonas aeruginosa* (*P. aeruginosa*, Gram-negative bacteria model), *Staphylococcus aureus*, (*S. aureus*, Gram-positive bacteria model) and *Saccharomyces cerevisiae* (*S. cerevisiae*, yeast model) were resolved.

2. Experimental

2.1. Electrodes

A platinum disc working electrode (WE) with an area of 0.5 mm^2 surrounded by a platinum counter electrode (CE) of 1.4 mm^2 were integrated on a silicon nitride substrate using sputtering. Electrode production was carried out in-house at the IMB-CSIC Barcelona. The electrodes were 0.08 mm apart, ensuring near-homogeneous polarization of the working electrode [24].

2.2 Preparation of the microbiological mixed suspensions

Microorganism were grown in separate under the experimental conditions that favoured their proliferation and in specific culture media, namely ABMM for *P. aeruginosa* (CGSC 5073 K12), LB medium for *S. aureus* (ATTC 6530) and the universal medium for yeasts DSMZ 186 (DSMZ, Germany) for *S. cerevisiae*. Bacteria were grown overnight at 37 ºC but yeasts, with a longer duplication time, required at least 48 hours growing under the same conditions to reach an initial concentration of around 10^9 colony forming units per mL (CFU mL^{-1}). Cells were then isolated and cleaned. 10 mL of culture medium were centrifuged for 15 min at 1600 g. The supernatant liquid was removed and cells (the pellet) were resuspended in 5 x 10^{-3} M KCl. The process was repeated twice in order to remove metabolic products, membrane fragments and cytoplasmatic proteins. The final pellet was resuspended in 10 mL of 5 x 10^{-3} M KCl and then counted using plating on agar containing LB medium. The suspension was then serially diluted down to 1 CFU mL^{-1} in decade steps.

The mixed response to *P. aeruginosa* and *S. aureus*, to *P. aeruginosa* and *S. cerevisiae* and to *S. aureus* and *S. cerevisiae* was evaluated. A total amount of 22 mixed suspensions were manually prepared, with values selected randomly that completely covered the linear range of response of each microorganism. Before measurements, biological samples were stored in the fridge at 4 °C to slow growth. All of the manipulations were performed under sterile conditions.

2.3 Impedance measurements

An external Ag|AgCl electrode, 5240 (Crison, Barcelona, Spain), was used as a reference electrode in a 10 mL electrochemical cell together with the WE/CE chip. The electrode was connected to a potentiostat (Solartron 1287 (Solartron Analytical, Hampshire, UK)) which itself was connected to an impedance analyzer (Solartron SI 1260A). EIS spectra were recorded using the Z-Plot software (Scribner Associates Inc., North Carolina, USA). A 25 mV AC potential was applied at the cell open circuit potential (+0.26 ± 0.05 V vs. Ag|AgCl) over a frequency range between 100 kHz and 10 Hz.

Mixed suspensions were introduced in the electrochemical cell which was thermostatically kept at 20 ºC. Impedance measurements were made 50 seconds after introducing the mixed suspension in the electrochemical cell.

2.3 ANN Modelling

ANNs were used to model the combined response of three binary mixtures of microorganism and the mixed response to these cells was modelled with 22 manually prepared mixed suspensions, whose values were selected randomly, as previously detailed. 22 samples were proved to be enough to model correctly the combined response of two species and considered sufficient examples of interactions among them [25].

The whole impedance spectrum, recorded after 50 seconds of attachment was treated with ANNs as a calibration tool. The total set of samples was randomly divided into two subsets: (1) the training set (75 % of impedance spectra), which served to determine the model's parameters, and (2) the test set (25 % of impedance spectra), which enabled the model's predictive ability to be evaluated [26].

Calculations were made by developing the corresponding programs in MATLAB (MATLAB 6.1, Mathworks, USA) which employed its Neural Network Toolbox (Neural Network Toolbox 4.0.2, Mathworks, USA). In all cases, the ANNs used were feedforward networks and were trained using backpropagation algorithms, viz. Bayesian Regularization (BR), specially efficient with small data sets, given it does not employ an internal validation subset [27].

3. Results and Discussion

3.1 Determination of individual calibration curves for each microorganism using EIS

Impedance data for each individual microorganism in a range of concentrations from 10^1 to 10^9 CFU mL^{-1} were fitted using the *Z-View* software to the equivalent circuit shown in Figure 1.

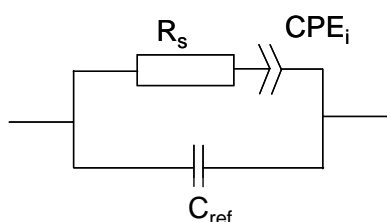

Fig. 1. Equivalent circuit used for the fitting of the impedance data, which contains the capacitor associated to the reference electrode (C_{ref}), the solution resistance (R_S) and the interface Constant Phase Element (CPE$_i$).

The CPE magnitude from the fitting was then normalized using Eq. 1. K_i is the value of CPE at any concentration and $K_i(m)$ is the value of

CPE of the culture medium in absence of bacteria.

$$\Delta K_i = \frac{K_i - K_i(m)}{K_i(m)} \cdot 100 \qquad (1)$$

Figure 2 shows the correlation of the normalized CPE$_i$ magnitude with the suspended concentration of each individual microorganism.
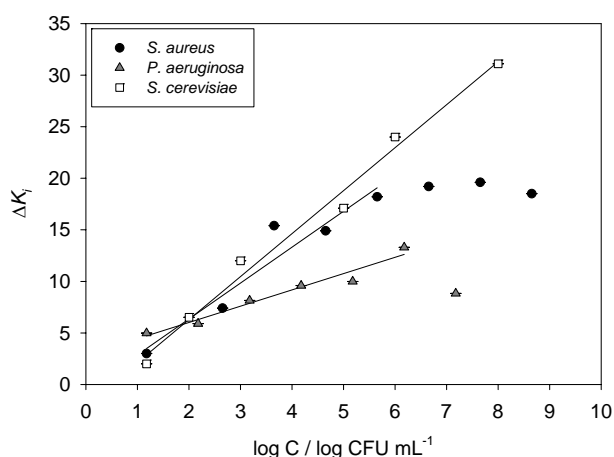

Fig. 2. Representation of the normalized magnitude of the interface capacitance, ΔK_i, with the suspended concentration of *S. aureus*, *P. aeruginosa* and *S. cerevisiae*. This calibration curve was used for obtaining the linear range of response of each microorganism.

All of these microorganism showed capacity to attach to the platinum electrode surface and thus modifying the structure of the electrode-solution interface [28, 29]. However, the magnitude of the response differed between microorganisms. EIS was found to be extremely sensitive to the changes produced in the interface structure by *S. cerevisiae* attachment in a vast range of concentrations, from 10^1 to 10^8 CFU mL^{-1}. This may be associated to the fact that yeasts are much bigger than bacteria and may produce deeper changes in the interface structure when attaching. Regarding to bacteria, the impedimetric approach was more sensitive (in terms of slope of the calibration curve) to the changes caused by *S. aureus* than those caused by *P. aeruginosa*. An explanation of this fact could be obtained by considering the composition of the external membranes of these bacteria: the presence of teichoic acids, highly charged molecules, in the external layers of *S. aureus* may be though to cause deeper changes in the interface structure than the lipopolysaccharides that surround *P. aeruginosa*.

Although experimental data showed differences between microorganisms, they were not visible

to the naked eye and powerful statistical methods were applied, specifically ANNs.

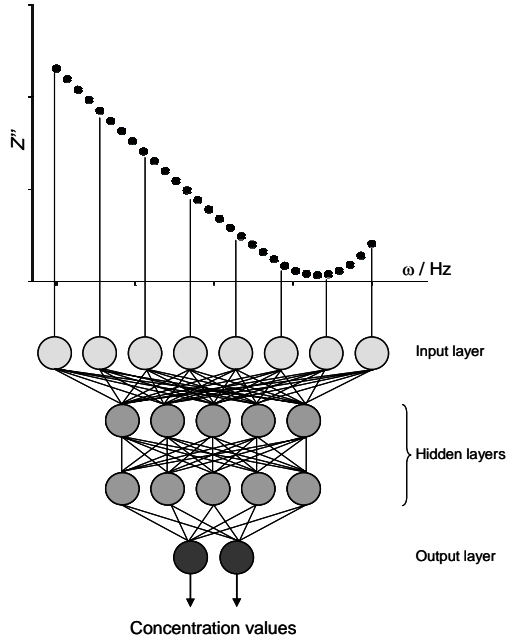### 3.2 Building of the response models and interpretation of ANNs results

Fig. 3. Scheme of the approach used in the study. Each imaginary component (Z'') of the impedance spectra was taken as input in the ANN. Appropriate training was made until the targets were reached within the established errors.

As stated above, three sets of 22 mixed suspensions were prepared in order to build the response models. The concentration range was chosen to practically coincide with the linear response range of each microorganism to the method in use, avoiding the boundary values. Regarding the previous calibration curves, the ranges from 10^1 to 10^6 CFU mL^{-1}, 10^2 to 10^6 CFU mL^{-1} and 10^1 to 10^7 CFU mL^{-1} were respectively selected for *S. aureus*, *P. aeruginosa* and *S cerevisiae*. Each set of samples was then randomly subdivided into two different subsets, namely training and test, which comprised 16 and 6 points, respectively. It has to be noted that the extreme values were reserved for the training subset to avoid the adjusted ANN to extrapolate these points out of the obtained model.

In the impedimetric approach here described, the interface capacitance, CPE$_i$, was found to correlate with the concentration of microorganism, whereas resistive elements, such as the solution resistance, remained invariant. Thus, the imaginary component of the 22 impedance spectra corresponding to each binary mixture of microorganism were considered as the input vectors in the ANN (a total of 30 values, corresponding to the 30 scanned frequencies), being the corresponding concentrations the targets that the modelling should reach. Figure 3 shows the schematic way of action of the proposed ANN modelling.

In order to choose the ANN that best fulfilled this purpose, different structures with supervised learning were considered. In all cases, some features of the structure were established in advance: 30 neurons in the input layer (one for each imaginary component of the impedance spectrum), two neurons in the output layer (one for each microorganism to be quantified in the binary mixture) and linear transfer functions in both input and output layers. The use of two hidden layers was found to be necessary when modelling EIS data [23]. Thus, the evaluated structures always had two hidden layers with a variable number of neurons (from 3 to 6 in the first hidden layer and from 3 to 20 in the second one). Finally, all possible combinations of transfer functions (*tansig*, *logsig* and *radbas*) in both hidden layers were tested.

Table 1
Obtained RMSE values for different combinations of transfer functions in hidden layers and number of neurons in these layers.

Neurons number (hidden layer 1-hidden layer 2)	Transfer function (hidden layer 1-hidden layer 2)	RMSE (log CFU mL^{-1})
S. aureus – P. aeruginosa mixed samples		
4-10	*radbas-logsig*	0.8196
5-10	*radbas-tansig*	1.1871
3-15	*radbas-logsig*	1.1605
6-20	*logsig-tansig*	2.2085
S. aureus – S. cerevisiae mixed samples		
3-5	*radbas-tansig*	2.0050
4-10	*radbas-logsig*	1.2530
5-15	*tansig-radbas*	1.9926
6-10	*logsig-radbas*	2.1557
P. aeruginosa – S. cerevisiae mixed samples		
3-10	*tansig-logsig*	2.0553
4-15	*tansig-radbas*	2.2239
5-5	*radbas-tansig-*	1.7902
6-10	*radbas-logsig*	1.4337

The modelling capacity of the ANN was evaluated in terms of the root mean squared error (RMSE):

$$ RMSE = \sqrt{\frac{\sum_{ij}\left(c_{ij} - \hat{c}_{ij}\right)^2}{2n-1}} \qquad (2) $$

where n is the number of samples ($2n$, as many as two species were determined) and c_{ij} and $\hat{c}_{ij}$ are the expected concentration value and that provided by the ANN, respectively, for each

Table 2
Correlation between obtained and expected values in training ($n = 16$) and external test ($n = 6$) sets employing the final ANN configuration.

		Slope	Intercept (log CFU mL^{-1})
S. aureus – P. Aeruginosa mixed samples			
Training	*S. aureus*, $r = 0.996$	0.96 ± 0.05	0.10 ± 0.15
	P. Aeruginosa, $r = 0.998$	0.97 ± 0.03	0.12 ± 0.13
Test	*S. aureus*, $r = 994$	1.0 ± 0.2	-0.2 ± 0.5
	P. Aeruginosa, $r = 0.996$	0.89 ± 0.11	0.1 ± 0.4
S. aureus – S. cerevisiae mixed samples			
Training	*S. aureus*, $r = 0.999$	0.996 ± 0.012	0.02 ± 0.05
	S. cerevisiae, $r = 0.999$	0.998 ± 0.005	0.02 ± 0.02
Test	*S. aureus*, $r = 977$	1.0 ± 0.3	-0.2 ± 1.3
	S. cerevisiae, $r = 0.997$	1.03 ± 0.11	-0.1 ± 0.5
P. aeruginosa – S. Cerevisiae mixed samples			
Training	*P. Aeruginosa*, $r = 0.996$	0.94 ± 0.06	0.2 ± 0.2
	S. cerevisiae, $r = 0.988$	0.94 ± 0.10	0.2 ± 0.5
Test	*P. Aeruginosa*, $r = 994$	0.87 ± 0.14	0.3 ± 0.6
	S. cerevisiae, $r = 0.989$	1.0 ± 0.2	-0.2 ± 0.8

r is the correlation coefficient. Uncertainties calculated at 95% confidence level.

compound, with *i* denoting samples and *j* species.

Table 1 shows the magnitude of the RMSE for some relevant tested combinations. It has to be emphasized that, for each tested combination, the RMSE magnitude was an average from three reinitialisations of the ANN. Before reinitializing, the weight values were reset and fixed to random values. Thus, the ANN was retrained to see if the model converged in similar situations or whether it reached local minima.

In all cases, low RMSEs were found when using the *radbas* and the *logsig* transfer functions for the first and the second hidden layers, respectively. However, the optimum number of neurons depended on the case, being 4 and 10 for the first and second hidden layers when resolving binary mixtures containing *S. aureus* (*S. aureus - P. aeruginosa* or *S. aureus - S. cerevisiae*) or 6 and 10 by binary mixtures of *P. aeruginosa* and *S. cerevisiae*.

The global behaviour of the modelling system for the external test set was also evaluated by plotting the predicted values (from the ANN) against the expected ones (from plating on agar). Good models should display comparative lines with high correlation, a slope equal to one with zero intercept. Best models were found to coincide with those that previously showed low RMSEs.

The regression parameters of the comparative lines between predicted and expected values for the optimal ANN configurations are shown in Table 2. In all cases, very good correlation was obtained with comparison lines indistinguishable from the theoretical values.

4 Conclusions

In this work the combination of EIS and ANNs has been able to quantitatively solve three binary mixtures of microorganism, namely *P. aeruginosa*, *S. aureus* and *S. cerevisiae*. In all cases, best models have been found to be made up by two hidden layers, using the *radbas* transfer function in the first one and the *logsig* in the second one. Configurations with lowest RMSEs have been always found to use 10 neurons in the second hidden layer. However, the optimal number of neurons in the first hidden layer has been shown to vary depending on the case: 4 when resolving binary mixtures containing *S. aureus* (*S. aureus - P. aeruginosa* or *S. aureus - S. cerevisiae*) or 6 by binary mixtures of *P. aeruginosa* and *S. cerevisiae*. Finally, the predictive ability of the final modelling system has been evaluated by comparing the predicted values (from the ANN) against the expected ones (from plating on agar). In this case, very good correlation has been obtained with comparison lines indistinguishable from the theoretical values (slope equal to one with zero intercept in the three cases under study).

References

[1] P. Stoodley, K. Sauer, D.G. Davies and J.W. Costerton, Annu. Rev. Microbiol., 56 (2002) 187.
[2] W.G. Characklis and K.C. Marshall, eds. *Biofilms*. Wiley series in ecological and applied

microbiology, ed. c. John Wiley. 1990, John Wiley, cop.: New York.

[3] H.M. Lappin-Scott and J.W. Costerton, eds. *Microbial Biofilms*. 1995, Cambridge University Press: Cambridge.

[4] R.I. Amann, B.J. Binder, R.J. Olson, S.W. Chisholm, R. Devereux and D.A. Stahl, Appl. Environ. Microbiol., 56 (1990) 1919.

[5] W.P. Charteris, P.M. Kelly, L. Morelli and J.K. Collins, Int. J. Food Microbiol., 35 (1997) 1.

[6] C.Y. Boquien, G. Corrieu and M.J. Desmazeaud, Appl. Microbiol. Biot., 30 (1989) 402.

[7] L. Mariey, J.P. Signolle, C. Amiel and J. Travert, Vib. Spectrosc., 26 (2001) 151.

[8] L.C. Thomas and J.E.S. Greenstreet, Spectrochim. Acta, 6 (1954) 302.

[9] D. Naumann, V. Fijala, H. Labischinski and P. Giesbrecht, J. Mol. Struct., 174 (1988) 165.

[10] I. Horbach, D. Naumann and F.J. Fehrenbach, J. Clin. Microbiol., 26 (1988) 1106.

[11] H. Oberreuter, F. Mertens, H. Seiler and S. Scherer, Lett. Appl. Microbiol., 30 (2000) 85.

[12] G.D. Sockalingum, W. Bouhedja, P. Pina, P. Allouch, C. Mandray, R. Labia, J.M. Millot and M. Manfait, Biochem. Bioph. Res. Co., 232 (1997) 240.

[13] J. Bastert, H.C. Korting, P. Traenkle and A.F. Schmalreck, Mycoses, 42 (1999) 525.

[14] C. Amiel, L. Mariey, M.-C. Curk-Daubié, P. Pichon and J. Travert, Le Lait, 80 (2000) 445.

[15] É.M. Timmins, D.E. Quain and R. Goodacre, Yeast, 14 (1998) 885.

[16] S.H. Beattie, C. Holt, D. Hirst and A.G. Williams, FEMS Microbiol. Lett., 164 (1998) 201.

[17] M. Kansiz, P. Heraud, B. Wood, F. Burden, J. Beardall and D. McNaughton, Phytochemistry, 52 (1999) 407.

[18] T. Udelhoven, D. Naumann and J. Schmitt, Appl. Spectrosc., 54 (2000) 1471.

[19] M. Cortina, A. Gutes, S. Alegret and M. del Valle, Talanta, 66 (2005) 1197.

[20] M. Ramis and M.C. García, Quimiometría. Vol. 8, Síntesis, Madrid, 2001

[21] J.A. Freeman and D.M. Skapura, Neural Networks: Algorithms, Applications and Programming Techniques, Addison-Wesley, Reading, MA, USA, 1991

[22] M. Cortina-Puig, X. Muñoz-Berbel, M.A. Alonso-Lomillo, F.J. Muñoz-Pascual and M. del Valle, Talanta, 72 (2007) 774.

[23] M. Cortina-Puig, X. Muñoz-Berbel, M. del Valle, F.J. Muñoz and M.A. Alonso-Lomillo, Anal. Chim. Acta, 597 (2007) 231.

[24] J.E. Harrar and I. Shain, Anal. Chem., 38 (1966) 1148.

[25] M. Cortina, M. del Valle and J.-L. Marty, Electroanalysis, 20 (2008) 54.

[26] J.C. Mackay, Network: Comp. Neural, 6 (1995) 469.

[27] H. Demuth and M. Beale, Neural Network Toolbox, for Use with MATLAB, Mathworks Inc, Natick, MA, USA, 1992

[28] X. Muñoz-Berbel, N. Vigués, A.T.A. Jenkins, J. Mas and F.J. Muñoz, Biosens. Bioelectron., In Press, Accepted Manuscript.

[29] X. Muñoz-Berbel, N. Vigués, J. Mas, A.T.A. Jenkins and F.J. Muñoz, Electrochem. Commun., 9 (2007) 2654.